AN *IN VITRO* INVESTIGATION OF BIOCHEMICAL AND MOLECULAR MARKERS OF NANOMATERIAL TOXICITY TO THE INTESTINE

Victor Chibueze Ude

Submitted for the degree of Doctor of Philosophy

Heriot-Watt University

Institute of Biological Chemistry, Biophysics and Bioengineering

Engineering and Physical Sciences

July 2018

The copyright in this thesis is owned by the author. Any quotation from the thesis or use of the information contained in it must acknowledge this thesis as the source of the quotation or information.

Abstract

Application of nanomaterials (NMs) cuts across all facets of life, including agriculture, food, medicine, cosmetics, textiles and electronics, and can lead to ingestion by humans. Although researchers have investigated the toxicity of NMs, there is still a paucity of studies which have assessed NM toxicity to the gastrointestinal (GI) tract. The Caco-2 cell line is most commonly used to assess impacts of NMs on the GI tract, but *in vitro* co-culture models that are more complex can be used to better mimic intestinal physiology. Therefore, the aim of this research was to identify the most appropriate *in vitro* model, and biochemical and molecular markers for assessing the toxicity of NMs to the intestine *in vitro*. Undifferentiated Caco-2 cells, differentiated Caco-2 cells, Caco-2/HT29-MTX (mucus secreting intestinal model) and Caco-2/Raji B (M cell) co-cultures were used for this study. Copper oxide (CuO) NMs were investigated and copper sulphate (CuO_4) included as an ionic control. CuO NMs are useful due to their antimicrobial properties for wood preservation, inks, cosmetics, textiles and food contact materials and their incorporation in these products may enhance oral exposure. CuO NMs and $CuSO_4$, impaired the function of the intestinal barrier (as indicated by a reduction in transepithelial electrical resistance (TEER) and Zonular occludens (ZO-1) staining intensity), and shortened microvilli in all differentiated *in vitro* intestinal models tested. An increase in interleukin (IL)-8 secretion, upregulation of haem oxygenase (*HMOX*)*1*, *IL8*, metallothionein (*MT*) *1A* and *2A* and *mucin* (*MUC*) *2* expression were also observed following exposure of all models to CuO NMs and $CuSO_4$. CuO NMs and $CuSO_4$ increased reactive oxygen species (ROS) production in acellular conditions, but only $CuSO_4$ induced ROS production in the cell models. The Caco-2/Raji B co-culture demonstrated the highest level of NM translocation. Silica NMs and montmorillonite nanoclays did not stimulate a toxic response. The toxicity of CuO NMs and $CuSO_4$ was typically 2 fold greater in undifferentiated Caco-2 cells, suggesting that undifferentiated cells may overestimate the toxicity of NMs. Therefore, it is suggested that differentiated Caco-2 cells, Caco-2/HT29-MTX and Caco-2/Raji B co-cultures are powerful *in vitro* intestinal models and can be used to assess NM toxicity to the intestine. In addition, *HMOX1*, *IL8*, *MT2A* and *MUC2* expression, IL-8 protein, TEER measurement, ZO-1 staining and light microscopy to assess cell morphology and viability are presented as biomarkers for investigating the intestinal toxicity of NMs across *in vitro* models of varied complexity.

Dedication

The thesis is dedicated to my Dad (Late Mr Patrick Uwaezuoke Ude) and Mum (Mrs Patricia Chimaruife Ude) for their sacrifices towards my training.

Acknowledgements

My profound gratitude goes to my supervisors, Dr Helinor Johnston and Professor Vicki Stone for their loving advice, support, kindness, encouragement, inspirational feedbacks and more especially for taking up the job of supervising this project. My sincere thanks to Dr David Brown for allowing me to tap from his great wealth of knowledge. Truly, I count myself privileged to have worked with you in the same laboratory.

I am grateful to Dr Nilesh Kanase for training me when I initially arrived the laboratory and all his words of encouragement. Thanks to Dr Matthew Boyle, Dr Mona Connoly, Krystyna, Leagh, Daniele, Dr Rachel Verdon, Suzanne and the entire Nanogroup for their advice, encouragement and for adding fun to the journey of this PhD research. I am very grateful to Professor Peter Morris for his advice and encouragement in difficult time and Professor Ted Henry and Dr Ferry Melchels members of my PhD review committee.

I am very grateful to Mr Leonard Khama, Barr Okpala, and Professor Diribe for their support. I would like to thank my wonderful friends by name Dr Amadike Ugbogu, Dr Ifeyinwa R. Kanu, Dr Emeka Nebo, Dr Noel, Elijah, Ikenna, Ambrose, Mavis, Olumide and those I could not mention their names here.

I wish to say a big thanks to my ever-loving Mum, my mother and father in-law, brothers (Madubike, Henry and Ebere) and sisters (Pauline, Gladys and Patience) for their love, prayers and support. More importantly, I appreciate your sacrifices, love, caring, prayers and encouragement my amiable wife (Angela Ude) and children (Sochideberem, Chijindum and Chizuberem). Thanks to all of you.

I thank You my God for if not your grace, wisdom and knowledge, nothing would have been possible.

ACADEMIC REGISTRY

Research Thesis Submission

Name*:*	**VICTOR CHIBUEZE UDE**		
School:	**Engineering and Physical Sciences**		
Version: *(i.e. First, Resubmission, Final)*	**Final**	Degree Sought:	**PhD (Biochemistry)**

Declaration

In accordance with the appropriate regulations, I hereby submit my thesis and I declare that:

1) the thesis embodies the results of my own work and has been composed by myself
2) where appropriate, I have made acknowledgement of the work of others and have made reference to work carried out in collaboration with other persons
3) the thesis is the correct version of the thesis for submission and is the same version as any electronic versions submitted*.
4) my thesis for the award referred to, deposited in the Heriot-Watt University Library, should be made available for loan or photocopying and be available via the Institutional Repository, subject to such conditions as the Librarian may require
5) I understand that as a student of the University I am required to abide by the Regulations of the University and to conform to its discipline.
6) I confirm that the thesis has been verified against plagiarism via an approved plagiarism detection application e.g. Turnitin.

* *Please note that it is the responsibility of the candidate to ensure that the correct version of the thesis is submitted.*

Signature of Candidate*:*		Date:	/07/2018

Submission

Submitted By *(name in capitals):*	**VICTOR CHIBUEZE UDE**
Signature of Individual Submitting:	
Date Submitted:	/07/2018

For Completion in the Student Service Centre (SSC)

Received in the SSC by *(name in capitals):*			
Method of Submission (Handed in to SSC; posted through internal/external mail):			
E-thesis Submitted (mandatory for final theses)			
Signature:		Date:	

Table of Contents

List of Figures

Chapter 1

Chapter 2

Chapter 3

Chapter 4

Chapter 5

Chapter 6

List of Tables

Chapter 1

Chapter 2

Chapter 6

Abbreviations

$\Omega.cm^2$	– Resistivity
%	– Percentage
A549 cell	– Human lung epithelial cell line
ANOVA	– Analysis of variance
AP	– Apical
ATCC	– American Type Culture Collection
BL	– Basolateral
BMD	– Benchmark dose
BSA	– Bovine serum albumin
Caco-2	– Human epithelial colorectal adenocarcinoma cell line
cDNA	– Complementary deoxyribonucleic acid
CO_2	– Carbon dioxide
Conc.	– Concentration
Cu	– Copper
Cu $\mu g/cm^2$	– Copper concentration in microgram per centimetre square
Cu µg/ml	– Copper concentration in microgram per millilitre
CuO	– Copper oxide
Ct	– Threshold cycle
DAPI	– 4, 6- diamido-2-phenylindole
DCFH-DA	– dichloro-dihyro-fluorescein diacetate
DLS	– Dynamic Light Scattering
DMEM	– Dulbecco's modified eagle medium
DNA	– Deoxyribonucleic acid
ECACC	– European Collection of Authentic Cell Culture
EDTA	– Ethylenediaminetetraacetic acid
ELISA	– Enzyme-linked immunosorbent assay
EPR	– Electron Paramagnetic Resonance
EVOM	– Epithelial voltohmmeter
ex/em	– Excitation/emission
FAE	– Follicle-associated epithelium
FBS	– Fetal bovine serum
SEM	– Scanning Electron Microscopy
FITC	– Fluorescein isothiocyanate
FTU	– Fluorescent unit

GALT	– Gut-associated lymphoid tissue
GAPDH	– Glyceraldehyde 3- phosphate dehydrogenase
GI	– Gastrointestinal
h	– Hour
H_2O_2	– Hydrogen peroxide
HBSS	– Hanks' Balanced Salt solution
HMOX1	– Haem oxygenase 1 gene
HNO_3	– Nitric acid
HT29	– Colon adenocarcinoma cell line
ICAM-1	– Intercellular adhesion molecule-1
ICP-OES	– Inductively coupled plasma optical emission spectrometry
IL-8	– Interleukin-8
JRC	– Joint Research Centre
L-Glu	– Levo glutamine
LDH	– Lactate dehydrogenase
M	– Molar
M cell	– Microfold cell
MALT	– Mucosal-associated lymphoid tissue
MEM	– Minimum essential medium eagle
min	– Minutes
mM	– Milli molar
MMT	– Montmorillonite
mRNA	– Messenger ribonucleic acid
MT	– Metallothionein
MTX	– Methotrexate
MUC2	– Mucin-2
mV	– Millivolt
MWCNT-COOH	– Carboxylated multi-walled carbon nanotubes
MWCNT-PVP	– Poly (4-vinylpyrrolidone) wrapped multi-walled carbon nanotubes
NEAA	– Non-essential amino acid
nM	– Nano molar
nm	– Nano mitre
NMs	– Nanomaterials
NOEL	– No-observed-effect-level

o/n	– Overnight
P_{app}	– Apparent permeability coefficient
PBS	– Phosphate buffered saline
PCR	– Polymerase chain reaction
PdI	– Polydispersity index
Pg/ml	– Pictogram/ millilitre
PPs	– Peyers patches
PVP	– Poly (4-vinylpyrrolidone)
Raji B cells	– Human Burkitti's lymphoma; B lymphocyte
RNA	– Ribonucleic acid
ROS	– Reactive oxygen species
RPM	– Revolution per minute
RT	– Room temperature
RT qPCR	– Real time quantitative polymerase chain reaction
sec.	– Seconds
SEM	– Scanning electron microscopy
SEM	– Standard error mean
SiO_2	– Silicon dioxide
SWCNT-COOH	– Carboxylated single-walled carbon nanotubes
TEER	– Transepithelial electrical resistance
TEM	– Transmission electron microscopy
TNF-α	– Tumour necrosis factor alpha
WGA	– Wheat germ agglutinin
ZO-1	– Zonula occludens-1

List of Publications

Peer reviewed paper:

- Ude, V. C., Brown, D., Viale, L., Kanase, N., Stone, V. and Johnston, H. J. (2017). Impact of copper oxide nanomaterials on differentiated and undifferentiated Caco-2 intestinal epithelial cells; assessment of cytotoxicity, barrier integrity, cytokine production and nanomaterial penetration. Particle and Fibre Toxicology 14(7).

Conference presentations:

- Ude, V. C., Stone, V. and Johnston, H. J. (2017). Investigation of the toxicity of ingested copper oxide nanomaterials (CuO NM) to the intestine *in vitro*. Inhaled Particles XII Conference, 25-27 September 2017, Glasgow UK.

- Ude, V. C., Stone, V. and Johnston, H. J. (2017). Comparative study of the impact of CuO NMs and CuSO4 on differentiated Caco-2 intestinal cells and a co-culture mucus secreting Caco-2 model. 53rd EUROTOX Congress: Connecting for a Safer Future, Toxicology Letters, Bratislava, Slovakia (280).

Chapter 1: Introduction

1.0. Nanotechnology

In recent years, research on nanotechnology has been in exponential growth due to its potential application in advanced technology, consumer products, agriculture, processing, packaging, engineering, drug or food supplement delivery and biomedicine (Bouwmeester et al. 2009, Aueviriyavit et al. 2014). Nanotechnology is an interdisciplinary area of research and technological development involving the development and use of engineered nanomaterials as well as the fabrication of structures, devices and systems at the nanoscale (1-100 nm). Nanomaterials are materials which have at least one dimension measuring 1-100 nm in size (European-Commision 2011). At the nanometre scale (nanoscale), the properties of materials change compared to their ionic, or bulk (microscale) counterparts (Johnston et al. 2015, Aitken et al. 2006). For example, NMs can have greater catalytic efficiency, increased electrical conductivity, and improved hardness, strength, magnetic, mechanical, thermal, or optical properties, which are highly desirable for applications in commercial, medical, military, and environmental sectors (Chakraborty et al. 2011, Aitken et al. 2006).

The physicochemical properties of NMs such as particle size, chemical composition, agglomeration state, crystal structure, surface area, charge, shape/structure, solubility, and surface coatings control their behaviour (Oberdörster et al. 2005, Gatoo et al. 2014, Braakhuis et al. 2014). The size of NMs impacts greatly on the biological response. For example, a significantly greater neutrophil influx into the rat lung was observed after instillation of 64 nm polystyrene particles in relation to 202 and 535 nm particles (Brown et al. 2001), and 23.5 nm copper NMs and cupric ions ($CuCl_2 \cdot 2H_2O$) demonstrated higher toxicity compared to 17 μm micro-copper particles after oral gavage (Chen et al. 2006). A high surface area per unit mass often correlates with higher biological reactivity (Ahamed et al. 2014), suggesting that decrease particle size, and increased surface area can enhance NM toxicity (Brown et al. 2001, Duffin et al. 2007).

In addition, reports have demonstrated that NM shape can influence their toxicity. For example, rod shaped CuO NMs were more toxic than their spherical counterparts to intestinal epithelial Caco-2 cells (Piret et al. 2012b) and human hepatocyte carcinoma (HepG2) cells (Piret et al. 2012a). NM surface charge regulates cellular uptake, plasma protein binding, blood-brain barrier integrity, transmembrane permeability and colloidal behaviour (Pietroiusti et al. 2011, Goodman et al. 2004, Gatoo et al. 2014, Clift et al.

2011a). Agglomeration is the clumping together of small particles to form larger structures leading to an increase in size and reduction in surface area (Nichols et al. 2002). Agglomeration of NMs is a function of size, chemical composition surface charge and other physicochemical properties. Agglomeration may lead to increased or decreased toxicity of NMs. For example Lim et al. (2012) reported no impact of agglomeration of nano-sized carbon black on its toxicity after exposure to rats through venturi nozzles (pulmonary route). In contrast, agglomeration of carbon nanotubes led to an increase in toxicity in a mesothelioma cell line (MSTO-211H) (Wick et al. 2007) and silver NMs agglomeration caused a reduced toxicity in fish (alevin and juvenile rainbow trout) (Kalbassi et al. 2013). Therefore, the impact of agglomeration on NM toxicity is likely to be dependent on the NM in question, and model under investigation. Presently, there are numerous types of NMs, which can be made from all the elements of the periodic table, sometimes in combination. The composition of NMs can influence their toxicity, with some NMs inherently more toxic than others (Brown et al. 2018, Kermanizadeh et al. 2013a)

1.1. Nanomaterial routes of exposure

The route of exposure of toxic substances determines the level and site of toxicity. The human body is equipped anatomically, biochemically and physiologically to prevent the entrance of toxic materials into the systemic environment. For example, the GI tract is equipped with tight junctions between adjacent epithelial cells (selective absorption), mucus (trapping pathogens and particulate matters) and M cells (for antigen sampling) to prevent the entrance of pathogens, antigens and other particulate matter (Hansson 2012, Kucharzik et al. 2000). In addition, the interaction of NMs with cells, (locally at the exposure site and at the site distal to site of entry), body fluids (e.g. lymph and blood) and biological molecules (e.g. proteins and lipids) has an essential role in the distribution and biological effects of NMs in the body. For example, protein interactions with NMs (often termed the protein corona) may lead to the formation of complexes, which could be more mobile or stable thereby affecting cell and tissue accessibility (Nel et al. 2006, Brown et al. 2014).

There are four main routes of human exposure to NMs: inhalation, dermal, ingestion (oral) and parenteral (e.g. injection) (Figure 1.1), which can occur in environmental,

consumer and occupational settings (The Royal Society 2004). Some of the possible applications of NMs that could enhance oral exposure include the use of NMs as food pigments, health supplements and /or flavour, texture and taste enhancers (Bouwmeester et al. 2009, Wijnhoven et al. 2009, Bergin and Witzmann 2013). For example, the use of titanium dioxide (TiO_2) NMs as a food additive (pigment) will lead to the direct ingestion of NMs (Duncan 2011). Ag NMs have antimicrobial activities and are used for coatings for food and drink containers, clothing, personal care products (e.g. toothpaste, shampoo, detergents), wound dressings, toys and humidifiers (Benn et al. 2010), which may lead to exposure via ingestion, inhalation or dermal. Ag NMs are also incorporated into food packaging to increase the shelf life of food, and nanoclays are used to improve the barrier properties of food and drink packaging (Majeed et al. 2013). The leaching of these NMs into food and drink (Benn and Westerhoff 2008, Hauri and Niece 2011) from such products could lead to the accidental ingestion of NMs.

In addition to ingested NMs, inhaled NMs may also have access to the GI tract through mucociliary clearance from the respiratory tract (Takenaka et al. 2001, Hoet et al. 2004) (Figure 1.1). However, it has been reported that inhaled particles trapped into mucus are not capable of moving (Kirch et al. 2012, Geiser and Kreyling 2010). This suggests that the mucus layer in the respiratory tract may immobilize the NMs once inhaled, thereby hindering their bioavailability. Therefore, the physicochemical properties of NMs may influence their interaction with mucus, and hence the potential for transfer to the GI tract from the lungs. Inhaled NMs may be cleared by the mucociliary escalator or transported into the circulatory system followed by distribution to secondary target organs such as the liver, kidneys, intestine, lymph nodes, spleen, heart, and the brain (Mailänder and Landfester 2009, Geiser and Kreyling 2010).

Possible modes of NM exposure to the skin could be occupational, or via the direct application of NM including products such as sunscreens or cosmetics (Christensen et al. 2010). NMs used for producing sunscreen and cosmetics may be deposited into the GI tract through the process of hand to mouth exposure in occupational and consumer settings (Peixe et al. 2015). Nanotoxicology research papers are dominated by *in vivo* and *in vitro* studies, which investigate the toxicity of NMs following inhalation (Johnston et al. 2015, Brown et al. 2004, Brown et al. 2010, Hussain et al. 2005, Gaiser et al. 2013, Kermanizadeh 2012, Kermanizadeh et al. 2013a, Kermanizadeh et al. 2013b).

Conversely, there are lack of studies, which have assessed the impact of ingested NMs on the gastrointestinal (GI) tract (Stone et al. 2014, House of the Lords 2009, Stone et al. 2016).

Various researchers have used animal models and cell lines to study the impact of NM inhalation on the lungs (Suliman et al. 2015, Brown et al. 2004, Farcal et al. 2015, Banga et al. 2012, Mura et al. 2011, Derk et al. 2015) and they reported cytotoxic effects, release of pro-inflammatory cytokines, genotoxicity, oxidative stress and intracellular production of ROS. This information on the cellular and molecular events underlying NM toxicity to the lungs, can be used to guide investigations which evaluate the toxicity of NMs at other target sites, such as GI tract.

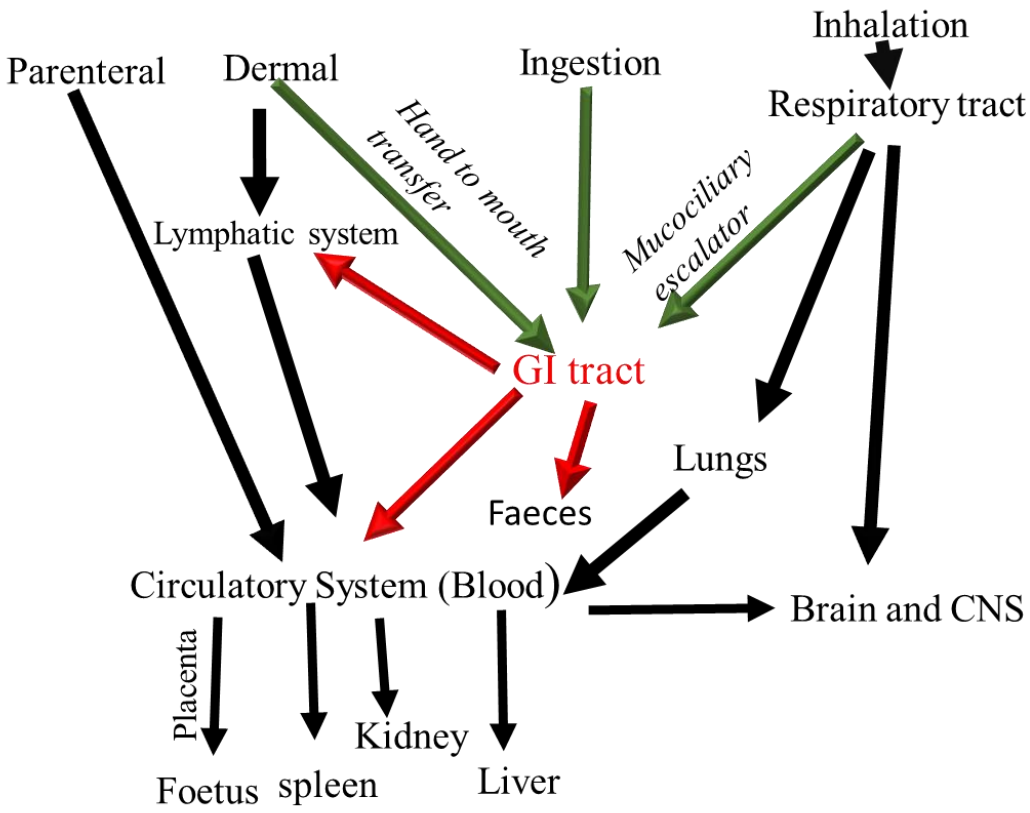

Figure 1.1: Exposure routes of nanomaterials.

Exposure to NMs may occur via parenteral, dermal, oral and pulmonary routes. Following exposure, NMs may enter the circulation and become more widely distributed. The green arrows show the possible exposure routes of NMs to the GI tract whereas the red arrows indicate the potential fate of NMs on leaving the GI tract.

1.2. The gastrointestinal tract structure and function

The functions of the GI tract include digestion and absorption of nutrients and electrolytes, maintenance of water homeostasis, elimination of undigested fraction of macromolecular antigens and the exclusion of pathogens (Bellmann et al. 2015). The GI tract is a complex barrier-exchange system and a boundary between the intestinal contents and the internal medium of the human body. However, daily consumption of food and drink exposes the GI tract to various potentially harmful substances such as chemicals (e.g. pharmaceuticals, pesticides and NMs), and microorganisms.

The GI tract consists of the oral cavity, oesophagus, stomach, small intestine, and large intestine, which are separated by sphincters. The length of the GI tract from mouth to anus is approximately 5 m, of which two-thirds is the small intestine, with some variation between individuals (Helander and Fändriks 2014). The oral cavity begins the process of digestion by receiving, chewing and mixing food with saliva. The oral cavity, the oesophagus and the stomach have very low surface area, of which the oral cavity and the oesophagus are about 0.02 m^2 while the stomach is approximately 0.05 m^2 (Helander and Fändriks 2014). Little is known about absorption and transport in the oral cavity, the oesophagus and the stomach (Bellmann et al. 2015, Helander and Fändriks 2014).

The major site of absorption is the small intestine, which is divided into three segments; the duodenum, jejunum and ileum, and are covered by extended microvilli (Sancho et al. 2004) (Figure 1.2). The small intestine is the longest part of the GI tract with the highest surface area (30 m^2) due to the presence of villi and microvilli at the outermost surface, which increases the surface area of small intestine 9-16 fold (Helander and Fändriks 2014). The duodenum, being the first part of the small intestine, regulates digestion by neutralising gastric acid and increasing pH to about 6.5 (Evans et al. 1988, Hörter and Dressman 2001).

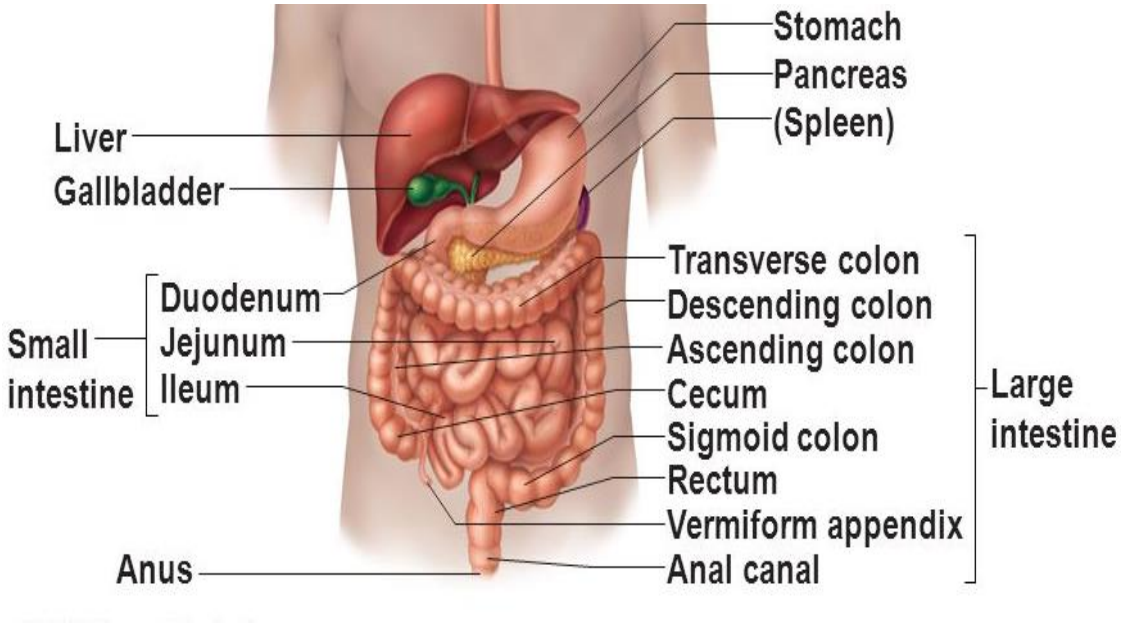

Figure1.2: The human gastrointestinal tract

Adapted from (Baricevic 2012).

Most nutrients are absorbed in the jejunum because of the presence of crypts of Lieberkühn, villi and microvilli, which leads to an increase in the surface area (Sancho et al. 2004). The jejunum also secretes mucins, lactoferrin, albumin and other proteins. The large intestine, also known as the colon, is divided into the ascending, transverse, descending and sigmoid colon (Helander and Fändriks 2014). It has a relatively short length and lacks villi. The diameter of the large intestine is 4.8 cm while the surface area of the colon is about 2 m^2 (Helander and Fändriks 2014). It stores indigestible food materials and waste products prior to excretion, absorbs vitamin K and maintains water balance.

1.2.1. The intestinal epithelium

The intestinal epithelium is made up of the enterocytic cells, endocrine cells, Paneth cells (provides host defence against microbes), goblet cells, and microfold cells (Madara 2011) (Figure1.3). A single layer of epithelial cells forms the epithelium lining of the GI tract and is constantly renewed from intestinal stem cells (ISCs) by continuous production of progeny. The proliferation of ISCs usually occurs at the base of the crypts (deep invaginations of the epithelium around the villi) and the progeny eventually emerge as

differentiated absorptive or secretory lineages. During differentiation, enterocytes, goblet cells, and microfold cells, migrate from the crypts to the epithelial surface, while Paneth cells migrate to the crypt base (Gassler et al. 2006, Mahe et al. 2015). The protective barrier function of the GI tracts is as a result of well differentiated enterocytes (which prevent transport of molecules between cells), the tight mucosal lining, presence of mucus secreting (goblet) cells, well developed innate immunity and presence of immune tissue and cells (Garrett et al. 2010). The integrity of the epithelial barrier is dependent on epithelial cells being joined together by tight junctions, which are essential to the establishment and maintenance of cell polarity (Snoeck et al. 2005). The intestinal epithelial cells separate the intestinal lumen from the systemic environment and regulate nutrient and ion absorption. They also protect the systemic environment from invasion of microorganisms, some of which are in a symbiotic relationship with the host (human intestine) (section 1.2.1.5). For example, commensal bacteria benefit from the host's anaerobic and nutrient rich luminal environment (Halpern and Denning 2015, LeBlanc et al. 2013) and help degrade bile acids and metabolise essential vitamins such as riboflavin, vitamin B12, which is of benefit to the host (LeBlanc et al. 2013, Morowitz et al. 2011). The interaction of the microorganisms and the host also enhances the barrier function and intestinal epithelial structure (Halpern and Denning 2015).

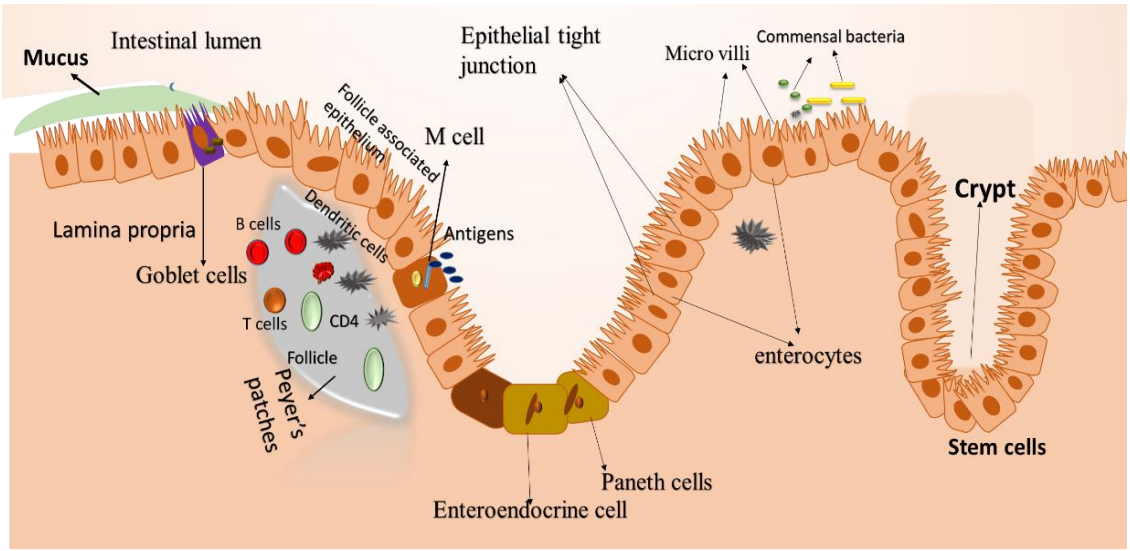

Figure1.3: Structural representation of the small intestine

1.2.1.1. Tight junctions

The majority of the cells in GI tract are enterocytes. The individual cells of the intestinal epithelium are sealed together by tight junctions, which prevent the translocation of substances from the intestinal lumen to the systemic environment (Landy et al. 2016). A compromise in tight junction function leads to inflammation and penetration of toxic compounds to the systemic environment (Schulzke et al. 2009, Ma et al. 2012).

There are ~40 tight junction proteins such as zonula occludens (ZO-1, ZO-2, ZO-3), claudin, tricelluin, occludin, junctional adhesion molecule (JAM) and tight junction-associated marvel protein (TAMP) (Ma et al. 2012, Lee 2015, Halpern and Denning 2015, Landy et al. 2016). The functions of all the tight junction associated proteins are not known, however; ZO-I and occludin have been demonstrated to play a role in tight junction stabilization (cell-cell contact) and regulation, while claudin is essential for cell to cell adhesion and formation of a selective barrier (Lee 2015). Occludin and claudin bind with ZO-1, which then interacts with the actin cytoskeleton and cytoskeleton proteins (König et al. 2016, Fanning et al. 2002, Lee 2015).

In vitro, the function of tight junctions is monitored by performing permeability studies (using inulin or mannitol) and via measurement of transepithelial electrical resistance (TEER). TEER measures the ability of the cell monolayer to separate ionic charge across the epithelium (Ma et al. 2012). Intestinal monolayers have been classified as leaky or tight based on their electrical resistance and tight junction discriminate between substances based on charge and size (Ma et al. 2012). TEER measurement has been used to study the toxicity of chitosan NMs (Vllasaliu et al. 2010), Ag NMs (Bouwmeester et al. 2011, Georgantzopoulou et al. 2016) and TiO_2 NMs (Brun et al. 2014) using different cell types including differentiated Caco-2 cells, lung adenocarcinoma (Calu-3) cells, Caco-2/Raji B cells and a Caco-2/HT29 co-culture.

In vitro studies suggest that TiO_2 NMs cause a reduction in tight junction (ZO-1) staining intensity at 24 h post exposure to a Caco-2/HT29 co-culture (Brun et al. 2014). Calu-3 cells treated with chitosan NMs also demonstrated a reduction in intensity of ZO-1 staining after 24 h exposure (Vllasaliu et al. 2010), indicating that NMs may affect the tight junctions of epithelial cells. The regulation of tight junctions is influenced by nutrition (the composition of food intake), pharmacological (ingested medication), physiological (enzymes secreted into lumen fluid composition of the mucosal and luminal

compartment), microbial (luminal microbial load) and inflammatory factors (inflammatory state of the intestinal mucosa, inflammatory and pro-inflammatory mediators present in lumen) (Ma et al. 2012).

1.2.1.2. Villi and microvilli

The apical surface of the intestinal epithelium is covered by microvilli, often-termed the brush border. The microvilli were first visualised using electron microscopy in 1950 by Granger and Baker (1950) and are known to be essential for nutrient absorption, as the presence of microvilli increases the intestinal surface area. Thousands of microvilli, which possess a uniform diameter and length of about 100 nm X 1-3 µm, project into the intestinal lumen and are arranged in an orderly manner in such a way that the brush border can be viewed in a hexagonal array of microvilli (Helander and Fändriks 2014). Intact and densely packed microvilli are present in the small intestine (Helander and Fändriks 2014, Crawley et al. 2014). Disruption of the orderly arrangement or shortening of the microvilli may lead to impairment in its absorptive function. Previous studies have demonstrated shortening of microvilli after exposure of differentiated Caco-2 cells to CuO NMs (Ude et al. 2017), TiO_2 NMs (Koeneman et al. 2010, Faust et al. 2014a) and ion (III) oxide (Fe_2O_3) NMs (Zhang et al. 2010, Faust et al. 2014b).

1.2.1.3. Goblet cells

The goblet cell is a mucus-secreting cell and an essential part of the mucosal barrier. The goblet cells in the intestinal epithelium are responsible for mucus secretion, forming a mucus layer (Liu et al. 2015). The mucus layer protects the epithelial surface, interacts and traps foreign particles and pathogens thereby preventing their contact with the enterocytes. Mucus is a complex network which is formed from extremely branched macromolecules and glycoproteins and acts as a first barrier that every material taken orally must cross before accessing the intestinal epithelium (Crater and Carrier 2010). The most abundant mucin of the intestinal mucus is mucin (MUC) 2, (Johansson et al. 2008, Johansson et al. 2011). Mucus is continuously secreted and shed or digested, therefore pathogens, drugs and other particles delivered to mucosal surface have to move "upstream" via the mucus layer before they can adhere to the surface of epithelial cells (Cone 2009).

The ability of pathogens, drugs and other particles to transverse the mucus layer are dictated by the adhesive and viscoelastic nature of the mucus (Crater and Carrier 2010). The viscosity of mucus is affected by rehydration and for mucus to transport particles and pathogens it must have appropriate viscoelasticity (Cone 2009). Therefore, for NMs to interact with the intestinal epithelium and be absorbed, they must pass through the sticky mucus layer efficiently. Physicochemical characteristics (Liu et al. 2015) such as particle size and solubility determines if a substance will be able to have contact with the epithelial tissue since soluble substances hardly adhere to the mucus (Sigurdsson et al. 2013). In addition, materials that can adhere to mucus are typically restrained from crossing the mucus layer while non-adherent materials easily cross (Bannunah et al. 2014). There is less interaction of mucus with the lamellar layer (thin layer membrane or tissue) in the small intestine and this allows access of the intestinal contents to the epithelium (Bannunah et al. 2014, Johansson et al. 2011, Round et al. 2012). The thin layer of mucus in the small intestine is likely to explain why most absorption occur in the small intestine as it leads to high epithelial cell accessibility by particles and pathogens (Atuma et al. 2001, Round et al. 2012, Bannunah et al. 2014). Reports have demonstrated that the presence of mucus reduces the rate of absorption of NMs in cellular and acellular *in vitro* models (Crater and Carrier 2010, Vllasaliu et al. 2011).

1.2.1.4. Gut-associated lymphoid tissue (GALT)

The human GI tract needs to control whether an immune response is elicited in response to antigen from external environment (via food, water and other chemicals (drugs)). GALT includes specialized areas of the intestinal epithelium comprising of isolated and aggregated lymphoid follicles. The follicle-associated epithelium (FAE) forms a boundary between the GALT and the luminal microenvironment (Corr et al. 2008) (Figure 1.3). GALT is one of the largest lymphoid organs because of its high immunocyte content (70 % of the body's immunocytes) (Jung et al. 2010).

Aggregated lymphoid follicles known as Peyer's patches (PPs) were named after the Swiss pathologist Johann Conrad Peyer who described PPs in detail in 1667 (Jung et al. 2010) and are responsible for luminal sampling of particles and antigens. M cells are located in the follicle-associated epithelium of intestinal PPs of gut-associated lymphoid tissue. M cells are also found in the isolated lymphoid follicles, appendix and the

mucosal-associated lymphoid tissue (MALT) (Corr et al. 2008, des Rieux et al. 2006). M cells make up approximately 1% of the in the intestinal epithelium surface (Bellmann et al. 2015, des Rieux et al. 2006, Giannasca et al. 1999). Some of the characteristics of M cells that distinguish them from other enterocytes include reduced and weakly organised brush border, short and irregular microvilli, lack of apical glycoprotein of alkaline phosphatase and sucrose-isomaltase activity, absence of thick glycocalyx and a unique intraepithelial invagination or 'pocket' (Gebert et al. 1999, Corr et al. 2008, Kanaya et al. 2007, Brayden et al. 2005).

M cells transport materials across the intestinal epithelial barrier from the lumen of the intestine to underlying immune cells, the point of processing and initiation of an immune response. The transportation of materials may inhibit or activate an immune response and could therefore either cause tolerance or a systemic immune response (Corr et al. 2008). NMs and microorganisms can also utilize the M cell as a point of entry into the systemic environment (Teitelbaum et al. 1999, Gullberg and Soderholm 2006). Other functions of M cells may include releasing a co-stimulatory signal for T- and B- cell proliferation thereby aiding the induction of an immune response to the antigen they are transporting (Corr et al. 2008). The determinants of the mechanism of particle or microorganism uptake by M cells include size, local surface pH, surface charge, temperature, hydrophobicity, concentration of the material and presence or absence of an M cell-specific receptor (des Rieux et al. 2005). Interestingly, researchers have demonstrated the transport of particles such as latex beads, nanoparticles, carbon particles and liposomes and macromolecules including ferritin, horseradish peroxidase, cholera toxin-binding subunit, lectins and antivirus antibodies across M cells *in vitro* (Gebert et al. 1996, des Rieux et al. 2005, Shakweh et al. 2004).

In vivo study of M cells has been a difficult task due to the minute quantity of M cells found in the intestinal epithelium. This led to the design of different types of *in vitro* models in order to investigate M cell functions. *In vitro* models of M cells are usually a co-culture of Caco-2 cells with freshly isolated murine lymphocytes or Raji B cells, (Gullberg et al. 2000, des Rieux et al. 2007, Kernéis et al. 1997). *In vitro* models are found to mimic the *in vivo* M cell by having short or no microvilli at the apical surface, broad microfold cells, thinner glycocalyx and ability to transport particulate matter (Brayden et

al. 2005). *In vitro* M cell models are presently being employed in drug and particulate transport studies (des Rieux et al. 2005, Gullberg et al. 2000, Shakweh et al. 2004).

1.2.1.5. The intestinal microbiota

The gut microbiota (sometimes termed the microflora) is the entire population of microorganisms including bacteria, fungi, archaea, viruses, and protozoan that inhabit the GI tract *(e.g.* Bifidobacteria *(Bifidobacterium bifidum),* Lactobacteria *(Lactobacillus acidophilus, Lactobacillus plantarum, Lactobacillus rhamnosus),* Propionobacteria, Peptostreptococci and Enterococci*).* The gut microbiota enhance food digestion, nutrient metabolism, drug metabolism, prevent pathogenic microorganism's colonization of the intestine and help in maintaining intestinal barrier function (Jandhyala et al. 2015). Alteration of the gut microflora is associated with numerous human diseases such as obesity, colitis, immunological dysfunction and inflammatory bowel disorders (Pietroiusti et al. 2016). Many NMs are exploited for their antimicrobial properties, and thus their ingestion could lead to a change in the abundance and diversity of the gut microflora, which may lead to adverse health effects. Silver NMs have been shown to affect the microflora in rats following ingestion shifting the gut microflora to a greater percentage of gram positive bacteria (Williams et al. 2015). In addition, zinc oxide (ZnO), caesium oxide (CeO) and TiO_2 NMs were demonstrated to affect short-chain fatty acid production, hydrophobicity, sugar content of the extracellular polymeric substance, and electrophoretic mobility using an *in vitro* model of colon gut microbiota (Taylor et al. 2015).

1.2.1.6 Intestinal pH

pH is a logarithmic measure of hydrogen ion concentration and could also be defined as a measure of acidity and alkalinity of a solution, where pH less than 7 is acidic and greater than 7 is alkaline (Abbasi et al. 2012). The pH of the stomach is highly acidic at pH 1 to 2 (Beasley et al. 2015). The duodenum has a pH of 6, whilst the ileum has the pH 7.4, which decreases to pH 5.7 in caecum and finally increases to 6.7 in the rectum (Fallingborg 1999). The differences in the pH of the different segments of the GI tract pose difficulty in the *in vitro* study of absorption and toxicity. Researchers have applied different approaches such as mimicking the saliva, gastric juice, and duodenal juice *in*

vitro to improve the physiological relevance of the models (Brandon et al. 2006, Versantvoort et al. 2005, Oomen et al. 2003, Oomen et al. 2002). Importantly, pH may also affect the physicochemical properties of NMs. For example, the solubility of NMs (e.g. Ag) is enhanced at acidic pH, which may influence its toxicity and availability for absorption in the GI tract (Lefebvre et al. 2015, Bellmann et al. 2015).

1.2.2. Ingested NM penetration across the intestinal epithelium

Particulate matter does not undergo simple diffusion into the basolateral compartment (des Rieux et al. 2006), which could be attributed to the physical characteristics of the particles such as surface charge and inability to dissolve. Ingested NMs may translocate across the GI tract via four processes. The first is endocytosis, an energy dependent movement of macromolecules and particles across the intestinal barrier via the epithelial cells. The second is transcytosis, where macromolecules and particles are transported across the intestinal barrier through microfold (M) cells at the surface of intestinal lymphoid tissue or via other epithelial cells. Third, persorption occurs where old enterocytes are extruded from the villus into the gut lumen, leaving holes in the epithelium, allowing translocation of large particles. Fourth, the paracellular (passive transport) route across tight junctions of the epithelial cell layers (Martirosyan and Schneider 2014, Martirosyan et al. 2012, Powell et al. 2010) (Figure 1.4). The transportation of particulate materials is dependent on the physical and chemical properties of substance (Bellmann et al. 2015). The most efficient transport mechanism for the transportation of intact macromolecules through the epithelial cells is the vesicular transcytosis (endocytosis) which requires energy from the cell. Therefore, most NM uptake only occurs via an active transport mechanism through interaction with the microfilament actin cytoskeleton and microtubules (Bellmann et al. 2015, Catto-Smith et al. 2008). However, transportation of NMs through endocytosis is very low because of the low metabolic activity of the small intestine (des Rieux et al. 2006). In the GI tract, large particles, viruses and bacteria are absorbed via phagocytosis and M cells employ receptor-mediated endocytosis and phagocytosis in intestinal lumen sampling (Bellmann et al. 2015).

The size of paracellular spaces is dependent on the region of the gut; the small intestine has a diameter of one nanometre while the upper duodenum and large intestine could

allow the passage of a material with a diameter of 7 and 3 nm respectively (Bellmann et al. 2015). Although the paracellular spaces hinder the access of substances into the intestinal epithelium, other conditions such as inflammation, diarrhoea, irradiation insult and other intestinal insults (Bellmann et al. 2015) may lead to an increase in transcellular permeability, thereby promoting the transport of material through tight junctions of the epithelial surface. Therefore, it could be inferred that most NMs are absorbed through the M cells, with transport via endocytosis and damaged tight junctions also likely (Bellmann et al. 2015, Shakweh et al. 2004, des Rieux et al. 2006). Translocation of NMs across the intestinal barrier *in vivo* is size dependent (with smaller NMs translocating to a greater extent) and there is evidence that translocated NMs are distributed throughout the body following ingestion (Schleh et al. 2012). *In vitro* studies have also demonstrated a similar size dependent translocation of NMs (Zhou et al. 2017).

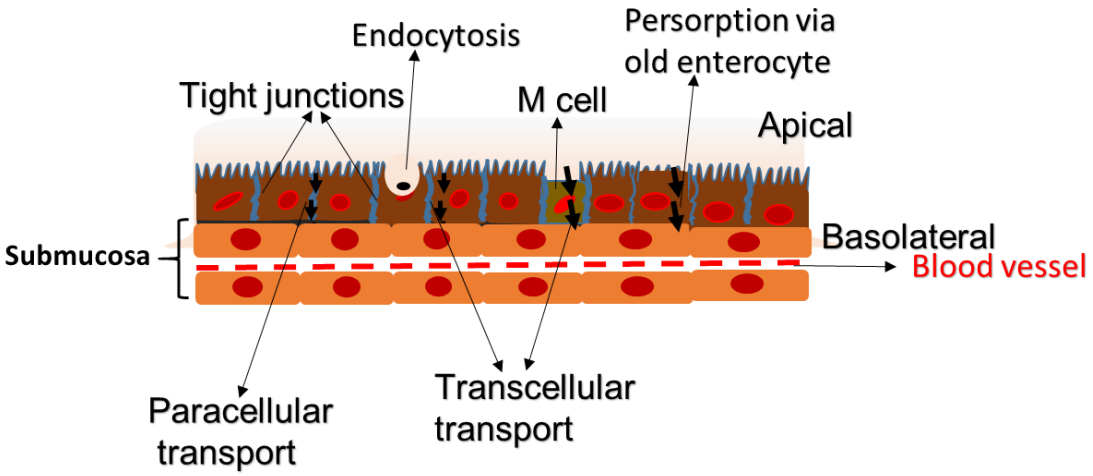

Figure 1.4: Translocation of ingested NMs.

1.2.3. Human gastrointestinal models for studying NM transportation and toxicity

Studying the toxicity of NMs to the human GI tract is a complicated task due to its diversity and complexity. Beside the complexity of human GI tract, the physicochemical characteristics of NMs may also affect its toxicity in different ways. For example, some NMs may dissociate in acidic medium leading to increased toxicity. Several models of the human GI tract have been employed when investigating the toxicity of chemicals and pathogens including *in vivo* animal models, *ex vivo* tissue models, *in vitro* cell culture models, *in vitro* non-cellular models, and *in silico* computational models (Lefebvre et al. 2015, Gamboa and Leong 2013). Each of these models have their own advantages and

limitations and therefore, for effective study of absorption and toxicity of NMs in the GI tract there is the often a need to employ more than one model.

1.2.3.1. In vivo models

In vivo animal models have been used to investigate NM (local and systemic) toxicity and translocation. *In vivo* models have also been used to investigate the efficacy and bioavailability of oral nanomedicines (section 1.3.4). Animal models used for *in vivo* studies may be healthy, genetically modified or induced with human pathological disease such as cancer, diabetes, ulcer or any other disease state the researcher is interested in (Vandamme 2014). Typically, rats, mice, pig and human volunteers are exposed to NMs dispersed in liquid, incorporated in food or administered via oral gavage for *in vivo* toxicity studies (e.g. Bouwmeester et al. 2018, Pele et al. 2015). The use of animal models for toxicity testing is advantageous as it involves the use of living organism with an organised GI tract that is anatomically and physiologically similar to humans (Vandamme 2014). However, some drawbacks are associated with their use. For example, a difference in the length of the GI tract, peristalsis movement and gastrointestinal arrangement of the animal model and humans. When NMs are incorporated into food it is difficult to ascertain the amount of NMs that actually reached the intestine without forming other complexes with the food materials and the animal may not eat all the food or drink all the liquid containing the NMs (Bouwmeester et al. 2018). Other disadvantages include cost, time and ethical considerations. A desire to reduce reliance on animal testing led to the emergence of alternative approaches such as *in vitro* or *in silico* models (Lefebvre et al. 2015). Although, *ex vivo* and *in vitro* models cannot totally replace *in vivo* models, they could be used first before deciding whether to use an animal model thereby embracing the 3Rs principles (Replacement, Reduction and Refinement of animal testing) (Burden et al. 2017). This is particularly important for NMs, as there are many NMs whose safety needs to be assessed (Burden et al. 2017).

1.2.3.2. Ex vivo models

Ex vivo models typically use tissues obtained from humans or animals to investigate toxicity, and are often regarded as a bridge between *in vivo* and *in vitro* models. By retaining cytoarchitecture, physiological function, intercellular connections and

metabolic processes, and *ex vivo* models closely resemble the *in vivo* setting (Ong et al. 2013, Dusinska et al. 2017). Indeed studies have shown that mice lung slices (*ex vivo*) and mice (*in vivo*) exposed to SiO_2 (10 nm), CeO_2 (23 and 88 nm) and TiO_2 (10 and 100 nm) demonstrated similar pattern of toxicity (Kim et al. 2014). GI tract sections can be inverted so that anything taken up across the epithelium will collect in the lumen of the GI tract section, allowing its quantification (Alam et al. 2008, Au - Mateer et al. 2016). Uptake and translocation of TiO_2 NMs have been studied *ex vivo* using rainbow trout intestinal gut sac and the result demonstrated a titanium metal concentration increase in the mucosa (Al-Jubory and Handy 2013). *Ex vivo* experiments also provide researchers with the opportunity to perform experiments, which ordinarily would not be possible *in vivo*. For example, uptake studies using confocal and electron microscopy can easily be studied using *ex vivo* or *in vitro* models as they require series of treatments and washes (Brun et al. 2014, Estrela-Lopis et al. 2011, Wang et al. 2012, Peckys and de Jonge 2011, Elsaesser et al. 2011). In addition, investigation of the impact of NMs on epithelial cell integrity via TEER measurement is only possible in either *ex vivo* or *in vitro* models (Lefei et al. 2017, Brun et al. 2014, Zhang et al. 2010). The use of *ex vivo* models are only applicable for short term experiments (~3 h) (Lundquist and Artursson 2016) and their use often requires fresh tissue, which may not always be available, or could be expensive as the entire animal model may be sacrificed for the tissue to be collected (Ong et al. 2013), hence the study may also have ethical limitations. *Ex vivo* models also lack circulation and the sub-epithelial muscle layer, thereby hindering nerve signalling and peristaltic movement signalling (Lundquist and Artursson 2016). However, co-culture *in vitro* models which make use of different cell types also mimic the *in vivo* situation and could last longer in cell culture than the *ex vivo* models (Clift et al. 2011b).

1.2.3.3. In vitro models

Due to cost and ethical implications of performing *in vivo* studies, the desire to increase the implementation of 3Rs principles, and to make testing more rapid, it has become important to develop and use alternative (non-rodent) models to reduce the requirement for animal testing. Human cell lines are a useful tool to study the toxicity of materials to target cells (Lefebvre et al. 2015). To date the study of the effect of pathogen exposure/infection and toxicity of substances (e.g. chemicals, pharmaceuticals, NMs) in the GI tract has used different types of *in vitro* cell models from humans and animals such

as primary cell cultures and cell lines from normal tissue (e.g. IEC 16, IEC 17 and IEC 18). Others include cell lines transfected with regulatory genes (e.g. IEC 16 transfected with Cdx-2 gene), and established cell lines of tumour origin (e.g. Caco-2, HT29 and HCT 8) (Sambuy et al. 2001). However, most of the models are considered inefficient as they are faced with different drawbacks ranging from inability to form villi, microvilli, functional tight junctions, differentiate into intestinal enterocyte and express characteristic enzymes of the normal living intestinal epithelial cells. Primary cells maintain some degree of differentiation when cultured in the laboratory however, differentiation to mature enterocytes lasts for only three to six days, preventing long term study with primary cells (Sambuy et al. 2001). Therefore, the need to obtain a regular supply of cells limits their widespread use. In addition, there is inter-individual variability in the response measured when primary cells are used.

Cell lines obtained from normal intestinal tissue express most of the epithelial cell markers like cytokeratin, organized F-actin bundles, tight junction proteins, and microvillus proteins, but do not form functional tight junctions as a result of their inability to survive for a long time in culture and do not express disaccharidase and peptidase (Sambuy et al. 2001). Cell lines obtained from normal tissue, which are usually derived from rats, have been found to differentiate poorly and so they do not mimic the differentiated intestinal epithelium. All these drawbacks led to further research and the discovery of cell line from tumour origin of which Caco-2, HT 29 and T 84 are the mostly used models (Sambuy et al. 2001, Ferrec and Fardel 2012). The Caco-2 cell line is most commonly used as it expresses most of the characteristics of mature enterocytes. This is because these cells spontaneously differentiate to form a monolayer of highly polarised cells, joined by functional tight junctions with well-developed and organised microvilli on the apical (AP) membrane after two to three weeks (Sambuy et al. 2001, Sambuy et al. 2005, Ferruzza et al. 2012a). Both undifferentiated and differentiated Caco-2 cells have been used in existing nanotoxicology studies (e.g. Abbott Chalew and Schwab 2013, Bony et al. 2006, des Rieux et al. 2005). For example, barrier permeability and cytotoxic effects of different-sized ZnO NMs have been studied using differentiated Caco-2 cells. This study demonstrated that the penetration and cytotoxicity of ZnO (20 nm) NMs was greater than those with a diameter of 1-5 μm and 90-200 nm after 24 h exposure (Chang et al. 2011). Furthermore, differential toxicity of rod and spherical shape CuO NMs were

investigated with differentiated Caco-2 cells and they observed that rod shaped NMs are more toxic than the spherical shaped CuO NMs (Piret et al. 2012b).

Whilst simple monocultures of (undifferentiated and differentiated) Caco-2 cells have been commonly used to investigate NM toxicity, more complex *in vitro* co-culture models (with 2-3 cell types) have also been used to better mimic the *in vivo* situation. For example, *in vitro* co-culture models comprised from Caco-2 and HT29-MTX mucus secreting cells (Mahler et al. 2009), Caco-2 and Raji B cells for M cell model (des Rieux et al. 2005, des Rieux et al. 2007), and Caco-2 and THP-1 (macrophage) cells for an immune cell model (Manabe et al. 2002, Kämpfer et al. 2017) have been employed in existing studies. A triple co-culture with Caco-2, HT29-MTX and Raji B cells has M cells and secretes mucus has also been used to assess NM transport (Schimpel et al. 2014, Antunes et al. 2013). Currently these triple and double co-culture models are mostly used for NM absorption and translocation studies (des Rieux et al. 2005, des Rieux et al. 2007, Beatriz et al. 2014, Akbari et al. 2017, Araújo et al. 2014, Antunes et al. 2013). Therefore, use of these models to assess the toxicity of NMs would also be prudent.

1.3. Copper

Copper (Cu) is a transition element with an atomic number of 29 and atomic mass of 63.5 g/mol. Cu, on exposure to atmospheric oxygen slowly reacts to form copper oxide (CuO). Cu is an essential micronutrient present in all tissues and is necessary for peptide amidation, cellular respiration, pigment formation, neurotransmitter biosynthesis and connective tissue strength (Desai and Kaler 2008, Araya et al. 2003). Low concentrations of Cu may result in incomplete development, while excessive Cu intake could be harmful and can cause gastrointestinal symptoms such as nausea, vomiting, diarrhoea, and abdominal pain (Dameron and Harrison 1998, Araya et al. 2003, Ellingsen et al. 2007, Gotteland et al. 2001). Some of the enzymes that use Cu as a cofactor include ceruloplasmin, tyrosinase, dopamine-β-hydoxylase, peptidylglycine-α-amidating mono-oxygenase, hephaestin, cytochrome *c* oxidase and copper/zinc superoxide dismutase (Kaler 1998, Desai and Kaler 2008, Rinaldi 2000, Zucconi et al. 2007, Joanne et al. 2006).

The pathogenesis of many neurological diseases such as aceruloplasminemia, Alzheimer's disease, amyotrophic lateral sclerosis, Huntington's disease, Menkes disease, occipital horn syndrome, Parkinson's disease, prion disease, and Wilson disease

are associated with high Cu levels in humans (Kaler 1998, Gaggelli et al. 2006). Cu has also been implicated in development and maintenance of both innate and acquired immunity (Erickson et al. 2000, Muñoz et al. 2005). Although Cu toxicity in humans is rare, Cu can replace other metals in metalloproteins (proteins containing a metal ion cofactor) and the higher binding affinity of Cu compared to other metals may lead to disruption of protein structure hence inactivating the protein or leading to over activity (Foster et al. 2014, Valdez et al. 2014). It is therefore essential to avoid this deleterious indiscriminate binding of Cu by maintaining its concentration at a minimum level. A high Cu level in the human body can also activate the generation of damaging free radicals. The presence of Cu-ATPase (ATP7A and ATP7B), allows the body to eliminate excess Cu via the intestine as faeces, the liver as a bile product, and the mammary gland as milk (Lutsenko et al. 2007, Usman et al. 2013).

1.3.1. Copper Oxide Nanomaterials (CuO NMs)

CuO NMs can be synthesized via three methods including simple precipitation (Ahamed et al. 2014), *Gloriosa superba* L. plant extract as fuel by solution combustion synthesis (Naika et al. 2015) and thermal decomposition (Xu et al. 2002). Copper oxidizes to CuO and Cu_2O then to Cu^+ on exposure to the ambient environment. Presently, CuO NMs have been useful as antimicrobials integrated into textiles, inks, food contact materials, wood preservation solutions and intrauterine devices (Gabbay 2006, Ren et al. 2009). Cu is cheap and readily available and therefore, could replace silver and gold for antimicrobial activity. CuO NMs are also incorporated into heat transfer fluids and/ or semiconductors (Chang et al. 2005, Aruoja et al. 2009). It has been reported that modification of Cu NMs with organic compounds to form copper-based metal-organic framework NMs (Cu-MOF NMs) can reduce the toxicity of Cu NMs, (Xiao et al. 2018). These applications of CuO NMs may lead to their being exposed to the GI tract. For example, CuO NMs may be exposed to GI tracts via direct ingestion of foods or water contaminated by leachates from food contact materials, hand to mouth contact of consumer products or in environmental/occupational setting and mucocilary escalator when inhaled.

1.3.2. CuO NM toxicity in vitro

Previous studies have reported CuO NM toxicity *in vitro* using various cell types including human lung epithelial (A549) cells (Sun et al. 2012, Strauch et al. 2017, Titma et al. 2016), human colon (Caco-2) cells (Titma et al. 2016, Piret et al. 2012b), human bronchial epithelial (BEAS-2B) cells (Strauch et al. 2017), human cervix (HeLa) cells (Strauch et al. 2017) and human liver (HepG2) cells (Siddiqui et al. 2013, Piret et al. 2012a). However, the toxicity of CuO NMs is cell type dependent with some cells exhibiting greater sensitivity to CuO NM toxicity. CuO NMs were demonstrated to be the most potent in terms of cytotoxicity and DNA damage to A549 human lung epithelial cells among TiO_2, ZnO, $CuZnFe_2O_4$, Fe_3O_4, and Fe_2O_3, and could not be explained solely by Cu^{2+} ion release since CuO NMs showed more toxicity than the same quantity of Cu^{+} (Karlsson et al. 2008). CuO NM exposure to cells has been shown to exhibit its toxicity via DNA damage (Angelé-Martínez et al. 2017), ROS production (Karlsson et al. 2008, Angelé-Martínez et al. 2017), stimulation of an inflammatory response (Misra et al. 2014), activation of DNA damage inducible genes and down reregulation of DNA repair genes, glutathione depletion and cell cycle arrest (Strauch et al. 2017). Other studies have also reported the involvement of the autophagy pathway (Sun et al. 2012) and reduction of mitochondrial membrane potential (Siddiqui et al. 2013) in CuO NM toxicity. In addition, CuO NMs have been shown to translocate across the Caco-2 cell monolayer *in vitro* (Chen et al. 2015) and decrease barrier integrity (as indicated by a reduction in TEER) (Piret et al. 2012b). Ag NMs have demonstrated a lack of impact on the Caco-2/HT29-MTX co-culture via assessment of IL-8 and ROS at 24 and 2 h respectively (Georgantzopoulou et al. 2016). Reports have also shown an increase in oxidative stress and metal binding genes (*HMOX1*, *MT2A*, *MT1G*, *MT1M*, *MT1F*) at 4 h post exposure of Caco-2/Raji B cells to Ag NMs but no impact was observed on TEER at 24 h post exposure (Bouwmeester et al. 2011). Although, toxicity of CuO NMs has been studied using different cell types, only a few studies have used Caco-2 cells and none have compared its toxicity using undifferentiated Caco-2 cells, differentiated Caco-2 cells and co-culture models (Caco-2/HT29-MTX and Caco-2/Raji B cells).

1.3.3. CuO NM toxicity in vivo

Translocation of ingested CuO NMs *in vivo* using animal models has not been investigated previously. However, other NMs such as TiO_2 and Au NMs have been shown to translocate across the intestinal barrier of rats. For example, Au (1.4-18 nm) (Schleh et al. 2012) and TiO_2 NMs (50 nm) (Kreyling et al. 2017) translocated across the gastrointestinal barrier 1 h post exposure of rats via intra-oesophageal instillation. Most *in vivo* studies conducted to date have investigated the biodistribution of ingested rutile or anatase TiO_2 NMs (Jones et al. 2015, Pele et al. 2015). TiO_2 NMs (15 nm) showed a peak absorption (~13 µg/l) between 8 and 12 h following oral administration, when the titanium level was assessed in the urine and blood samples over 4 days (Jones et al. 2015). In addition, Pele et al. (2015) reported a peak absorption (~11 µg/l) 12 h after administration of 100 mg/ml of TiO_2 NMs, suggesting low absorption as there was no significant absorption compared to a micro sized counterpart (Jones et al. 2015).

Few studies have investigated the toxicity of ingested NMs to the intestine *in vivo*. For example investigation of the toxicity of CuO, TiO_2 and Al_2O_3 NMs following exposure of rats for 14 days via oral gavage demonstrated an increase in total oxidants status, activity of Ca-ATPase, Mg-ATPase, alanine amino transferases (ALT) and aspartate amino transferases (AST) in the blood, which indicates liver damage (Canli and Canli 2017). Inhibition of Na, K-ATPase was also observed and CuO and Al_2O_3 NMs increased alkaline phosphatase (ALP) activity. Oral exposure of rats to Cu NMs (25 nm) mediated a dose related increase in Cu concentration in urine and induced red blood cell, thymus, spleen, kidney and liver damage at doses of 100, 200 and 400 mg/kg body weight (Lee et al. 2016), indicating that Cu NMs can be absorbed from the intestine. They also observed elevated airway hyper-responsiveness, inflammatory cell counts, pro-inflammatory cytokine secretion, ROS production, and mucus secretion.

Oral administration of gold NMs at a dose of 0.57mg/kg for 8 weeks to mongrel white male rats demonstrated that gold NMs (5 nm) accumulated in the connective tissue sheath of the testes (Velikorodnaya et al. 2015). In addition, though little presence of gold NMs was observed in the lumen of convoluted seminiferous tubules there was no impact on the expression of proliferation proteins (KI-67 and D1 cyclin) and activity of apoptosis in the spermatogenic epithelium (Velikorodnaya et al. 2015). DNA damage and permanent genome alterations, and modulation of DNA repair gene expression in the

mice liver was investigated for polyvinylpyrrolidone (PVP)-coated Ag NMs (33.6 nm) following ingestion (Kovvuru et al. 2015). The observation was that Ag NMs induce large DNA deletions in developing embryos, irreversible chromosomal damage in bone marrow, and double strand breaks and oxidative DNA damage in peripheral blood and/or bone marrow after 5 days of oral gavage administration. Ag NMs also altered expression of 36 of the 84 DNA repair genes, where 24 genes were downregulated and 12 genes were upregulate out of the altered genes (Kovvuru et al. 2015). Oral administration of Ag NMs (7.9 nm) showed that the majority of the NMs were eliminated via faeces, while their blood concentration was very low, an indication of low absorption through the GI tract whereas a high blood silver level after tail vein injection of Ag NMs was observed (Park et al. 2011).

Most *in vivo* studies have investigated CuO NM toxicity to the lung (Gosens et al. 2016). Inhalation and intratracheal instillation of CuO NMs mediated an increase in ROS and cell death via apoptosis in mice exposed to 2.5, 5 and 10 mg/kg body weight (Lai et al. 2018). Another researcher also reported that exposure of mice to 25, 50 and 100 µg/kg body weight of CuO NMs daily via intranasal instillation for three days to Balb/c mice and ovalbumin-induced asthma murine model caused an increase in inflammatory cytokines and ROS production in the lungs, and intensified the development of Asthma (Park et al. 2016).

1.3.4. Impact of NMs on microorganisms

Varieties of metal NMs are bactericidal however, the antimicrobial properties of CuO, Au, Ag, ZnO, TiO_2 and SiO_2 NMs are the most studied (Ahamed et al. 2014, Usman et al. 2013, Argueta-Figueroa et al. 2014, Kasemets et al. 2009, Awwad et al. 2015, Zhou et al. 2012, Beyth et al. 2015, Zhang et al. 2015, Yang et al. 2017). The mechanism of toxicity of metal NMs on bacteria have been attributed to the release of ions, cellular uptake, ROS production and oxidative stress as reviewed by Besinis et al. (2014). The anti-bacterial activity of CuO NMs has been demonstrated on *Escherichia coli*, *Pseudomonas aeruginosa*, *Klebsiella pneumonia*, *Enterococcus faecalis*, *Shigella flexneri*, *Salmonella typhimurium*, *Proteus vulgaris*, *Staphylococcus aureus* (Ahamed et al. 2014). A reduction in the growth of yeast, e.g. *Candida albicans, Candida krusei and Candida glabrata* has also been observed (Amiri et al. 2017) including a 60-fold greater

toxicity than bulk CuO on *Saccharomyces cerevisiae* (Kasemets et al. 2009). Aruoja and colleagues also reported antimicrobial effects of CuO NMs on algae (*Pseudokirchneriella subcapitata*, bacterial species (*Vibrio fischeri, E.coli, S. aureus*) and protozoa (*Tetrahymena thermophile*) (Aruoja et al. 2015). Ag NMs have been effective against drug resistant bacterial such as *E. coli, P. aeruginosa, Staphylococcus pyogens S. aureus, lactobacilli* (*Lactobacillus delbrueckii subsp. bulgaricus and Lactobacillus*), *Bacillus subtilis, and Bacillus cereus* (Lara et al. 2010, Tian et al. 2018, Syed et al. 2015). Ag, TiO_2 and SiO_2 NMs have been shown to exert anti-microbial properties against *Streptococcus mutans* (Besinis et al. 2014). In addition, Au NMs also demonstrated bactericidal effect on *Bacillus subtilis, Bacillus cereus, Bacillus thuringiensis, S. aureus, Staphylococcus epidermidis, and P. aeruginosa* (Zhang et al. 2015, Kumari et al. 2012). Therefore, NMs may be useful in antimicrobial formations and incorporation in food packaging materials. However, following ingestion NMs may impact on the gut microflora, which can have implications for gut health (e.g. Merrifield et al. 2013).

1.4. Mechanism of NM toxicity

The mechanism of toxicity of NMs are hinged on some of the properties of NMs such as particle size, surface area, surface characteristics, dissolution, agglomeration/aggregation, chemical composition, as well as the exposure route, target organ and concentration (Oberdörster et al. 2005, Gatoo et al. 2014). For example, the surface area of NMs increases as the size of NMs decreases, which is known to enhance the NM cellular uptake, translocation, accumulation, reactivity and interaction with biomolecules (e.g. Duffin et al. 2007). It is established that NMs of varied physicochemical properties can exert toxicity via oxidative stress and inflammation (Williams et al. 2015). Existing knowledge of NM toxicity can inform the design of studies which investigate NM toxicity to the intestine *in vitro*.

1.4.1. Dissolution

It is generally believed that dissolution of metal containing NMs such as CuO, Ag, ZnO and Ce_3O_4 is fundamental to their toxicity, as reviewed by Ivask et al. (2014) and Bondarenko et al. (2013). However, investigation of the contribution of ions to their toxicity is difficult, as the available methods such as detection of free and labile metal

ions, qualitative determination of the presence of dissolved metal ions by chelation, and separation of dissolved metal ions by filtration or centrifugation is challenging (Ivask et al. 2012). Previous studies commonly include an 'ionic control' that is typically a metal salt (e.g. silver nitrate) to help identify the contribution of ions to NM toxicity. When soluble NMs are internalised by cells in a particle form, they tend to dissociate intracellularly (in acidic lysosomes) thereby exhibiting a Trojan horse-type mechanism of toxicity (Cho et al. 2011, Shinohara et al. 2017). CuO, ZnO and Ag NMs, which are soluble, have been shown to be more toxic than the non-soluble SiO_2 and TiO_2 NMs *in vitro* (Karlsson et al. 2008, Farcal et al. 2015, Johnston et al. 2015, Kermanizadeh et al. 2013b). However, more direct comparisons of the toxicity of an array of soluble and non-soluble NMs using the same experimental design (e.g. cell model, NM dispersion protocol, NM concentrations and exposure time) is required to verify these findings. Previous studies have also shown that Ag NMs dissociated intracellularly in an immortalized murine microglial cell line (BV-2) when internalised, inducing toxicity via a Trojan horse mechanism (Hsiao et al. 2015). ZnO and Ag NM toxicity correlates well with ion release indicating that the toxicity of ZnO and Ag NMs may be dependent on dissolution as reviewed by Ma et al. (2013) and McShan et al. (2014). However, it has been reviewed that both particles and ionic effects contribute to the toxicity of ZnO and Ag NMs (Chang et al. 2012, Hsiao et al. 2015). For example, studies have also shown that CuO NM toxicity involves a combination of particle and ion mediated effects in differentiated Caco-2 and A549 cells (Piret et al. 2012b, Wang et al. 2012) and that CuO NMs may dissociate to Cu ions after internalisation, as reviewed by Ivask et al. (2014). Although, dissolution is implicated in metal containing NM toxicity as mentioned above, separation of particle from ion effects and determination of the actual ion or particle that will have contact with the cell is pertinent for understating of their mechanism of toxicity.

1.4.2. Uptake

The uptake of NMs by intestinal cells may be an important determinant in their toxicity. NM uptake is dependent on their physicochemical properties such as size, agglomeration/aggregation, surface charge, morphology and interaction with biomolecules (Yao et al. 2015, Fröhlich 2012, Shaw et al. 2016, Zhou et al. 2017, Florez et al. 2012). The uptake of NMs by cells can lead to increased bioavailability and it has been suggested that when CuO NMs are internalized, it may lead to the release of Cu ions

(Ivask et al. 2014). Only one published paper has demonstrated the uptake of CuO NMs (10-20 nm) by differentiated Caco-2 cells, and the authors reported that CuO NMs were present in the cytoplasm, nuclei, lysosomes and membrane bound vesicles after 1 h exposure (Chen et al. 2015). Reports have shown a size dependent increase in Au NM (15, 50 and100 nm) uptake by differentiated Caco-2 cells, demonstrating an increase in uptake as the size decreases (Yao et al. 2015). Silicon oxide NMs (50, 150 nm) demonstrated a very low level of uptake by differentiated Caco-2 cells with higher uptake for the smaller SiO_2 (50 nm) NMs (Ye et al. 2017). An increased uptake and translocation of rod shaped polystyrene NMs (50-100 nm) was demonstrated compared to spherical NMs using Caco-2/HT-29 and Caco-2/HT-29/Raji-B intestinal models (Banerjee et al. 2016). Whereas increased uptake of triangular shaped Au NMs (60-70 nm) was observed compared to rod and star shaped NMs using murine macrophage cells (Xie et al. 2017). Thus, the shape of NMs may influence NM cell interactions and therefore cellular dose.

It has been shown using A549 cells and mouse macrophage cells (J774A.1 cells) that the uptake of NMs may occur by micropinocytosis, phagocytosis, passive diffusion, active endocytosis, clathrin and caveolae-mediated process depending on the physicochemical properties (e.g. size) of the NMs and cell type under investigation (Kuhn et al. 2014, Fröhlich 2012). For example, Li and Monteiro-Riviere (2016) demonstrated that Au NMs (80 nm) was internalised in a size dependent manner via active endocytosis, clathrin and caveolae-mediated endocytocysis in human epidermal keratinocytes. NMs or previous injury to the cell can affect the integrity of the plasma membrane or cell monolayer (barrier integrity) leading to increased translocation (Ivask et al. 2014). It has been shown that the uptake of Fe_3O_4 NMs (20, 50 and 200 nm) occurred in a size dependent manner and was enhanced in inflamed Caco-2 cells (Zhou et al. 2017). However, most studies, which have investigated the uptake and translocation of NMs using Caco-2 cells have used NMs other than CuO. Therefore, the study of uptake and translocation of CuO NMs is essential for proper knowledge of its toxicity.

1.4.3 Oxidative stress

Oxidative stress is an imbalance between the production of ROS and their detoxification by antioxidants (Johnston et al. 2018). ROS are oxygen-derived small molecules with an unpaired electron (e.g. superoxide, hydroxyl, peroxyl hypochlorous acid, ozone and

hydrogen peroxide) (Huang et al. 2010). ROS are very reactive and damaging to proteins, DNA and lipids and can lead to cell death as reviewed in Johnston et al. (2018). ROS are important for physiological functions, for example wound healing, tissue repair processes and destruction of invading pathogens. In addition, signalling pathways involved in cell proliferation, cell growth, apoptosis, inflammation and metastasis are often regulated by ROS. However, higher concentrations could be very detrimental to human cells and tissues. Mitochondrial and cytochrome P-450 enzymes, endotoxin-activated macrophages, cytokine activated neutrophils and hypoxia-activated hypoxanthine-xanthine oxidase system found in the intestinal mucosa are the major producers of ROS in mammals (Granger and Kvietys 2015, Bhattacharyya et al. 2014). Transition metals including Cu induce ROS production via Fenton or Haber-Weiss reactions (Gaggelli et al. 2006, Chumakov et al. 2016) and CuO NMs have also be reported to likely stimulate ROS production via these processes (Angelé-Martínez et al. 2017). The reduction of molecular oxygen to water in the mitochondrial electron transport chain, leads to stepwise addition of four electrons and thereby formation of several hydrogen containing ROS like superoxide radical, hydroxyl radical and hydroperoxyl radical (Gaggelli et al. 2006). Although the superoxide ion is usually generated by the electron transport chain in mitochondria and microsomes via electron leakage, superoxide radicals can also be produced by metal ion-dependent oxidative reactions through Fenton and Haber-Weiss chemistry (Gaggelli et al. 2006).

The human body regulates ROS levels to maintain physiological homeostasis via the activity of non-enzymatic and enzymatic antioxidants. Antioxidants scavenge ROS to control cellular levels. Non-enzymatic antioxidants include glutathione, melatonin, thioredoxin, vitamin E, vitamin C, vitamin A, minerals (zinc, copper, manganese, iron and selenium) and polyphenols (flavonoids) (Bhattacharyya et al. 2014, Kim et al. 2012). Whilst enzymatic antioxidants include haem oxygenase, catalase, superoxide dismutase, glutathione reductase and glutathione peroxidase (Kim et al. 2014, Bhattacharyya et al. 2014, Verma et al. 2013, Ock et al. 2012). There are many approaches that can be used to assess whether oxidative stress is activated in cells including assessment of antioxidants (e.g. glutathione) depletion, antioxidant activity (e.g. superoxide dismutase), intracellular ROS production and expression of antioxidants genes (e.g. *HMOX1* and glutathione reductases expression).

There is evidence that NMs of varied physicochemical properties can stimulate oxidative stress. For example, carbon NMs can stimulate a depletion of glutathione in lung epithelial cells *in vitro* (Stone et al. 1998). The capacity of NMs to induce intracellular production of ROS is commonly assessed in hazard studies as an indicator of their potential to cause oxidative stress. For example, CuO NMs have been shown to generate an increased level of ROS compared to TiO_2, ZnO, $CuZnFe_2O_4$, Fe_3O_4 and Fe_2O_3 NMs after exposure to the A549 human lung epithelial cells, and it was concluded that CuO NMs seem to be more toxic than the other NMs (Karlsson et al. 2008). Assessment of CuO NMs showed a depletion of glutathione in A549 cells indicating that CuO NMs toxicity may occur as a result of oxidative stress (Boyles et al. 2016). It has also been shown that ultrafine carbon can induce toxicity via oxidative stress in human monocytes (Brown et al. 2004). There are several pathological conditions associated with oxidative stress in the GI tract, which includes inflammatory bowel disease, gastrointestinal ulcer and various intestinal malignancies (Bhattacharyya et al. 2014, Kim et al. 2014). It is therefore prudent to assess whether NMs induce ROS production in intestinal cells and antioxidant enzymes to determine the possible mechanism of CuO NM toxicity in the GI tract.

I.4.4. Inflammation

Oxidative stress and inflammation are intimately linked. NM mediated oxidant production causes the activation of several signalling pathways, transcription factors and cytokine cascades leading to a myriad of cellular responses (Brown et al. 2004, Brown et al. 2010, Zhang et al. 2016, Marano et al. 2011, Yan et al. 2016). For example, oxidative stress may lead to an inflammatory response via activation of the redox sensitive nuclear factor kappa B (NF-κB) and nuclear factor erythroid related factor (Nrf) 2 signalling pathways, which are responsible for controlling the transcription of pro-inflammatory genes like interleukin-1 beta (IL-1β), interleukin-8 (IL-8), and tumour necrosis factor-alpha (TNF-α) as well as cytoprotective proteins such as antioxidants (Huang et al. 2010). Gosens et al (2016) demonstrated that CuO NMs caused an inflammatory response in the lungs following inhalation. Research has shown production of pro-inflammatory cytokine such as MCP-1, IL-8, TNF-α, IL-1, and IL-6 on exposure of cells to NMs (Johnston et al. 2015, Huang et al. 2010, Piret et al. 2012a, Piret et al. 2012b). CuO NMs have been shown to induce IL-8 release by differentiated Caco-2, HepG2 and A459 cells (Piret et al. 2012b,

Piret et al. 2012a, Boyles et al. 2016). There is evidence that carbon black particles and ultra-fine carbon can induce toxicity via the release of cytokines (TNF α and IL-8) in human monocytes and A549 cells (Brown et al. 2004, Brown et al. 2010). Au NMs (20 and 100 nm) have been shown to induce toxicity due to inflammation by stimulating cytokine (IL-6, MCP-1, 1L-1β) release in primary hepatocytes, the hepatocyte cell line (C3A) and macrophages (Brown et al. 2014). The production of pro-inflammatory cytokines may be mediated by ROS as report has a reduction of cytokine production after exposure of cells with antioxidant prior to NM exposure (Brown et al. 2004). Since NM toxicity may occur through activation of an inflammatory response, there is the need to investigate the toxicity of CuO NMs via assessment of the stimulation of inflammation (such as investigation of cytokine release *in vitro*).

1.4.5. Disruption of metal homeostasis

Copper is essential for several processes in the human body including for example respiration, connective tissue formation, protection from oxidative stress, iron absorption and metabolism (Nose et al. 2006, Prohaska 2008, Lutsenko et al. 2007, Lutsenko 2010). Due to the participation of Cu in important physiological functions, the intracellular concentration is tightly controlled. In humans, the Cu transporter 1(CTR1) regulates intestinal Cu absorption (Nose et al. 2006). An increase in extracellular Cu concentration induces the movement of CTR1from the plasma membrane into the cytoplasm thereby decreasing Cu uptake. When the concentration of Cu reduces CTR l returns to the plasma membrane (Burkhead et al. 2009, Molloy and Kaplan 2009). Copper-transporting P-type ATPases (ATP7A and ATP7B) are also involved in Cu homeostasis (La Fontaine and Mercer 2007). ATP7A controls the transport of Cu into the trans-Golgi network for biosynthesis of Cu containing enzymes and importation into the intestine whereas ATP7B is essential for homeostasis in the liver, placenta, brain, kidney and small intestine (La Fontaine and Mercer 2007, Lutsenko et al. 2007, Prohaska 2008). Increased levels of Cu may overwhelm homeostatic control mechanisms and alter Cu homeostatic proteins leading to its accumulation and toxicity (Prohaska 2008, Lutsenko 2010). Reports have shown that alteration of homeostatic mechanisms of physiologically important metals may lead to toxicity, as reviewed in Chang et al. (2012).

1.4.6. Interaction of NMs with proteins

Several proteins require one or more metals for their optimum activity. Metals such as Ni, Cu, Zn, Fe, Mn and Co function as cofactors and are essential for enzymatic catalysis, electron transfer, structural maintenance and signalling. Proteins may interact with metal ions derived from NMs via non-covalent binding and the coordination effect (Chang et al. 2012, Ueno et al. 2007, Quintanar and Rivillas-Acevedo 2013). More specifically, the binding of ligand to a central metal atom of a protein is usually essential for the activity of the protein. When the original central atom (e.g. metal ion) is substituted, it can lead to protein unfolding and structural changes, which may affect the activity of the protein (Chang et al. 2012). A greater percentage of *in vivo* molecules coordinate with nitrogen atoms (of histidine), oxygen atoms (of aspartate and glutamate), and sulphur atoms (of cysteines and methionine residues) (Quintanar and Rivillas-Acevedo 2013). These atoms have the capability of bonding with metals such as Cu ions by donating one electron. Therefore, since the coordination atoms are located at the active site, the replacement of the metal may affect the specificity of the protein leading to functional disruption. Cu ions have high affinity for thiol and amino group present in proteins and have the ability to dislodge other metals (Letelier et al. 2005). The presence of clusters of these functional groups in a protein (e.g. metallothionein) may enhance Cu storage in the cell and prevent its toxicity. However, increased levels of Cu may lead to its binding to other thiol groups unrelated to Cu metabolism or homeostasis (Letelier et al. 2005). For example, Cu can dislodge Zn from metallothionein at toxic level, which have been shown to induce ROS production (Ogra et al. 2016).

1.4.6.1. Metallothioneins

Metallothioneins (MTs) are low molecular weight cysteine-rich, metal-binding proteins first isolated in 1957 from the cortex of the horse kidney (Margoshes and Vallee 1957). These low molecular weight (7 KDa) proteins contain 61- 68 amino acids, of which about 20 are cysteine, which can bind to both essential metals (zinc and copper) and toxic metals (cadmium and mercury). MTs have no aromatic amino acid residues and may contain 7 to 12 metal atoms (such as zinc, copper, silver, cadmium or mercury) in each molecule (Calvo et al. 2017). The cysteine residue can cluster in Y-Cys-Cys-Y, Y-Cys-Y-Cys-Y and Y-Cys-Y-Y-Cys. Where Y is any other non-aromatic amino acid (Figure 1.5). MTs

are known to have a high content of thiol groups as a result of their rich cysteine (33 mol %) content and could bind to many transition metals such as cadmium, copper, platinum, mercury, and silver (Romero-Isart and Vašák 2002, Ruttkay-Nedecky et al. 2013).

MT detoxifies heavy metals like mercury and cadmium and regulates the concentration of essential metals such as copper and zinc. MT can protect against ROS, DNA damage, oxidative stress, cell damage, angiogenesis, apoptosis, and increase cell proliferation (Takahashi 2012, Carpene et al. 2007, Ruttkay-Nedecky et al. 2013). MT proteins are encoded by a family of genes located on chromosome 16q13 and are broadly classified into major and minor isoforms, in which MT-1 and MT-II are known as the major isoforms having MT-IA, MT-IB, MT-IE, MT-IF, MT-IG, MT-IH, MT-IX and MT-IIA as the known functional members (Takahashi 2012). The minor isoforms are MT-III and MT-IV (Romero-Isart and Vašák 2002, Takahashi 2012, Cherian et al. 2003). Some of the functions of the four isoforms are outlined in table 1.1.

Treatment of human hepatoblastoma cells (HepG2) with 100 mM of Cu for 2 weeks led to a 28-fold elevation in intracellular Cu and concurrently exhibited a seven-fold increase in total MT concentration with an increase in its saturation with Cu from 45 to 86% (Jiménez et al. 2002). Therefore, MT could account for around 38% of Cu in the cytosolic fraction (Jiménez et al. 2002). At excessive concentrations of Cu, synthesis of MT is induced by gene transcription (Bremner 1987, Suzuki et al. 2002). However, when the concentration of Cu goes above the storable level by MT, the thiol groups are saturated and the Cu-MT complex becomes unstable. The instability of the complex triggers the release of Cu ions leading to free radical generation; thereby MT may begin to function as a pro-oxidant (Jiménez et al. 2002, Liu et al. 2001).

Researchers have also demonstrated that during Cu deficiency, Cu binds MT (Suzuki et al. 2002). MT expression was strongly upregulated in Ag NM treated astrocytes with an average hydrodynamic diameter of 75±20 nm (Luther et al. 2012). Using an immunoblot, it was observed that exposure of 0, 6.25, and 12.5 µg/ml Ag NMs for 24 h showed a dose-dependent increase in MT expression in Caco-2 and NHBE (human bronchial epithelial) cells, whereas RAW 264.7 (murine macrophage), THP-1, (human macrophage) and RLE-6TN (rat lung epithelial-T-antigen negative) cells did not show increased expression, though their exposure to $CdCl_2$ triggered increased MT expression (Zhang et al. 2015).

This suggests a cell specific MT isotype upregulation. However, more studies are needed in intestinal cells to quantify the expression level of MT after NM exposure.

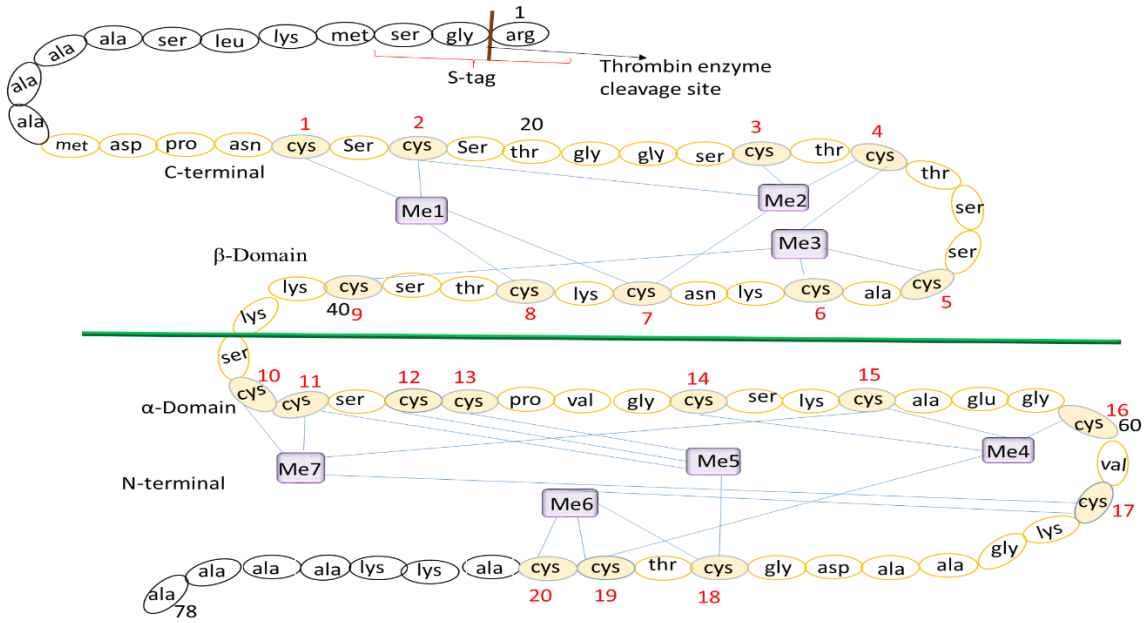

Figure 1.5: Schematic representation of peptide sequence and metal binding domains of metallothionein 1

The 20 cysteines are numbered with red (1-20), metal biding domain (Me1-Me7) and thrombin cleavage site are indicated with a brown line.

Table 1.1: Isoforms, organ of expression and functions of metallothionein,

MT ISOFORMS	ORGANS OF EXPRESSION	FUNCTIONS
MT-I	Expressed ubiquitously in all organs such as liver, intestine, kidney and brain	Essential for copper and zinc homeostasis, cell transcription, detoxification of heavy metals, play a role in immune function, and are necessary for a variety of GI tract functions (Thirumoorthy et al. 2011). They also protect against oxidative stress caused by ROS, nitrogen species and other free radicals (Calvo et al. 2017). Their expression is inducible by external stimuli.
MT-II	Expressed ubiquitously in all organs such as liver, intestine, kidney and brain	Essential for copper and zinc homeostasis, cell transcription, detoxification of heavy metals, play a role in immune function, and are necessary for a variety of GI tract functions (Thirumoorthy et al. 2011). They also protect against oxidative stress caused by ROS, nitrogen species and other free radicals (Calvo et al. 2017). Their expression is inducible by external stimuli.
MT-III	Expressed in brain, central nervous system, stratified epithelia and pancreas	Play a major role in the development, organization and programmed cell death in the brain (Thirumoorthy et al. 2011, Cherian et al. 2003). Their expression is not inducible by external stimuli.
MT-IV	Expressed in brain, central nervous system, stratified epithelia and upper GI tract	Regulates stomach acid pH, taste and texture discrimination of the tongue. Protects against sunburn and other skin traumas (Thirumoorthy et al. 2011, Cherian et al. 2003). Their expression is not inducible by external stimuli.

1.5 General aims and objectives

It is not appropriate to rely on animal testing to assess NM toxicity, as animals are expensive, time consuming and their use is associated with ethical issues. Reducing reliance on the use of animal models in NM toxicity studies is therefore very essential to align studies with the 3Rs principles (Burden et al. 2017). *In vitro* models can be used to test a panel of NMs, at a range of concentrations and time points to make testing high throughput, efficient, and lower cost. There is a lack of studies, which have assessed the toxicity of ingested NMs, however existing knowledge of how NMs exert toxicity can inform which cellular responses are prioritised when screening toxicity to the intestine. Whilst there are a variety of different intestinal *in vitro* models available, these models have not been widely used to investigate the toxicity of NMs to the intestine (Stone et al. 2016, Lefebvre et al. 2015, Bouwmeester et al. 2018). Therefore, the general aims of this study are:

1. To identify biochemical and molecular biomarkers for testing the toxicity of NMs to a model of the intestine *in vitro*.
2. To compare the response to NMs using *in vitro* intestinal models of varied complexity.

1.6. General hypotheses

i. NMs will induce cytotoxicity in intestinal cell models *in vitro*
ii. NMs will elicit ROS production in intestinal cell models *in vitro*.
iii. NMs will induce cytokine production in intestinal cell models *in vitro*.
iv. NMs will impair barrier integrity (i.e. a reduction in TEER, disruption of tight junction staining), which will lead to Cu ion translocation across differentiated intestinal cell models *in vitro*.
v. NMs will upregulate expression of genes related to inflammation, oxidative stress, mucus secretion and metal binding (metallothionein) in intestinal cell models *in vitro*.
vi. The impact of CuO NMs on intestinal *in vitro* models will be similar to copper sulphate ($CuSO_4$).
vii. The toxicity of CuO NMs to intestinal cell models *in vitro* will be similar to silica SiO_2 NMs and montmorillonite (MMT) nanoclay.

viii. The toxicity of NMs will be comparable across all *in vitro* models under investigation.

CHAPTER 2: Impact of copper oxide NMs and copper sulphate on undifferentiated Caco-2 cells

2.1. Introduction

The human Caco-2 cell line originated from a human colon adenocarcinoma and was first isolated in the Sloan Kettering Institute, New York, NY by Fogh and colleagues (Fogh et al. 1977). Caco-2 cells spontaneously differentiate to a mature human intestinal epithelium after culturing for 15-21 days (Sambuy et al. 2001, Sambuy et al. 2005, Natoli et al. 2011). Differentiated cells share many morphological and functional characteristics of enterocytes *in vivo* such as the presence of microvilli. Interestingly, the origin of Caco-2 cells is the colon of the large intestine, which do not have microvilli and its associated proteins. Caco-2 cells can be used to develop co-culture models, which mimic different characteristics of the human small intestine including mucus secreting goblets cells (co-culture of Caco-2 and HT29 cells) (Gamboa and Leong 2013, Lefebvre et al. 2015), M cells (Caco-2 and Raji B co-culture) (des Rieux et al. 2007, des Rieux et al. 2005), and microvilli (Sambuy et al. 2001, Sambuy et al. 2005). The healthy and diseased state of the human intestine has also been modelled using Caco-2 cells (Kämpfer et al. 2017). Although Caco-2 cells are of colon tumour origin, it has been widely employed as an *in vitro* model for the study of intestinal epithelial cell function (Wang et al. 2008), drug discovery/development, mode of transport and mechanism (Kumar et al. 2010, Cheng et al. 2008, Liu et al. 2017, Hubatsch et al. 2007). In addition, undifferentiated Caco-2 cells are also useful in the study of NM toxicity (Jepson 2012, Gerloff et al. 2013, Gerloff et al. 2009, Tarantini et al. 2015b), pathogens (O'Flaherty and Klaenhammer 2012, Naresh et al. 2009), pharmaceuticals (Li et al. 2011, Taipalensuu et al. 2001) and industrial chemical waste (Velarde et al. 1999).

Undifferentiated Caco-2 cells lack some biochemical and morphological characteristics of human enterocytes but they represent proliferating cells (Tarantini et al. 2015b), hence they depict more closely the intestinal crypt epithelial cells. Undifferentiated Caco-2 cells have been shown to be more sensitive than differentiated Caco-2 cells to NM toxicity (Gerloff et al. 2013, Ude et al. 2017), but they can be used for a rapid and cheap screen of a high number of substances (e.g. NMs, drugs) at a range of concentrations and time points before employing more complicated models. More especially, the culture of differentiated cells requires transwell plates and takes up to 21 days to develop. In contrast, undifferentiated cells can be grown in 96 well plates and can be used 24 h post seeding, which means that they are cheaper and quicker to use. Although there has been

a lack of studies, which have assessed the response of the intestine to ingested NMs (Stone et al. 2016), the majority of existing *in vitro* studies have used Caco-2 cells as a model system. For example, undifferentiated Caco-2 cells have been used for the study of the toxicity of cadmium selenium (CdSe) quantum dots (QD), in which cell viability and cell attachment were studied as indicators of toxicity (Wang et al. 2008). Reports have also shown that titanium dioxide (TiO_2, 305-311 nm), silver (Ag, 202-227 nm) and zinc oxide (ZnO, 212-260 nm) NMs led to increased IL-8 production from undifferentiated Caco-2 cells but no significant reactive oxygen (ROS) formation was stimulated (Abbott Chalew and Schwab 2013). Toxicity, genotoxicity and pro-inflammatory effects of amorphous nanosilica (SiO_2, 15 and 55 nm) have also been studied using undifferentiated Caco-2 cells (Tarantini et al. 2015b). These researchers observed that SiO_2 of 15 nm generated more ROS than the 55 nm SiO_2 and IL-8, while 55 nm SiO_2 did not stimulate IL-8 secretion and both sizes did not cause genotoxicity. Although there are many studies, which have used undifferentiated Caco-2 cells to study the toxicity of NMs, there is no report on toxicity of CuO NMs and $CuSO_4$ using undifferentiated Caco-2 cells. The majority of existing studies have assessed similar endpoints to screen NM toxicity; namely, cytotoxicity, inflammation and oxidative stress, and this will inform the endpoints investigated in this study.

Undifferentiated Caco-2 cells were selected for the study of CuO NM and $CuSO_4$ toxicity because the Caco-2 cell line is the basis on which other, more complex models for this project will be built on. Thus, it is important to understand the "baseline" response in undifferentiated cells prior to applying more complex models. It is also very easy, cheap and quick to screen a wide range of concentrations of NMs with undifferentiated cells and so it is intended that the results obtained will inform the selection of NM concentrations that will be used for further experiments. Of benefit is that common cellular responses can be measured across undifferentiated cells, and more complex models allowing for comparisons in model sensitivity to be made.

2.1.1. Aim and objectives

The aim of this chapter was to investigate the use of undifferentiated Caco-2 cells for the study of ingested NM toxicity *in vitro*, and to identify the biochemical and molecular biomarkers of NM toxicity in the intestinal model *in vitro*. In addition, the toxicity of

CuO NMs and $CuSO_4$ will be compared to help dissect out the contribution of particle and ionic effects to NM toxicity.

The specific objectives include:

i. To determine the effect of CuO NMs and $CuSO_4$ on undifferentiated Caco-2 cells via assessment of cytotoxicity (Alamar blue assay), cytokine production (ELISA) and ROS formation (DCFH-DA assay).
ii. To assess the impact of CuO NMs and $CuSO_4$ on undifferentiated Caco-2 cell morphology (light/electron microscopy) and expression of genes related to inflammation (*IL8*), oxidative stress (*HMOX1*), mucus secretion (*MUC2*) and metal binding (e.g. metallothionein (*MT1A* and *2A*).

2.1.2. Hypotheses

i. CuO NMs and $CuSO_4$ will induce a loss of viability in undifferentiated Caco-2 cells.
ii. CuO NMs and $CuSO_4$ will stimulate ROS production in undifferentiated Caco-2 cells.
iii. CuO NMs and $CuSO_4$ will stimulate cytokine production in undifferentiated Caco-2 cells.
iv. CuO NMs and $CuSO_4$ will upregulate the expression of genes related to inflammation, oxidative stress, mucus secretion and metal binding in undifferentiated Caco-2 cell.
v. The impact of CuO NMs on undifferentiated Caco-2 cell will be similar to $CuSO_4$.

2.2. Materials and Methods

2.2.1. Nanomaterial preparation

CuO NMs were obtained from Plasma Chem, GmbH (Berlin, Germany), in a powdered form as a kind gift from project partners in the FP7 funded project Sustainable Nanotechnologies (SUN). The CuO NMs are a crystalline material with a size range of 15–20 nm (size provided by manufacturer). Brunauer–Emmett–Teller (BET) method was used to evaluate the specific surface area ($47 m^2/g$ and a density ($6.3 g/cm^3$) (manufacturer data sheet). Previously, a detailed characterisation of the CuO NMs was performed using

Transmission Electron Microscopy (TEM), X-ray diffraction (XRD), and Inductive Coupled Plasma Optical Emission Spectrometry (ICP-OES) (Gosens et al. 2016).

2.2.2. Nanomaterial preparation

CuO NMs and $CuSO_4$ were dispersed following the procedure developed by (Jacobsen et al. 2010). Briefly, CuO NMs and $CuSO_4$ were dispersed in 2 % heat inactivated fetal bovine serum (FBS) in Milli Q de-ionised water and sonicated for 16 min without pause. Following the sonication step, all samples were used immediately. To determine the acute toxicity of CuO NMs, concentrations between 0.37 to 78.13 Cu µg/cm^2 (equivalent to 1.17 to 250 Cu µg/ml) were used. After sonication, the required concentration for each experiment was obtained by serial dilution in the appropriate medium.

2.2.3. Cell Culture

The human colon colorectal adenocarcinoma Caco-2 cell line was obtained from the American Type Culture Collection (ATCC) (USA). The cells were maintained in minimum essential medium eagle (MEM) (Sigma) supplemented with 10 % heat inactivated FBS (Gibco Life Technologies), 100 U/ml Penicillin/Streptomycin (Gibco Life Technologies), 100 IU/ml nonessential amino acid (NEAA) (Gibco Life Technologies), and 2 mM L- glutamine (L-Glu) (Gibco Life Technologies), at 37 ºC and 5 % CO_2. The cells were sub-cultured three times a week at 70 to 80 % confluency using trypsin-EDTA (0.05 %) (Gibco Life Technologies).

2.2.4. Dynamic light scattering

Dynamic Light Scattering (DLS) measures hydrodynamic diameter, zeta potential and the polydispersity index of NM suspensions. The instrument first measures the Brownian motion of particles by assessing scattered light, and applies the Stokes-Einstein equation to determine the size of the particle. The mean hydrodynamic diameter (z-average diameter) and the width of distribution (polydispersity index (PdI)) of the particle are calculated. In addition, the zeta potential of NMs are usually measured in a cell containing two gold electrodes and application of voltage to the electrode leads to movement of particles towards opposite charge electrode then velocity is measured as a function of voltage.

The hydrodynamic diameter, zeta potential and PdI of CuO NMs suspended in biological medium (MEM and DMEM complete cell culture medium) was determined using DLS (Malvern Zetasizer Nano series) at 0 h and at 24 h (following incubation at 37 °C). Briefly, CuO NMs were dispersed by bath sonication in 2 % FBS (in water) for 16 min (at a concentration of 1 mg/ml). The concentration was adjusted to 50 Cu µg/ml in phenol red free MEM or DMEM cell culture medium supplemented with 10 % FBS (Gibco Life Technologies), 100 U/ml Penicillin/Streptomycin (Gibco Life Technologies), 100 IU/ml NEAA (Gibco Life Technologies), and 2 mM L-Glu (Gibco Life Technologies). The hydrodynamic diameter, polydispersity index (PdI) and Zeta potential of the samples were measured in triplicate following 120 sec equilibrations.

2.2.5. Alamar blue cell viability assay

Alamarblue (resazurin) is a non-toxic, cell-permeating compound that is blue in colour and virtually non-fluorescent. Upon entering cells, resazurin is reduced to the fluorescent product (resorufin) by mitochondrial enzymes. Only viable cells convert resazurin to resorufin, thereby generating a quantitative measure of viability (Al-Nasiry et al. 2007). For viability assessment, a concentration of 1.56 x 10^5 cells /cm^2 of Caco-2 cells were seeded into a 96 well plate (surface area 0.32 cm^2) (Costar Corning Flintshire UK) and incubated at 37 ºC and 5 % CO_2. After 24 h 100 % confluency was reached, and the cell culture medium was removed. The cells were washed twice with PBS (Gibco Life Technologies) and exposed to cell culture medium (negative control), 0.1 % triton-X 100 (positive control) and a range of concentrations of CuO NMs or $CuSO_4$ (0.37 to 78.13 Cu µg/cm^2 equivalent to 1.95 to 250 Cu µg/ml) at a volume of 100 µl. The concentration of the CuO NMs and $CuSO_4$ were standardized to ensure that the cells were exposed to the same concentration of Cu for both CuO NMs and $CuSO_4$ at each concentration. The cells were incubated for 24 h at 37 ºC and 5 % CO_2 and then the supernatant was removed, and the cells were washed twice with PBS. Cells were then exposed to 100 µl of Alamar blue reagent (0.1 mg/ml in MEM cell culture medium) (Sigma, Poole). The cells were incubated for 4 h at 37 ºC, 5 % CO_2 and fluorescence measured with a microplate reader (SpectraMax M5) at a wavelength of 560/590 nm (excitation/emission). Data was analysed using PROAST 38.9 software to obtain the Benchmark dose response (BMD) 20 (the concentration of CuO NMs that increase cell death by 20 %). Data are expressed as mean % viability of the control.

2.2.6. Nuclei counting

Undifferentiated Caco-2 cells seeded at a concentration of 3.13 x 10^5 cells/cm^2 were grown on a glass coverslip in a 24 well plate (Costar Corning, Flintshire, UK) for 24 h. The cells were exposed to cell culture medium (control), 6.34 and 12.68 Cu µg/cm^2 of CuO NMs or $CuSO_4$. After 24 h, the cells were fixed with 4 % formaldehyde for 25 min at RT and 50 mM ammonium chloride was used to quench excess aldehyde groups at RT for 10 min. The cells were then permeabilized with 0.1 % triton X100 for 10 min at RT. The nuclei of the cells were stained with 300 nM of 4, 6- diamido-2-phenylindole (DAPI) for 15 min at RT and then washed with PBS three times. The glass coverslips were mounted with mowiol containing DABCO (1, 4-Diazobicyclo-(2,2,2-octane, antifading agent, (Sigma, Poole UK)) onto a microscope slide, sealed with nail polish and allowed to dry at 4 ^oC for 24 h before visualizing with Zeiss fluorescent Microscope, Carl Zeiss Axio Scope A 1 Upright Research Microscope (Germany) fitted with camera (ZEISS Axiocam ERc 5s). At least five fields of view were imaged and analysed (each field of view was 140.80 X 105.60 microns). Data are expressed as mean % of unexposed control.

2.2.8. Romanowsky staining: Cell morphology

Rapid Romanowsky stains combine the basic (cationic) dye, methylene blue (azure) and the acid (anionic) dye, eosin Y. The basic dye binds negatively charged nuclei thereby generating a purple colour while the acid dye binds to the cytoplasm producing a red colour (Horobin 2011).

For light microscopy, undifferentiated Caco-2 cells seeded at a concentration of 3.13 x 10^5 cells/cm^2 were grown on a 10 mm glass coverslip in a 24 well plate (Costar Corning, Flintshire, UK) for 24 h. The cells were exposed to MEM cell culture medium (control), 6.34 and 12.68 Cu µg/cm^2 of CuO NMs or $CuSO_4$. After 24 h, the cells were stained with Rapid Romanowsky stain (TCS Biosciences, England). Cells were fixed by rinsing the coverslip 10 times in methanol. To stain the cells the coverslips were rinsed in eosin Y solution 10 times and then the methylene blue solution 10 times. The cells were thoroughly washed in distilled water, air-dried and mounted with DPX mountant (Sigma, Poole UK). The samples were examined using light microscopy- Zeiss fluorescent microscope, Carl Zeiss Axio Scope A 1 Upright Research Microscope (Germany) fitted with camera (ZEISS Axiocam ERc 5s) (magnification 40 X).

2.2.7. Scanning electron microscopy (SEM)

SEM uses an electron gun located at the top of an SEM instrument to shoot out a highly concentrated electron beam towards the specimen. To maximise the efficiency, the electron is directed towards the specimen via the series of lenses located in the vacuum chamber. The vacuum chamber helps to prevent the obstruction of the electron beam as obstruction of the chamber may lead to unclear result and the more the electron that reach the specimen the more powerful the magnification obtained. As the beam of the electrons (incident beam) hits the specimen, X-rays, primary backscattered electrons, secondary electrons and Auger electrons are emitted. The electrons used by the SEM are the primary backscattered and secondary electrons. The rebounding electrons are picked up by electron recorder and the imprint recorded. Finally, the information is translated onto a screen, which allows a clear representation of three-dimensional images (Gree 2015).

For this experiment, undifferentiated Caco-2 cells were seeded at a concentration of 3.13 x 10^5 cells/cm^2 onto a 10 mm glass coverslip in a 24 well plate (Costar Corning, Flintshire, UK) and grown for 24 h. The cells were treated with cell culture medium (control) or 12.68 Cu µg/cm^2 of CuO NMs. After 24 h, the cells were washed with PBS twice, fixed with 5 % glutaraldehyde (in 0.1 M sodium cacodylate) for 2 h at 4 ^oC. The cells were washed three times with 0.1 M sodium cacodylate followed by dehydration in graded ethanol (25, 50, 70, 80 and 90 %) for 10 min in each ethanol grade at RT. The cells were further dehydrated in 100 % ethanol three times for 15 min each then, submerged in 2:1 fresh solution of hexamethyldisilazane (Sigma, Poole):100 % ethanol. The glass coverslips containing the cells were dried in 100 % hexamethyldisilazane (Sigma, Poole) and mounted on SEM specimen stubs (Aluminium, 12.5 mm diameter, 3.2 x 6 mm pin Agar Scientific UK). Finally, the specimens were coated with gold and examined with Scanning Electron Microscopy (SEM). More than 5 views were imaged and a representative image presented.

2.2.9. Oxidative stress assays

2.2.9.1. Evaluation of acellular ROS production: DCFH-DA assay

The oxidant activity of CuO NMs in acellular conditions was assessed using the dichloro-dihyro-fluorescein diacetate (DCFH-DA) probe. The presence of oxidizing species

converts the non-fluorescent DCFH-DA probe to the fluorescent dichloro-dihyro-fluorescein (DCF) species. In acellular conditions, the acetate is removed via chemical or enzymatic hydrolysis as the enzyme capable of hydrolysing DCFH-DA is absent in a cell free environment. The acellular ROS formation by CuO NMs and $CuSO_4$ was investigated by modifying the methods described by Foucaud et al. (2007) and Sauvain et al. (2013). Briefly, 10 mM DCFH-DA (in methanol) was hydrolysed by diluting 10 mM DCFH-DA to 1 mM in methanol and then to 0.2 mM in 0.01M NaOH. The solution was incubated at RT for 30 min in the dark and 0.1 M PBS (pH 7.4) was then added to stop the reaction (to give a concentration of 0.05 mM DCF). The reaction mix was placed on ice and used immediately. As a control, an equivalent volume of 0.01 M NaOH, 0.1 M PBS solution (pH 7.4) and methanol was prepared without DCFH-DA.

The DCFH reaction mix or the mixture without DCFH-DA was transferred to the wells of a black clear bottom 96 well plate (225 µl/well) in triplicate This was followed by addition of 25 µl MEM complete cell culture medium without phenol red (negative control), 1 mM/cm^2 H_2O_2 and 3.17, 6.34 or 12.68 Cu µg/cm^2 of CuO NMs or $CuSO_4$ (in complete cell culture medium without phenol red). The fluorescence generated by the DCF oxidation was measured at time zero and every 15 min for 75 min then every 30 min for 1 h 30 min 485/530 nm (ex/em) with constant shaking at RT. Data was expressed as fold change or fluorescence units.

2.2.9.2. Evaluation of intracellular ROS production: DCFH-DA assay

Intracellular reactive oxygen species (ROS) levels were evaluated using the non-florescent probe DCFH-DA. The diacetate allows for the penetration of DCFH-DA in to the cell, which is then cleaved inside the cell. Existing studies have varied with respect to the protocol used to assess ROS production using the DCFH-DA assay (e.g. DCFH probe concentration, the time point at which ROS production is quantified, and whether cells are preloaded with dye then exposed to NMs or exposed to NMs then the DCFH-DA probe). Thus, the protocol had to be optimised for Caco-2 cells and CuO NMs. The DCFH-DA concentration was optimized and identified to be 150 µM. Undifferentiated Caco-2 cells (1.56 x10^5 cells /cm^2) were grown in a 96 well plate (Costar Corning) and maintained at 37 ^oC, 5 % CO_2 and 95 % humidity for 24 h. Cells were then washed twice with PBS and 150 µM of DCFH-DA (in Hanks' Balanced Salt solution (HBSS)) was added (100 µl). The cells were then incubated for 1 h in the dark at 37 ^oC, 5 % CO_2 and

95 % humidity. Next, the cells were washed with PBS and exposed to 100 µl HBSS (control), H_2O_2 (1 mM), CuO NMs or $CuSO_4$ (3.17, 6.34 and 12.68 Cu µg/cm^2) diluted in HBSS and incubated at 37 ^oC, 5 % CO_2 and 95 % humidity. The fluorescence was measured at time 0 and then every 1 h for 6 h at a wavelength of 485/530 nm (ex/em) using micro plate reader, SpectraMax M5 (California USA). The fluorescence reading was used to identify the appropriate time point for performing the DCFH-DA assay and the chosen time (2 h) was used for further experiments. The same experiment was repeated with undifferentiated Caco-2 cells with the same concentrations of CuO NM, $CuSO_4$ and H_2O_2 and following the procedure as stated above. The fluorescent readings were taken at 0 h and 2 h. Data was expressed as fold change or fluorescence unit.

2.2.10. Cytokine analysis

2.2.10.1. Proteome profiling

A proteome profiler provides a platform in which multiple cytokines can be detected concurrently within a sample. Proteome profiling was performed using a Human Cytokine Array kit (R&D System, Inc., Minneapolis, MN USA) following the manufacturer's protocol. Briefly, undifferentiated Caco-2 cells (1.56 x10^5 cells /cm^2) were cultured in 96 well plate (Costar Corning) and maintained at 37 ^oC, 5 % CO_2 and 95 % for 24 h. Cells were exposed to 4.44 Cu µg/cm^2 of CuO NMs for 24 h. The supernatant was stored at -80 ^oC and then thawed on the day of the experiment. After blocking the membrane with the array buffer-4 (supplied by the manufacturer) for 1 h, 1 ml of the thawed supernatant was added to 0.5 ml of array buffer-4 plus 15 µl human cytokine array detection antibody cocktail and incubated overnight (o/n) at 4 ^oC with a rocking plat form shaker. After 24 h the membrane was treated with 2 ml of streptavidin-HRP and incubated for 1 h at RT. This was followed by treatment with chemiluminescence reagent and the membrane was visualized and a photograph taken using a ChemiDoc XRS+ imager (ChemiDoc, version 4.1, Bio-Rad).

2.2.10.2. IL-8 production

Caco-2 cells were seeded at a concentration of 1.56 × 10^5 cells/cm^2 into the wells of a 96 well plate (Costar Corning Flintshire, UK) and incubated for 24 h at 37 °C and 5 % CO_2 until 100 % confluency was reached. Cells were then exposed to cell culture medium

(control), 200 ng/ml TNF-α (positive control), 2.22, 4.44 and 8.88 Cu μg/cm^2 of CuO NMs or $CuSO_4$ for 6 or 24 h. The cell supernatants were collected and stored at −80 °C until required. On the day of the cytokine analysis, the supernatants were thawed, and human IL-8 levels quantified using Enzyme-linked Immunosorbent Assay (ELISA) (R&D System, Inc., Minneapolis, MN USA) following the manufacturer's protocol. The absorbance of human IL-8 production was measured using a microplate reader, SpectraMax M5 (California USA) at wavelength 450 nm and the concentration in pg/ml was obtained from the standard curve. Data are expressed as mean IL-8 concentration (pg/ml).

2.2.11. Gene expression

2.2.11.1. Ribonucleic acid (RNA) isolation

Caco-2 cells were seeded into a 24 well plate (Costar Corning, Flintshire, UK) at a concentration of 1.56×10^5 cells/cm^2 and were incubated at 37 ^oC, 5 % CO_2 for 24 h. The cells were then exposed to cell culture medium (control), 3.17, 6.34 and 12.68 Cu μg/cm^2 of CuO NMs or $CuSO_4$ and incubated for 4, 8, 12 and 24 h at 37 ^oC. The RNA was isolated using the MagMAX^{TM} 96 Total RNA Isolation Kit (Ambion, USA) following the manufacturers protocol. Briefly, after, the specified time point, the medium was removed and 140 μl of lysis/binding solutions were immediately transferred into the plates, which were shaken for one minute before transferring to the processing plates.

Thereafter, 20 μl of bead mix was added and shaken for 5 min. The RNA binding beads were captured magnetically, and the supernatant discarded. The beads were washed with wash solutions (provided by the manufacturer). Diluted TURBO DNase (50 μl) was then added and the samples shaken at RT for 15 min, followed by addition of 100 μl of ribonucleic acid (RNA) rebinding solution and further shaken for 3 min. The RNA binding beads were washed twice with a wash solution and the beads were dried by shaking for 2 min. The RNA was eluted with 30 μl of the elution buffer. The RNA concentration and purity were measured with a Nanodrop 2000c system (Thermo Scientific, UK) and only isolated RNA samples with A260/A280 ratio of 2 to 2.1 were used for cDNA synthesis.

2.2.11.2. Complementary deoxyribonucleic acid (cDNA) synthesis

The RNA was transcribed to cDNA using a Precision nanoScript^{TM}2 Reverse Transcription kit (Primerdesign, UK) following the manufacturer's protocol. Briefly, RNA (900 ng) was added into thin walled 0.2 ml PCR tubes followed by 0.5 µl each of oligo-dT and random nanomer primer and made up to 10 µl with RNase/DNase free water. The samples were heated to 65 ^{o}C for 5 min using Life Pro thermal cycler (Bioer Service Life, China) and immediately cooled in ice. A mixture of 5 µl of nanoScript Buffer 4 X, 1 µl of 10 mM dNTP mix, 1µl of nanoScript 2 enzyme and 3 µl of RNase/DNase free H_2O was transferred to the reaction tube on ice. The reaction tube was pulse centrifuged and heated at 25 ^{o}C for 5 min, 42 ^{o}C for 20 min and 75 ^{o}C for 10 min using Life Pro thermal cycler (Bioer Service Life, China). The cDNA was stored at -20 ^{o}C immediately until when needed.

2.2.11.3. Real time quantitative polymerase chain reaction (RT qPCR)

RT qPCR was performed with a 7900 RT fast PCR system and SDS 2.3 software using 384 well plates (Applied Biosystems, USA), using a custom designed real-time PCR assay with Double-Dye probe and Precision PLUS qPCR Master Mix (Primerdesign, UK) following the manufacturer's instructions. Approximately 25 ng cDNA (calculated from RNA concentration prior to cDNA synthesis) was used for RT qPCR. The enzyme activation step was measured at 95 ^{o}C for 2 min, denaturation (95 ^{o}C for 10 s) and data collection (60 ^{o}C for 1 min) for 40 cycles. Glyceraldehyde 3- phosphate dehydrogenase (GAPDH) was used as an internal control/housekeeping gene as GAPDH have been shown to be the best housekeeping gene for Caco-2 cell (Piana et al. 2008, Vreeburg et al. 2011). The fluorogenic data was collected through FAM channel. Sequences of primers of genes indicative of activation of inflammation (*IL8*), oxidative stress (haem oxygenase (*HMOX1*)), mucus secretion (*MUC2*) and metal binding (*MT1A* and *MT2A*) used for the RT qPCR are shown in Table 2.1. The threshold cycle (Ct) value indicates the cycle number at which the fluorescence generated within a reaction is above the threshold, therefore the Ct value is the point of accumulation of a sufficient number of amplicons in the process of the reaction. The relative level of mRNA expression is a ratio of optical density of the experimental groups to that of GAPDH (endogenous housekeeping gene). Data are expressed as mean fold change.

Table 2.1: Primers used for RT qPCR analysis.

GENE	PRIMER	
	Sense	Anti-sense
HMOX1	5'-GGAAGCCCCCACTCAACA-3'	5'-GCATAAAGCCCTACAGCAACT-3'
IL8	5'-CAGAGACAGCAGAGCACAC-3'	5'-AGCTTGGAAGTCATGTTTACAC-3'
MT1A	5'-GCCCTGCTCGAAGATATAGAAAG-3'	5'-AATACAGTAAATGGGTCAGGGTT-3'
MT2A	5'-GACTCTAGCCGCCTCTTCAG-3'	5'-GGCAGCAGGAGCAGCAG-3'
MUC2	5'-ACCTCCATCAATAACTCCTCCTA-3'	5'-CTCCACCTGGTTTGTGAAAGT-3'

2.2.12. Data analysis

Each experiment was repeated at least three times (on different days) and all data generated from these experiments are expressed as the mean ± standard error of the mean (SEM). The figures were generated using Graph Pad Prism. After checking normality of the data, a one-way analysis of variance (ANOVA) and the Tukeys multiple comparison was employed to investigate statistical significance using Minitab 17 software. PROAST version 38.9 software was used to analyse Benchmark dose-response. The microscope images and nuclei counts were analysed with image J software.

2.3. Results

2.3.1. Characterisation of CuO NMs

CuO NMs were characterised by measuring the hydrodynamic diameter, zeta potential and PdI using DLS (Table 2.2) after dispersion in MEM and DMEM complete cell culture medium (at 0 and 24 h). DLS analysis demonstrated that CuO NMs were agglomerated in both media at time zero since the average hydrodynamic diameter was 104.86±9.03 and 117.63±7.88 nm in MEM and DMEM complete cell culture medium respectively. The average hydrodynamic diameter significantly decreased to 25.26±0.91 and

23.74±0.64 in both MEM and DMEM complete cell culture medium after incubation for 24 h at 37 ºC, 5 %, CO_2 and 95 % humidity. There was no significant difference in the hydrodynamic diameter of CuO NMs diluted in MEM complete cell culture medium compared to that of DMEM complete cell culture medium at both 0 h and 24 h post incubation. The Zeta potential did not vary significantly between media and remained negative at 0 and 24 h. The PdI at 0 and 24 h time points were less than one, which is a confirmation that CuO NM suspensions were suitable for DLS analysis.

Table 2.2: Hydrodynamic diameter, zeta potential and polydispersity index (PdI) of CuO NMs in MEM and DMEM complete cell culture medium.

CuO NMs were suspended in MEM and DMEM complete medium at a concentration of 50 Cu µg/ml, and measurements taken at 0 and 24 h post incubation at 37 ºC. Data are expressed as mean ± SEM (n=3). Asterisk (*) represents significant (P<0.05) difference between 0 h and 24 h.

	Time (h)	*0*	*24*
Complete MEM	Hydrodynamic diameter (nm)	104.86±9.03	25.26±0.91*
	Zeta Potential (mV)	-8.76±0.66	-9.12±0.82
	PdI	0.29±0.01	0.47±0.07*
Complete DMEM	Hydrodynamic diameter (nm)	117.63±7.88	23.74±0.64*
	Zeta Potential (mV)	-9.39±0.52	-9.22±0.26
	PdI	0.58±0.02	0.41±0.03

2.3.2. Viability of undifferentiated Caco-2 cells after exposure to CuO NMs and $CuSO_4$

When the viability of undifferentiated Caco-2 cells was assessed using the Alamar blue assay a concentration dependent decrease in viability was observed 24 h post exposure with CuO NMs and $CuSO_4$ (Figure 2.1). There was no impact on the viability of undifferentiated Caco-2 cells at lower concentrations (0.61 to 1.22 Cu µg/cm^2) of CuO NM and $CuSO_4$. Significant decreases in cell viability were observed at concentrations above 4.89 Cu µg/cm^2 for both CuO NMs and $CuSO_4$. For example, cell viability was reduced from 87 to 3 % from 2.44 to 19.53 Cu µg/cm^2 of CuO NMs and $CuSO_4$ and up

to 90 % cell death was observed at concentrations above 19.53 Cu µg/cm^2 of CuO NMs after 24 h. There was no significant difference between the toxicity of CuO NMs and $CuSO_4$ when concentration was expressed as Cu µg/cm^2.

PROAST 38.9 software was used to calculate the concentration of CuO NMs and $CuSO_4$ required to kill 20 % (Benchmark dose (BMD) 20) of the cells (EFSA 2009). The BMD 20 for CuO NMs and $CuSO_4$ were 4.44 and 4.25 Cu µg/cm^2 respectively (Figure 2. 2). This data was used to select concentrations of CuO NMs and $CuSO_4$ (2.22, 3.17, 4.44, 6.34, 8.88 and 12.68 Cu µg/cm^2) for investigating sub-lethal impacts on Caco-2 cells. The viability of undifferentiated Caco-2 cells were also studied by staining the nuclei of the undifferentiated Caco-2 cell after exposure to 6.34 and 12.68 Cu µg/cm^2 of CuO NMs and $CuSO_4$, using DAPI in order to assess cell number. A significant concentration dependent decrease in number of nuclei compared to unexposed control was observed for both CuO NMs and $CuSO_4$, suggesting that there was a loss of cells (Figure 2.3).

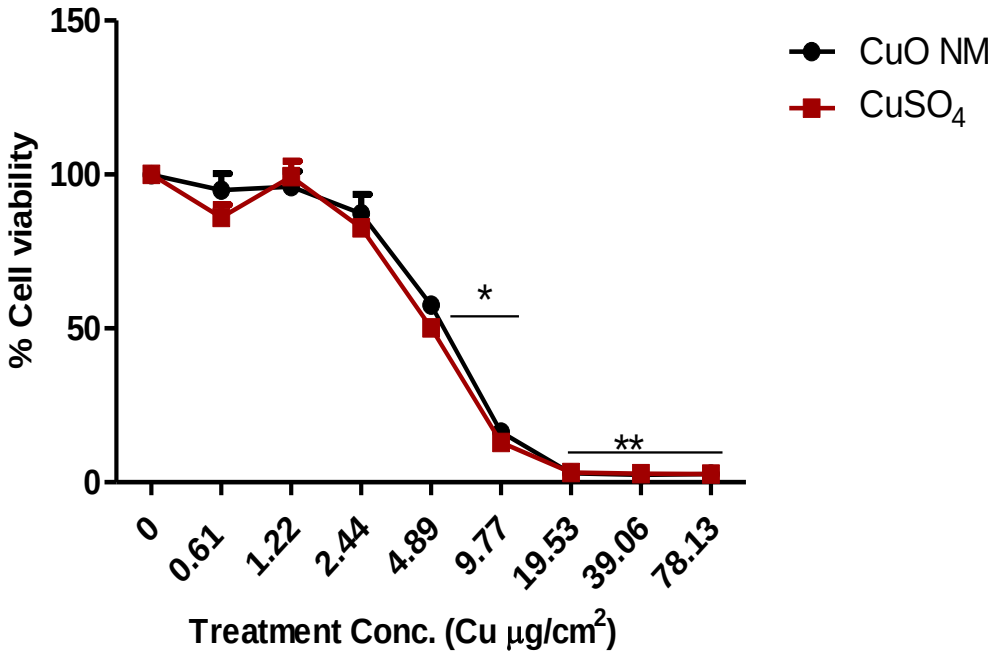

Figure 2.1: Cytotoxicity of CuO NMs and $CuSO_4$ to undifferentiated Caco-2 cells.

*Viability of undifferentiated Caco-2 cells was assessed using the Alamar blue assay following exposure of cells to MEM complete cell culture medium (control), CuO NMs or $CuSO_4$ at concentrations ranging from 0.61 to 78.13 Cu µg/cm^2 for 24 h. Viability of Caco-2 cells was expressed as a % of the control (i.e. % viability). Data are expressed in mean ± SEM (n = 3) and significance is indicated by * = P < 0.05, ** = P < 0.01 compared to control.*

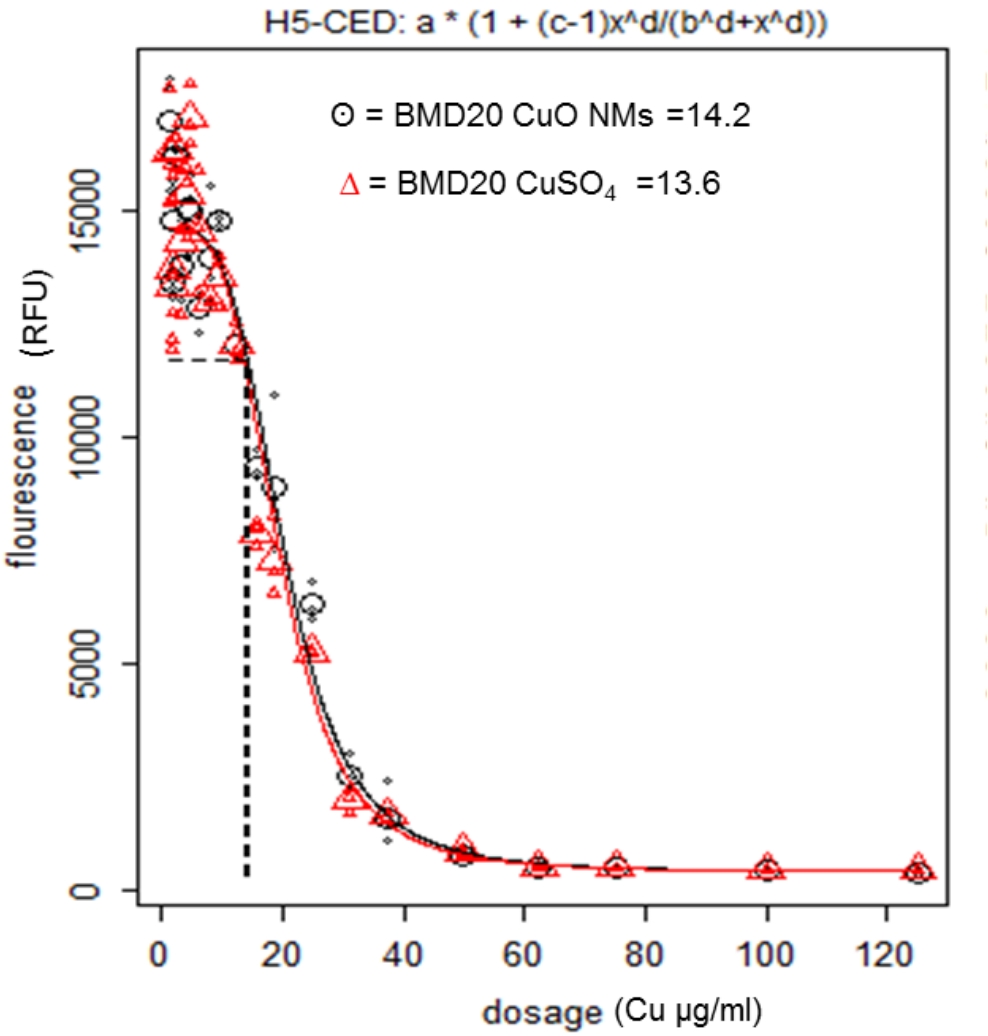

Figure 2.2 Determination of 20% Benchmark dose (BMD20) following exposure of undifferentiated Caco-2 cells to CuO NMs and $CuSO_4$.

Viability of undifferentiated Caco-2 cells was assessed using the Alamar blue assay following exposure to cell culture medium (control), CuO NMs or $CuSO_4$ at concentrations ranging between 1.17 and 125 Cu µg/ml Cu for 24 h. Data are expressed as fluorescence intensity Data were analysed using PROAST 38.9 software to obtain the BMD 20.

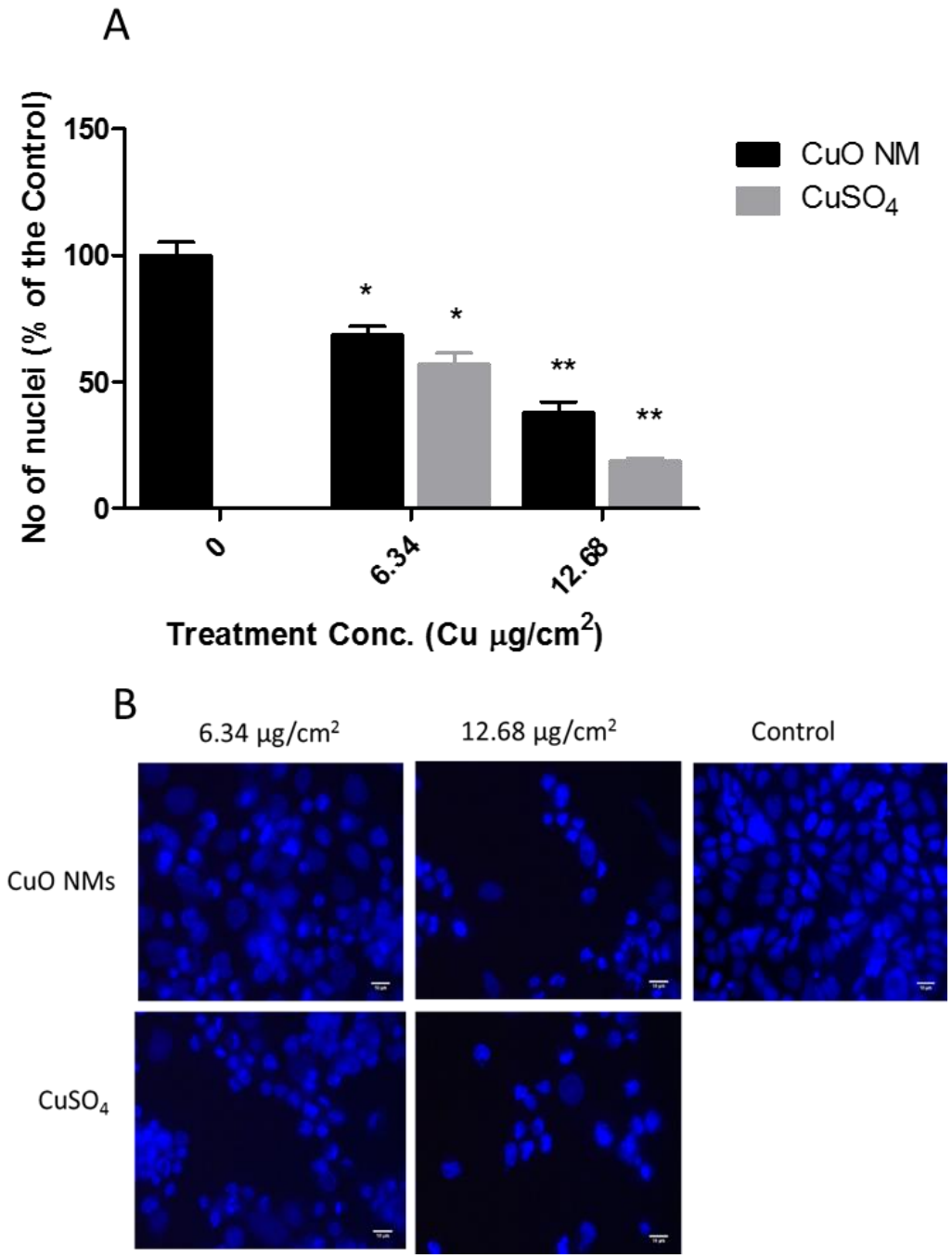

Figure 2.3: Assessment of the viability of undifferentiated Caco-2 cells using nuclei staining with DAPI.

*Undifferentiated Caco-2 cells were treated with 6.34 and 12.68 Cu µg/cm^2 of CuO NMs and $CuSO_4$, fixed and the nuclei stained with DAPI and images obtained with Zeiss fluorescent Microscope, Carl Zeiss Axio Scope A 1 Upright Research Microscope (magnification 40 X) and the nuclei counted (A) using Image J software. Data are presented as the number of nuclei (expressed in % of the unexposed control) ± SEM (n = 3) and significance are indicated by * = P < 0.05, ** = P < 0.01 compared to control. Representative images are presented (B), and Scale bar = 10 µm (n= 3).*

2.3.3. Impact of CuO NMs on cell morphology

The morphology of undifferentiated Caco-2 cells was assessed using SEM (Figure 2.4) and it was shown that for the control, the entire surface was covered with cells demonstrating they were 100 % confluent. However, only poorly developed microvilli resembling those of crypt cells were observed on the cell surface of the cell monolayer. Cells exposed to CuO NMs (12.68 Cu µg/cm^2) showed a loss of cells compared to the control. Light microscopy was also used to verify the morphology of the undifferentiated Caco-2 cells (Figure 2.5). The unexposed control cells were all healthy and the cells covered the entire surface of the coverslip. Wells exposed to 6.34 or 12.68 Cu µg/cm^2 CuO NMs or $CuSO_4$ for 24 h show a clear concentration dependent loss of cells.

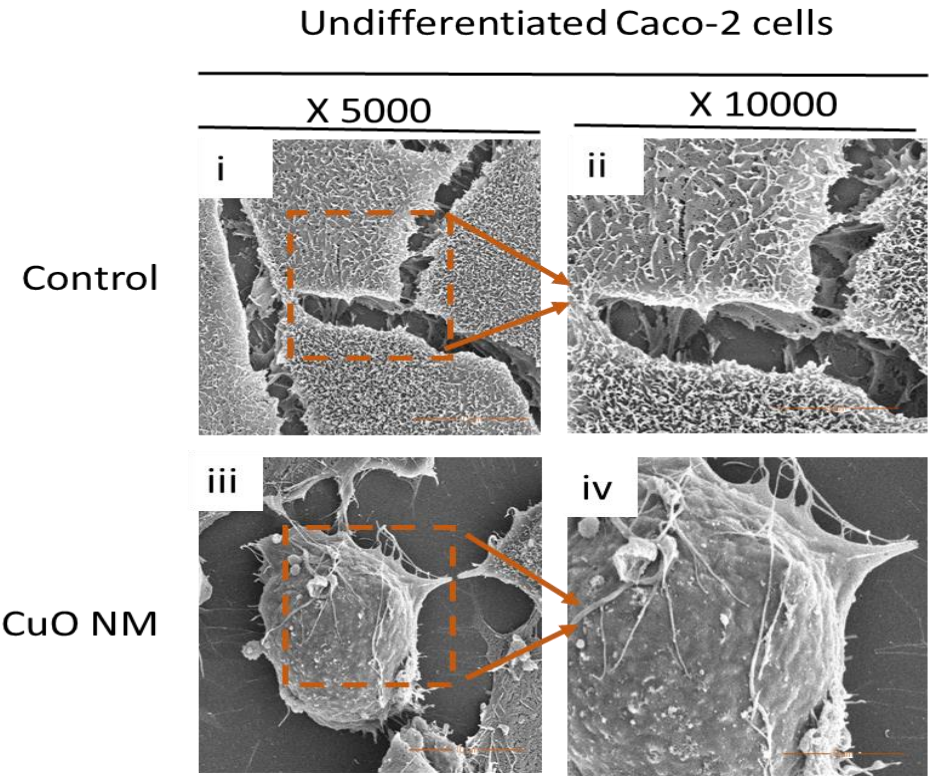

Figure 2.4: SEM images of undifferentiated Caco-2 cells exposed to CuO NMs for 24 h.

Cells were exposed to 12.68 Cu µg/cm^2 of CuO NMs or cell culture medium (control) for 24 h and then were washed, fixed, dehydrated, dried and examined by SEM. Specimens i) and ii) are control undifferentiated Caco-2 cells imaged at magnifications of X 5000 and X 10000 respectively. iii) and iv) are undifferentiated Caco-2 cells exposed to 12.68 Cu µg/cm^2 of CuO NMs imaged at a magnification of X 5000 and X 10000 respectively. Representative images are shown (n=3).

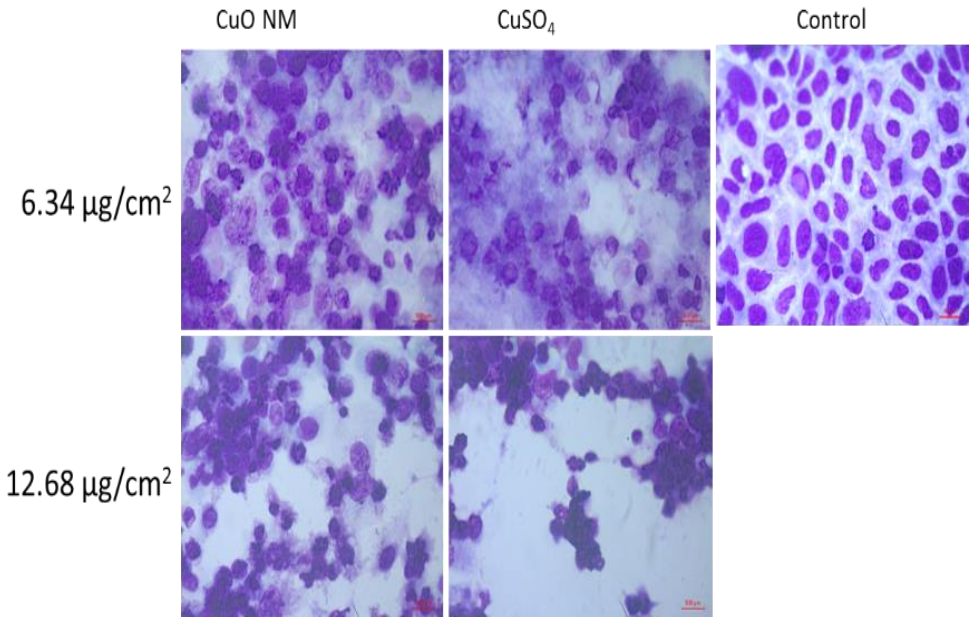

Figure 2.5: Impact of CuO NMs and $CuSO_4$ on undifferentiated Caco-2 cell morphology using light microscopy.

Cells were exposed to cell culture medium (control), and 6.34 or 12.68 Cu µg/cm^2 CuO NMs or $CuSO_4$ for 24 h. The cells were then fixed, stained and visualised using light microscopy (magnification 40X, scale bar=50 µm. Representative images are shown (n=3).

2.3.4. Oxidative stress

2.3.4.1. Acellular ROS Production

Figure 2.6 shows acellular ROS production by CuO NMs and $CuSO_4$ over time, with an increase in fluorescence indicative of an increase in ROS production. At all the time points assessed a similar trend was observed for CuO NMs and $CuSO_4$. This data was used to identify the optimum time point for assessment of acellular ROS production. A significant ROS production was observed at 2 h post incubation hence, was taken as the optimum time point. CuO NMs and $CuSO_4$ significantly increased ROS formation compared to the control in a concentration dependent manner; with increasing concentration stimulating increased ROS production at 2 h post incubation (Figure 2.7). The greatest increase in ROS production was observed at a concentration of 12 Cu µg/cm^2 for both CuO NMs and $CuSO_4$. However, the level of ROS formation stimulated by $CuSO_4$ was double that stimulated by CuO NMs at concentrations of 3.17 and 6.34 Cu

µg/cm^2 and more than three-fold higher at highest concentration of 12 Cu µg/cm^2 (Figure 2.7).

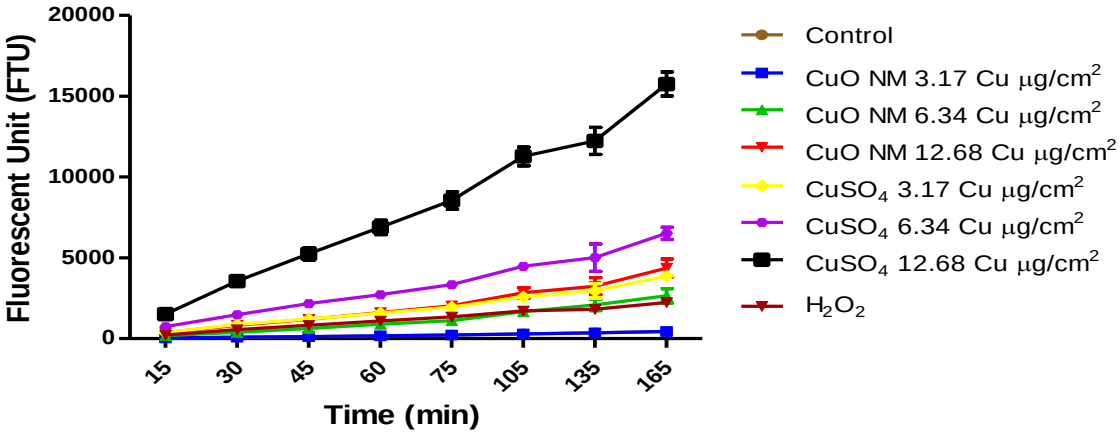

Figure 2.6: Acellular ROS formation by CuO NMs and $CuSO_4$ over time.

Acellular ROS production by CuO NMs and $CuSO_4$ was determined using the DCFH-DA assay concentrations of 3.17, 6.34 and 12.68 Cu µg/cm^2. Cell culture medium were included as a negative control and H_2O_2 (1 mM/cm^2) as positive control and assessed at regular intervals up to 2 h 45 min. Data are expressed as fluorescence units (FTU) ± SEM (n = 3).

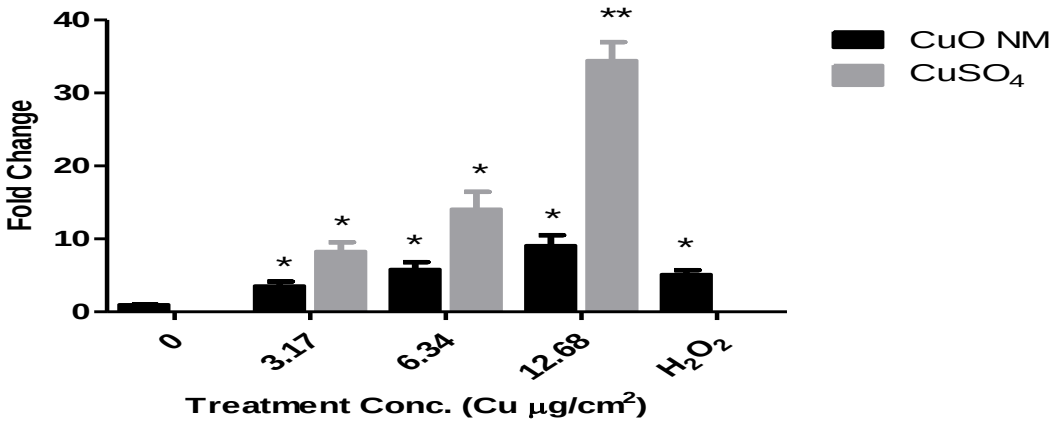

Figure 2.7: Acellular ROS formation by CuO NMs and $CuSO_4$ at 2 h.

*Acellular ROS production by CuO NMs and $CuSO_4$ was determined using the DCFH-DA assay at concentrations of 3.17, 6.34 and 12.68 Cu µg/cm^2. Cell culture medium was included as a negative control and H_2O_2 (1 mM/cm^2) as a positive control and assessed at 2 h post incubation. Data are expressed as mean fold change (compared to control) ± SEM (n = 3). Significance are indicated by * P<0.05 and ** = P<0.01 compared to control.*

2.3.4.2. ROS Production by undifferentiated Caco-2 cells

The potential role of ROS production in the toxicity of CuO NMs to undifferentiated Caco-2 cells was evaluated by measuring the level of intracellular ROS formation by undifferentiated Caco-2 cell after exposure to CuO NMs and $CuSO_4$ using the DCFH-DA assay. In the first instance, the optimal concentration of DCFH-DA to use was determined by measuring ROS production at different concentrations of DCFH-DA (25, 100 and 150 μM) (Figure 2.8). A concentration of 150 μM DCFH-DA was chosen based on the result of this pilot study (Figure 2.8) as a significant increase in ROS production was observed at this concentration. The time point used to assess ROS production was also selected based on the results of a pilot study (Figure 2.9). A 2 h time point was selected to monitor changes in ROS production in cells as measurable increase in ROS formation in treated cells, compared to the control was observed (Figure 2.9. Longer time points were avoided as ROS formation due to cell death may occur in cells, since the assay is conducted in HBSS, which does not contain essential nutrients required for cell growth. Following exposure of undifferentiated Caco-2 cells to CuO NMs and $CuSO_4$ for 2 h, CuO NMs showed a non-significant concentration dependent increase in ROS formation compared to control (Figure 2.10). However, $CuSO_4$ demonstrated a significant concentration dependent increase (more than 6-fold increase) in ROS production in cells (Figure 2.10). ROS was not produced when undifferentiated Caco-2 cells were treated with CuO NMs and $CuSO_4$ for 24 h (Data not shown).

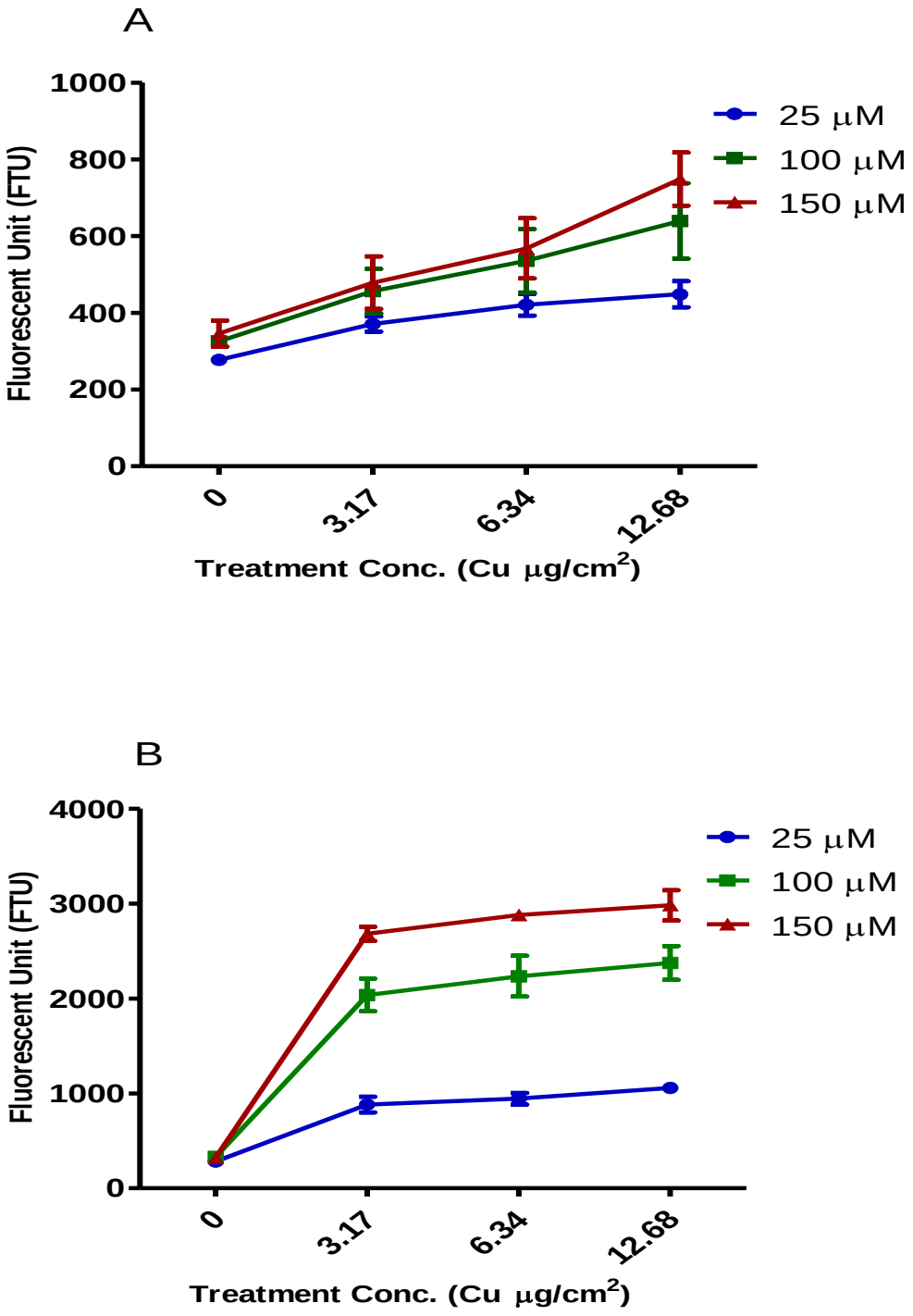

Figure 2.8: Determination of optimum concentration for DCFH assay with undifferentiated Caco-2 cells.

Undifferentiated Caco-2 cells were treated with 25, 100, and 150 µM DCFH-DA for 1 h prior to exposure to MEM complete cell culture medium containing (0), 3.17, 6.34 and 12.68 Cu µg/cm^2 and I mM H_2O_2. A) CuO NMs, B) $CuSO_4$ Data are expressed in fluorescence units (FTU) ± SEM (n = 3).

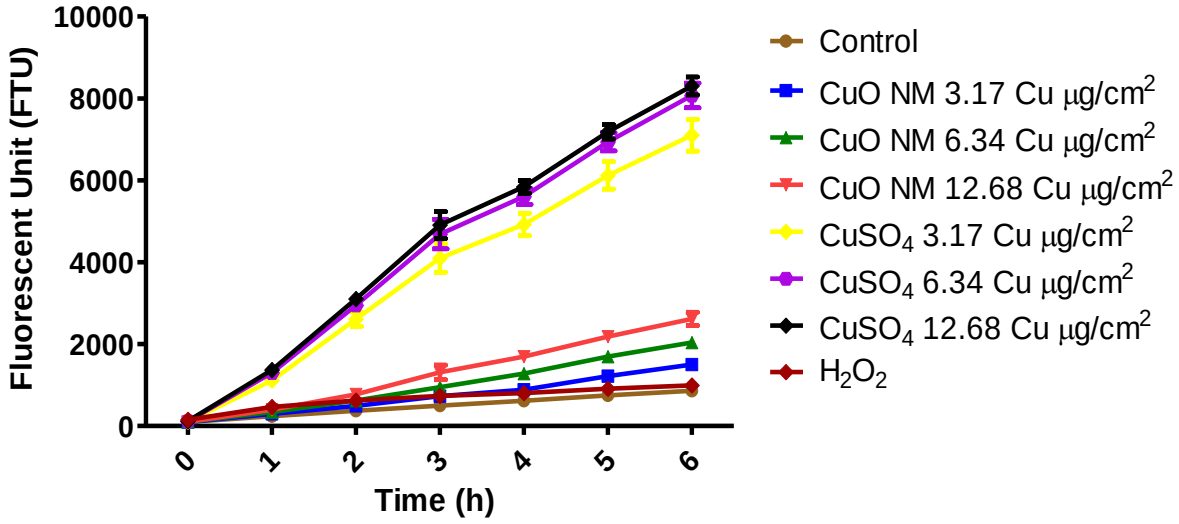

Figure 2.9: ROS formation by undifferentiated Caco-2 cells following exposure to CuO NMs and $CuSO_4$.

Intracellular ROS production by cells exposed to cell culture medium (0), 1mM H_2O_2, CuO NMs and $CuSO_4$ at concentrations of 3.17, 6.34 and 12.68 Cu µg/cm^2 using the DCFH-DA assay. Data are expressed as mean fluorescence unit (FTU) ± SEM (n = 4).

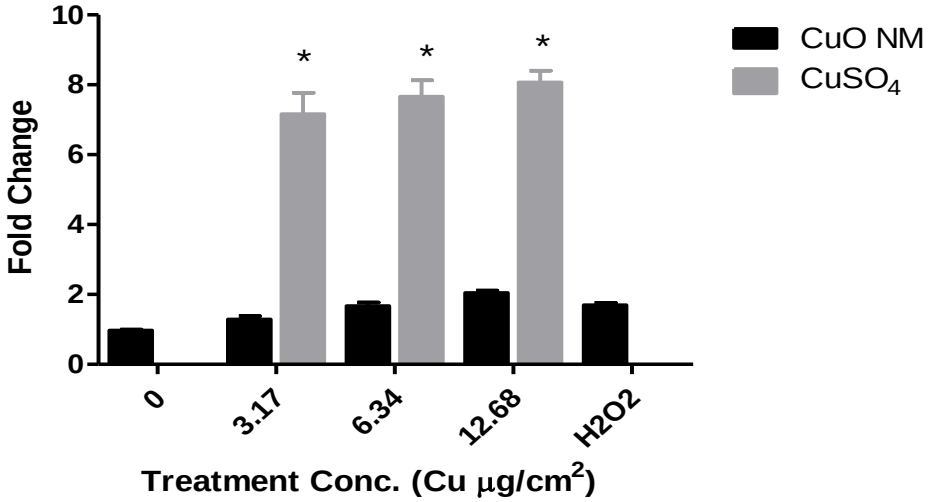

Figure 2.10: ROS formation by undifferentiated Caco-2 cells 2 h post exposure to CuO NMs and $CuSO_4$.

*Intracellular ROS production by cells exposed to cell culture medium (0), 1mM H_2O_2, CuO NMs and $CuSO_4$ at concentrations of 3.17, 6.34 and 12.68 Cu µg/cm^2 using the DCFH-DA assay. Data are expressed as the mean fold change in ROS production (compared to control) ± SEM (n = 4). Significance are indicated by * = P<0.05 compared to control.*

2.3.5. Cytokine production

For cytokine production, a protein profiler was used to identify which cytokines were produced by undifferentiated Caco-2 cells after exposure to CuO NMs (Figure 2.11). An increase in IL-8 and ICAM-1 was observed, and investigation of IL-8 was prioritised for further studies, which quantified cytokine production using an ELISA. CuO NMs and $CuSO_4$ stimulated a significant increase in IL-8 production by undifferentiated Caco-2 cells 24 h post exposure at all concentrations tested, compared to control. The greatest level of cytokine production was observed at a concentration 4.44 Cu µg/cm^2 for both CuO NMs and $CuSO_4$, with IL-8 production of ~ 1000 pg/ml (Figure 2.12). The positive control (cells treated with 200 ng/ml TNFα) stimulated an increase in IL-8 concentration (275 ± 35.04 pg/ml) and IL-8 production was below detection level (31.13 pg/ml) for the control group. No significant change in IL-8 secretion was observed at 6 h post exposure for all concentrations of CuO NMs and $CuSO_4$ (Figure 2.12).

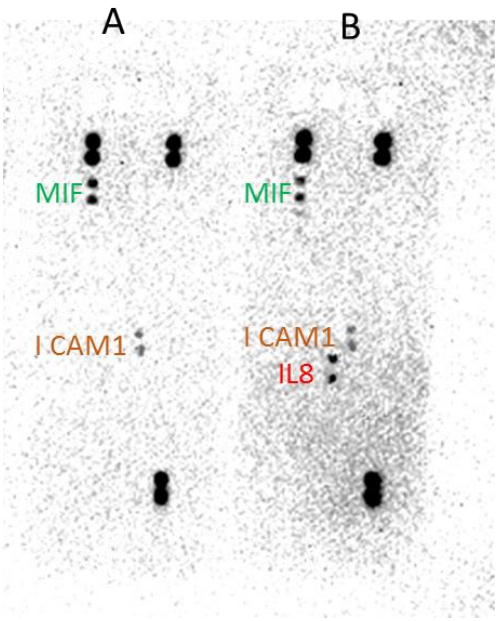

Figure 2.11: Assessment of cytokine expression by undifferentiated Caco-2 cells using a proteome profiler.

Cells were exposed to cell culture medium (control, 0), or 4.44 Cu µg/cm^2 of CuO NMs for 24 h. Cytokines were detected using human cytokine array kits. Double dots represent a different cytokine and only MIF, ICAM-1 and IL-8 were detected. Unexposed cells (A). Cells exposed to 4.44 Cu µg/cm^2 CuO NMs (B).

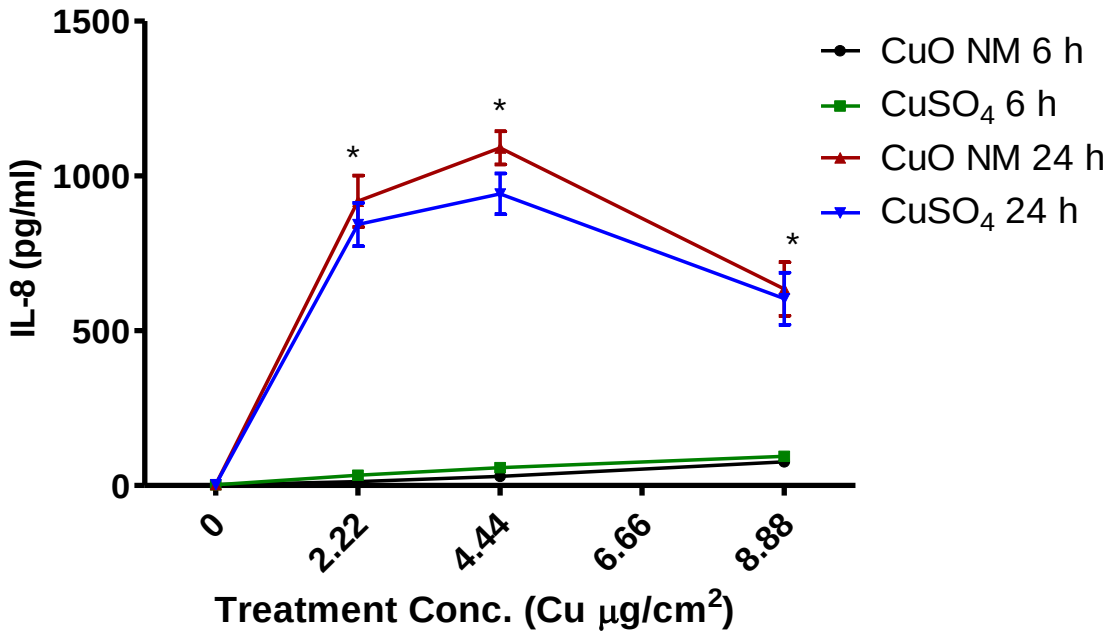

Figure 2.12: IL-8 production by undifferentiated Caco-2 cells following exposure to CuO NMs and $CuSO_4$.

*Cells were exposed to cell culture medium (control, 0), CuO NMs or $CuSO_4$ at concentrations of 2.22, 4.44 or 8.88 Cu μg/cm^2 for 6 or 24 h. The level of IL-8 in the cell supernatant was determined using an ELISA. Data are expressed as mean IL-8 concentration (pg/ml) ± SEM (n = 3). Significance are indicated by * = P<0.05 compared to control.*

2.3.6. Gene expression analysis

The impact of CuO NMs and $CuSO_4$ on the expression of *HMOX1*(antioxidant) and *IL8* (pro-inflammatory cytokine) was investigated to further probe the involvement of oxidative stress and an inflammatory response in the Caco-2 cells response to CuO NMs and $CuSO_4$. Mucin 2 (*MUC2*) was included as this is a gene responsible for mucus formation in the intestine and metallothionein (*MT1A* and *MT2A*), a gene for metal binding known to have high affinity for copper, in order to assess the impact of CuO NM and $CuSO_4$ on mucus formation and metal binding proteins. CuO NMs and $CuSO_4$ induced a significant increase in *HMOX1* expression compared to controls at all concentrations and time points in undifferentiated Caco-2 cell. The highest level of expression was observed at 12 h, with a fold increase in expression ranging from 39 to 78

fold, followed by 8 h (29 to 68 fold) and although reduced at 24 h, detectable expression was still significant for CuO NMs and $CuSO_4$ (Figure 2.13A).

IL8 expression significantly increased at all concentrations and time points tested. The highest significant increase in *IL8* expression was observed at 12 h post exposure to CuO NMs and $CuSO_4$ (76 to 265 fold), and the lowest significant increase was observed at 24 h post exposure (45 to 115 fold) (Figure 2.13B). A significant increase in expression was observed at the highest concentrations of CuO NMs (12.68 $\mu g/cm^2$) compared to $CuSO_4$ at 8, 12 and 24 h time points.

MT1A demonstrated a significant increase in expression at 8 h post exposure to CuO NMs at concentration of 3.17 and 6.34 $\mu g/cm^2$ with a fold increase of 3.2 and 2.7 fold respectively, and at 12 h post exposure to $CuSO_4$ (3.17 $\mu g/cm^2$) (2.9 fold) compared to control (Figure 2.13C). No significant change in gene expression was observed at all other concentrations and time points (Figure 2.13C).

Expression of *MUC2* showed a concentration and time dependent increase from 4 to 12 h exposure. The highest significant increase in expression of *MUC2* was observed at 12 h post exposure to CuO NMs at concentrations of 12.68 $\mu g/cm^2$ with fold increase of ~26 fold. *MUC2* expression was lowest at 4 and 24 h post exposure of CuO NMs and $CuSO_4$ with a significant increase in expression at concentrations of 12.68 $\mu g/cm^2$ at 4 h and concentrations of 6.34 and 12.68 $\mu g/cm^2$ at 24 h post exposure (Figure 2.13D).

A fold change in *MT2A* expression could not be calculated because the untreated control did not express *MT2A* at a detectable level. Therefore, the results are presented as CT values in Table 2.3. Since the untreated control did not express *MT2A* at a detectable level (Ct value > 40), it can be deduced that CuO NMs and $CuSO_4$ increased *MT2A* expression at all concentrations and time points tested. However, there was no significant change in Ct values across the concentrations at all time points (Table 2.3). The expression of all the genes are represented at Figure 2.14 in heatmap form for easy comparison. Generally, the highest expression of all the genes were observed at 12 h post exposure of CuO NMs and $CuSO_4$ and gene expression is greatest at the highest concentration tested (Figure 2.13).

A: HMOX-1

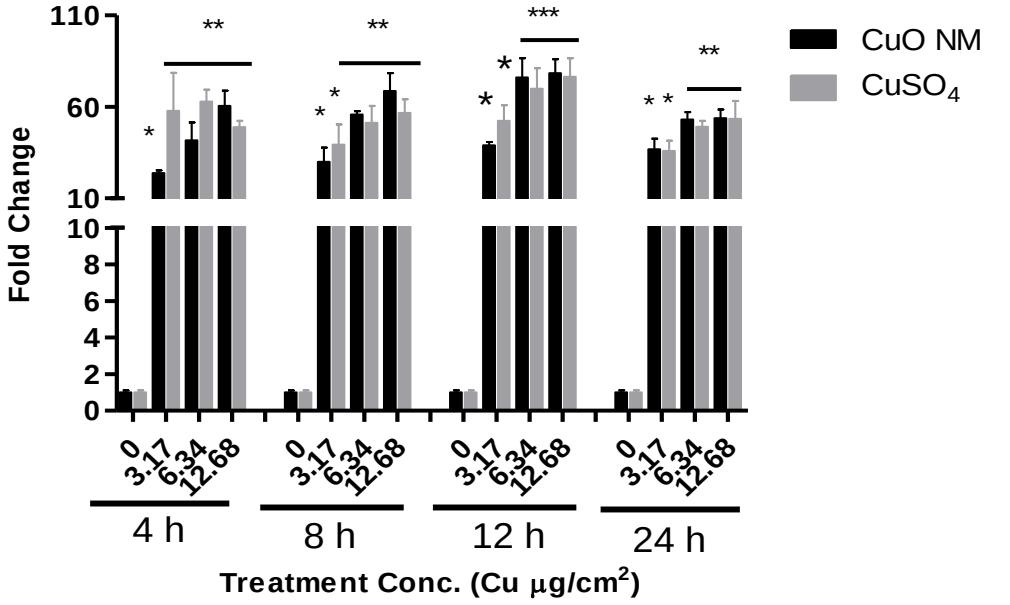
CuO NM
CuSO4
Fold Change
110
60
10
10
8
6
4
2
0
0
3.17
6.34
12.68
4 h
8 h
12 h
24 h
Treatment Conc. (Cu μg/cm²)

B: IL-8

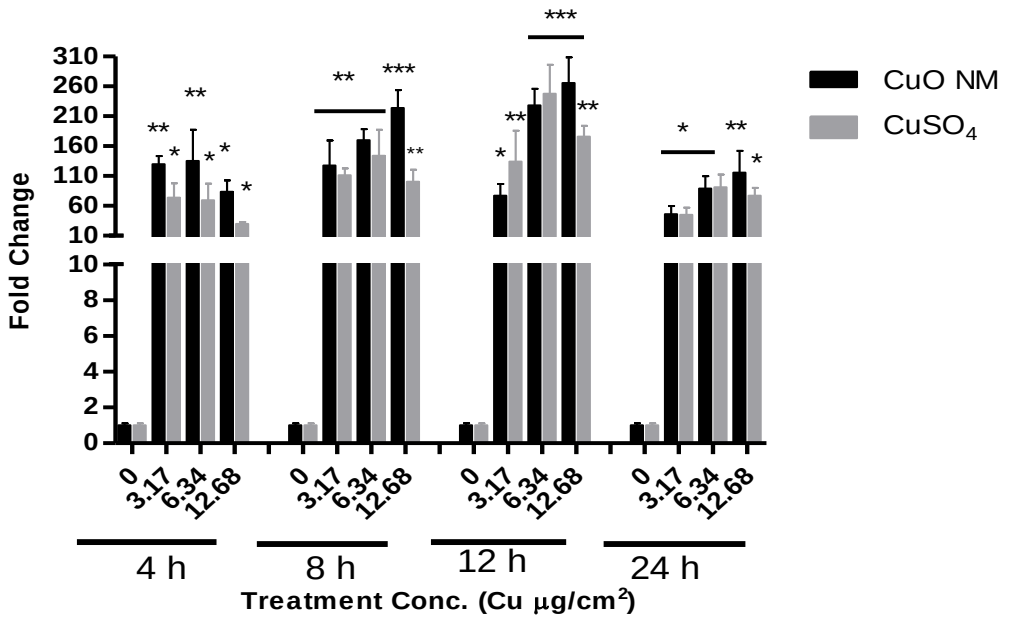
CuO NM
CuSO4
Fold Change
310
260
210
160
110
60
10
10
8
6
4
2
0
0
3.17
6.34
12.68
4 h
8 h
12 h
24 h
Treatment Conc. (Cu μg/cm²)

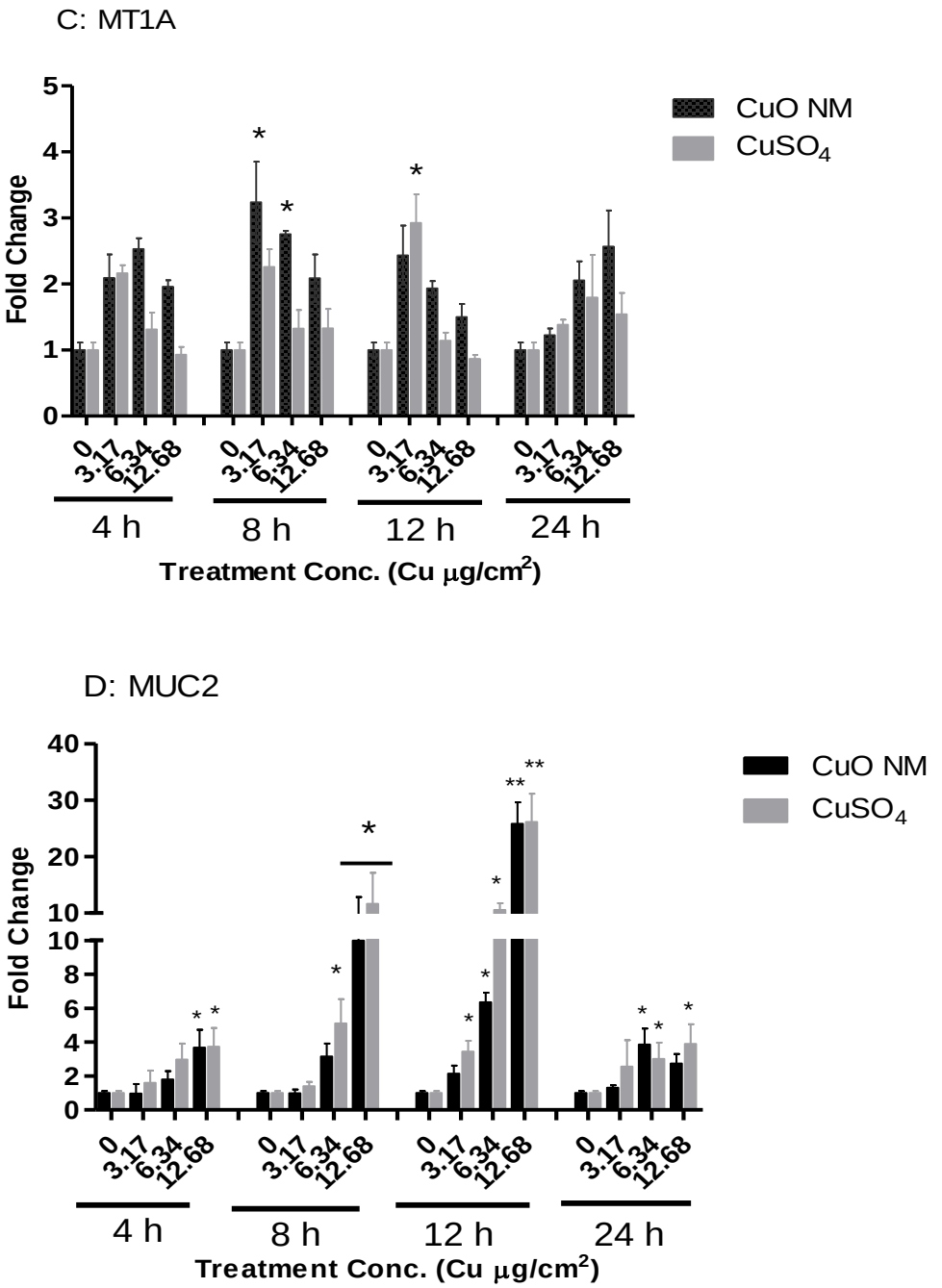

Figure 2.13: Effect of CuO NMs and $CuSO_4$ on undifferentiated Caco-2 cell gene expression.

*Undifferentiated Caco-2 cells were exposed to cell culture medium (control, 0), CuO NM or $CuSO_4$ at concentration of 3.17, 6.34 or 12.68 Cu μg/cm^2 for 4, 8, 12 and 24 h and changes in HMOX1 (A), IL8 (B), MT1A (C) and MUC2 (C) expression assessed using qPCR. Data were expressed as mean fold-change (compared to control) ± SEM (n = 3). Significance are indicated by * P<0.05, ** P<0.01, *** P<0.001 compared to control.*

Table 2.3: Effect of CuO NMs and $CuSO_4$ on undifferentiated Caco-2 cell MT2A expression.

Undifferentiated Caco-2 cells were exposed to cell culture medium (control, 0), CuO NMs or $CuSO_4$ at concentrations of 3.17, 6.34 or 12.68 Cu µg/cm^2 for 4, 8, 12 and 24 h. Data were expressed as mean Ct value ± SEM (n = 3). Gene expression was not detected for the control (Ct value>40).

	CuO NMs (Cu µg/cm^2)			$CuSO_4$ Cu µg/cm^2)		
Time (h)	3.17	6.34	12.68	3.17	6.34	12.68
4	18.84±0.69	17.37±0.31	17.19±0.47	17.49±0.36	18.26±0.74	18.89±0.50
8	17.68±0.30	16.75±0.33	17.18±0.80	17.56±0.33	17.88±0.23	18.85±0.20
12	18.23±0.22	17.30±0.27	17.96±0.38	18.14±0.25	18.34±0.21	19.67±0.37
24	17.88±0.55	18.05±0.66	17.96±0.38	17.78±0.55	18.74±0.58	19.47±0.41

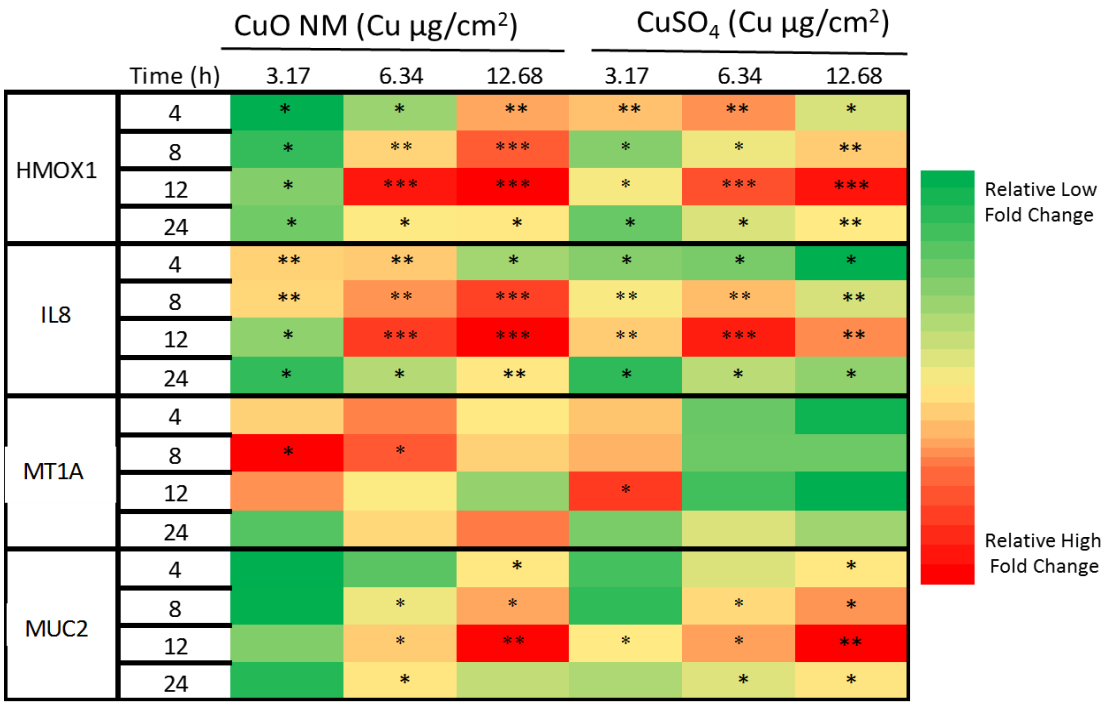

Figure 2.14: Heatmap representation of gene expression in undifferentiated Caco-2 cells after exposure to CuO NMs and $CuSO_4$.

*Undifferentiated Caco-2 cells were exposed to CuO NMs and $CuSO_4$ at concentrations of 3.17, 6.34 or 12.68 Cu µg/cm² and expression of HMOX1, IL8, MT1A and MUC2 assessed at 4, 8, 12 and 24 h post exposure using qPCR. Genes were compared separately for significance within each time point. Significance are indicated by * = P<0.05, **= P<0.01, ***= P<0.001 compared to control.*

2.4. Discussion

In this chapter, the physicochemical characteristics of CuO NMs in cell culture media, and their toxicity to undifferentiated Caco-2 cells was assessed via investigation of cytotoxicity, ROS production, cytokine production, and cell morphology (via light microscopy and SEM). For all cellular responses, the toxicity of CuO NMs was compared to $CuSO_4$. The impact of CuO NMs on the expression of *HMOX1*, *IL8*, *MT1A* and *MT2A* was also investigated by RT qPCR. This study revealed that CuO NMs reduced cell viability, caused a change in cell morphology, stimulated IL-8 production and upregulated *HMOX1*, *IL8*, *MUC2*, *MT1A* and *MT2A* expression in a comparable manner to $CuSO_4$ in an undifferentiated Caco-2 *in vitro* model. There was comparable impact of CuO NMs and $CuSO_4$ on undifferentiated Caco-2 cell for all the markers used to assess

the toxicity of CuO NMs, with the exception of acellular and cellular ROS formation. More especially, $CuSO_4$ stimulated 2-fold higher response than CuO NMs in both acellular and cellular ROS assays. Using a battery of tests, it has therefore been demonstrated that both CuO NMs and $CuSO_4$ stimulate inflammatory and oxidative stress driven responses in undifferentiated Caco-2 cells. The result also suggests that the toxicity of CuO NMs is partly dependent on its dissolution (i.e. is ion mediated).

2.4.1. Physicochemical properties of CuO NMs

The potential usefulness and toxicity of NMs is dependent on their physicochemical properties, which includes size and size distribution, shape, agglomeration/aggregation state, surface charge, crystal structure, surface area, chemical composition, porosity, and surface chemistry (Oberdörster et al. 2005, Karlsson et al. 2008). NMs tend to agglomerate in biological medium. There are various approaches for preparing NMs including use of dispersants such as solvents, proteins, detergents and/or physical and mechanical process such as probe and bath sonication, or varying pH (Wang et al. 2018, Lin et al. 2017, Tsuda and Gehr 2014). However, it is necessary to use a method that will not disrupt the NM structure and characteristics as this may alter or enhance the toxicity of the NMs (Foucaud et al. 2007). Furthermore, there is evidence that chemicals used to disperse NMs can enhance their toxicity (Foucaud et al. 2007). In this study, CuO NMs were sonicated in 2 % FBS, then diluted in cell culture medium, as this method has been widely employed to disperse NMs used for toxicity studies (Jacobsen et al. 2010, Kermanizadeh et al. 2013b, Kermanizadeh et al. 2013a, Johnston et al. 2015). The hydrodynamic diameter of the NMs in complete MEM and DMEM were 104.86±9.03 and 117.63±7.88 nm respectively. The primary particle size of the CuO NMs investigated is approximately 10 nm (Gosens et al. 2016) suggesting that the NMs were agglomerated in biological media. Other studies have also demonstrated that dispersion of NMs in biological medium can influence their physicochemical properties (e.g. agglomeration) (Kang et al. 2013, Oberdörster et al. 2005). Incubation at 37 ^{o}C for 24 h after dispersion and dilution in cell culture medium reduced the hydrodynamic diameter of the NMs to 25.26±0.91 and 23.74±0.64 in complete MEM and DMEM. This suggests that there is a reduction in particle size in biological media over time, perhaps due to a reduction in agglomeration due to the presence of proteins in the dispersion media and dissociation of

the CuO NMs to ionic form. No TEM analysis was performed to confirm the change in CuO NM agglomeration status over time, but could be performed in future studies.

The comparable toxicity of $CuSO_4$ and CuO NMs in this study is an indication that the toxicity of CuO NMs may be partly mediated by ions. ICP OES analysis of the CuO NMs used for the study demonstrated dissociation of CuO NM to Cu ions over time after dispersion in MEM (47.79 and 53.53 % at 1 and 24 h respectively) and DMEM (59.91 and 67.41 % at 1 and 24 h respectively) (Ude et al. 2017). Therefore, as the CuO NMs were not 100 % soluble at 24 h, but had equivalent toxicity to $CuSO_4$, it suggests that CuO NMs exert toxicity via ion and particle effects.

2.4.2. Cytotoxicity

The Alamar blue assay was employed to assess the viability of undifferentiated Caco-2 cells 24 h post exposure. The BMD 20 value was then calculated. The BMD helps in eliminating the challenges of no-observed-effect-level (NOEL), which regulators normally expect when deciding allowable daily intake of substances for risk assessment. BMD also uses full dose-response raw data for the statistical analysis hence uncertainty quantification in the data is possible (Chen and Chen 2014). Undifferentiated Caco-2 cells were employed for quick screening of viability, as it is cheaper, easier, and quicker and could accommodate a wide range of NM concentrations. It is beneficial to perform more than one viability/cytotoxicity assay when investigating the toxicity of NMs, due to issues with NM interference in biochemical assays and to increase confidence in findings (Ong et al. 2014, Kroll et al. 2012). The lactate dehydrogenase (LDH) assay uses the cell supernatants to assess a decline in plasma membrane integrity, which is indicative of cell death, and can be performed in combination with the Alamar blue assay, to maximise the results obtained from each experiment. However, it is established that CuO NMs interfere with the LDH assay (Han et al. 2011) hence, assessment of CuO NM toxicity with LDH assay was unreliable in this case.

Therefore, the viability of undifferentiated Caco-2 cells were also investigated by assessing the impact of CuO NMs on cell morphology using light microscopy after staining with Romanowisky stain and by performing nuclei counts after staining cells with DAPI. These methods were performed as the use of more complex *in vitro* models (Chapters 3, 4 and 5) requires the culture of cells on transwell plates, which means that

the Alamar blue assay cannot be performed. Thus, it was prudent to identify if alternative approaches to assess the impacts of NMs on cell viability provided comparable findings to the more traditionally used biochemical assays (e.g. the Alamar blue assay). Imaging of cell morphology using light microscopy, SEM and nuclei staining revealed a loss of undifferentiated Caco-2 cells exposed to CuO NMs and $CuSO_4$, which is indicative that there was a loss of cell viability.

All the methods used to screen cell viability were in agreement with a concentration dependent decrease in the viability of undifferentiated Caco-2 cells observed after exposure to CuO NMs. All approaches agreed that there was no significant difference between the toxicity of CuO NMs and $CuSO_4$. As discussed above, the toxicity of CuO NMs is therefore, likely to be mediated by both particle and ion effects. Furthermore, following uptake of CuO NMs by the cell, the particle may dissociate intracellularly (Trojan horse mechanism), therefore promoting ion-mediated effects. Existing research using human adenocarcinoma cell line (A549) has attributed the toxicity of CuO NMs to intracellular release of copper ions (Strauch et al. 2017). Piret et al also reported that the shape of CuO NMs could cause toxicity in differentiated Caco-2 cell with predominant effect from copper ion release (Piret et al. 2012b). Similar reports have been made for other soluble NMs, such as silver and cobalt oxide (Co_3O_4) (Bossi et al. 2016, Park et al. 2010, Hsiao et al. 2015, McShan et al. 2014, Ortega et al. 2014). Although, not investigated in this study, the contribution of intracellular Cu ion release to CuO NM toxicity could be investigated by detection of free and labile metal ions, qualitative determination of the presence of dissolved metal ions by chelation, and separation of dissolved metal ions by filtration or centrifugation (Ivask et al. 2012).

Previously published studies have investigated the cytotoxicity of ZnO (10 nm), SiO_2 (14 nm), TiO_2, iron oxides and Ag (25 nm) to undifferentiated Caco-2 cells (Gerloff et al. 2009, Gerloff et al. 2013, Gerloff et al. 2012, Chen et al. 2016, Karlsson et al. 2008). The CuO NMs tested in this study appear more toxic, as they elicit toxicity at lower NM concentrations. However, it should be stressed that there is a need for side-by-side experiments with these NMs for more meaningful comparison as the experimental design used was not the same across all studies (e.g. cell concentration, NM dispersion method, approach to measure cell viability).

2.4.3. ROS formation

It is generally established that many NMs can exhibit toxicity via stimulation of an oxidant response (Fu et al. 2014, Manke et al. 2013, Abdal Dayem et al. 2017, Sabella et al. 2014, McShan et al. 2014). ZnO, TiO_2 and Ag NM (Chen et al. 2016, Ryu et al. 2014, Long et al. 2006) produce ROS in a range of cell types (e.g. human keratinocytes, Caco-2 cells and immortalized brain microglia). In addition, CuO NMs has also been shown to produce ROS in A549, hepatocellular carcinoma (HCC), well-differentiated (HepG2) and poorly differentiated (SK-Hep-1) hepatocytes and airway epithelial (HEp-2) cells (Wang et al. 2012, Kung et al. 2015, Fahmy and Cormier 2009). However, there is no published paper on ROS production by CuO NMs and $CuSO_4$ in undifferentiated Caco-2 cells at this time. Interestingly, $CuSO_4$ produced > 2 fold increase in ROS production in both acellular and cellular conditions compared to CuO NMs. This is likely to derive from the fact ROS measurements were made at 2 h, and the CuO NMs will not be fully soluble at this time point. It is hypothesised that ROS production by CuO NMs and $CuSO_4$ may have occurred through the Fenton process. In order to confirm the involvement of oxidative stress in NM toxicity antioxidant levels (e.g. glutathione) could be measured or the ability of antioxidants to ameliorate CuO NM toxicity assessed (Chakraborty and Pradhan 2011, Halasi et al. 2013). Interestingly, the level of the antioxidant *HMOX1*expression was increased by both CuO NMs and $CuSO_4$ (see section 2.3.6).

2.4.4. IL-8 production

CuO NMs and $CuSO_4$ stimulated a concentration and time dependent increase in IL-8 protein production in undifferentiated Caco-2 cells. IL-8 is widely produced by a range of cell types in response to pathogenic invasion, tumour necrosis factor, cellular stress and NMs (Puthothu et al. 2006, Hoffmann et al. 2002). IL-8 contributes to the initiation and amplification of inflammatory processes and is a neutrophil chemoattractant (Puthothu et al. 2006, Hoffmann et al. 2002, Kermanizadeh et al. 2013a). A peak production of IL-8 was observed at 24 h at a concentration of 6.34 Cu $\mu g/cm^2$ with production still significant, but reduced at 12.68 Cu $\mu g/cm^2$. The lower effect at 12.68 Cu $\mu g/cm^2$ could be a result of cell death. In addition, the cytokine may adsorb onto the NM surface, preventing its detection at higher NM concentrations (Brown et al. 2010). Limited studies have investigated cytokine production by Caco-2 cells following NM

exposure. When cytokine production is assessed, investigation of IL-8 production has dominated in existing studies (Chen et al. 2016, Piret et al. 2012b). In order to inform the selection of cytokines, a literature review was performed to identify what cytokines were commonly investigated in Caco-2 cells (following exposure to pathogens, pharmaceuticals etc.), and a proteome profiler was used to qualitatively assess cytokine production after exposure to CuO NMs. Results obtained suggest that IL-8 production should be routinely used to assess Caco-2 response to NMs. At 6 h, IL-8 protein production was not observed, and this may be because the produced *IL8* mRNA has not been translated to IL-8 proteins, as *IL8* mRNA was upregulated at 4 h post exposure (section 2.4.5).

2.4.5. Gene expression

Previous studies, which have investigated Caco-2 cell responses to NMs, have neglected to assess changes in gene expression. However, results from this study demonstrate that exposure of Caco-2 cells to NMs may lead to modification in the expression of gene, which control inflammation, oxidative stress (e.g. antioxidant), metal binding and mucus production. HMOX-1 is an active anti-oxidant enzyme known to play an important role in protection and preservation of GI tract mucosa from acute and chronic inflammation (Zhu et al. 2011). HMOX-1 protein has the capability of regulating stress caused by hypoxia, ROS and heat shock (Cooper et al. 2009, Tsuji et al. 2009, Chang et al. 2009). In the present study, CuO NMs upregulated *HMOX1* at all concentrations and time points indicating that *HMOX1* mRNA expression study could be useful in assessing the toxicity of NMs in the intestine *in vitro*. An increase in *HMOX1* expression by CuO NMs suggests that they stimulate an oxidant response.

Various reports have also demonstrated this type of up regulation of *HMOX1* in response of a variety of cell types to NMs. For example Ag NMs (5-37 nm) upregulated *HMOX1* expression after exposure to HeLa and A549 cells (Miura and Shinohara 2009, Sthijns et al. 2017) while ZnO was demonstrated to upregulate *HMOX1* in a monoculture of A549 cells and a co-culture of A549 and human coronary artery endothelial cells (HCAECs) (Yan et al. 2017). An increase in *HMOX1* expression was shown in Caco-2 cells after exposure to Au (5nm) (Bajak et al. 2015) and CuO NMs up regulated *HMOX1*in the A549 cell line (Strauch et al. 2017). In addition, SiO_2 was also shown to

upregulate *HMOX1* in HaCat cell line but not in Caco-2 cells (Ebabe Elle et al. 2016). Thus, there are likely to be cell and NM specific changes in *HMOX1* expression.

IL-8 is secreted at a high concentration at the site of inflammation and is responsible for stimulating increased recruitment and migration of neutrophils (Struyf et al. 2005, Kermanizadeh et al. 2013a). As discussed above (section 2.4.4) CuO NMs and $CuSO_4$ stimulated a significant increase in IL-8 production at 24 h. This study also demonstrates a significant increase in expression of *IL8* by CuO NMs and $CuSO_4$ at all concentration and time points. The lack of protein secretion at 6 h but high level of gene expression at 4 h may be attributed to the fact that the genes expressed have not been translated to a detectable protein level at shorter time point. Therefore, this result suggests that at shorter time points (4 h), *IL8* expression could be used as a sensitive, and rapid approach to assess NM toxicity to Caco-2 cells, whilst the protein assay will be more useful at longer time exposure (24 h). Expression of *IL8* at 4 h has been reported after exposure of undifferentiated Caco-2 cells to ZnO and SiO_2 NMs previously (Gerloff et al. 2013).

The key players in *MT* induction include stress (Haq et al. 2003) and hypoxia, which may be as a result of reactive oxygen radicals from metal overload (Murphy et al. 1999). MT proteins are known to possess metal detoxifying properties and have the ability to scavenge excess metals (Sahu et al. 2013). Although the fold change of *MT2A* was not calculated due to its absence in the control at a detectable level, *MT2A* was significantly upregulated at all concentrations and time points following exposure to CuO NMs and $CuSO_4$. *MT1A* was not significantly upregulated, which shows that *MT2A* is more sensitive to CuO NMs and $CuSO_4$ than *MT1A* in undifferentiated Caco-2 cells. Expression of *MT1A* and *2A* by CuO NMs and $CuSO_4$ were comparable. Induction of *MT* genes in this study are likely as a result of copper ion and not particle as metal ions are responsible for activation of *MT* expression. CuO NMs has been shown to upregulate *MT2A* expression in human bronchial epithelial (BEAS-2B) cells (Strauch et al. 2017) and a marked upregulation in *MT2A* expression has been reported after exposure of HeLa cell line with Ag NMs, which was attributed to oxidative stress (Miura and Shinohara 2009).

MUC2 was also upregulated in a concentration and time dependent manner from 4 to 12 h and decreased at 24 h post exposure. It is possible that the observed upregulation of *MUC2* at higher concentrations of CuO NMs and $CuSO_4$ is a means of protection against

toxic substances. Expression of *MUC2* has been reported to continue after inflammation, with altered structure and reduction in oligosaccharide chain content to 50 % leading to loss of viscoelastic properties and then barrier integrity dysfunction (Cornick et al. 2015). *MUC2* expression has not been previously investigated for Caco-2 cell responses to NMs, although it has been investigated for other chemicals/pathogens (Elamin et al. 2014, Cobo et al. 2015, Azzam et al. 2011). The results from this study suggest that it could be assessed more routinely when investigating NM toxicity to Caco-2 cells. It is also important to state here that the impact of CuO NMs on undifferentiated Caco-2 cells using gene expression should be assessed at early time points as *HMOX1*, *IL8* and *MT2A* mRNA expression was very high at 4 h post exposure. Therefore, IL-8 protein production and expression of *HMOX1*, *IL8* and *MT2A* can be used as a quick and early molecular marker for evaluating toxicity of CuO NMs in undifferentiated Caco-2 cells. In future, other genes such as *MT1B*, *MT1M*, *MT1L*, *MT1E*, *MT1F*, *MT1X*, *MT1G*, *MT1H* and *GPX*), antioxidant genes (catalase, glutathione peroxidase, superoxide dismutase), apoptosis genes (caspases 3 and 7) can be studied to help elucidate the mode and mechanism of NM toxicity.

2.5. Conclusions

In this chapter, CuO NMs and $CuSO_4$ demonstrated a similar degree of toxicity to undifferentiated Caco-2 cells. Markers of CuO NM toxicity to Caco-2 cells were identified namely: cytotoxicity, ROS production, IL-8 production, and gene expression (*HMOX1*, *IL8*, *MUC2*, *MT1A* and *MT2A*). Studies investigating NM toxicity normally assess inflammatory and oxidative effects and it is apparent that these endpoints are also relevant to the intestine. The comparable effect of CuO NMs and $CuSO_4$ in most of the biochemical and molecular markers (except ROS formation) and knowledge that CuO NMs are not fully soluble at the time points investigated indicates the possibility that CuO NMs mediate toxicity via particle and ion effects. Undifferentiated Caco-2 cells have been shown to be very sensitive to CuO NMs and $CuSO_4$ toxicity. However, the toxicity of NMs can be overestimated using undifferentiated Caco-2 cells since they lack various characteristics of mature intestine. It is therefore essential to use more complex *in vitro* models, which better mimics *in vivo* conditions when assessing NM toxicity.

CHAPTER 3: Impact of copper oxide NMs and copper sulphate on differentiated Caco-2 cells: an intestinal epithelial cell model

3.1. Introduction

Undifferentiated Caco-2 cells lack tight junctions, microvilli and other associated proteins and so they do not accurately represent human small intestinal epithelial cells (section 2.1). However, culturing Caco-2 cells for 15-21 days, without growth factor supplementation, leads to spontaneous differentiation to mature enterocyte-like cells, which have better resemblance to mature enterocytes of the human small intestine (Sambuy et al. 2001, Sambuy et al. 2005, Natoli et al. 2011, Jepson 2012). Functional tight junctions joining the cells in the monolayer and well developed microvilli at the apical (AP) side form during the culture period (Sambuy et al. 2001). In addition, the AP membrane of differentiated Caco-2 cells express characteristic hydrolases such as sucrose-isomaltase, lactase, aminopeptidase N and dipeptidyl peptidase IV of the absorptive enterocytes of small intestine (Ferruzza et al. 2012b, Sambuy et al. 2001). The above characteristics of differentiated Caco-2 cells make them more appropriate *in vitro* model to represent human mature intestinal epithelial cells. For this reason, it is the most frequently used model for the study of absorption, toxicity and metabolism in the intestinal epithelium (Ferrec and Fardel 2012). However, there are some drawbacks associated with their use, as, for example, differentiated Caco-2 cells lack mucus layer and a microfold cells, and do not contain digestive enzymes and physiological conditions associated with the small intestine. Differentiated Caco-2 cells have been used to study the toxicity of SiO_2 (14 nm) and ZnO (10 nm) NMs via assessment of cytotoxicity, *IL8* expression and IL-8 protein production (Gerloff et al. 2013). Piret et al. (2012b) also investigated the impact of CuO NMs on TEER, viability, IL-8 secretion and penetration of across differentiated Caco-2 cell monolayer 24 h post exposure. Although both undifferentiated and differentiated Caco-2 cells have been used to investigate NM toxicity (Piret et al. 2012b, Gerloff et al. 2013, Gerloff et al. 2012, Gerloff et al. 2009), few studies have compared the response of both models, despite concern that differentiated and undifferentiated cells may not provide the same response. It is more expensive and time consuming to work with differentiated cells, which limit their widespread use.

The development of fully differentiated cells is monitored by measurement of TEER (Jepson 2012, Ferruzza et al. 2012b, Ferruzza et al. 2012a), staining of tight junction proteins (e.g. Zonula occludens, occludins) (Jain et al. 2011, Natoli et al. 2011), assessment of microvilli development and presence of alkaline phosphatase (Ferruzza et

al. 2012b, Ferruzza et al. 2012a). TEER values of differentiated Caco-2 cells range from 260 up to 1200 Ω.cm depending on the frequency of media changes, number of days the cells are cultured and constituents of the medium in the AP and basolateral (BL) membrane. Caco-2 cells can be considered to be differentiated if the TEER value is greater than 250 $\Omega.cm^2$ (Ferruzza et al. 2012a). TEER measurement is a parameter used to ascertain the integrity, confluency and viability of the cell monolayer and a decrease in TEER value is an indication of loss of barrier integrity (Gamboa and Leong 2013). Differentiated Caco-2 cells have been used to investigate the transport of substances and pathogens across the intestinal barrier. However, the rate of paracellular (passive) transport in differentiated Caco-2 cells has been reported lower than that of undifferentiated Caco-2 cells and the human intestine as reviewed by Jepson (2012). However, other molecules (such as drug and nutrients) that are passively transported show good correlation with human colon and rectum biopsy but actively transported molecules do not correlate well (Lefebvre et al. 2015, Chen et al. 2010, Walter et al. 1996).

Differentiated Caco-2 cells have been used to study drug transport across the intestinal monolayer (Liu et al. 2017, Hubatsch et al. 2007) as well as the penetration of NMs. For example the translocation of silica nanoparticles (50 and 150 nm) (Ye et al. 2017). Cell permeability and cytotoxic effects of different-sized zinc oxide (ZnO) NMs were studied using differentiated Caco-2 cells and it was observed that the penetration of 20 nm ZnO NMs across the intestinal monolayer was greater, and that they were more cytotoxic than larger particles (1-5 µm and 90-200 nm) at 24 h post exposure (Chang et al. 2011). Differentiated Caco-2 cells have also been used to study the toxicity of NMs. For example, differential toxicity of rod and spherical shape CuO NMs with differentiated Caco-2 cells and they observed that rod shaped NMs were more toxic than the spherical shaped CuO NMs via assessment of IL-8 and TEER value (Piret et al. 2012b).

3.1.1. Aim and objectives

Most of the studies using differentiated Caco-2 cells to investigate NM toxicity have focused on assessment of translocation, cytotoxicity and IL-8 secretion without much consideration of other endpoints. Here, as differentiated Caco-2 cells are a widely accepted model of the intestinal epithelium. They were selected to study biochemical and

molecular markers of nanomaterial toxicity to the GI tract using CuO NMs and $CuSO_4$ employing wide range of endpoints including barrier integrity (using TEER measurement, SEM, immunostaining of the tight junction), light microscopy. In addition, cytokine production, ROS formation, NM translocation and gene expression (using markers of oxidative stress (*HMOX1*), inflammatory response (*IL8*), mucus secretion (*MUC2*) and metal binding (*MT1A* and *MT2A*)) were also assessed.

The aim of this chapter is to determine the potential use of differentiated Caco-2 cell as an *in vitro* model for the study of the toxicity of ingested NMs and to identify biochemical and molecular biomarkers of NM toxicity that could be employed in the assessment of NM toxicity to the intestine *in vitro*. Furthermore, the toxicity of CuO NMs and $CuSO_4$ was compared to explore the contribution of particle and ionic effects in NM toxicity.

Specific objectives are as follows

i. To determine the impact of CuO NMs and $CuSO_4$ on differentiated Caco-2 cells on cytotoxicity, barrier integrity and cell morphology (tight junction staining, TEER measurement, light and electron microscopy).
ii. To investigate the impact of CuO NMs and $CuSO_4$ on cytokine production and oxidative stress in differentiated Caco-2 cells via assessment of IL-8 production, ROS formation and expression of genes related to inflammation, oxidative stress, mucus secretion and metal metabolism (metallothionein).
iii. To assess the translocation of CuO NMs and $CuSO_4$ across differentiated Caco-2 cells.

3.1.2. Hypotheses

i. CuO NMs and $CuSO_4$ will induce loss of differentiated Caco-2 cell viability.
ii. CuO NMs and $CuSO_4$ will elicit ROS production in differentiated Caco-2 cells.
iii. CuO NMs and $CuSO_4$ will induce cytokine production in differentiated Caco-2 cells.
iv. CuO NMs and $CuSO_4$ will impair barrier integrity (i.e. a reduction in TEER, disruption of tight junctions), which will lead to Cu ion translocation across the differentiated Caco-2 cell monolayer.

v. CuO NMs and $CuSO_4$ will upregulate the expression of genes related to inflammation, oxidative stress, mucus secretion and metal binding (metallothionein) in the differentiated Caco-2 cells.

vi. The impact of CuO NMs on differentiated Caco-2 cells will be similar to $CuSO_4$.

3.2. Materials and Methods

3.2.1. Cell culture

The source of the Caco-2 cell line and its maintenance are described previously (section 2.2.3).

3.2.2. Differentiation of Caco-2 cells

Differentiated Caco-2 cells were cultured on 3.0 µm pore polycarbonate transwell inserts in a 12 well plate with a growth area of 1.12 cm^2 (Costar corning, Flintshire, UK). Cells were seeded at a concentration of 3.13 x 10^5 cells/cm^2 (500 µl/well) in complete cell culture medium into the AP compartment of the transwell insert, and the BL compartment was filled with 1.5 ml of complete cell culture medium. The cells were cultured at 37 ^oC, 5 % CO_2 and 95 % humidity for 18-21 days. The medium was changed every other day for the first 16 days and then every day until 21 days. The medium was changed by aspirating the medium in the BL compartment followed by AP compartment and replaced by filling the AP compartment with 500 µl of the medium first then the BL compartment with 1.5 ml of the cell culture medium. Differentiation of cells was confirmed via measurement of TEER, tight junction staining and SEM (for microvilli) (see sections 3.2.3, 3.2.5 and 3.2.7).

3.2.3. Measurement of trans-epithelial electrical resistance (TEER)

Trans-epithelial electrical resistance was measured using an epithelial voltohmmeter EVOM (World precision instrument, Sarasota, USA). The voltohmmeter was set to resistance and placed vertically on the insert making sure that the short electrode is placed in the AP compartment while the long electrode is placed in the BL compartment touching the cells. The resistance reading in ohms was taken once the reading stabilized and measurements were taking every 2 days until 21 days starting from the fifth day.

The resistivity was calculated using equation 1.

$Resistivity\ (\Omega.cm^2) = ohm2 - ohm1 \times A$---------- Equation 1

Where Ohm1 = Resistance of the insert with cell culture medium only.

Ohm 2 = Resistance of the insert with cell.

A = Surface area of the insert in cm^2

TEER are reported as resistivity.

Only Caco-2 cell monolayers with TEER values greater than 500 $\Omega.cm^2$ were used for experiments.

3.2.4. Investigation of the impact of CuO NMs and $CuSO_4$ on the barrier integrity of differentiated Caco-2 cells

The impact of CuO NMs and $CuSO_4$ on the barrier integrity of differentiated Caco-2 cells was assessed by measuring TEER. Differentiated Caco-2 cells were exposed to complete cell culture medium (negative control), 0.1 % triton X100 (positive control), CuO NMs or $CuSO_4$ at a concentration of 6.34 and 12.68 Cu µg/cm^2 (500 µl/well). The sub-lethal concentrations selected for investigation were based on the findings from undifferentiated cells (section 2.3.2) and the Cu concentration was standardized for CuO NMs and $CuSO_4$. The TEER values were taken at time zero immediately after exposure with CuO NMs and $CuSO_4$ and then every 3 h for 15 h and at 24 h post exposure. The resistivity was calculated using equation 1. Data are expressed as mean resistivity ($\Omega.cm^2$).

3.2.5. Immunostaining of differentiated Caco-2 tight junctions

Differentiated Caco-2 cells were exposed to cell culture medium (control), CuO NMs or $CuSO_4$ (6.34 Cu µg/cm^2) (500 µl/well) for 24 h at 37 ^oC and then washed twice with PBS. The cells were fixed with 4 % formaldehyde for 25 min at RT and 50 mM ammonium chloride was used to quench excess aldehyde groups at RT for 10 min. The cells were permeabilized with 0.1 % triton X100 for 10 min and nonspecific binding was blocked with 10 % BSA for 2 h at the RT. Cells were then incubated with 1 µg/ml (diluted in 1 % BSA) anti ZO-1 tight junction protein antibody (Abcam, Cambridge, UK) overnight (o/n) at 4 ^oC. Cells were incubated with Alexa Fluor 488 goat anti-rabbit IgG H&L (Abcam, Cambridge, UK) (secondary antibody), diluted to 4 µg/ml (in 1 % BSA) for 1 h. This was followed by counter staining with DAPI (300 nM) for 15 min at RT for nuclei. After each

step, cells were washed three times with PBS except after treatment with secondary antibody, which was washed five times. The polycarbonate inserts were carefully excised, mounted with mowiol containing DABCO (antifading agent), covered with a glass coverslip and then sealed with nail polish. The slides were incubated at 4 ^{o}C for 24 h before cells were visualized using a Zeiss LSM880 confocal microscope (Germany) and the results analysed using the Zen program and Image J software.

3.2.6. Nuclei counting (cytotoxicity)

Differentiated Caco-2 cells were exposed to cell culture medium (control), CuO NMs or $CuSO_4$ (6.34 or 12.68 Cu µg/cm^2) (500 µl/well) for 24 h at 37 ^{o}C, and then were washed twice with PBS and processed as described in section 2.2.6 to stain the nuclei. The polycarbonate inserts were carefully excised and mounted with mowiol containing DABCO (anti fading agent) onto a microscope slide and covered with a glass coverslip, which was then sealed with nail polish and allowed to dry at 4 ^{o}C for 24 h before visualizing with a Zeiss fluorescent microscope, Carl Zeiss Axio Scope A 1 Upright Research Microscope (Germany) fitted with a camera. At least five fields of view (each field of view was140.80 X 105.60 microns) were imaged for each sample. The results were analysed with Image J software and data are expressed as mean nuclei number ± SEM, and representative images presented.

3.2.7. Scanning electron microscopy (SEM)

Differentiated Caco-2 cells were exposed to cell culture medium (control) or 12.68 Cu µg/cm^2 of CuO NMs (500 µl/well) for 24 h at 37 ^{o}C. The inserts were then processed as described in section 3.2.4. The polycarbonate membranes were carefully excised and mounted on SEM specimen stubs (Aluminium, 12.5 mm diameter, 3.2 x 6 mm pin Agar Scientific UK). Then, specimens were coated with gold and examined with SEM. More than 5 views were imaged and representative images presented.

3.2.8. Romanowsky staining (assessment of cytotoxicity and cell morphology)

Differentiated Caco-2 cells were exposed to cell culture medium (control), 6.34 and 12.68 Cu µg/cm^2 of CuO NMs or $CuSO_4$ (500 µl/well) at 37 ^{o}C. After 24 h, the cells were stained with Rapid Romanowsky stain (TCS Biosciences, England). Briefly,

differentiated Caco-2 cells were fixed by rinsing the insert 15 times in methanol. To stain the cells the inserts were then rinsed with eosin Y solution 15 times and then methylene blue solution 15 times. The inserts were thoroughly washed in distilled water and air-dried. The polycarbonate inserts were carefully excised, then mounted with DPX (Sigma, Poole UK) and covered with a glass coverslip. The specimens were viewed and imaged using a light microscope-Zeiss fluorescent microscope, Carl Zeiss Axio Scope A 1 Upright Research Microscope (Germany) fitted with camera (ZEISS Axiocam ERc 5s) (magnification 40 X).

3.2.9. Determination of Cu ion in medium

Differentiated Caco-2 cells were exposed to complete cell culture medium (control), 3.17, 6.34 and 12.48 Cu µg/cm^2 of CuO NMs and $CuSO_4$ (500 µl/well) for 24 or 48 h at 37 ^oC, 5 % CO_2 and 95 % humidity. This was followed by removal of the cell culture medium from AP and BL compartments. The medium from AP (300 µl) and BL (900 µl) compartments were digested with 5 ml of 4 % HNO_3 (Sigma), filtered with Puradisc 25 mm 0.2 µm PES filter media (Whatman). The volume was made up to 10 ml with Milli Q deionised H_2O to obtain final acidic concentration of 2 % HNO_3.

The cells were also digested following the method described by (Bolea et al. 2014). Briefly, to detach the cells, 25 mM trypsin EDTA (100 µl) was added into the apical compartment of the transwell plate and incubated for 5 min at 37 ^oC, 5 % CO_2 and 95 % humidity. The cells were then digested by adding 1 ml of 20 % HNO_3 followed by shaking with a rotatory shaker, PMS-1000, Grant-bio (Cambridge UK) at high speed for 4 h, at RT. The cell suspension was then diluted with Milli Q H_2O to get an acidic concentration of 2 % HNO_3, and then filtered with Puradisc 25 mm 0.2 µm PES filter media (Whatman). The copper ion content in the acidic extracts of medium (from AP and BL compartment) and cell were analysed by Dr. Lorna Eades (University of Edinburgh) using Inductive Coupled Plasma Optical Emission Spectrometry (ICP-OES) (Perkin Elmer Optima 5300 DV USA). Radio frequency (RF) forward power of 1400 W, with argon gas flows of 15, 0.2 and 0.75 L/min for plasma, auxiliary, and nebuliser flows was employed respectively. Data are expressed as % of the exposed concentration.

Apparent permeability coefficients (P_{app}) of Cu were calculated using equation 2 (des Rieux et al. 2007).

$$Papp\ (cm/s) = \frac{\Delta Q}{\Delta t} \times \frac{1}{A} \times Co$$----------Equation 2

Where ΔQ/Δt is the amount of Cu transported into the BL compartment per unit time (t), A is the surface area of the insert (Caco-2 cell monolayer) and Co is the initial concentration of the substance in the donor (AP) compartment.

3.2.10. Evaluation of intracellular ROS production: DCFH-DA assay

Differentiated Caco-2 cells were washed twice and150 µM DCFH-DA (in HBSS) was added (500 µl) into the apical compartment of each of the wells. The cells were then incubated for 1 h in the dark at 37 ^{o}C, 5 % CO_2 and 95 % humidity. Next, the cells were washed with PBS and exposed to 500 µl of HBSS (control), H_2O_2 (1 mM), CuO NMs or $CuSO_4$ (3.17, 6.34 and 12.68 Cu µg/cm^2) diluted in HBSS (500 µl/well) and incubated at 37 ^{o}C, 5% CO_2 and 95 % humidity for 2 h. The fluorescence reading was measured at time 0 and after 2 h at a wavelength of 485/530 nm (excitation/emission) using a micro plate reader, SpectraMax M5 (California USA) Data are expressed as mean fold change in fluorescence (compared to control).

3.2.11. Cytokine analysis

4.2.11.1. Proteome profiling

Proteome profiling was performed using a Human Cytokine Array kit (R&D System, Inc., Minneapolis, MN USA). Supernatants collected after treatment of differentiated Caco-2 cells with 6.34 Cu µg/cm^2 of CuO NM for 24 h (section 3.2.3), which had been stored at -80 ^{o}C were thawed and used for Proteome profiling following the manufacturer's protocol as described above (Section 2.2.10.1). The results from this experiment informed the selection of cytokine (IL-8) to be analysed.

3.2.11.2. IL-8 production

Differentiated Caco-2 cells were exposed to cell culture medium (negative control), 200 ng/ml tumour necrosis alpha (TNF-α) (positive control), 3.17, 6.34, or 12.68 Cu µg/cm^2 of CuO NMs and $CuSO_4$ (500 µl/well) for 24 or 48 h at 37 ^{o}C. The cell supernatants were collected from the AP and BL compartments of differentiated cells and stored at −80 °C

until required. IL-8 level was quantified using an ELISA as described previously (section 3.2.10.2.).

3.2.12. Gene expression

3.2.12.1. Ribonucleic acid (RNA) isolation

Differentiated Caco-2 cells were exposed to cell culture medium, 3.17, 6.34 and 12.68 Cu μg/cm^2 of CuO NMs or $CuSO_4$ (500 μl/well) and incubated for 4, 12 and 24 h at 37 ^oC. The medium was then removed, and the inserts washed twice with PBS followed by addition of trypsin EDTA (100 μl) into the AP compartment of each wells of the insert and the cells were incubated for 5 min at 37 ^oC. Trypsinisation was stopped by addition of cell culture medium (500 μl). The cells were transferred to 1.5 ml microfuge tubes and centrifuged for 5 min at 2000 rpm using an Eppendorf refrigerated microcentrifuge 5424 (Cole- Palmer UK). The cell pellet was re-suspended in PBS (30 μl) and transferred to the processing plate then, lysis/binding solutions (140 μl) were added and the samples were shaken for 1 min and RNA was isolated following the protocol described in section 2.2.11.1.

3.2.12.2. Complementary deoxyribonucleic acid (cDNA) synthesis

The RNA was transcribed to cDNA using Precision nanoScript^{TM}2 Reverse Transcription kit (Primerdesign, UK) following manufacturers protocol as described in section 2.2.11.2.

3.2.12.3. Quantitative polymerase chain reaction (qPCR)

qPCR was performed with a 7900 RT fast PCR system and SDS 2.3 software with 384 well plates (Applied Biosystems, USA), using Custom designed real-time PCR assay with Double-Dye probe and Precision PLUS qPCR Master Mix (Primerdesign, UK) following the manufacturer's instructions as described in section 2.2.11.3.

3.2.13. Data analysis

Each experiment was repeated at least three times (on different days) and all data generated from these experiments are expressed as the mean ± Standard error of the mean (SEM). The figures were generated using Graph Pad Prism. After checking normality of

the data, a one-way analysis of variance (ANOVA) with a Tukeys multiple comparison was employed to investigate statistical significance using Minitab 17 software. The microscope images were analysed with image J software.

3.3. Results

3.3.1. Verification of differentiation of Caco-2 cells and impact of CuO NM and $CuSO_4$ on barrier integrity (TEER value and tight junction staining)

Caco-2 cell differentiation was monitored by measurement of TEER. Measurement of TEER commenced 5 days post seeding to avoid disruption of the monolayer. The TEER value increased, with time (Figure 3.1). More specifically, there was an increase in TEER value from day 5 (76 $\Omega.cm^2$) reaching approximately 600 $\Omega.cm^2$ at the 17^{th} day (Figure 3.1). The increase in TEER value was minimal from the 17 to 21^{st} day (760 $\Omega.cm^2$) (Figure 3.1). Only differentiated Caco-2 cells with a TEER value greater than 500 $\Omega.cm^2$ were used throughout (Figure 3.1).

Measurement of TEER value following exposure to CuO NMs and $CuSO_4$ was then used to assess impacts on the barrier integrity. The TEER value of the control cells at the start of the experiment was between 824 and 861 $\Omega.cm^2$ (Figure 3.2). After 24 h, there was no change in the TEER value for the control cells over the duration of the experiment (0 – 24 h) (Figure 3.2). A concentration and time dependent decrease in TEER values was observed following exposure to CuO NMs and $CuSO_4$ compared to control (Figure 3. 2). Whilst the TEER value of differentiated Caco-2 cells exposed to 6.34 and 12.68 Cu $\mu g/cm^2$ of CuO NMs and $CuSO_4$ remained virtually constant up to 9 h post exposure, the TEER value significantly decreased from 12 h post exposure (Figure 3.2). The level of reduction of TEER value of both CuO NMs and $CuSO_4$ was greatest after 24 h for both tested concentrations (6.34 and 12.68 Cu $\mu g/cm^2$).

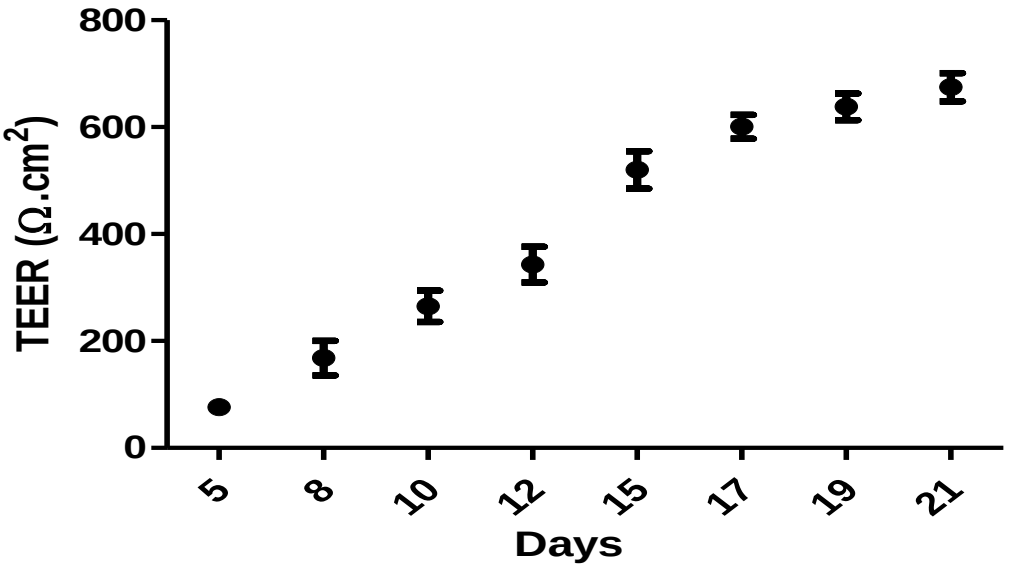

Figure 3.1: TEER value of Caco-2 cell over 21 days.

Caco-2 cells were grown in transwell plates and TEER measurements made at regular intervals to monitor cell differentiation. Data are expressed as mean TEER value ± SEM (n = 3).

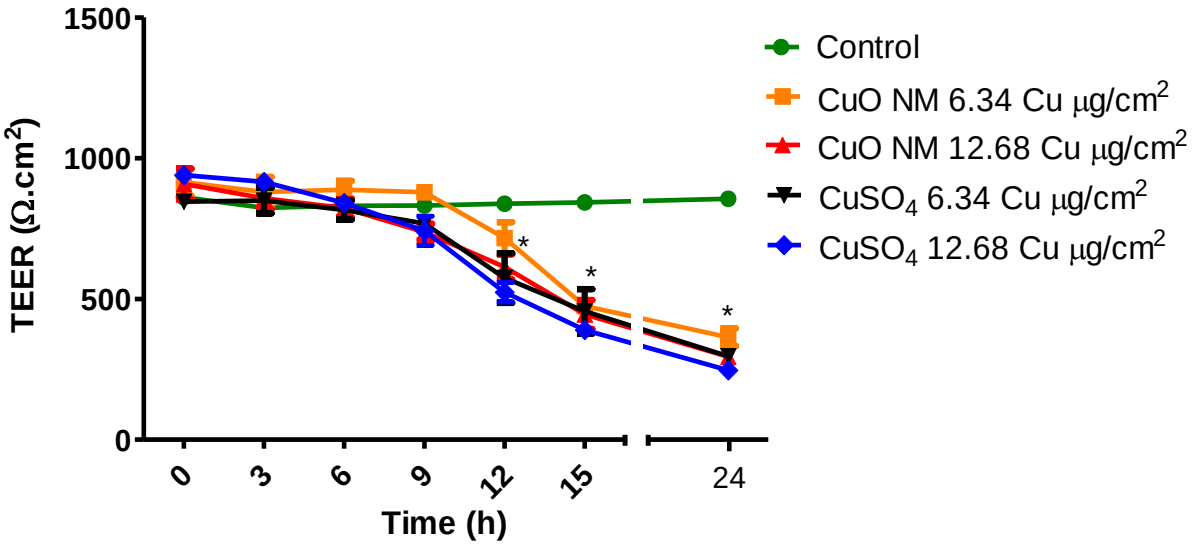

Figure 3.2: Impact of CuO NMs and $CuSO_4$ on differentiated Caco-2 cell TEER values.

*Differentiated Caco-2 cells were exposed to cell culture medium (control, 0), CuO NMs or $CuSO_4$ at concentrations of 6.34 or 12.68 Cu µg/cm^2 for24 h. The TEER values were measured using epithelial volt-ohmmeter EVOM every 3 h. Data are expressed as mean ± SEM (n = 3). Significance at $P<0.05$ is indicated by * compared with control.*

3.3.2. Verification of tight junction formation and impact of CuO NMs and $CuSO_4$ on tight junction protein (ZO-1) of differentiated Caco-2 cells

The ability of differentiated Caco-2 cells to form tight junctions is a characteristic of intact intestinal epithelial cells and was verified by staining for the Zonula occludens-1 (ZO-1) a tight junction protein. After culturing for 21 days, tight junctions were visualised in differentiated Caco-2 monolayers, confirming that the cells differentiated (Figure 3.3). Undifferentiated Caco-2 cells were also included as a control, and did not show any tight junction staining (Appendix 2). Differentiated Caco-2 cells exposed to 6.34 Cu µg/cm^2 of CuO NMs, and $CuSO_4$ for 24 h were stained for ZO-1 and the intensity of tight junction protein staining was reduced for both treatments compared to control suggesting a loss of barrier integrity (Figure 3.3). The extent ZO-1 staining intensity may be quantified to confirm the impact of CuO NMs and $CuSO_4$ on the tight junction protein.

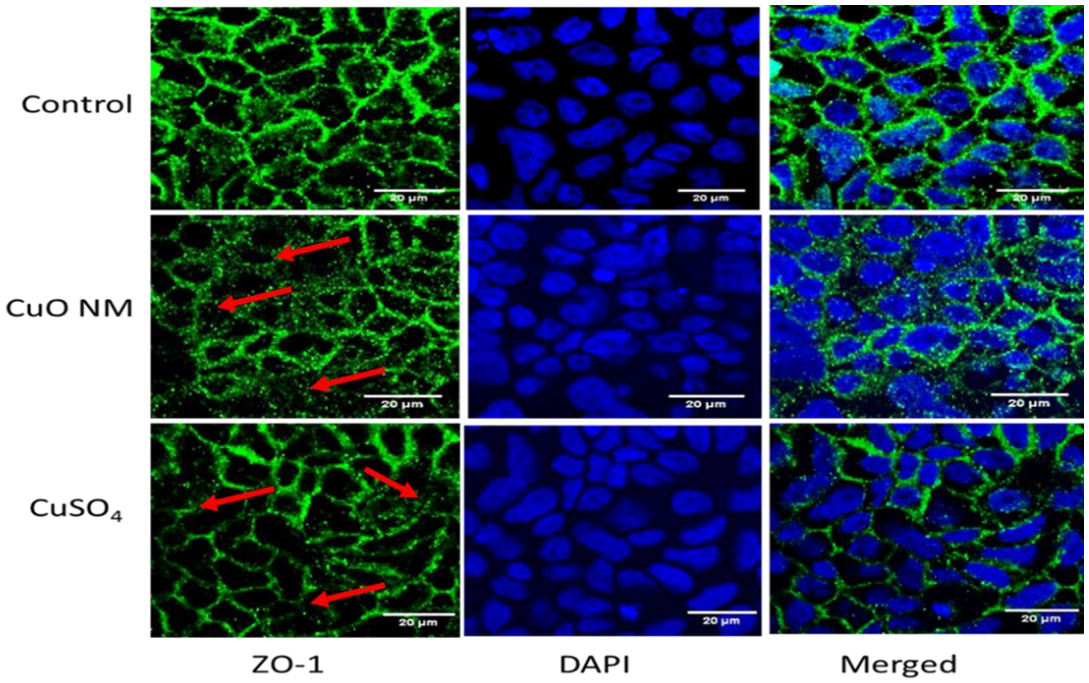

Figure 3.3: The impact of CuO NMs and $CuSO_4$ on differentiated Caco-2 cell tight junction protein.

Following differentiation, Caco-2 cell monolayers were exposed to cell culture medium (control) or 6.34 Cu µg/cm^2 of CuO NMs and $CuSO_4$ for 24 h, then fixed, and stained for the tight junction protein ZO-1 (green) and nucleus with DAPI (blue). The images of extended focus were obtained with Zeiss LSM880 confocal microscope using the Zen program for data analyses. Red arrows indicate areas where there is a reduction in ZO-1 staining intensity. Scale bar = 20 µm. Representative images are shown (n=3).

3.3.3. Verification of microvilli formation and assessment of CuO NMs and $CuSO_4$ impact on differentiated Caco-2 cell viability and morphology

To assess the differentiation status of Caco-2 cells (e.g. microvilli development) and to investigate the effect of CuO NMs and $CuSO_4$ on cell morphology, SEM and light microscopy was used. SEM revealed that control differentiated Caco-2 cells covered the entire surface with extended microvilli development evident (Figure 3.4), which is one of the characteristics of the human intestinal epithelium. Differentiated Caco-2 cells exposed to CuO NMs (12.68 Cu µg/cm^2) covered the cell surface like their control counterparts but the microvilli were shorter on some of the cells, compared to control (Figure 3.4).

To confirm the viability of the cells, microscopy and nuclei counts were performed. Using light microscopy, it was observed that there was no difference in cell number of cells between the control differentiated cells and cells treated with CuO NMs or $CuSO_4$ at concentrations of 6.34 or 12.68 Cu µg/cm^2 24 h post exposure, suggesting that there was no loss of cells following treatment (Figure 3.5). Differentiated Caco-2 cells were stained with DAPI and the nuclei counted in order to count cell number as an indicator of cell viability (Figure 3.6). There was no significant difference in the number of nuclei counted in the CuO NMs or $CuSO_4$ exposed cells compared to the control cells, which suggests that there was no cell death (Figure 3.6A). Representative images confirming the number of counted nuclei are shown in figure 3.6B.

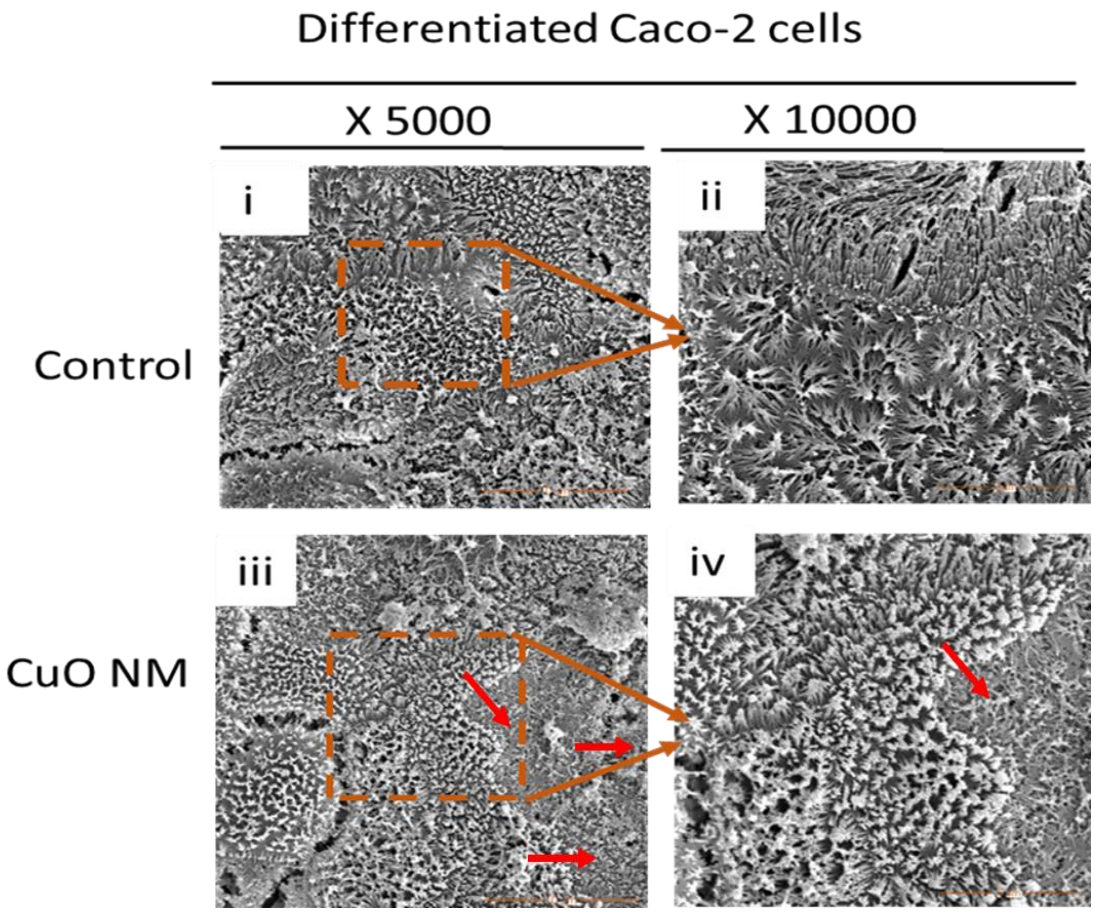

Figure 3.4: SEM images of differentiated Caco-2 cells exposed to CuO NMs for 24 h.

Differentiated Caco-2 cells were exposed to cell culture medium (control) or 12.68 Cu µg/cm^2 of CuO NMs for 24 h and were then washed, fixed, dehydrated, dried and examined by SEM. Specimens i) and ii) are control differentiated Caco-2 cells imaged at a magnification of X 5000 and X 10000 respectively. iii) and iv) are differentiated Caco-2 cells exposed to 12.68 Cu µg/cm^2 of CuO NMs imaged at a magnification of X 5000 and X 10000 respectively. Representative images are shown (n=3). Red arrows indicate area of shortened microvili.

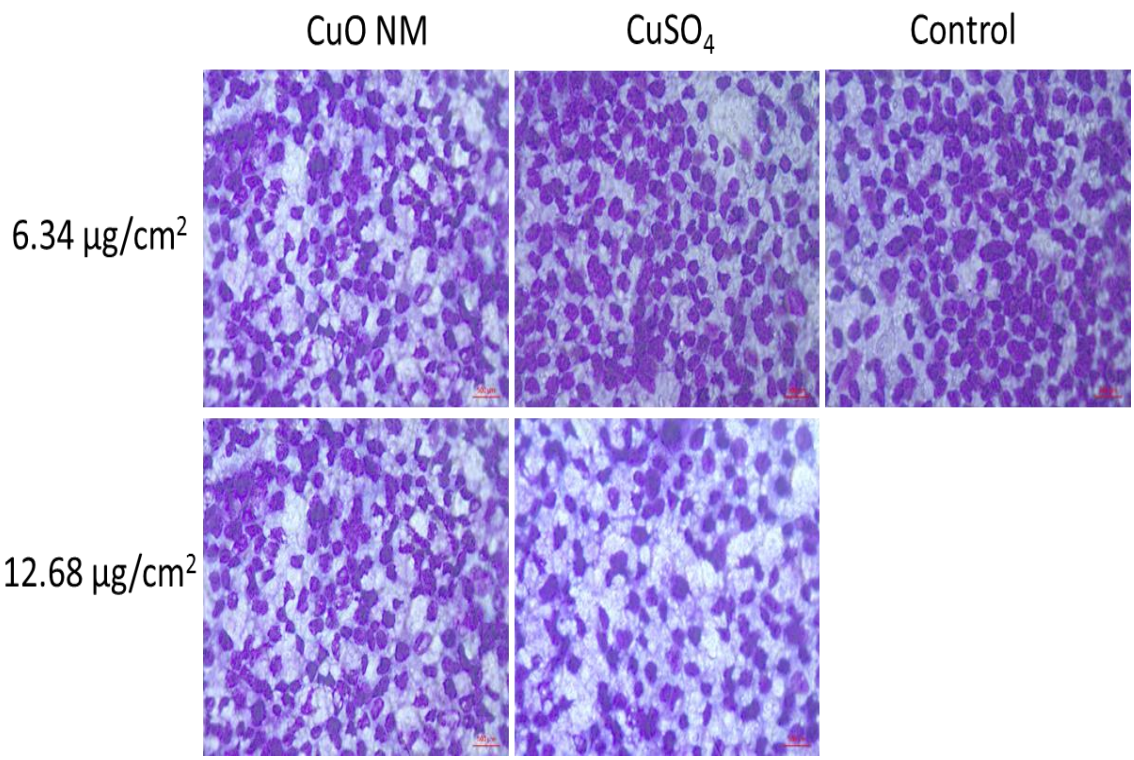

Figure 3.5: Impact of CuO NMs and $CuSO_4$ on differentiated Caco-2 cell morphology and cell number using light microscopy.

Differentiated Caco-2 cells were exposed to cell culture medium (control) or 6.34 or 12.68 Cu µg/cm^{2}of CuO NMs or $CuSO_4$ for 24 h. The cells were then fixed, stained and visualised using light microscopy (magnification 40 X, scale bar= 50 µm. Representative images are shown (n=3).

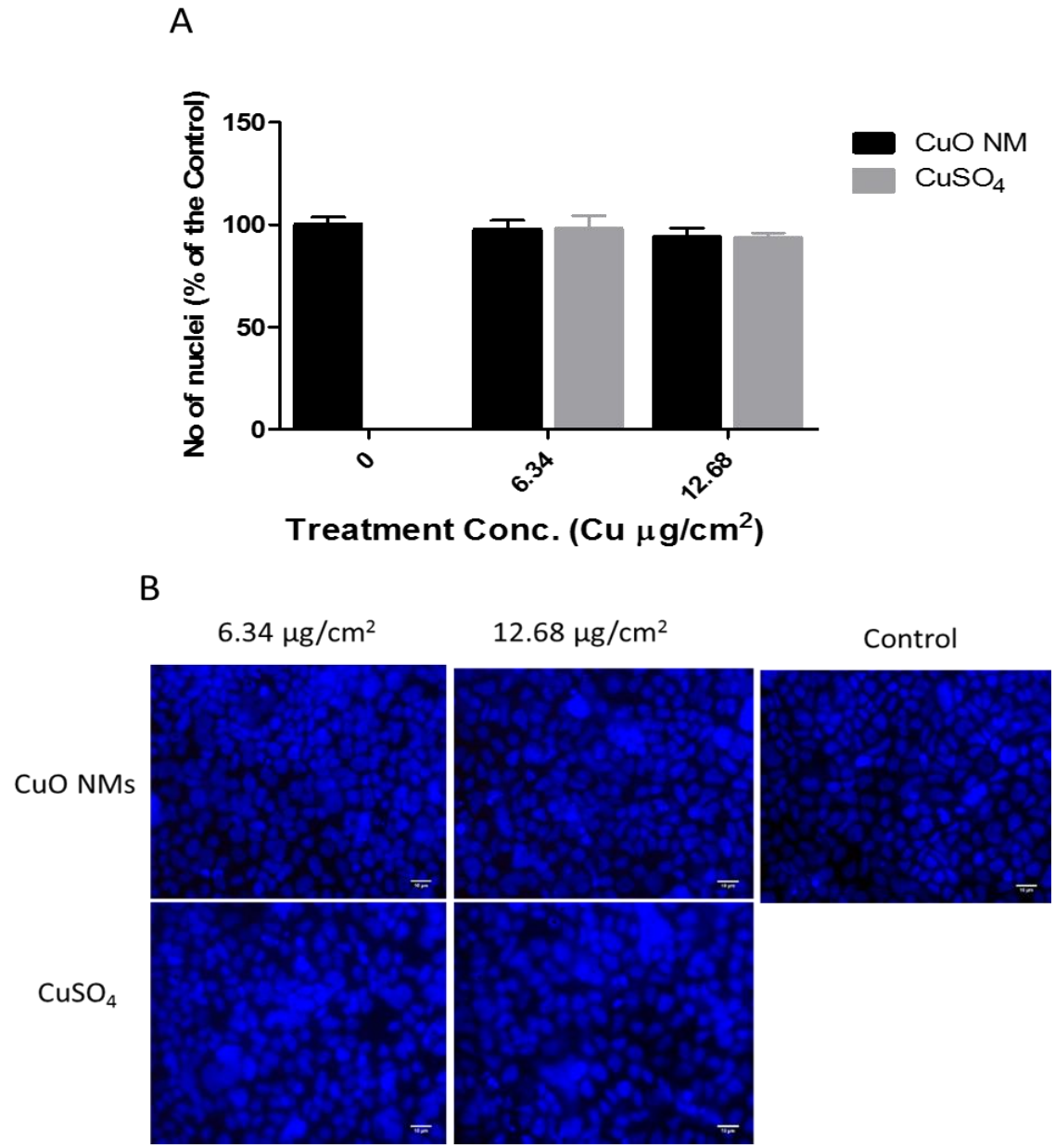

Figure 3.6: Assessment of the viability of differentiated Caco-2 cells using nuclei staining with DAPI.

*Differentiated Caco-2 cells were treated with CuO NMs and $CuSO_4$ at a concentration of 6.34 and 12.68 Cu µg/cm^2 fixed and the nuclei stained with DAPI. Images were obtained with a Carl Zeiss Axio Scope A 1 Upright Research Microscope (magnification 40X) and the nuclei counted using Image J software (A). Data are expressed as the number of nuclei (% of the unexposed control) ± SEM (n = 3). Significance at P<0.05 is indicated by * compared to unexposed control. Representative images are presented (B), and Scale bar = 10 µm (n= 3).*

3.3.4. Cellular uptake and translocation of Cu across the intestinal monolayer

A concentration and time dependent decrease in the concentration of Cu was observed in the AP compartment of differentiated Caco-2 cells 24 h post exposure with CuO NMs and $CuSO_4$ (Figure 3.7A). Approximately, 87 to 96 % of the initial treatment concentration was detectable in the media of the AP compartment after 24 h treatment with 3.17 Cu µg/cm^2 of CuO NMs and $CuSO_4$, which declined to about 77 to 85 % at 48 h post exposure. At the highest treatment concentration (12.68 Cu µg/cm^2) of CuO NMs and $CuSO_4$, the detectable Cu concentration in the media of the AP compartment was between 58 to 61 % of the initial treatment concentration 24 h post exposure and the detectable concentration further decreased to 27 to 29 % after 48 h post exposure (Figure 3.7A).

The concentration of Cu in the BL compartment increased in a time and concentration dependent manner, which was suggestive of Cu translocation across the intestinal barrier. The concentration of Cu was lowest in the BL media when cells were exposed to 3.17 Cu µg/cm^2 CuO NMs and $CuSO_4$ 24 h post exposure, and greatest for cells exposed to CuO NMs and $CuSO_4$ at the highest concentration of 12.68 Cu µg/cm^2 at longest time point of 48 h. A significantly higher translocation of Cu was observed after 48 h for $CuSO_4$ compared to 24 h post exposure at both concentrations (3.17 and 6.34 Cu µg/cm^2) (Figure 3.7B). The level of translocated Cu from AP to BL compartment was highest at a concentration of 12.68 Cu µg/cm^2 for both CuO NMs and $CuSO_4$ compared to all other treatment concentrations at both 24 and 48 h post exposure. The cellular retention of CuO NMs or $CuSO_4$ was very low (< 3 % of the initial exposure concentration) at 24 and 48 h, for all the tested concentrations with only cells exposed to $CuSO_4$ 6.34 Cu µg/cm^2 for 48 h having significantly higher uptake compared to 24 h post exposure (Figure 3.7C). Cu was not detected in the untreated control. No significant difference was observed in transport and uptake of CuO NMs and $CuSO_4$ at 24 and 48 h post exposure (Figure 3.7C).

Expression of the data to obtain an apparent permeability coefficient (P_{app}) demonstrated a time and concentration dependent increase in permeability following exposure of differentiated Caco-2 cells to CuO NMs and $CuSO_4$. A significant increase in P_{app} (indicative of an increase in permeability) was observed after exposure of differentiated Caco-2 cell monolayer with 12.68 Cu µg/cm^2 of CuO NM and $CuSO_4$ for 24 and 48 h.

The permeability of the monolayer increased over time, as was an enhanced P_{app} value at 48 h post exposure compared to 24 h (Figure 3.8).

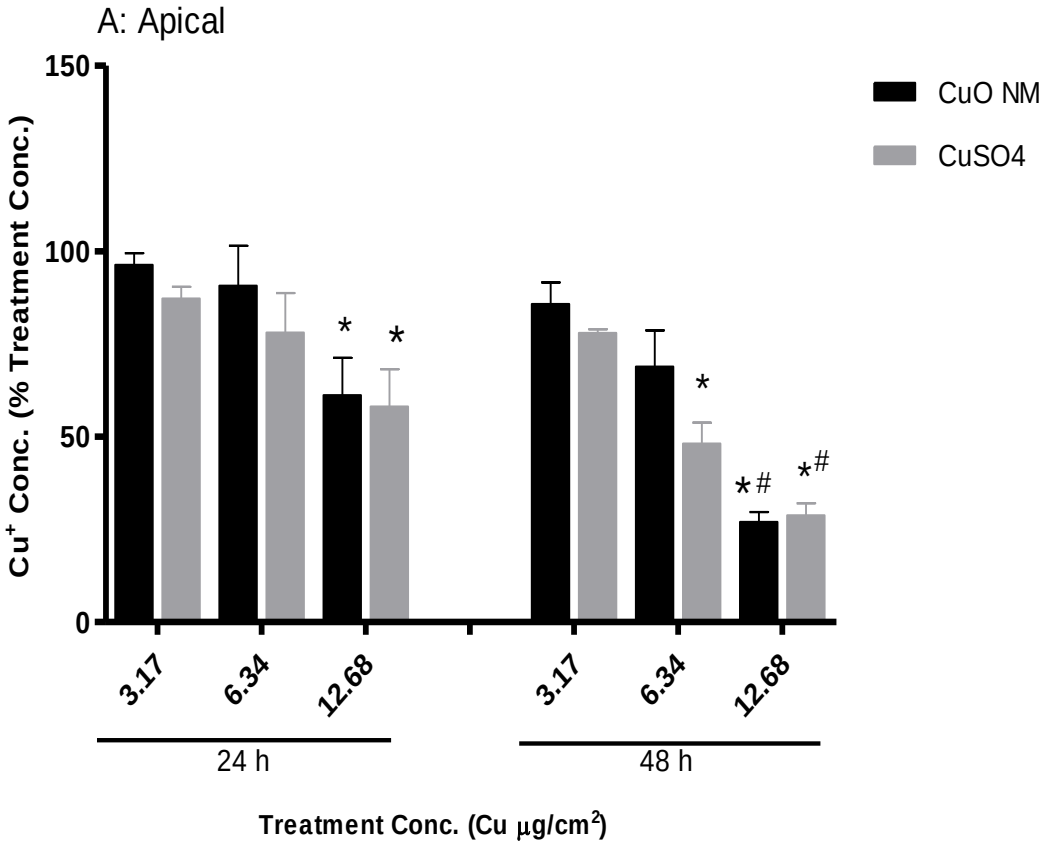

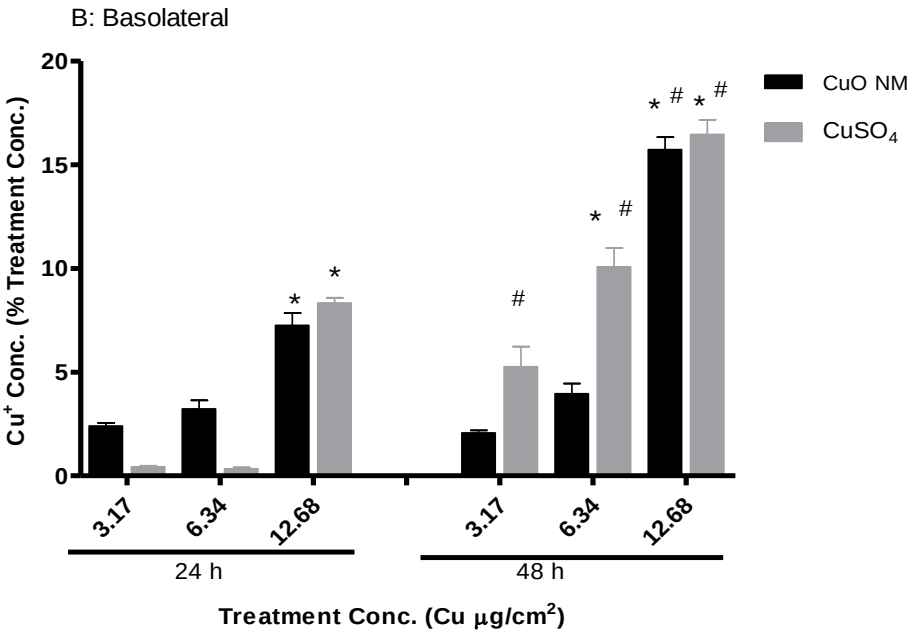

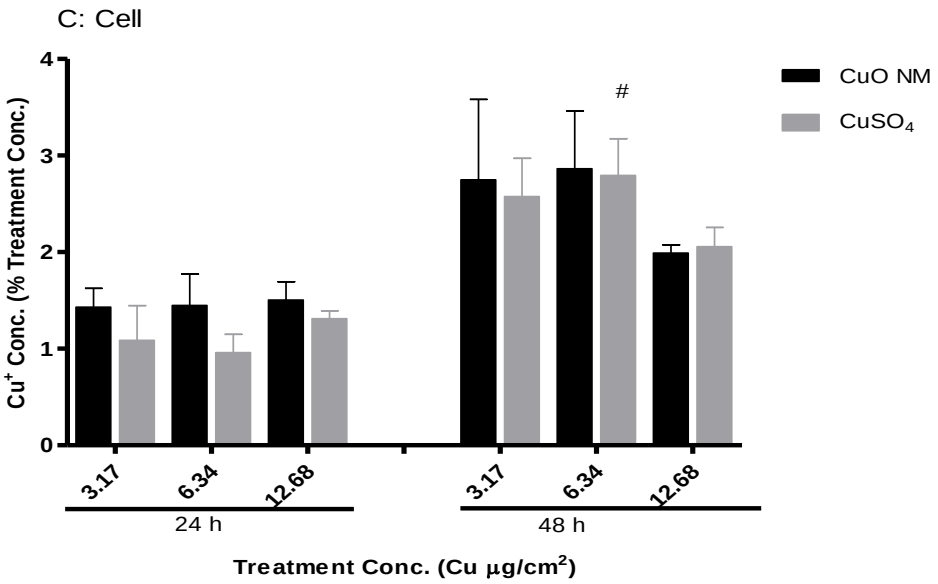

Figure 3.7: CuO NMs or $CuSO_4$ cellular uptake and translocation across differentiated Caco-2 cells.

*Differentiated Caco-2 cells were exposed to cell culture medium (control, 0), CuO NMs or $CuSO_4$ at concentrations of 3.17, 6.34 or 12.68 Cu µg/cm^2 for 24 and 48 h. The level of Cu in the AP (A), BL (B) compartments and the cells (C) was evaluated by ICP-OES. Sample preparation and data analysis was performed by Victor Chibueze Ude and Dr. Lorna Eades performed the ICP-OES analysis. Data are expressed as mean copper concentration (as a percentage of the treatment concentration) ± SEM (n = 3). Significance at P<0.05 are indicted by * for comparison of 24 h post exposure of 3.17 Cu µg/cm^2 of CuO NMs to other treatment concentration within each time point or # for comparison of equivalent concentrations between 24 and 48 h time points.*

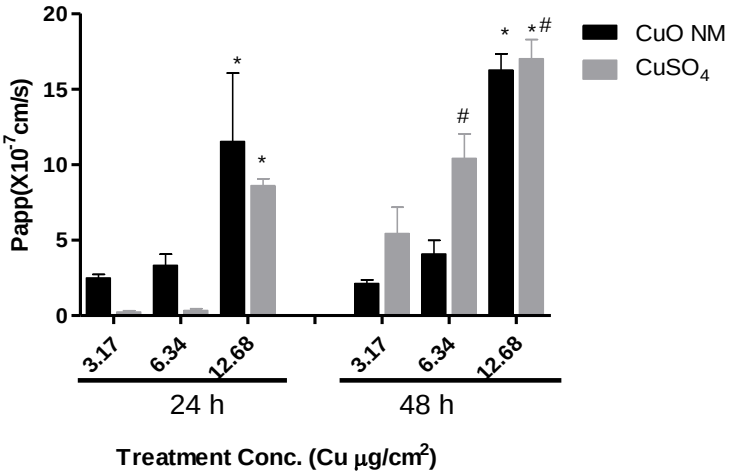

Figure 3.8: Apparent permeability coefficient (P_{app}) of CuO NMs and $CuSO_4$.

*Cells were exposed to cell culture medium (control, 0), CuO NMs or $CuSO_4$ at concentrations of 3.17, 6.34 or 12.68 Cu µg/cm^2 for 24 and 48 h. The concentration of Cu in the AP and BL compartment were determined by ICP-OES and P_{app} was calculated. Data are expressed as the mean P_{app} ± SEM x10^{-7} cm/s (n = 3). Significance at P<0.05 are indicted by * for comparison of 24 h post exposure of 3.17 Cu µg/cm^2 of CuO NMs to other treatment concentration within each time point or # for comparison of equivalent concentrations between 24 and 48 h time points.*

3.3.5. ROS formation

The level of ROS formation by differentiated Caco-2 cells after exposure to CuO NMs and $CuSO_4$ was determined using the DCFH-DA assay 2 h post exposure. $CuSO_4$ showed a concentration dependent increase in ROS generation (Figure 3.9). ROS production after exposure of cells to $CuSO_4$ was significantly higher than that stimulated by the negative control, positive control and CuO NMs. Although the level of ROS formation after exposure to positive control (1 mM H_2O_2) was higher than the cells treated with cell culture medium (negative control) the finding was not significant. No significant increase in ROS production was observed following exposure of cells to CuO NMs.

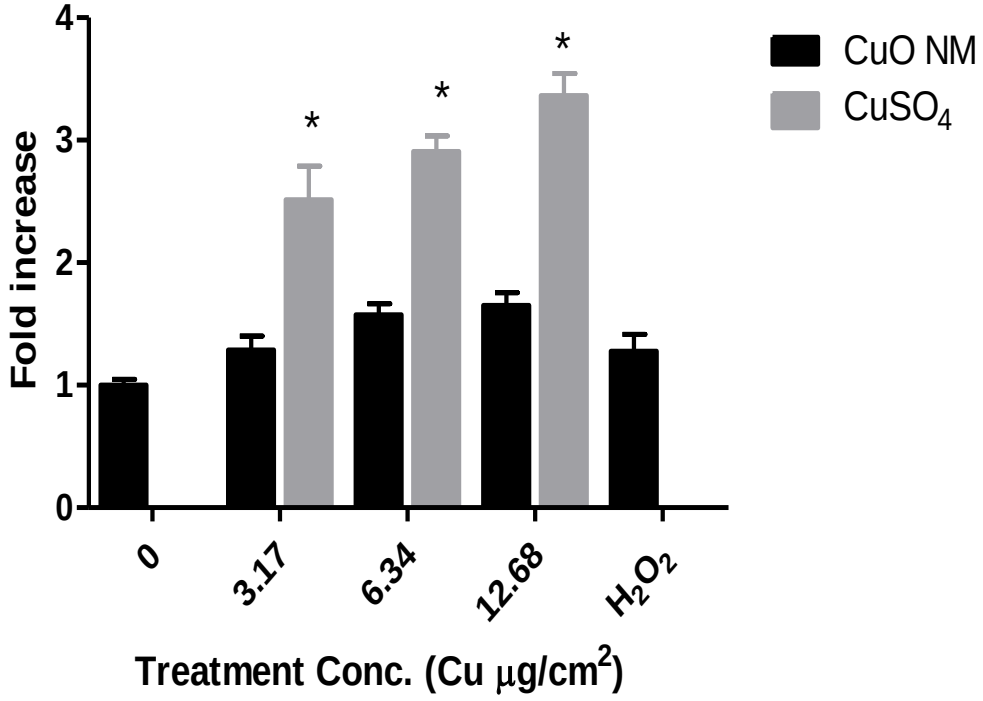

Figure 3.9: ROS formation by differentiated Caco-2 cells following exposure to CuO NMs and $CuSO_4$ at 2 h.

*Intracellular ROS levels were determined using the DCFH-DA assay 2 h post exposure of differentiated Caco-2 cells to CuO NMs and $CuSO_4$ at concentrations of 3.17, 6.34 and 12.68 Cu μg/cm^2. Data are expressed as the fold change in ROS production ± SEM (n = 3). Significance at $P<0.05$ is indicated by * compared to control.*

3.3.6. Cytokine production

For the selection of relevant cytokines secreted by differentiated Caco-2 cells, a proteome profiler was used as it is capable of screening up to 37 cytokines at a time. As observed for undifferentiated Caco-2 cells (section 2.3.5) IL-8 and ICAM-1 production was increased following exposure of differentiated Caco-2 cells to CuO NMs. IL-8 was prioritised because it is a known cytokine involved in inflammatory response to NMs, while ICAM-1 is secreted by all adherent cells and this was confirmed by equal intensity of spot on both CuO NMs and cell culture medium (control) exposed cells (Figure 3.10). CuO NMs and $CuSO_4$ demonstrated a significant increase in IL-8 production following

exposure of differentiated Caco-2 cells to CuO NMs and $CuSO_4$ at concentrations of 3.17, 6.34 and 12.68 Cu/µg cm^2 for 24 and 48 h compared to the control (Figure 3.11). No significant difference was observed in IL-8 production between CuO NMs and $CuSO_4$ treated differentiated Caco-2 cells, and no difference was observed between time points. IL-8 production was highest at 48 h post exposure to 3.17 Cu µg/cm^2 CuO NMs (421 pg/ml) and 24 h post exposure of 6.34 Cu µg/cm^2 $CuSO_4$ (451 pg/ml) IL-8 secretion was below the detectable level in the supernatant collected from the BL compartment of the exposed cells for all treatments, and in both the AP and BL compartment of the control group (data not shown). A concentration of 89.60 ± 4.77 pg/ml of IL8 was detected after treatment of differentiated Caco-2 cell with 200 ng/ml TNF-α (positive control) for 24 h.

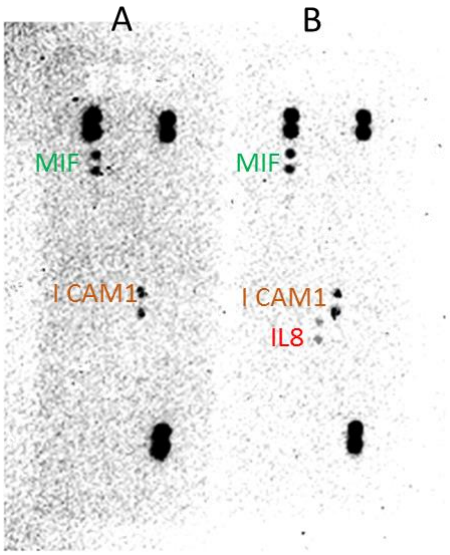

Figure 3.10: Assessment of Cytokine expression by differentiated Caco-2 cells using proteome profiler.

Cells were exposed to cell culture medium (control, 0, A), or 6.34 Cu µg/cm^2 of CuO NMs (B) for 24 h. Cytokines in the supernatant were detected using a human cytokine array kits. Double dots represent a different cytokine and only MIF, ICAM-1 and IL-8 were detected.

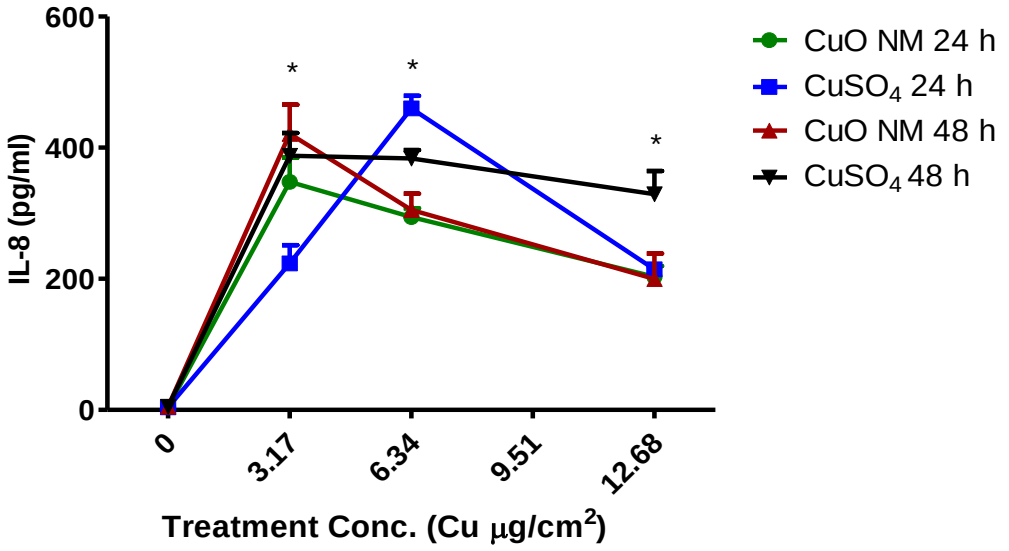

Figure 3.11: IL-8 production by differentiated Caco-2 cells following exposure to CuO NMs and $CuSO_4$.

*Cells were exposed to cell culture medium (control, 0), CuO NMs or $CuSO_4$ at concentrations of 3.17, 6.34 or 12.68 Cu μg/cm^2 for 24 or 48 h. The level of IL-8 in the cell supernatant was determined using an ELISA kit. Data are expressed as mean IL-8 concentration (pg/ml) ± SEM (n = 3). * indicates significance at P<0.05 compared to control.*

3.3.7. Gene expression

Exposure of differentiated Caco-2 cells to CuO NMs and $CuSO_4$ elicited a concentration and time dependent increase in *HMOX1* expression (Figure 3.12A). Expression of *HMOX1* was greatest at 4 h post exposure at a concentration of 12.68 Cu μg/cm^2 for both CuO NMs and $CuSO_4$. At 4 h post-exposure, the expression of *HMOX1* significantly increased (4 to 12 fold) at all concentrations compared to control. *HMOX1* expression was significantly increased after 12 and 24 h exposure of differentiated Caco-2 cells to higher concentrations of CuO NMs and $CuSO_4$ (6.34 and 12.68 Cu μg/cm^2) compared to control with the fold increase ranging from 4 to 13 fold (Figure 3.12A).

Expression of *IL8* by differentiated Caco-2 cells was increased in a concentration and time dependent manner (Figure 3.12B). No significant increases in *IL8* expression were observed at the lowest concentrations of CuO NMs and $CuSO_4$ (3.17 Cu μg/cm^2) at all the time points investigated (Figure 3.12B). CuO NMs and $CuSO_4$ (6.34 and 12.68 Cu μg/cm^2) induced a significant increase in *IL8* expression compared to control at 12 and

24 h post exposure with the fold change of between 4 and 12 (Figure 3.12B). The greatest expression was observed at 24 h post exposure (Figure 3.12B).

Differentiated Caco-2 cells demonstrated a time and concentration dependent increase in the expression of *MT1A* after exposure to CuO NMs and $CuSO_4$ (Figure 3.12C). Expression of *MT1A* was greatest at 24 h post exposure with a significant increase in expression observed at all concentrations. A significantly higher level of *MT1A* expression was also observed 4 and 12 h at concentrations of 6.34 and 12.68 Cu μg/cm^2 of CuO NMs and $CuSO_4$, with the fold increase ranging from 13.5 to 23. *MT2A* was the greatest expressed among all the genes assessed. The expression of *MT2A* by differentiated Caco-2 cells was significantly elevated at all time points and concentrations compared to control with the fold increase ranging from 11 to 116 fold (Figure 3.12E). The highest level of expression of *MT2A* was observed on cells exposed to CuO NMs and $CuSO_4$ for 12 h while there was no significant difference observed in *MT2A* expression between cells exposed to CuO NMs and $CuSO_4$ for 4 and 24 h.

MUC2 expression significantly increased at all concentrations after exposure of differentiated Caco-2 cells to CuO NMs and $CuSO_4$ for 24 h (Figure 3.12D). The greatest increase was observed at 24 h, with all concentration stimulating a significant increase in *MUC2* expression, with the fold increase ranging between 8 and 28 (Figure 3.12D). At shorter time points (4 and 12 h) the increase in *MUC2* expression was not significantly different compared to control, except for cells treated with 3.17 Cu μg/cm^2 CuO NMs and $CuSO_4$ for 4 h and 12.68 Cu μg/cm^2 12 h (Figure 3.12D) with fold increase of 3.4, 4.5 and 4.2 respectively. For all genes, there was no difference between the response stimulated by CuO NMs and $CuSO_4$. A heatmap, which provides a summary of the impact of CuO NMs and $CuSO_4$ on gene expression by differentiated Caco-2 cells is presented in figure 3.13. Overall, *MT2A* exhibited the strongest response compared to other genes. In general, the highest level of gene expression was observed at 24 h.

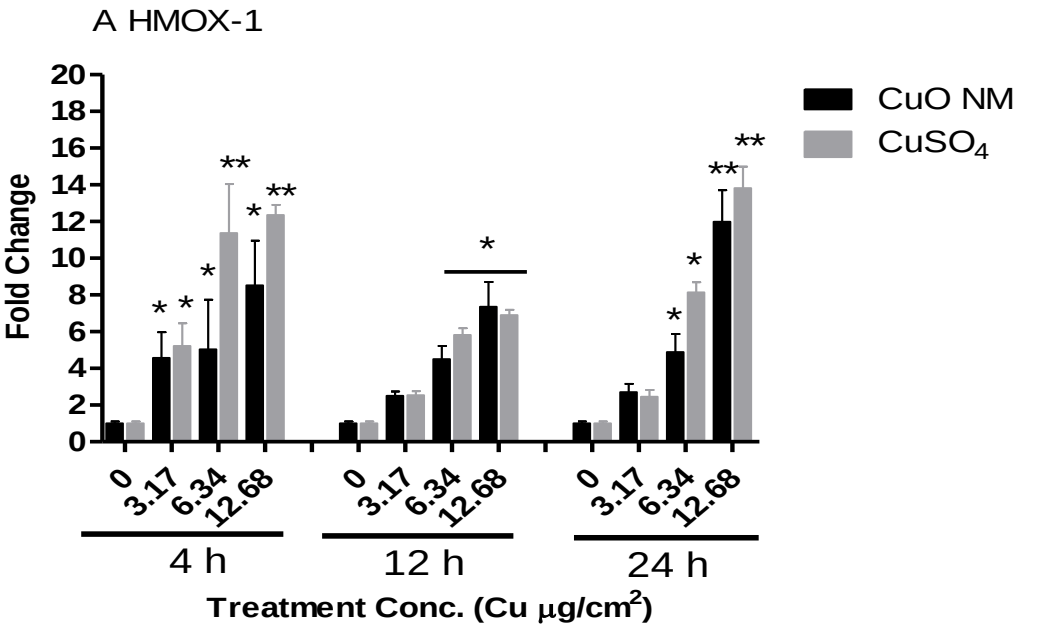
A HMOX-1
Fold Change
CuO NM
CuSO4
0
3.17
6.34
12.68
4 h
12 h
24 h
Treatment Conc. (Cu μg/cm2)

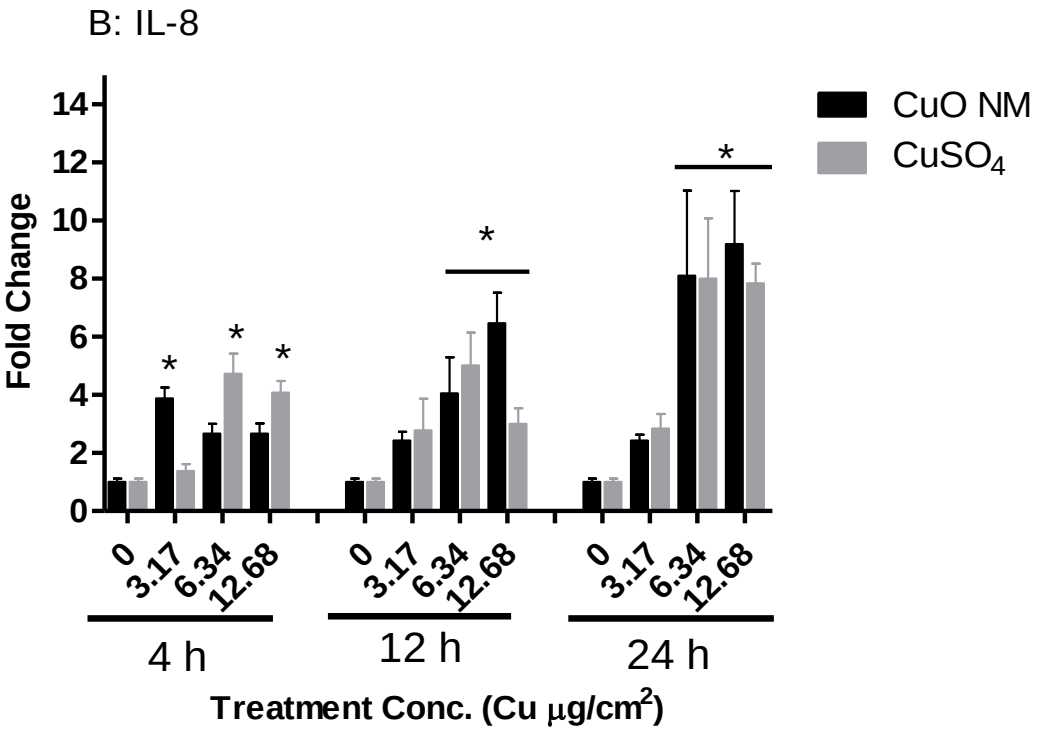
B: IL-8
Fold Change
CuO NM
CuSO4
0
3.17
6.34
12.68
4 h
12 h
24 h
Treatment Conc. (Cu μg/cm2)

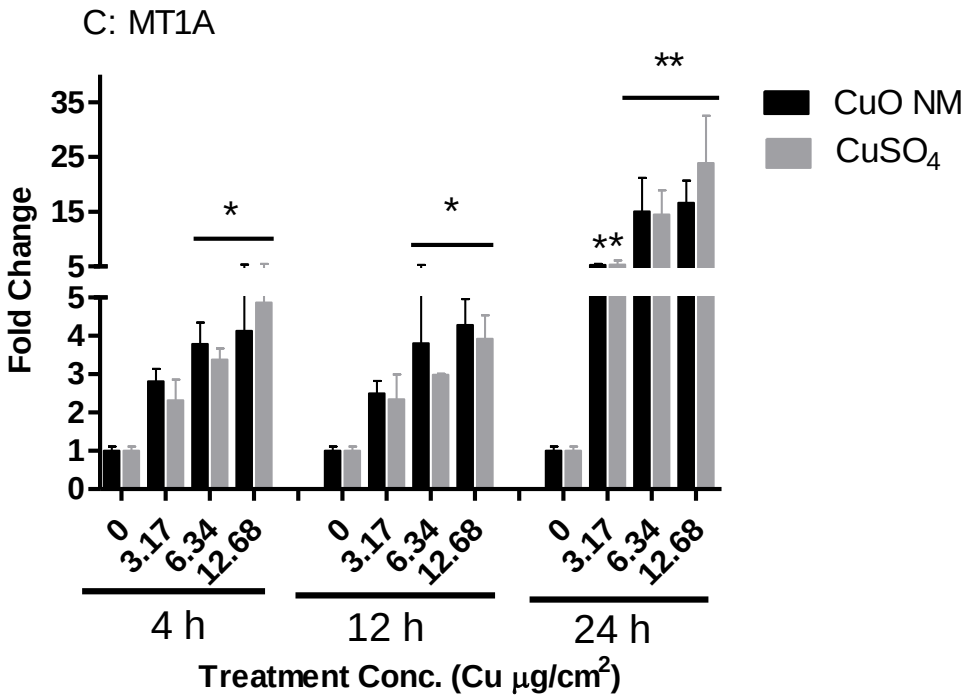
C: MT1A
CuO NM
CuSO4
Fold Change
35
25
15
5
5
4
3
2
1
0
*
*
**
**
0
3.17
6.34
12.68
4 h
12 h
24 h
Treatment Conc. (Cu μg/cm2)

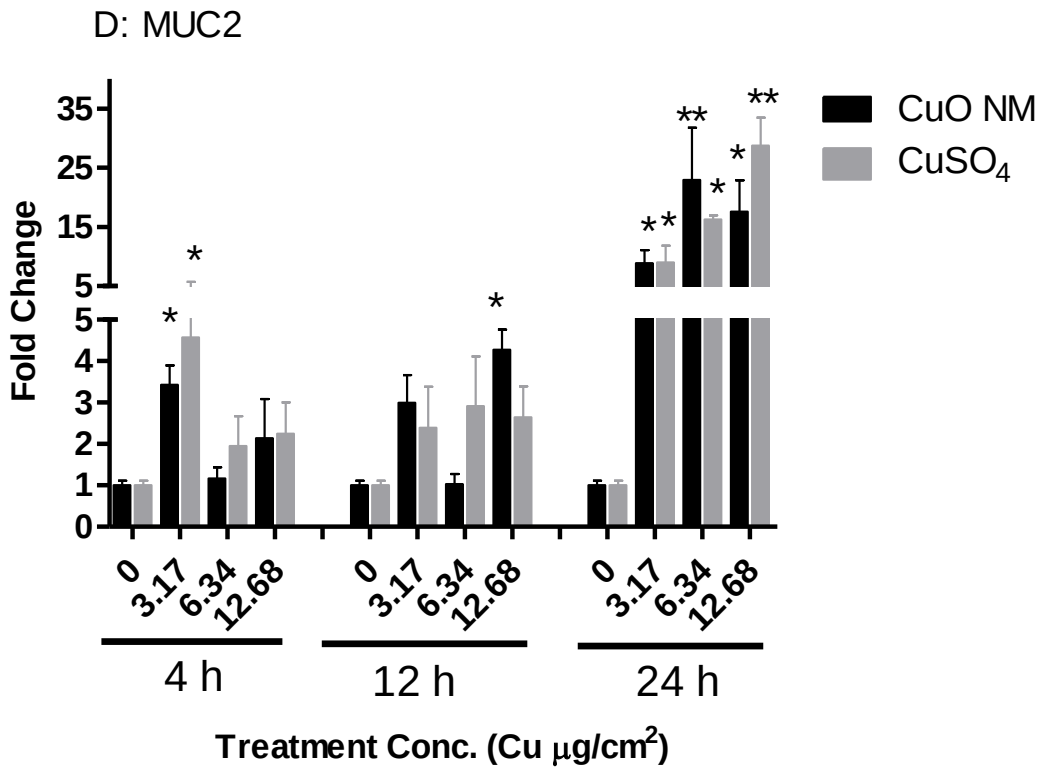
D: MUC2
CuO NM
CuSO4
Fold Change
35
25
15
5
5
4
3
2
1
0
*
*
*
*
**
**
*
0
3.17
6.34
12.68
4 h
12 h
24 h
Treatment Conc. (Cu μg/cm2)

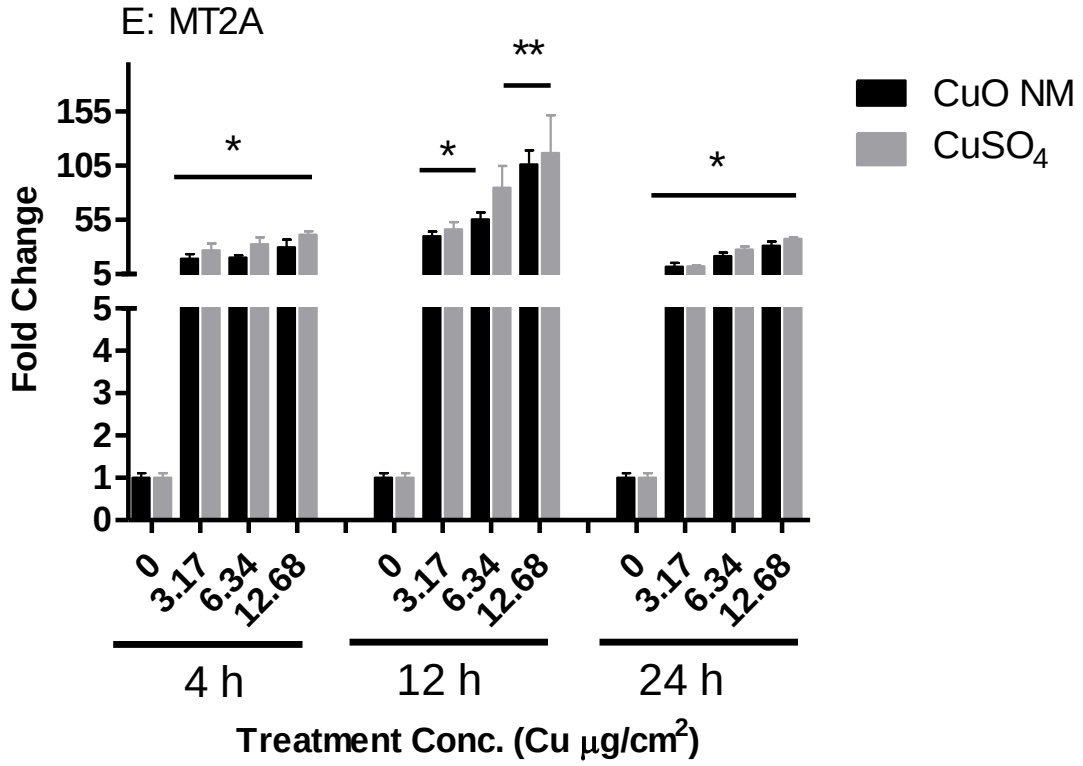

Figure 3.12: Effect of CuO NMs and $CuSO_4$ on differentiated Caco-2 cell gene expression.

*Differentiated Caco-2 cells were exposed to cell culture medium (control, 0), CuO NMs or $CuSO_4$ at concentrations of 3.17, 6.34 or 12.68 Cu μg/cm^2 for 4, 12 and 24 h and changes in A) HMOX1, B) IL8, C) MT1A, D) MUC2, E) MT2A expression assessed using qPCR. Data are expressed as mean fold change (compared to the control) ± SEM (n = 3). Significance indicated by * = P<0.05 and ** = P<0.01 compared to control.*

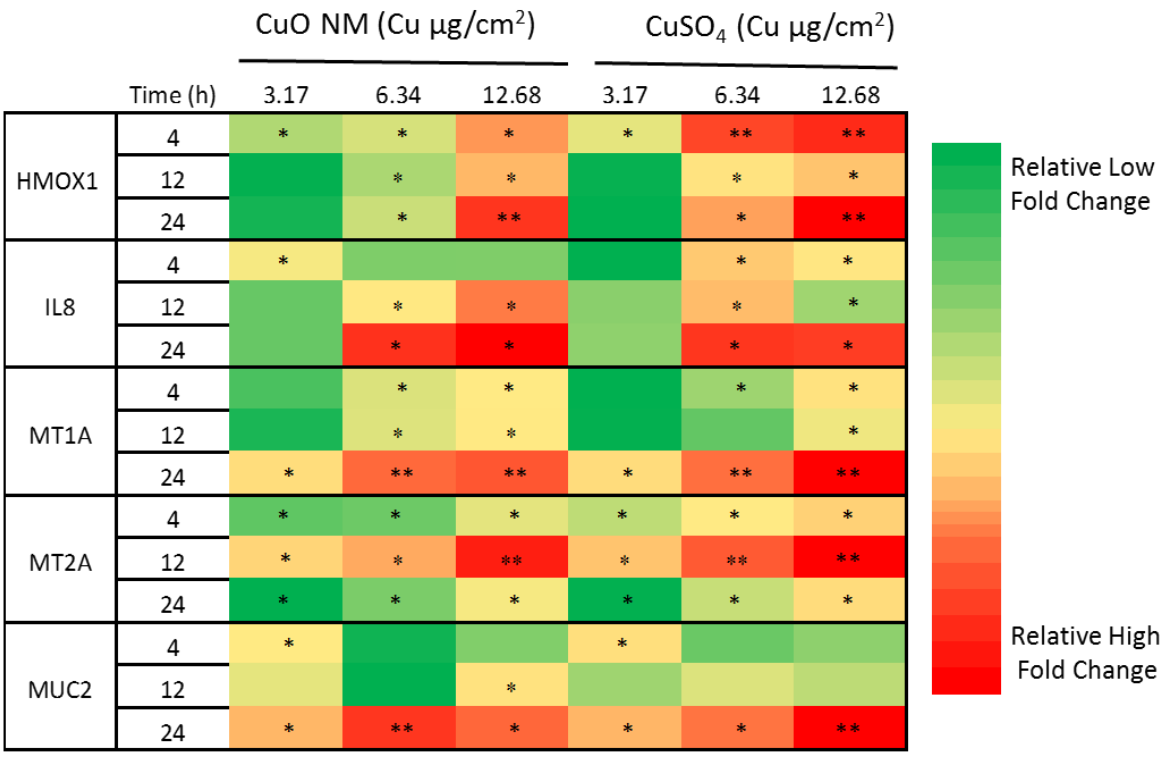

Figure 3.13: Heatmap representation of gene expression in differentiated Caco-2 cells after exposure to CuO NMs and $CuSO_4$.

*Differentiated Caco-2 cells were exposed to cell culture medium (control, 0), CuO NMs or $CuSO_4$ at concentrations of 3.17, 6.34 or 12.68 Cu µg/cm² for 4, 12 and 24 h and expression of A) HMOX1, B) IL8, C) MT1A, D) MUC2, E) MT2A assessed using qPCR. Genes were compared separately for significance. Significance indicated by * = P<0.05 and ** = P<0.01 compared to control.*

3.4. Discussion

In this chapter, the impact of CuO NMs and $CuSO_4$ on differentiated Caco-2 cells, was assessed via investigation of cell viability (nuclei count, light microscopy and SEM), ROS formation, cytokine production, cell morphology (via light microscopy) and barrier integrity (SEM, and ZO-1 staining) The translocation of Cu across the intestinal monolayer was also reported. According to the assays used, there was no significant cell death caused by the concentrations of CuO NMs and $CuSO_4$ tested at 24 and 48 h. However, CuO NMs and $CuSO_4$ caused barrier integrity dysfunction as evidenced via a reduction in TEER measurement and reduction in tight junction protein (ZO-1) staining Shortening of microvilli was also observed, indicating an impact on cell morphology. IL-

8 protein secretion was increased, which suggests that CuO NMs and $CuSO_4$ can stimulate an inflammatory response. Only $CuSO_4$ stimulated intracellular ROS formation. Expression of *HMOX1*, *IL8*, *MUC2*, *MT1A* and *MT2A* were upregulated. A concentration and time dependent translocation of Cu was also observed suggesting that CuO NMs and $CuSO_4$ may penetrate the intestinal barrier. For all the investigated endpoints, CuO NMs and $CuSO_4$ demonstrated a similar effect, except ROS formation.

3.4.1. Barrier integrity and cytotoxicity

The differentiation status of Caco-2 cells was monitored via measurement of TEER and confirmed using assessment of tight junction protein (ZO-1) staining and visualisation of the presence of microvilli with SEM in this study. Interestingly, the majority of studies, which assess Caco-2 differentiation in the published literature, rely on TEER measurements (Piret et al. 2012b, Nishitani et al. 2013, Susewind et al. 2016). By using a combination of approaches, it was possible to confirm the differentiation status of Caco-2 cells. It is recommended that TEER should be measured at least twice every week starting from the second week post seeding when culturing differentiated Caco-2 cells as it technically easier and cheaper than other approaches for assessing barrier integrity. Previous studies have used TEER measurement to monitor Caco-2 cell differentiation and to assess the impact of NM exposure to differentiated Caco-2 cell barrier integrity (Piret et al. 2012b, Nishitani et al. 2013, Susewind et al. 2016). However, their studies differ from this research as they only measured the impact of the NMs on TEER at 24 h post exposure whereas this study assessed impacts on TEER over time. Of benefit is that within one experiment multiple measurements of TEER can be made. In this study, it was revealed that TEER values decreased from 9 h post exposure indicating that an earlier measurement of toxicity could be made. It is therefore, recommended that future studies also monitor TEER over time when using differentiated Caco-2 cells to assess the toxicity of NMs in order to maximise the amount of information obtained from each experiment.

To further investigate the impact of CuO NMs and $CuSO_4$ on barrier integrity, differentiated Caco-2 cells treated with CuO NMs and $CuSO_4$ were stained for tight junction proteins (ZO-1). A reduction in tight junction staining in cells exposed to CuO NMs and $CuSO_4$ at 24 h confirmed the findings obtained from the TEER measurement. In addition, the shortening of the microvilli observed on some of the cells, as observed by

SEM, corroborated these findings. Loss of microvilli after food grade TiO_2 exposure to differentiated Caco-2 cells has been reported previously (Faust et al. 2014a, Koeneman et al. 2010). Other studies have demonstrated that NMs (e.g. Ag NMs, 20 nm) can impair barrier integrity (via assessment of TEER and ZO-1 staining) when differentiated Caco-2 cells have been used to assess NM toxicity (Martirosyan et al. 2012). Impairment of barrier integrity by NMs could have several implications for the function of the intestine. For example, it could enhance permeability to NMs to increase their translocation into the systemic circulation, increase microbial permeability and reduce nutrient absorption.

Since CuO NMs are known to interfere with the LDH assay (which uses the cell supernatant to assess cytotoxicity) (Han et al. 2011) and the transwell inserts used to culture differentiated cells are not compatible with the microplate reader, it was not possible to perform many biochemical assays that assess cell viability (e.g. Alamar blue assay). Thus, it was more challenging to use differentiated Caco-2 cells to evaluate NM mediated cytotoxicity. Assessment of cell morphology using light microscopy, and nuclei staining with DAPI to count cell number were employed to assess the viability of differentiated Caco-2 cells following NM exposure. Unlike the undifferentiated Caco-2 cells (Figure 2.3 and 2.4, Chapter 2), there was no loss of differentiated Caco-2 cells post exposure to CuO NMs, suggesting that the cells were viable. The SEM imaging also confirm that the cells were intact, suggesting the concentration and time point used for this experiment are non-toxic. A limited range of concentrations was studied in the differentiated cells. However, a concentration and time response experiment was not performed due to cost and insufficient time, but exposure to higher concentrations may have stimulate cytotoxic effect. Therefore, it suggests that undifferentiated cells may overestimated NM toxicity, and this may be because differentiated cells better mimic the robust nature of human intestine *in vivo* compared to the undifferentiated cells.

3.4.2. Translocation and cellular uptake

The bioavailability of NMs *in vivo* post oral exposure is a function of the physicochemical properties of the NMs including size, charge, time and the experimental set up (e.g. dose, time point) (Walczak et al. 2015b, Bellmann et al. 2015, Schleh et al. 2012, Kreyling et al. 2017, Lee et al. 2012). Several *in vivo* studies have therefore demonstrated that ingested NMs can penetrate the intestinal barrier and enter the circulation to become

distributed in the body (primarily the liver) (Schleh et al. 2012, Kreyling et al. 2017). In addition, polystyrene (50 nm) have been shown to cross the intestinal barrier *in vivo* (Walczak et al. 2015a). The level of penetration of NMs *in vivo* is low (typically <2 %). No studies were identified which investigated CuO NM translocation across the intestinal barrier *in vivo*. Differentiated Caco-2 cells have been commonly used as an *in vitro* model for the investigation of the translocation of pharmaceuticals and pathogens (Lubelska et al. 2012, Hubatsch et al. 2007, Lihua Chen et al. 2016). The transport of NMs (CuO and polystyrene) across the intestinal barrier has been investigated in vitro using differentiated Caco-2 cells (e.g. Chen et al. 2015, Walczak et al.2015b), with comparative studies demonstrating that the use of differentiated Caco-2 cells overestimates NM transport observed *in vivo* (e.g. Walczak et al. 2015a). Apart from studies carried out with *ex vivo* intestinal tissue (Brun et al. 2014) and Caco-2 co-culture models (Brun et al. 2014, Walczak et al. 2015b, Bouwmeester et al. 2011), only one research study has investigated the translocation of CuO NMs using differentiated Caco-2 cells (Chen et al. 2015). More specifically, Chen et al. (2015) assessed the concentration of Cu in the BL compartment only and used this information to identify the P_{app} value. In this thesis, the concentration of Cu in AP and BL compartments and cells was assessed, and the P_{app} value quantified to provide a more comprehensive assessment of Cu transport across the intestinal barrier.

Translocation of CuO NMs and $CuSO_4$ across the differentiated Caco-2 cell intestinal barrier occurred in a concentration and time dependent manner. Cu transport is likely to occur because of a compromise in the integrity of differentiated Caco-2 barrier by CuO NMs and $CuSO_4$ (see section 3.3.1), which enhance the paracellular transport of NMs and ions. A concentration and time dependent transport was observed at 3 h post exposure of differentiated Caco-2 cells to CuO NMs with the translocated concentration being ~1 % (Chen et al. 2015). Summation of copper concentration in the AP and BL compartments as well as the cells added up to approximately 100 % of the exposure concentration at the lowest concentration (3.17 Cu µg/cm^2) of CuO NMs and $CuSO_4$. Whereas at higher concentrations (6.34 and 12 .68µg/cm^2) of CuO NMs and $CuSO_4$, Cu was not completely recovered. The inability to recover Cu at 100 % may be attributed to increased activation of synthesis of thiol containing proteins including metallothionein proteins, which chelate Cu (Gaetke et al. 2014, Letelier et al. 2005), which is confirmed by the high expression of *MT2A* (section 3.3.7). Furthermore, reports have shown that metal ions may be lost as

a result of binding to materials used for cell culture and for the transport experiment (Malysheva et al. 2016, Sekine et al. 2015) such as cell culture plates and the insert polycarbonate membranes thereby preventing 100 % detection. In addition, as the cell monolayers are washed with PBS after removal of AP medium, and before cell digestion some of the NMs and ions may be lost at this stage.

Translocation of orally absorbed pharmaceuticals and xenobiotics in drug discovery are often predicted using P_{app} measurements *in vitro* and *ex vivo* (Hubatsch et al. 2007). The mechanism of translocation of substances across the intestinal barrier is likely to be via passive diffusion if the P_{app} values remain constant despite an increase in the concentration of the substance in the apical compartment (Chen et al. 2015). It has also been reported that when P_{app} values are less than $1x10^{-6}$ cm/s malabsorption is implicated in drug development whereas P_{app} values greater than 10 $x10^{-6}$ cm/s represent good absorption (Yee 1997, Walter et al. 1996). Interestingly, the P_{app} values of differentiated Caco-2 cells treated with all concentrations of CuO NMs and $CuSO_4$ for 24 h were less than $1x10^{-6}$ cm/s and were greater when exposed to 6.34 and 12.68 Cu µg/cm^2 $CuSO_4$ and 12.68 Cu µg/cm^2 of CuO NMs. This suggests that both CuO NMs and $CuSO_4$ are generally malabsorbed (i.e. translocation across the intestinal barrier is very slow) at lower concentrations and at the 24 h time point. This implies that translocation of CuO NMs or $CuSO_4$ is mediated by mostly tight junction stress and dysfunction. In comparison, the P_{app} value for CuO NMs or $CuSO_4$ at 24 and 48 h were greater than the P_{app} value obtained for mannitol (~5.0×10^{-7} cm/s) (Ferruzza et al. 2012b), which suggests that compromise to the intestinal barrier caused by CuO NMs was responsible for the translocation. The translocated CuO NMs and $CuSO_4$ in this study were greater than the *in vivo* studies with rats using Au (1.4-18 nm) (Schleh et al. 2012) and TiO_2 NMs (50 nm) (Kreyling et al. 2017) suggesting that NMs translocation may be overestimated using differentiated Caco-2 cells. The difference between these studies and this present study may be that CuO NMs is soluble whereas TiO_2 and Au NMs are not. However, *in vivo* studies for CuO NMs would be required to confirm this. CuO NMs uptake by cells was low (<3 %). Uptake was measured using ICP-OES, which does not differentiate particle and ion and was not confirmed by microscopy but should be performed in future.

3.4.3. ROS formation

It is established that NM toxicity can occur via an oxidant driven mechanism (Johnston et al. 2010, Fu et al. 2014, Abdal Dayem et al. 2017, Onodera et al. 2015, Abbott Chalew and Schwab 2013). However, only one published paper was identified, which has used differentiated Caco-2 cells to study the impact of Ag NMs on ROS formation (Georgantzopoulou et al. 2016), and no existing studies have used differentiated Caco-2 cells to study ROS production by CuO NMs. Hence, this study has addressed a gap in knowledge. $CuSO_4$ produced approximately double the level of ROS observed for CuO NMs. At the concentrations and time point (2 h) tested, CuO NMs did not stimulate ROS production. Only limited concentrations and time points were investigated in this study for time and financial reasons. Therefore, future studies could assess a wider range of NM concentrations and time points to provide a more comprehensive assessment of the contribution of ROS to CuO NM toxicity to differentiated Caco-2 cells. Transition metal ions are known to produce ROS via Fenton chemistry (Birben et al. 2012, Kleczkowski et al. 2002). Therefore the explanation for why ROS production by $CuSO_4$ was greater than that observed for CuO NMs could be that the CuO NMs are not completely soluble at 2 h post exposure (Ude et al. 2017). It is imperative to note here that the level of ROS produced by undifferentiated Caco-2 cells (section 2.3.4.2) were significantly higher than that of differentiated Caco-2 cells (section 3.3.5). This could be because differentiated Caco-2 cells are a more robust intestinal-like enterocyte and are less sensitive to NM toxicity compared to undifferentiated Caco-2 cells. Similar to our findings no ROS production was reported after exposure of differentiated Caco-2 cells to Ag NM (20 and 200 nm) to differentiated Caco-2 cells (Georgantzopoulou et al. 2016). Surprisingly, despite the lack of measurable ROS production the level of an antioxidant gene (*HMOX1*) was upregulated suggesting the involvement of oxidative stress in CuO NM toxicity. As described in chapter 2 (section 2.4.3) assessment of the glutathione depletion may be employed to better explain the involvement of oxidative stress in NM toxicity antioxidant levels in future.

3.4.4. IL-8 production

A concentration dependent increase in IL-8 production was observed in differentiated Caco-2 cells after exposure to CuO NMs and $CuSO_4$ with peak IL-8 production at 48 h

of exposure at a concentration of 3.17 µg cm^2 CuO NMs and after 24 h of exposure to $CuSO_4$ (6.34 µg cm^2). The earlier toxicity of $CuSO_4$ observed could be related to CuO NM solubility, as CuO NMs are unlikely to be fully dissolved at 24 h. It may also be due to NM interference as NM could bind to proteins preventing its detection. An increase in IL-8 secretion by differentiated Caco-2 cells has been reported after exposure to CuO NMs (15-20 nm) (Piret et al. 2012b), which was below the level detected in this present study. Furthermore, Gerloff and colleagues also reported an increase in IL-8 secretion after differentiated Caco-2 cells were exposed to ZnO NMs, with no response observed for SiO_2 NMs (Gerloff et al. 2013). In addition, 20 nm Ag NMs were shown to induce a significant increase in IL-8 compared to 200 nm in differentiated Caco-2 cells (Georgantzopoulou et al. 2016). IL-8 production was greater in undifferentiated Caco-2 cells compared to differentiated Caco-2 cells, which again suggests that use of differentiated cells may overestimate NM toxicity. Of the pro-inflammatory markers considered, only IL-8 was assessed as this cytokine was observed to be the most sensitive marker from the proteome profiler results. This corresponds with the published literature, in which IL-8 has most commonly been investigated. However, the proteome profiler result revealed that ICAM-1 secretion could also be assessed in future studies.

3.4.5. Gene expression

For undifferentiated Caco-2 cells (chapter 2), more time points were investigated and the findings informed the selection of time points for differentiated cells. Previously, researchers have studied the expression of *HMOX1* post exposure to Ag, ZnO, Au, and SiO_2 NMs using undifferentiated Caco-2 cells (Bajak et al. 2015, Ebabe Elle et al. 2016) and other cell types (A549, HCAECs, and Hela cells) (Sthijns et al. 2017, Yan et al. 2017, Miura and Shinohara 2009). For example, *HMOX1* expression was shown to increase in undifferentiated Caco-2 cells after exposure to Au (5nm) for 72 h (Bajak et al. 2015) but not SiO_2 post exposure for 24 h (Ebabe Elle et al. 2016). However, to date there are no published studies on the expression of *HMOX1* using differentiated Caco-2 cells. In the present study, CuO NMs and $CuSO_4$ stimulated a concentration and time dependent increase in *HMOX1* mRNA expression, which was lower than the level expressed by undifferentiated Caco-2 cells (section 3.3.5). The upregulation of the antioxidant *HMOX1* suggests that CuO NMs and $CuSO_4$ may stimulate an oxidant response in cells (Bansal et

al. 2014), however a more in depth investigation would be required to confirm the involvement of oxidative stress in CuO NM toxicity.

A concentration and time dependent significant increase in *IL8* expression was observed in differentiated Caco-2 cells in response to CuO NMs and $CuSO_4$, which was in accordance with the quantitative protein assay. A similar result was observed after treatment of differentiated Caco-2 cells with SiO_2 and ZnO NMs (Gerloff et al. 2013), suggesting that *IL8* is a good marker of NM toxicity for differentiated Caco-2 cells. *IL8* expression in differentiated Caco-2 cells was also lower than undifferentiated Caco-2 cell as was observed in protein secretion, again suggesting that undifferentiated Caco-2 cells may be more sensitive to NMs and can lead to an overestimation of impacts. As stated in section 2.4.5, MT have the capacity to detoxify metals and the ability to contain excess metal (Sahu et al. 2013). Binding of metal NMs to MTs may reduce their toxicity to cells. *MT1A* and *MT2A* demonstrated a concentration and time dependent increase in expression in differentiated Caco-2 cells following exposure to CuO NMs and $CuSO_4$. Existing studies have not investigated *MT* expression in differentiated Caco-2 cells following exposure to metal NMs. However, upregulation of *MT1X* and *MT2A* was also observed after exposure of HeLa and A549 cells with Ag NMs (Miura and Shinohara 2009, Miyayama and Matsuoka 2016), or with A549 and BEAS-2B cells with CuO NMs (Strauch et al. 2017). Whereas the highest expression was observed at 24 h post exposure for *MT1A, MT2A* expression was highest at 12 h post exposure and *MT2A* was significantly expressed at 4 h post exposure. This indicates that assessment of *MT2A* expression may be a sensitive indicator of NM toxicity.

A concentration and time dependent increase in *MUC2* expression was observed with differentiated Caco-2 cells. The increase in *MUC2* expression may be because *MUC2* expression increases after inflammation as a protective response (Cornick et al. 2015). For example, acetaldehyde has been shown to increase *MUC2* expression by intestinal goblet-like cells (LS174T) (Elamin et al. 2014). Overall, the results suggest that *HMOX1*, *IL8, MUC2, MT1A* and *MT2A* are sensitive markers of NM toxicity to the intestine *in vitro.*

3.5. Conclusions

CuO NMs and $CuSO_4$ demonstrated a markedly similar toxicity to differentiated Caco-2 cell. CuO NMs and $CuSO_4$ reduced the TEER value, ZO-1 staining intensity and shortened microvilli and thereby were observed to cause barrier integrity dysfunction. The compromise on monolayer integrity is likely to be responsible for the increased translocation of Cu across the intestinal monolayer for both treatments. CuO NMs and $CuSO_4$ also stimulated IL-8 secretion, and upregulated the expression of *HMOX1*, *IL8*, *MT1A, MT2A* and *MUC2*. ROS formation was greatest for $CuSO_4$. The similar toxic effect of CuO NMs and $CuSO_4$ is an indication that toxicity of CuO NMs was not only as a result of copper ion release, but a combination of both particles and ions. Obtained data demonstrate that differentiated cells are less sensitive to the toxicity of CuO NMs and $CuSO_4$ than undifferentiated cells. The results suggest that TEER measurement, tight junction protein staining, IL-8 production and gene expression (*HMOX1*, *IL8*, *MUC2* and *MT2A*) can be useful markers for investigating the toxicity of CuO NM in intestine using differentiated Caco-2 cells. The applicability of these markers to other NMs requires further investigation in the future.

CHAPTER 4: Impact of copper oxide NMs and copper sulphate on a Caco-2 and HT29-MTX co-culture-an intestinal mucus-secreting model

4.1. Introduction

The intestinal epithelium lined with mucus, which is secreted by the goblet cells and functions as a first line of defence against invading pathogens (Pelaseyed et al. 2014, Kim and Ho 2010). Mucus is also essential for digestion and absorption of food including egestion of undigested food, microorganisms and its by-products (Kim and Ho 2010). Mucus prevents infection and activation of inflammation, which could be damaging to the intestine by clearing and separating toxic materials such as pathogens from the epithelial cells to protect the intestinal epithelium (Hansson 2012). Mucus can enhance retention of substances in the intestinal lumen including NMs, which can be excreted with the mucus when the mucus layer are renewed, thereby preventing their interaction with the epithelial cells (Gamboa and Leong 2013). The secretory mucin glycoprotein (MUC2) is the largest component of the mucus in the intestine (Pelaseyed et al. 2014, Hansson 2012).

The human colon adenocarcinoma cell line (HT29) is frequently used as a cell line for mimicking mucus secretion *in vitro*. HT29 is derived from a primary tumour of a Caucasian woman aged 44 (Fogh and Trempe 1975), and is a mucus secreting cell line. Methotrexate (MTX) was used to transform HT29 cells to the HT29-MTX cell line (a mucus secreting cell). A monoculture of HT29 cells does not sufficiently mimic the human intestinal epithelium hence, a co-culture of Caco-2 and HT 29-MTX cells is used to solve this problem (Lefebvre et al. 2015). When co-cultured with differentiated Caco-2 cells a mucus layer forms within three to four weeks in culture, as muciporous goblets cells form (Sambuy et al. 2001).

Caco-2/HT29-MTX cells have been used to study the impact of the presence of mucus on intestinal transport of substances across the intestinal epithelium, since mucus is one of the essential protective barrier to pathogenic and particle uptake (Kavanaugh et al. 2013, Yuan et al. 2013, Martínez-Maqueda et al. 2015, Sigurdsson et al. 2013, Georgantzopoulou et al. 2016). It has been demonstrated previously that a co-culture of Caco-2 and HT 29-MTX cells develops a layer of mucus that is about 2-10 µm thick, and which is firmly bound completely covers the monolayer with the ability to withstand usual cell washing (Mahler et al. 2009). The development of Caco-2/HT29-MTX co-cultures has used several experimental approaches. For example, cells have been seeded at a ratio of 9:1, 8:2, 7:3 3:2 or 1:1 (of Caco-2:HT 29-MTX) (Georgantzopoulou et al.

2016, Mahler et al. 2009, Pan et al. 2015, Walczak et al. 2015b) into the AP chamber of a transwell membrane (Figure 4.1). Culturing of Caco-2 and HT29-MTX cells at a ratio of 9:1 has been demonstrated to develop a model with mucus secretion properties resembling that of the human intestine *in vivo* (Pan et al. 2015, Georgantzopoulou et al. 2016). As discussed previously, the integrity of the Caco-2 monolayer is ascertained using TEER measurement (Jepson 2012) and an increase in the ratio of HT29-MTX cell number in the co-culture decreases the TEER value (Gamboa and Leong 2013, Mahler et al. 2009). Therefore, there is the need to seed HT29-MTX cells at a concentration that will lead to mucus formation but still maintain the integrity of epithelium.

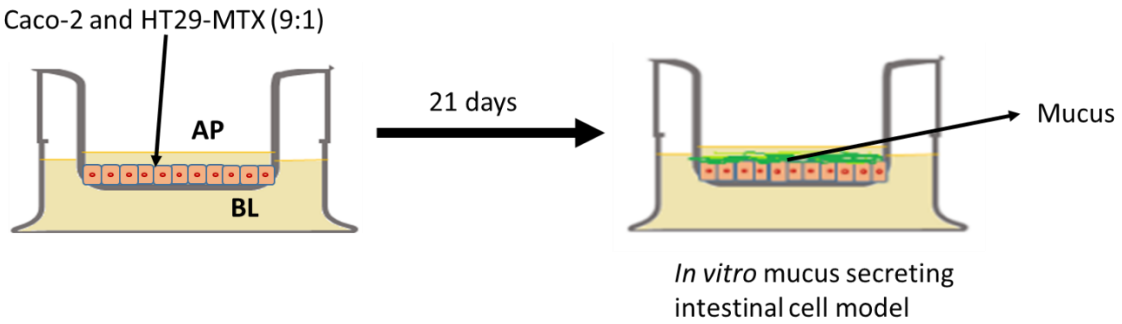

Figure 4.1: Schematic representation of mucus secreting co-culture model.

Caco-2 and HT29-MTX cells are seeded into the apical compartment of a transwell insert at ration of 9:1 and grown for 21 days. AP=apical, BL =basolateral.

Intestinal epithelial cells can produce mucin proteins. However, goblet cells are primarily responsible for mucus production, and there is evidence that mucin proteins MUC2 and MUC13 are expressed in the Caco-2/HT29-MTX co-culture (Navabi et al. 2013). It has been shown that exposure of acetaldehyde to human intestinal goblet-like (LS174T) cells led to increased MUC2 protein expression (Elamin et al. 2014). In addition, exposure of human bronchial ChaGo-K1 epithelial cells to TiO_2 NPs (<75 nm) stimulated mucin secretion (Chen et al. 2011). Mucin expression has not been quantified as a marker of NM toxicity in intestinal cell models to date. The Caco-2/HT29-MTX co-culture could represent a model of mucus secreting human intestinal epithelium for assessment of NM toxicity and transport.

Although the Caco-2 and HT29-MTX co-culture has been frequently used to investigate NM transport and toxicity (Walczak et al. 2015b, Lai et al. 2009, Akbari et al. 2017, Antunes et al. 2013, Araújo et al. 2014, Georgantzopoulou et al. 2016), only limited NMs

have been tested and only limited endpoints (cell viability, IL-8 and ROS production) have been used to assess the impact of NMs on the co-culture. More specifically the Caco-2/HT29-MTX *in vitro* model was used to investigate the toxicity of 20 and 200 nm Ag NMs and $AgNO_3$. The treatment had no impact on cell viability or oxidative stress, but could stimulate IL-8 release (Georgantzopoulou et al. 2016). For extensive assessment of the toxicity of NMs to the intestine *in vitro* using a mucus secreting models, a range of endpoints, including assessment of the impact on tight junction integrity (e.g. using TEER measurement and immunostaining of the tight junction protein), cell morphology (e.g. using SEM and light microscopy), IL-8 production, ROS formation and gene expression have been adopted in this study.

4.1.1. Aims and Objectives

This chapter is aimed at using the Caco-2/HT29-MTX mucus secreting co-culture *in vitro* model to assess the toxicity of ingested NMs and to identify the most appropriate biomarkers (biochemical and molecular) to employ in the assessment of NM toxicity to the intestine. The toxicity of CuO NMs and $CuSO_4$ will be compared to help decipher the involvement of particle and ions in NM toxicity.

Specific objectives are as follows

- **i.** To ascertain the impact of CuO NMs and $CuSO_4$ on a Caco-2/HT29-MTX co-culture via assessment of cytotoxicity, barrier integrity and morphology using tight junction staining, TEER measurement, light and electron microscopy and nuclei counts.
- **ii.** To determine the impact of CuO NMs and $CuSO_4$ on a Caco-2/HT29-MTX co-culture on cytokine production and oxidative stress via assessment of IL-8 production, ROS formation and expression of genes related to inflammation, oxidative stress, mucus secretion and metal binding (metallothionein).
- iii. To assess the translocation of CuO NMs and $CuSO_4$ across the intestinal epithelium using a mucus secreting Caco-2/HT29-MTX co-culture.

4.1.2. Hypotheses

i. CuO NMs and $CuSO_4$ will induce a loss of Caco-2/HT29-MTX co-culture viability.

ii. CuO NMs and $CuSO_4$ will elicit ROS production in the Caco-2/HT29-MTX co-culture.
iii. CuO NMs and $CuSO_4$ will induce cytokine production in the Caco-2/HT29-MTX co-culture.
iv. CuO NMs and $CuSO_4$ will impair barrier integrity (i.e. a reduction in TEER, disruption of tight junction staining) which will lead to Cu ion translocation across the Caco-2/HT29-MTX co-culture.
v. CuO NMs and $CuSO_4$ will upregulate expression of genes related to inflammation, oxidative stress, mucus secretion and metal binding (metallothionein) in the Caco-2/HT29-MTX co-culture.
vi. The impact of CuO NMs on Caco-2/HT29-MTX co-culture will be similar to $CuSO_4$.

4.2. Materials and Methods

4.2.1. Cell culture

HT29-MTX cells (Clone E-12) and the Caco-2 cell line were utilised for this study. The source and maintenance of Caco-2 cell line are as outlined in section 2.2.3. HT29-MTX cells were obtained from European Collection of Authentic Cell Culture (ECACC) (UK). HT29-MTX cells were maintained in 4.5 g/l glucose Dulbecco's modified eagle medium (DMEM) (Sigma) supplemented with 10 % heat inactivated FBS (Gibco Life Technologies), 100 U/ml Penicillin/Streptomycin (Gibco Life Technologies), 100 iu/ml NEAA (Gibco Life Technologies), and 2 mM L- glutamine (Gibco Life Technologies), at 37 ºC and 5 % CO_2 and 95 % humidity. The cells were sub-cultured three times a week at 70 to 80 % confluency using 0.05 % trypsin-EDTA (Gibco Life Technologies).

4.2.2. Culturing of the mucus secreting co-culture model

A mucus secreting co-culture model of the gastrointestinal epithelium was cultured by modifying the protocol of (Pan et al. 2015, Georgantzopoulou et al. 2016). Briefly, 3.13 x 10^5 cells/cm^2 of Caco-2 and HT29-MTX cells were seeded onto the AP compartment of 3.0 µm pore polycarbonate transwell inserts in a 12- well plate with growth area of 1.12 cm^2 (Costar corning, Flintshire, UK) at a ratio of 9:1. The co-culture was maintained in 4.5 g/l glucose Dulbecco's modified eagle medium (DMEM) (Sigma) supplemented

with 10 % FBS (Gibco Life Technologies), 100 U/ml Penicillin/Streptomycin (Gibco Life Technologies), 100 iu/ml nonessential amino acid (NEAA) (Gibco Life Technologies), and 2 mM L-glutamine (L-Glu) (Gibco Life Technologies). The cells were cultivated at 37 ^{o}C, 5 % CO_2 and 95 % humidity for 20-21 days and cell culture medium changed every other day for the first 16 days and then every day until the 21st day. The medium was changed by aspirating the cell culture medium in the BL compartment followed the AP compartment, and replaced with 500 µl medium in the AP compartment followed by 1.5 ml in the BL compartment. TEER was measured every two days for monitoring the development of the intact monolayer following the method described in section 3.2.3.

4.2.3. Alcian blue staining

In order to confirm that the Caco-2/HT29-MTX co-culture model produced mucus, Alcian blue staining was used. Alcian blue is a blue dye used to stain mucus due to its specificity to acidic glycoproteins (Pan et al. 2015) and can be imaged with light or electron microscopy. Briefly, the Caco-2 and Caco-2/HT29-MTX co-culture was washed twice with PBS and then fixed with 4% formaldehyde for 25 min at RT. The cells were washed thrice with PBS and stained with 10 mg/ml Alcian blue (in 3 % acetic acid) for 30 min at RT. The cells were washed with PBS and the inserts were then carefully excised and mounted onto a microscopic slide. The cells were covered with glass coverslip, visualised with Axiovert 40 C light microscope (ZEISS, Germany) and the image taken with camera (EOS 60D Canon, Japan).

4.2.4. Investigation of the impact of CuO NMs and $CuSO_4$ on barrier integrity using TEER measurement

The Caco-2/HT29-MTX co-culture was exposed to cell culture medium (control), 6.34 or 12.68 Cu µg/cm^2 of CuO NMs and $CuSO_4$ (500 µl/well), and the TEER value was measured as described in section 3.2.4.

4.2.5. Immunostaining of ZO-1 tight junctions

The Caco-2/HT29-MTX co-culture was exposed to cell culture medium (control), 6.34 Cu µg/cm^2 of CuO NMs and $CuSO_4$ (500 µl/well), processed, visualised and imaged as detailed in section 3.2.5.

4.2.6. Nuclei counting: Cytotoxicity

The Caco-2/HT29-MTX co-culture was exposed to cell culture medium (control), 6.34 or 12.68 Cu μg/cm^2 CuO NMs and $CuSO_4$ (500 μl/well). The cells were processed imaged and the nuclei number counted as described previously in section 3.2.6.

4.2.7. Scanning electron microscopy (SEM)

The Caco-2/HT29-MTX co-culture was exposed to cell culture medium (control) or 6.34 Cu μg/cm^2 of CuO NMs. The cells were processed and imaged as detailed in section 3.2.7.

4.2.8. Romanowsky staining: Cell morphology

The Caco-2/HT29-MTX co-culture was exposed to cell culture medium (control) 6.34 or 12.68 Cu μg/cm^2 of CuO NMs and $CuSO_4$ (500 μl/well), and then processed using the method outlined in section 3.2.8. The cells were imaged with a light microscope- Zeiss fluorescent microscope, Carl Zeiss Axio Scope A 1 Upright Research Microscope (Germany) fitted with a camera ((EOS 60D Canon, Japan)).

4.2.9. Assessment of Cu transport across the intestinal monolayer

The Caco-2/HT29-MTX co-culture was exposed to cell culture medium (control), 3.17, 6.34 or 12.68 Cu μg/cm^2 of CuO NMs and $CuSO_4$ (500 μl/well). Processing of the supernatant and cells including measurement of the Cu concentration were performed following the method described in section 3.2.9.

4.2.10. Evaluation of intracellular ROS production

The Caco-2/HT29-MTX co-culture was treated with cell culture medium (control), 6.34 or 12.68 Cu μg/cm^2 of CuO NMs and $CuSO_4$ (500 μl/well), and the level of ROS formation was determined as detailed previously in section 3.2.10.

4.2.11. IL-8 production

The Caco-2/HT29-MTX co-culture was treated with cell culture medium (control), 200 ng of TNFα (positive control), 3.17, 6.34 or 12.68 Cu μg/cm^2 of CuO NMs and $CuSO_4$

(500 µl/well), and IL-8 secretion was then assessed using ELISA following the method previously described in section 3.2.11.2.

4.2.12. Gene expression

The Caco-2/HT29-MTX co-culture was exposed to cell culture medium (control), 3.17, 6.34 or 12.68 Cu µg/cm^2 of CuO NMs and $CuSO_4$ (500 µl/well). The RNA was isolated as outlined in section 3.2.12.1 and the cDNA synthesised following the method described in section 2.2.11.2. qPCR was performed, and data analysed as described in section 2.2.11.3.

4.2.13. Data analysis

All data were analysed as described previously in section 3.2.13.

4.3. Results

4.3.1. Verification of mucus production and intact monolayer formation by Caco-2/HT29-MTX co-culture and impact of CuO NMs and $CuSO_4$ on barrier integrity

The development of tight junctions in the intestinal monolayer of the Caco-2/HT29-MTX co-culture was monitored by TEER measurement from 5 days after seeding the cells. The TEER value increased continuously over time and reached 870 Ω.cm^2 on the 21st day (Figure 4.2). For all the experiments, cells with a TEER value greater than 500 Ω.cm^2 were used. The impact of CuO NMs and $CuSO_4$ on the TEER value was assessed (Figure 4.4). The TEER value of control cells was unaffected during the experiment. CuO NMs and $CuSO_4$ caused a concentration and time dependent decrease in TEER value (Figure 4.4). A significant decrease in TEER was observed in cells exposed to 12.68 Cu µg/cm^2 of CuO NMs and $CuSO_4$ 15 h post exposure whilst those exposed at a concentration of 6.34 Cu µg/cm^2 were only affected significantly at 24 h post exposure compared to control (Figure 4.4). The presence of mucus on the surface or in the Caco-2/HT29-MTX co-culture was determined by staining with Alcian blue. A greater intensity of blue staining was present on Caco-2/HT29-MTX co-culture compared to differentiated Caco-2 cell monolayer, suggesting that there was greater mucus production (Figure 4.3).

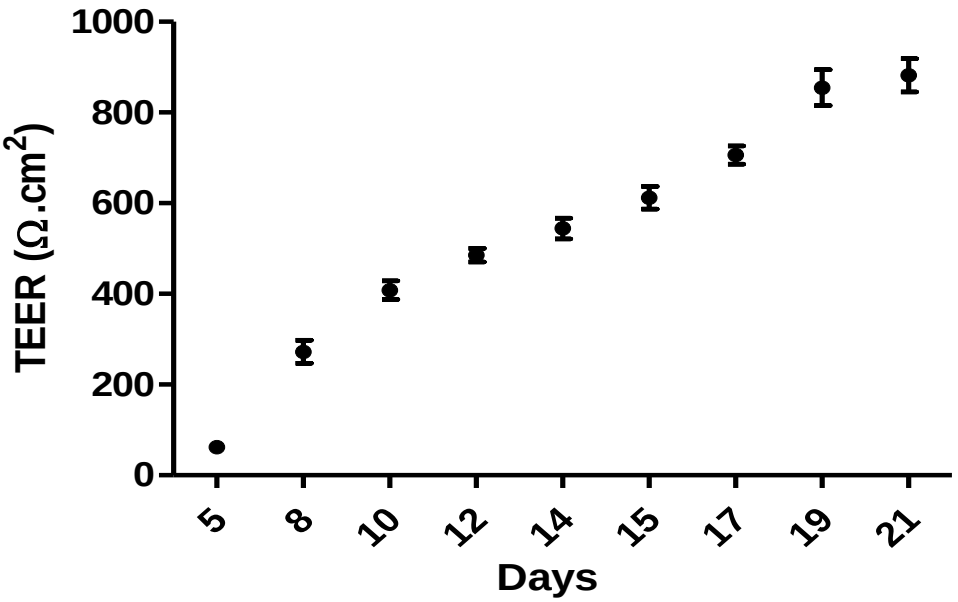

Figure 4.2: TEER value of the Caco-2/HT29-MTX co-culture over 21 days.

Caco-2/HT29-MTX cells were grown in transwell plates, and TEER measurement made at regular intervals to monitor cell differentiation. Data are expressed as mean TEER value ± SEM (n = 3).

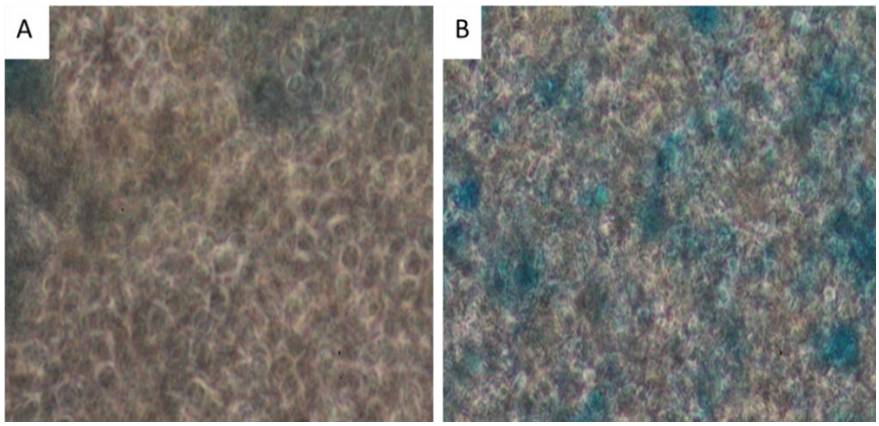

Figure 4.3: Mucus staining with Alcian Blue.

Differentiated Caco-2 cells (A) and the Caco-2/HT29-MTX co-culture (B) were stained with Alcian blue and imaged with a ZEISS light microscope fixed with camera (EOS 60D Canon, Japan. The blue colour is mucus stained with Alcian blue. Representative images are shown (n=3).

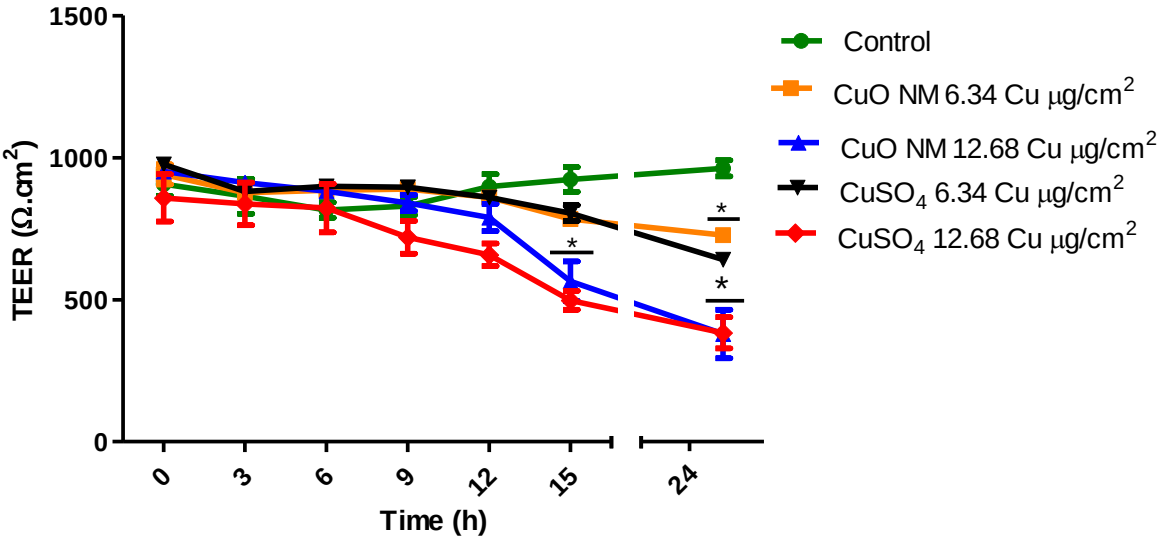

Figure 4.4: Impact of CuO NMs and $CuSO_4$ on Caco-2/HT29-MTX co-culture TEER values.

*Caco-2/HT29-MTX cells were exposed to cell culture medium (control, 0), CuO NMs or $CuSO_4$ at concentrations of 6.34 or 12.68 Cu µg/cm² for 24 h. TEER values were measured using epithelial volt-ohmmeter EVOM every 3 h. Data are expressed as mean TEER value ± SEM (n = 3). Significance at P<0.05 is indicated by * compared with control.*

4.3.2. Verification of tight junction formation using immunostaining and assessment of the impact of CuO NMs and $CuSO_4$ on the tight junction protein (ZO-1) of the Caco-2/HT29-MTX co-culture

The presence of tight junctions (one of the characteristics of mature intestinal epithelium) in the Caco-2/HT29-MTX co-culture was confirmed by staining the tight junction protein, ZO-1 (Figure 4.5). Following treatment with 6.34 Cu µg/cm² of CuO NMs, and $CuSO_4$ for 24 h, the intensity of the tight junction protein staining was similar to the control (Figure 4.5).

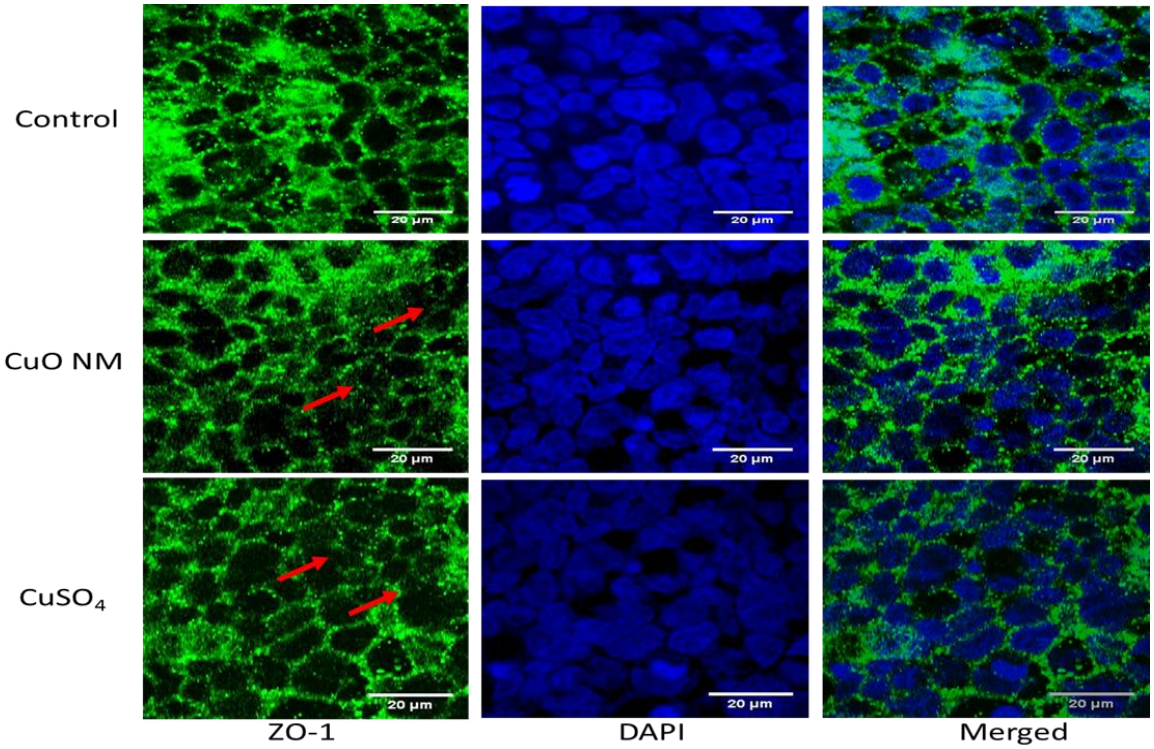

Figure 4.5: The impact of CuO NMs and $CuSO_4$ on Caco-2/HT29-MTX co-culture tight junction proteins.

The Caco-2/HT29-MTX co-culture was exposed to cell culture medium (control) or 6.34 Cu µg/cm^2 of CuO NMs and $CuSO_4$ for 24 h, then fixed, and stained for the tight junction protein ZO-1 (green) and nucleus (blue). The images of extended focus were obtained with Zeiss LSM880 confocal microscope using the Zen program for data analyses. Red arrows indicate areas where there is a reduction in ZO-1 staining intensity. Scale bar = 20 µm. Representative images are shown (n=3).

4.3.3. Verification of microvilli formation and impact of CuO NMs and $CuSO_4$ on Caco-2/HT29-MTX co-culture viability and morphology

The presence of microvilli in the Caco-2/HT29-MTX co-culture and impact of CuO NMs on microvilli and cell morphology was assessed with SEM and light microscopy. Using SEM, it was evident that extended microvilli covered the entire cell surface of control Caco-2/HT29-MTX co-culture cells (Figure 4.6). On exposure to CuO NMs (12.68 Cu µg/cm^2), the microvilli of some cells were shortened compared to control and there was no loss of cells (Figure 4.6). Using light microscopy, it was observed that CuO NMs and $CuSO_4$ did not impact on cell morphology or cell number (Figure 4.7). For assessment of viability, the Caco-2/HT29-MTX co-culture was stained with DAPI and a nuclei count performed. The co-culture treated with CuO NMs or $CuSO_4$ showed no significant

difference in nuclei number, compared to the control (Figure 4.8A) and the representative images shown in figure 4.8B confirmed this finding, which suggests that the treatment did not impact on cell viability.

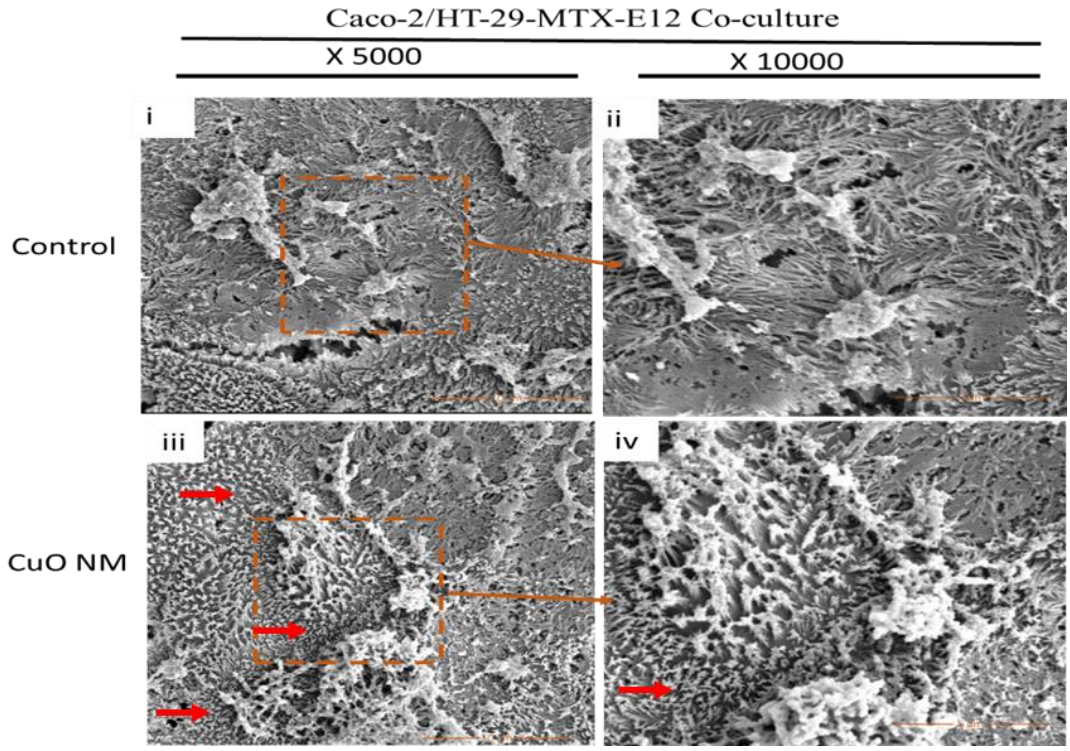

Figure 4.6: SEM image of the Caco-2/HT29-MTX co-culture exposed to CuO NMs for 24 h.

The Caco-2/HT29-MTX co-culture was exposed to cell culture medium (control) or 12.68 Cu µg/cm^2 of CuO NMs for 24 h. The cells were washed, fixed, dehydrated, dried and examined by SEM. Specimens i) and ii) are control Caco-2/HT29-MTX co-culture cells imaged at magnification of X 5000 and X 10000 respectively. iii) and iv) are Caco-2/HT29-MTX co-culture exposed to 12.68 Cu µg/cm^2 of CuO NMs imaged at magnification of X 5000 and X 10000 respectively. Representative images are shown (n=3). Red arrows indicate area of shortened microvili.

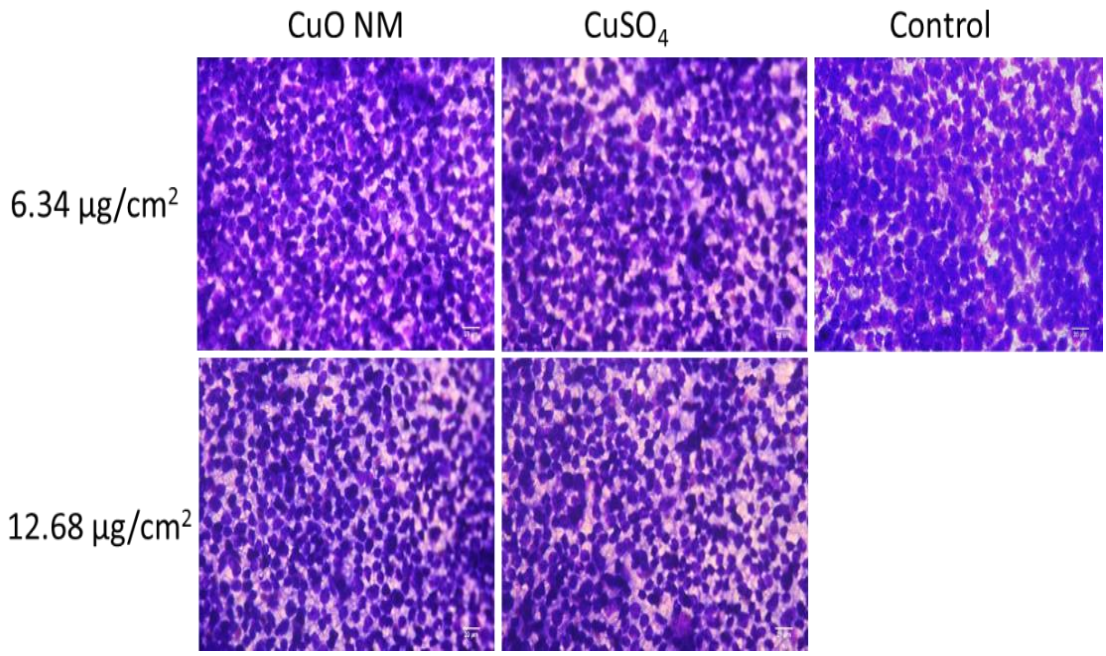

Figure 4.7: Impact of CuO NMs and $CuSO_4$ on Caco-2/HT29-MTX co-culture morphology.

The Caco-2/HT29-MTX co-culture was exposed to cell culture medium (control) and 6.34 or 12.68 Cu µg/cm² CuO NMs or $CuSO_4$ for 24 h. The cells were then fixed, stained and visualised using a light microscopy and imaged with a camera (EOS 60D Canon, Japan) (magnification 40 X, scale bar=20 µm. Representative images are shown (n=3).

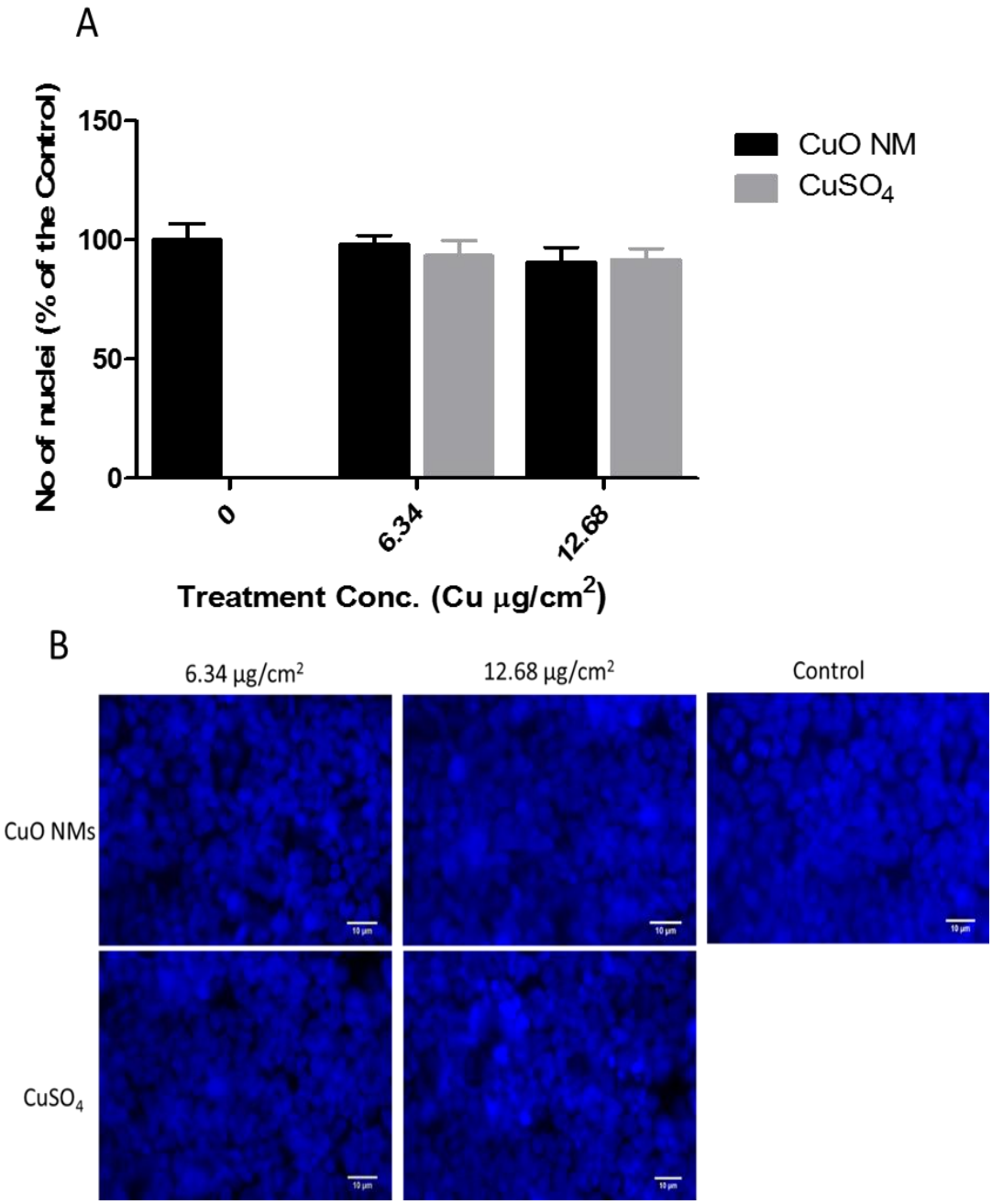

Figure 4.8: Assessment of the viability of the Caco-2/HT29-MTX co-culture using nuclei staining with DAPI.

*The Caco-2/HT29-MTX co-culture was treated with 6.34 and 12.68 Cu µg/cm^2 of CuO NMs and $CuSO_4$, fixed and the nucleus stained with DAPI and images obtained with Zeiss fluorescent Microscope, Carl Zeiss Axio Scope A 1 Upright Research Microscope (magnification 40X) (B). Nuclei were then counted using Image J software (A). Data are presented in number of nuclei (expressed in % of the unexposed control) ± SEM (n = 3). Significance at P<0.05 is indicated by * compared to unexposed control. Representative images are presented (n=3). Scale bar = 10 µm.*

4.3.4. Cellular uptake and translocation of Cu across the intestinal monolayer

After 24 h exposure of CuO NMs and $CuSO_4$, the detectable Cu concentration in the AP compartment ranged between 91 and 80 % (of the exposed concentration) whereas at 48 h post exposure the detectable level decreased slightly, and ranged between 69 and 83 (of % of the exposed concentration) (Figure 4.9A). However, no significant change in Cu concentration was observed between 24 and 48 h. At each time point, there seem to be a dose dependent decrease in Cu concentration in the AP compartment (Figure 4.9A) but this was not significant. There was no difference between the translocated Cu in CuO NMs and $CuSO_4$.

A time dependent significant increase in the concentration of Cu in the BL compartment was observed after treatment of the Caco-2/HT29-MTX co-culture with CuO NMs and $CuSO_4$, which suggests that Cu translocated from the AP compartment. The concentration of Cu detectable in the BL compartment at 24 h post exposure ranged between 1.6 and 5.8 % (of the exposed concentration) and 4.5 to 8.8 % (of the exposed concentration) at 48 h post exposure to CuO NMs and $CuSO_4$. This suggests that NM transport increased over time. There was no significant concentration dependent increase in detectable Cu in BL media between CuO NMs and $CuSO_4$ at either time point (Figure 4.9B). The concentration of Cu retained in the cell at all concentrations and time points was less than 3.1 % of the initial exposure concentration. However, the cellular retention of CuO NM or $CuSO_4$ significantly increased at 48 h (1.9 to 3.0 %) compared to 24 h (0.9 to 1.37 %) post exposure. The Caco-2/HT29-MTX co-culture did not demonstrate a significant treatment concentration dependent increase in detectable Cu in the cell (Figure 4.9C). The P_{app} of Caco-2/HT29-MTX co-culture exposed CuO NMs and $CuSO_4$ showed a significant time dependent increase at all concentrations (Figure 4.10), with a higher P_{app} value observed at 48 h.

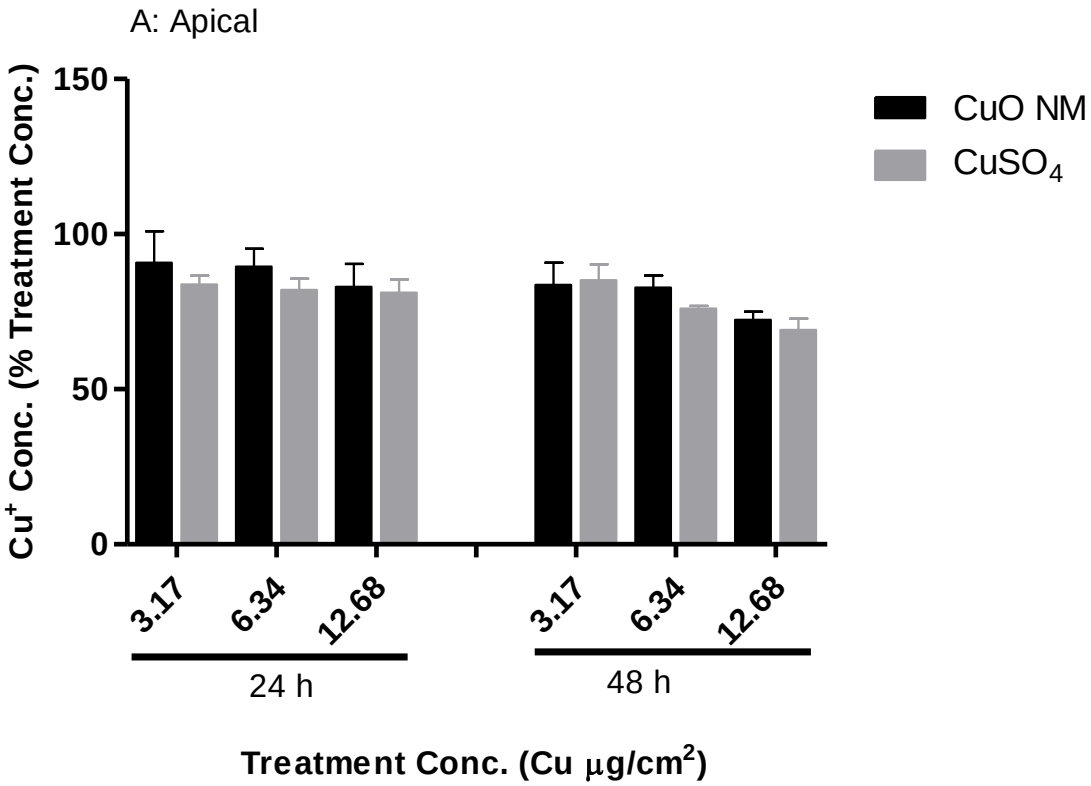
A: Apical
CuO NM
CuSO4
Cu+ Conc. (% Treatment Conc.)
150
100
50
0
3.17
6.34
12.68
3.17
6.34
12.68
24 h
48 h
Treatment Conc. (Cu μg/cm2)

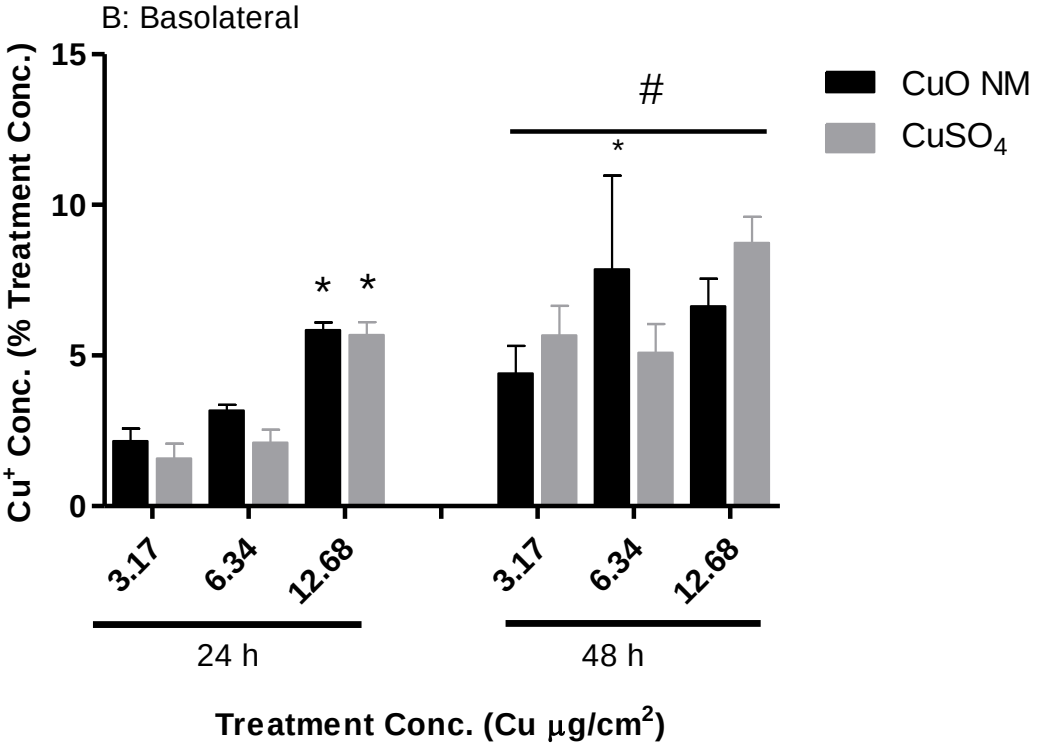
B: Basolateral
CuO NM
CuSO4
Cu+ Conc. (% Treatment Conc.)
15
10
5
0
#
*
* *
3.17
6.34
12.68
3.17
6.34
12.68
24 h
48 h
Treatment Conc. (Cu μg/cm2)

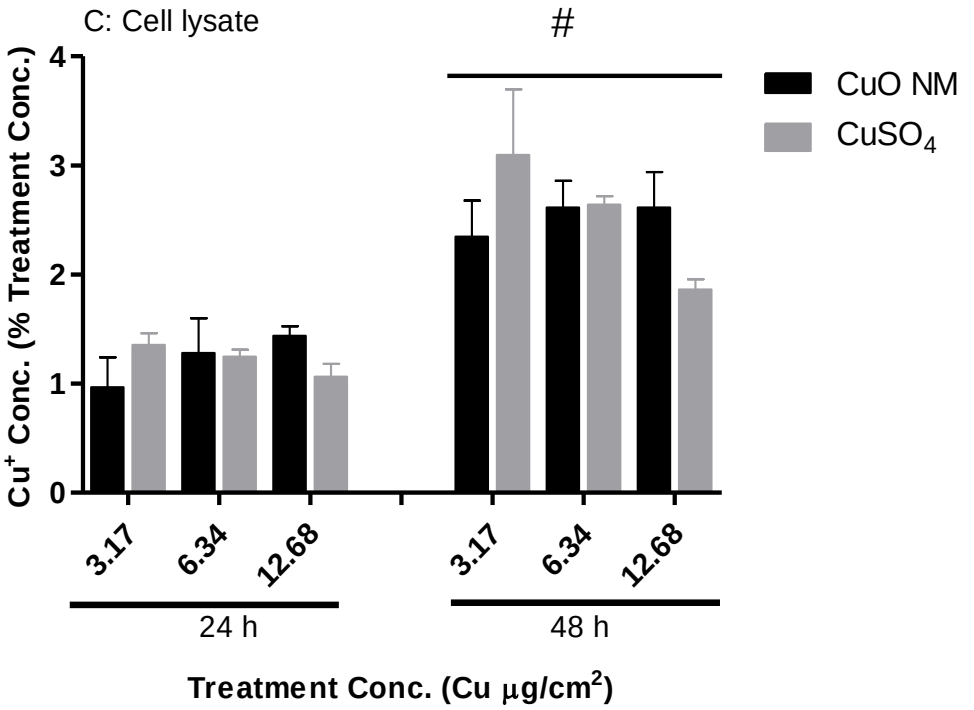

Figure 4.9: CuO NMs and $CuSO_4$ cellular uptake and translocation across Caco-2/HT29-MTX co-culture.

*The Caco-2/HT29-MTX co-culture was exposed to cell culture medium (control, 0), CuO NMs or $CuSO_4$ at concentration of 3.17, 6.34 or 12.68 Cu µg/cm^2 for 24 and 48 h. The level of Cu in the AP (A) and BL (B) compartments, and the cells (C) were evaluated by ICP-OES. Sample preparation and data analysis was performed by Victor Chibueze Ude and Dr. Lorna Eades performed the ICP-OES analysis. Data are expressed as mean copper concentration (as a percentage of the exposed concentration) ± SEM (n = 3). Significance at P<0.05 are indicted by * for comparison of 24 h post exposure of 3.17 Cu µg/cm^2 of CuO NMs to other treatment concentration within each time point or # for comparison of equivalent concentrations between 24 and 48 h time points.*

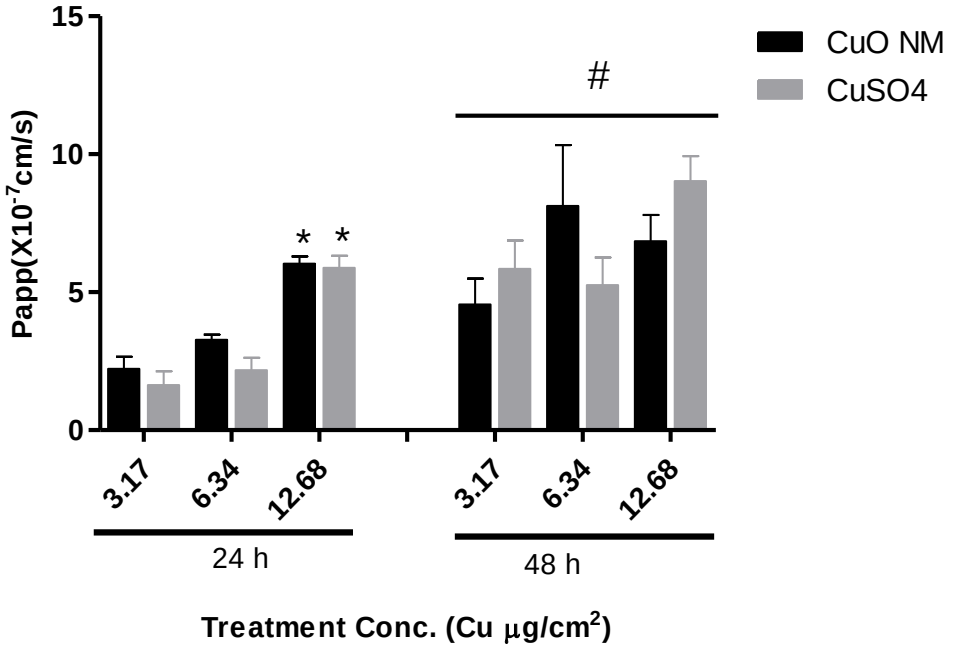

Figure 4. 10: Apparent permeability coefficient (P_{app}) of CuO NMs and $CuSO_4$.

*The Caco-2/HT29-MTX co-culture was exposed to cell culture medium (control, 0), CuO NMs or $CuSO_4$ at concentration of 3.17, 6.34 or 12.68 Cu µg/cm^2 for 24 and 48 h. The concentration of Cu in the AP and BL compartment was determined by ICP-OES and P_{app} was calculated. Data are expressed in mean P_{app} ± SEM x10^{-7} cm/s (n = 3). Significance at P<0.05 are indicted by * for comparison of 24 h post exposure of 3.17 Cu µg/cm^2 of CuO NMs to other treatment concentration within each time point or # for comparison of equivalent concentrations between 24 and 48 h time points.*

4.3.5. ROS formation

$CuSO_4$ mediated a significant increase in ROS formation in the Caco-2/HT29-MTX co-culture at 2 h post exposure, whereas CuO NMs did not. CuO NMs demonstrated less than a 2 fold increases in ROS production compared to control, whilst $CuSO_4$ increased ROS production more than 3 fold at all concentrations tested. ROS production by the co-culture exposed to $CuSO_4$ was significantly higher than the negative control, positive control (1 mM H_2O_2) and CuO NMs (Figure 4.11).

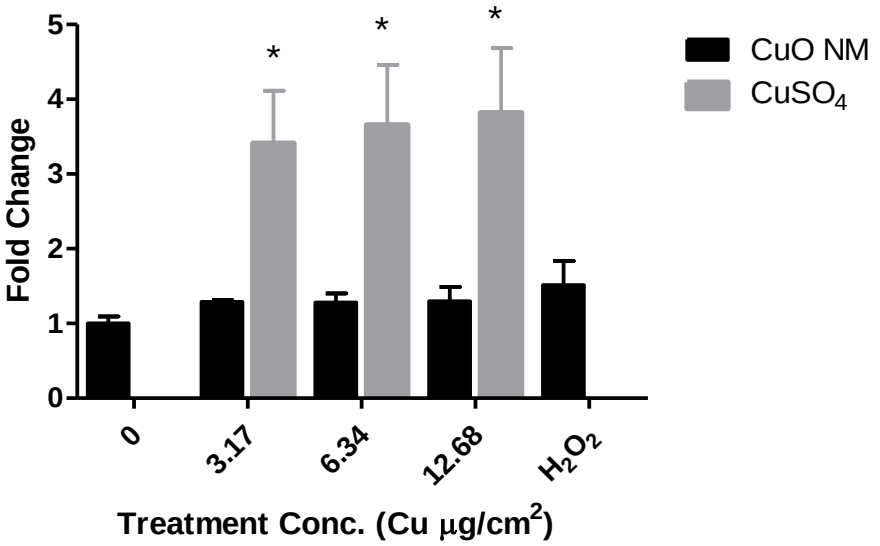

Figure 4.11: ROS formation by the Caco-2/HT29-MTX co-culture following exposure to CuO NMs and $CuSO_4$ for 2 h.

*Intracellular ROS levels were determined using the DCFH-DA assay 2 h post exposure of the Caco-2/HT29-MTX co-culture to cell culture medium (control, 0), H_2O_2 (1mM), CuO NMs and $CuSO_4$ at concentrations of 3.17, 6.34 and 12.68 Cu μg/cm^2. Data are expressed as fold change (compared to the control) ± SEM (n = 3). Significance at P<0.05 are indicated by * compared to control.*

4.3.6. IL-8 production

A concentration dependent increase in IL-8 secretion was observed following exposure of the Caco-2/HT29-MTX co-culture to CuO NMs and $CuSO_4$ for 24 h (Figure 4.12). Significant levels of IL-8 production were observed at all concentrations for both treatments, compared to the control (Figure 4.12). A similar level of IL8 was produced by cells exposed to CuO NMs and $CuSO_4$ at all concentrations. A below detectable level of IL8 was observed in the supernatant collected from the BL compartment for all treatments (data not shown). The positive control (200 ng/ml TNF-α for 24 h) secreted a concentration of 174.76 ± 41.44 pg/ml.

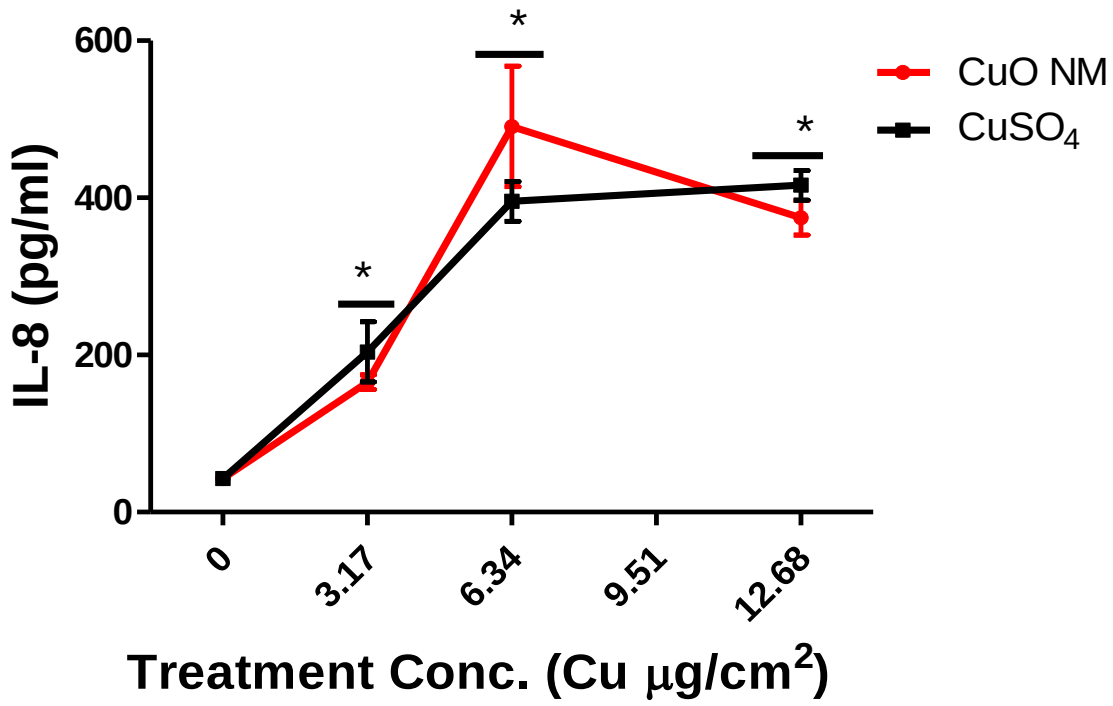

Figure 4.12: IL-8 production by the Caco-2/HT29-MTX co-culture following exposure to CuO NMs and $CuSO_4$.

*The Caco-2/HT29-MTX co-culture was exposed to cell culture medium (control, 0), CuO NMs or $CuSO_4$ at concentrations of 3.17, 6.34 or 12.68 Cu µg/cm^2 for 24 h. The level of IL-8 in the cell supernatant was determined using an ELISA. Data are expressed as mean IL-8 concentration (pg/ml) ± SEM (n = 3). Significance at P<0.05 is indicated by * compared to control.*

4.3.7. Gene expression

The Caco-2/HT29-MTX co-culture exposed to CuO NMs and $CuSO_4$ induced a concentration and time dependent increase in *HMOX1* expression, compared to control. The highest fold increase in expression was observed at12 h post exposure and was greatest at the highest concentration of 12.68 Cu µg/cm^2 for both CuO NMs and $CuSO_4$ with fold increase of approximately 21 fold. The lowest level of expression was observed at 24 h post exposure with the fold increase ranging from 3.4 to 8.5 fold (Figure 4.13A). This suggests a decrease in *HMOX1* expression at increased time point. There was no significant difference between *HMOX1* expression by CuO NMs and $CuSO_4$ exposed to the Caco-2/HT29-MTX co-culture.

IL8 expression after exposure of the Caco-2/HT29-MTX co-culture to CuO NMs and $CuSO_4$ significantly increased at all time points and concentrations compared to control except for cells exposed to CuO NMs and $CuSO_4$ at a concentration of 3.17 Cu μg/cm^2 for 12 h (fold increase ~1.4 fold) (Figure 4.13B). The maximum expression of *IL8* was observed at a concentration of 12.68 Cu μg/cm^2 CuO NM and $CuSO_4$ 12 h post exposure, with the fold increase ranging from 7 to 8) (Figure 4.13B). There was no significant difference between *IL8* expression by CuO NMs and $CuSO_4$ exposed Caco-2/HT29-MTX co-culture.

The lowest level of *MT1A* expression was observed for CuO NMs at a concentration of 3.17 Cu μg/cm^2 (2.5 fold increase), whilst the maximum expression of *MT1A* occurred at a concentration of 12.68 Cu μg/cm^2 $CuSO_4$ (14 fold increase) (Figure 4.13C). The expression of *MT1A* was not time or concentration dependent. $CuSO_4$ showed a significantly greater level of *MT1A* expression compared to CuO NMs at 24 h post exposure (12.68 Cu μg/cm^2).

$CuSO_4$ exposed to the Caco-2/HT29-MTX co-culture demonstrated a significant increase in *MUC2* expression at 4 and 12 h post exposure (3.4-4.9 fold) compared to control (Figure 4.13D). CuO NMs only stimulated a significant increase in *MUC2* expression by the co-culture at a concentration of 12.68 Cu μg/cm^2 (Figure 4.13D). However, for both CuO NMs and $CuSO_4$ the greatest increase in *MUC2* expression was observed at 24 h, with both treatments observed to induce a significant increase in *MUC2* expression 24 h post exposure at all concentrations compared to control with fold increase ranging from 9 to 16 (Figure 4.13D).

MT2A has the greatest level of expression compared to other genes. *MT2A* expression was significantly upregulated at all concentrations and time points after exposure of the Caco-2/HT29-MTX co-culture to CuO NMs and $CuSO_4$ compared to control with the fold increase ranging between 17 and 128. The highest fold increase in *MT2A* expression was observed at 12 h post exposure, reaching a maximum at a concentration of 12.68 Cu μg/cm^2 for both CuO NMs and $CuSO_4$ (128 and 119 fold increase respectively). The lowest level of *MT2A* expression was observed at 4 h post exposure with a fold increase of between 22 and 46 (Figure 4.13E). No significant difference was observed between gene expression by CuO NMs and $CuSO_4$ for *MT2A* expression. A heatmap summarising the findings from all genes is represented in figure 4.14, and allows visualization of the

concentration and time dependence of CuO NMs and $CuSO_4$ impacts on the gene expression to be compared.

A: HMOX-1

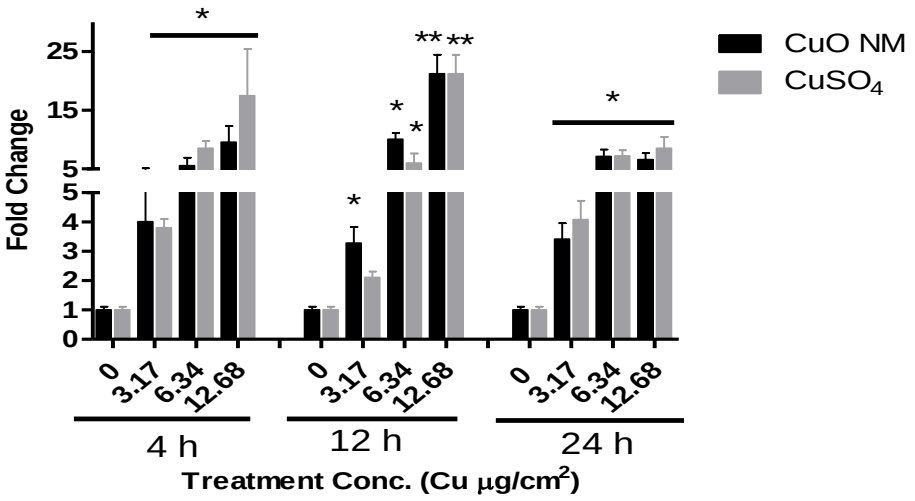

B: IL-8

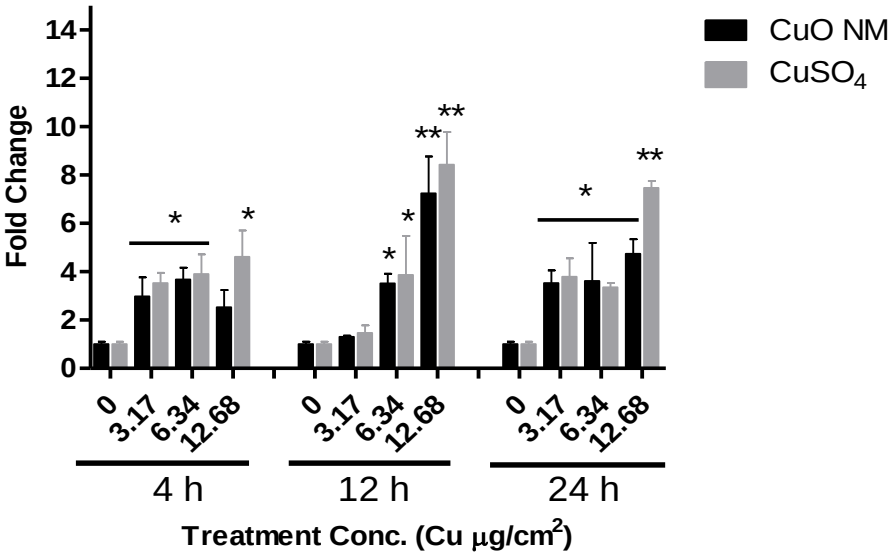

C: MT1A

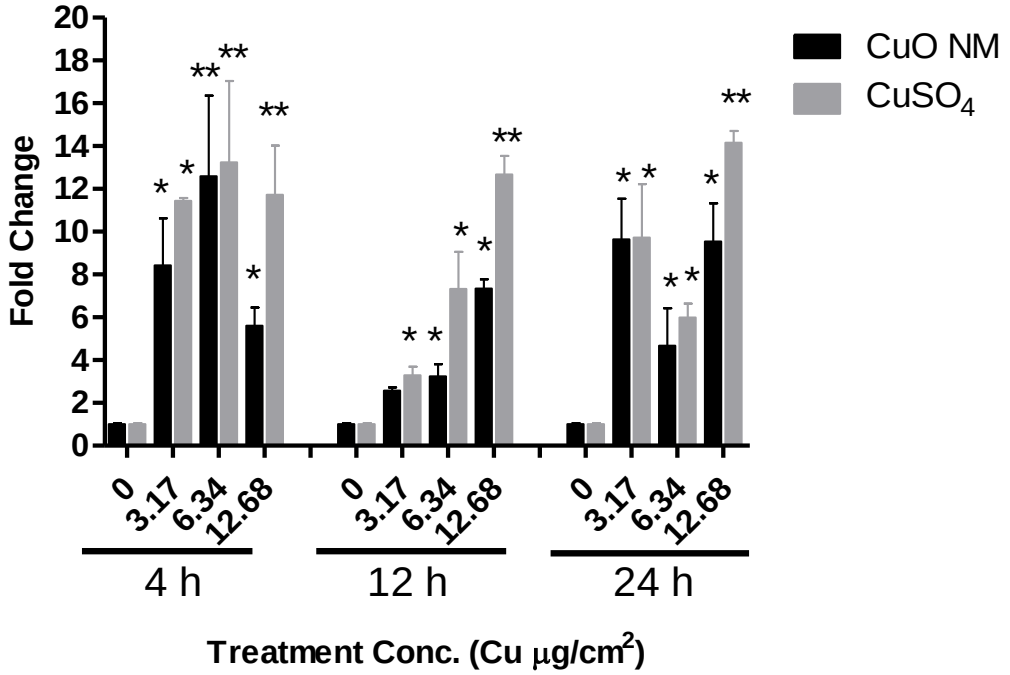
Fold Change
CuO NM
CuSO4
0
3.17
6.34
12.68
4 h
12 h
24 h
Treatment Conc. (Cu μg/cm2)

D: MUC2

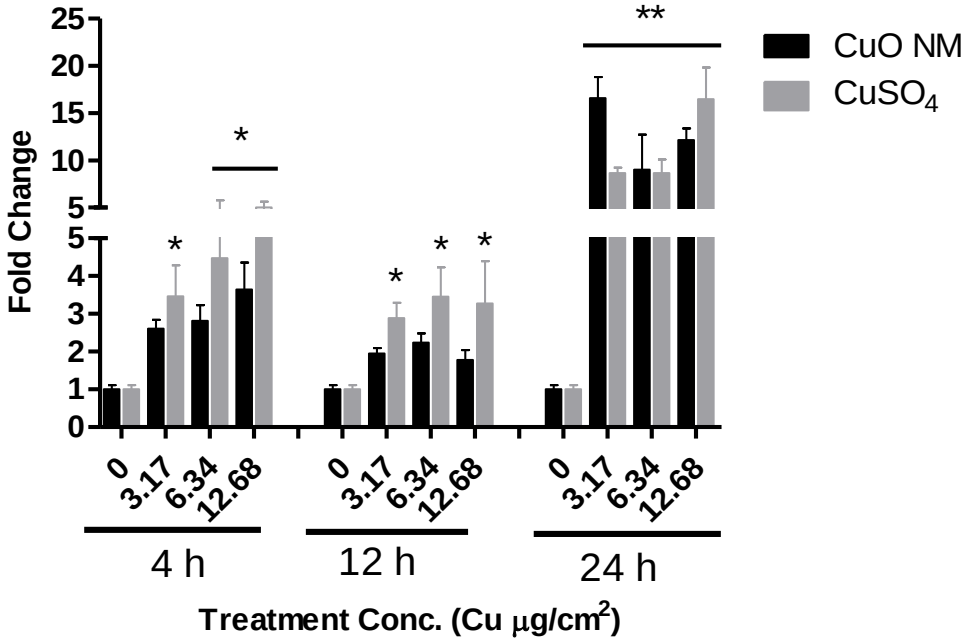
Fold Change
CuO NM
CuSO4
0
3.17
6.34
12.68
4 h
12 h
24 h
Treatment Conc. (Cu μg/cm2)

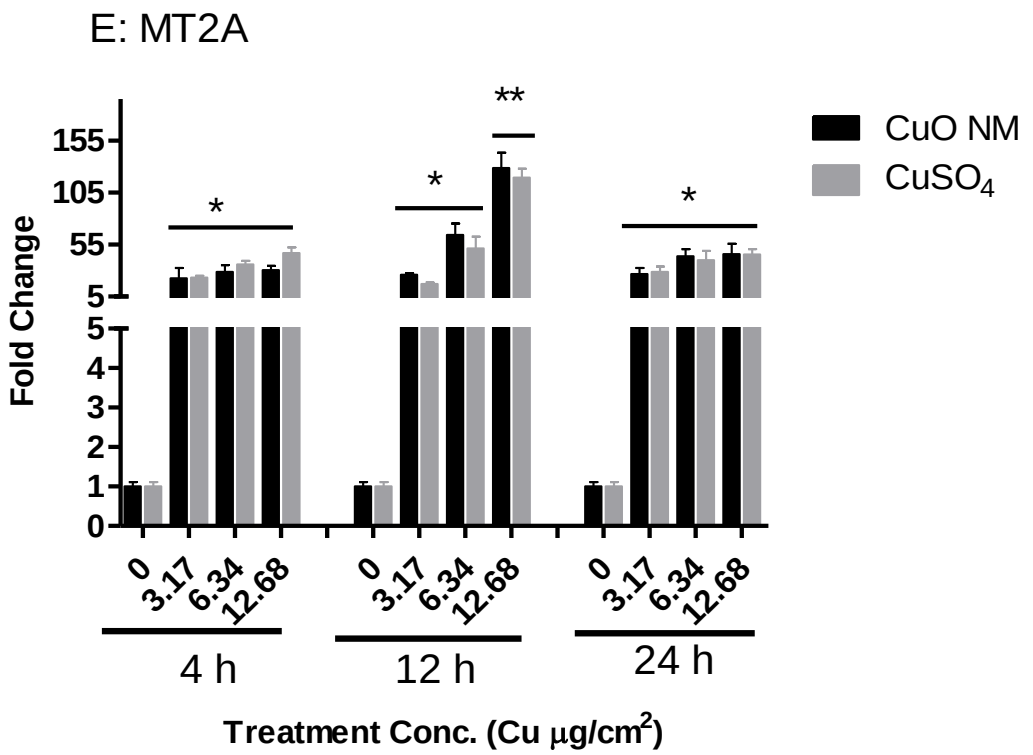

Figure 4.13: Effect of CuO NMs and $CuSO_4$ on gene expression in the Caco-2/HT29-MTX co-culture.

*Cells were exposed to cell culture medium (control, 0), CuO NM or $CuSO_4$ at concentrations of 3.17, 6.34 or 12.68 Cu μg/cm^2 for 4, 12 and 24 h and changes in HMOX1 A), IL8 B), MT1A C), MUC2 D), MT2A E) expression assessed using qPCR. Data were expressed as mean fold change (compared to the control) ± SEM (n = 3). Significance indicated by * = P<0.05 and ** = P<0.01 compared to control.*

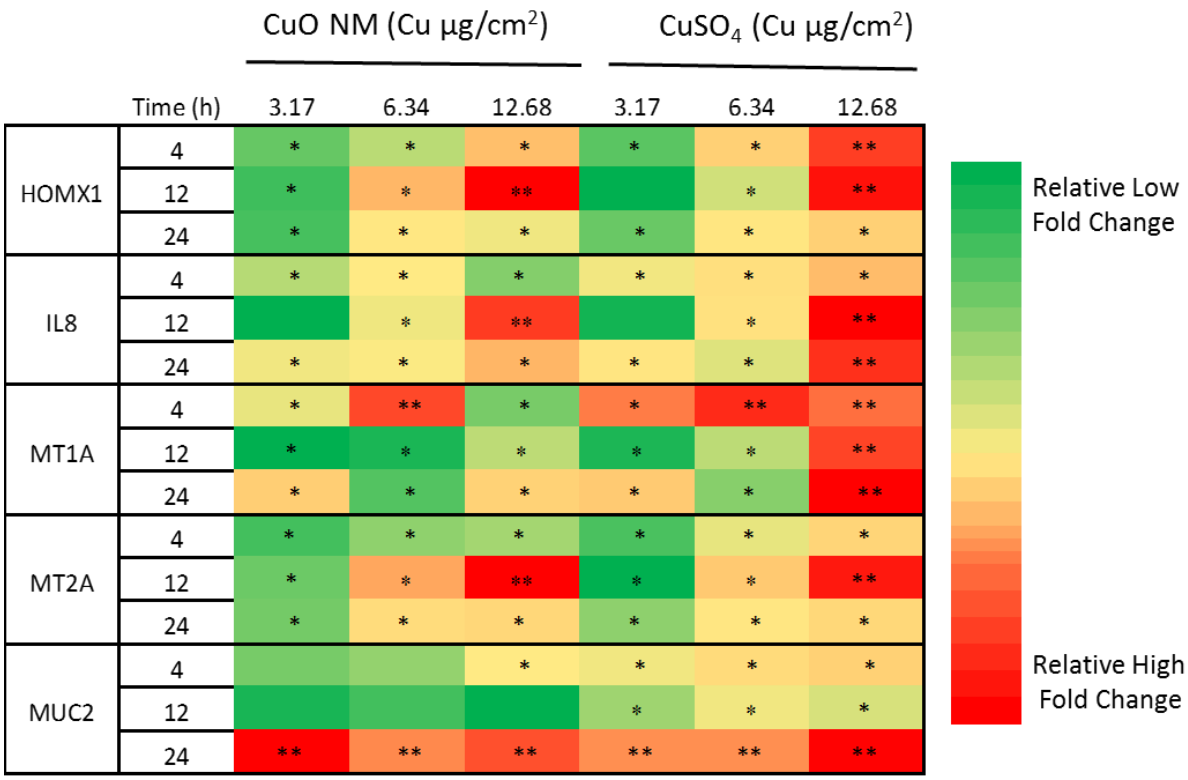

Figure 4.14: Heatmap representation of gene expression of Caco-2/HT29-MTX co-culture after exposure to CuO NM and $CuSO_4$.

*Caco-2/HT29-MTX cells were exposed to cell culture medium (control, 0), CuO NMs or $CuSO_4$ at concentrations of 3.17, 6.34 or 12.68 Cu µg/cm² for 4, 12 and 24 h and expression of HMOX1, IL8, MT1A, MUC2, MT2A assessed using qPCR. Genes were compared separately for significance. Data were expressed as mean fold change ± SEM (n = 3). Significance indicated by * = P<0.05 and ** = P<0.01 compared to control.*

4.4. Discussion

Here, the impact of CuO NMs and $CuSO_4$ on the Caco-2/HT29-MTX co-culture was studied via assessment of cell viability (nuclei count and light microscopy), cell morphology (light microscopy and SEM), IL-8 production, ROS formation and barrier integrity (SEM, TEER and ZO-1 staining). Presence of mucus on the Caco-2/HT29-MTX co-culture was determined by Alcian blue staining. Cu ion translocation and expression of *HMOX1*(oxidative stress gene), *IL8* (inflammatory response gene), *MUC2* (mucus secreting gene), *MT1A* and *MT2A* (metal binding genes) were also investigated. The presence of mucus on the surface of the co-culture monolayer is a clear indication of the

successful development of a mucus secreting *in vitro* intestinal model. CuO NMs and $CuSO_4$ induced no significant cell death on Caco-2/HT29-MTX cells as demonstrated by a lack of impact on nuclei number and morphology (via SEM and light microscopy). CuO NMs and $CuSO_4$ impaired barrier integrity, as revealed by a reduction in TEER. The reduction in barrier integrity is likely to be responsible for the concentration and time dependent translocation of Cu ions across the Caco-2/HT29-MTX barrier. CuO NMs and $CuSO_4$ also stimulated an increase in IL-8 production, and upregulated the expression of *HMOX1, IL8, MUC2, MT1A* and *MT2A*. In general, there was no difference between the impact of CuO NMs and $CuSO_4$ on Caco-2/HT29-MTX cells for all the endpoints employed for this study with the exception of ROS formation.

4.4.1. Barrier integrity and cytotoxicity

Mucus secretion is one of the characteristics of human intestinal epithelium. Alcian blue staining of the Caco-2/HT29-MTX co-culture demonstrated increased mucus staining compared to differentiated Caco-2 cells, suggesting that co-culturing of Caco-2 and HT29-MTX cells at the ratio of 9:1 stimulated mucus secretion, which could withstand the vigorous washing procedures. The level of mucus production and impact of NMs on mucus was not assessed. However, in future, mucus levels may be quantified using the method of enzyme-linked lectinosorbent assay (ELLA) that measured the reactivity of glycoproteins pre- and post-exposure to NMs (Even-Tzur et al. 2008). In addition to mucus secreting properties, the co-culture also maintained the characteristics of the intestinal epithelium *in vivo* such as presence of microvilli and tight junctions. Other researchers also reported similar result when a ratio of 9:1 of Caco-2 and HT29-MTX cells were co-cultured (Pan et al. 2015, Antunes et al. 2013).

Researchers have routinely used TEER measurement to determine the differentiation status of Caco-2/HT29-MTX co-culture (Brun et al. 2014, Akbari et al. 2017, Antunes et al. 2013, Walczak et al. 2015b, Calatayud et al. 2012). In this study, the TEER value was $> 250\ \Omega.cm^2$, which is suggested to be the minimum acceptable intestinal cell TEER value (Pan et al. 2015). This data indicates that the Caco-2/HT29-MTX co-culture developed an intact monolayer. The TEER value measured for Caco-2/HT29-MTX co-culture was comparable to that measured for differentiated Caco-2 cells (section 3.4.1). Assessment of TEER was also used to assess impacts of NMs on the integrity of the intestinal barrier.

Reduction in TEER in the Caco-2/HT29-MTX co-culture following exposure to polystyrene and TiO_2 NMs to the Caco-2/HT29-MTX co-culture has been reported, and was similar to these findings (Brun et al. 2014, Walczak et al. 2015b). However, this research differs from existing studies as TEER values were only assessed at one time point previously whilst in this study, a range of time points have been used to ascertain the impact of CuO NMs and $CuSO_4$ on TEER over time. Interestingly, when the Caco-2/HT29-MTX cells were exposed to 6.34 Cu µg/cm^2 of CuO NMs and $CuSO_4$, the TEER started decreasing at 15 h post exposure and was significant after 24 h of treatment. For the higher exposure concentration of 12.68 Cu µg/cm^2 of CuO NMs and $CuSO_4$ the TEER value of the co-culture model reduced significantly (P<0.5) as soon as 12 h post exposure. The TEER values of the Caco-2/HT29-MTX cell seemed to be less sensitive compared to differentiated Caco-2 cells (chapter 3, section 3.4.1) after exposure to CuO NMs and $CuSO_4$. Therefore, the presence of mucus may reduce the toxicity of the treatments depending on the treatment concentration.

Furthermore, to study the development of intact tight junctions (as confirmation of cell differentiation) and the impact of CuO NMs and $CuSO_4$ on the barrier integrity of the Caco-2/HT29-MTX co-culture, the ZO-1 protein was stained. The clear high intensity of ZO-1 staining on the control (untreated) indicates a development of intact tight junction by the Caco-2/HT29-MTX co-culture, again indicating that the cells were differentiated. Exposure of CuO NMs and $CuSO_4$ to the Caco-2/HT29-MTX co-culture did not seem to be much different, as the control staining was not a clear pattern. This may be due to the presence of mucin secreting cells providing a different pattern of staining, although the cells seem to be relatively intact. The decrease sensitivity of the Caco-2/HT29-MTX co-culture to CuO NMs and $CuSO_4$ toxicity therefore aligns with the findings from TEER measurements, discussed above. Tight junction protein staining has been used to monitor the development of tight junction by cells such as differentiated Caco-2 cells (Price et al. 2014, Qin et al. 2009), and Madin-Darby canine kidney (MDCK) cells (Tokuda et al. 2014), but only one published paper has used ZO-1 tight junction staining in Caco-2/HT29-MTX co-cultures (Brun et al. 2014), which was measured in response to TiO_2 NMs. More specifically, Brun et al. (2014) demonstrated that TiO_2, (12 to 140 nm) altered the staining intensity of ZO-1 protein in the Caco-2/HT29-MTX co-culture after 24 h

exposure. However, there is no other published papers on the impact of CuO NMs and $CuSO_4$ on the tight junctions of Caco-2/HT29-MTX co-culture to date.

SEM imaging of control Caco-2/HT29-MTX cells demonstrated the presence of microvilli, which shortened after exposure of CuO NMs for 24 h. This finding confirmed that Caco-2/HT29-MTX co-culture retained the characteristics of differentiated Caco-2 cells in addition to mucus secreting properties, which is in agreement with the previous findings (Pan et al. 2015). The shortening of the microvilli indicates that CuO NMs affected the cell structure of the Caco-2/HT29-MTX co-culture monolayer. The impact of CuO NMs on the microvilli of Caco-2/HT29-MTX cells has not been studied previously. Impact of CuO NMs on microvilli may be assessed further via villin protein staining. There was no impact on the nuclei number and cell morphology/number of Caco-2/HT29-MTX cells. These methods were used to assess impacts on viability, as the Alamar blue assay is not compatible with the transwell plates used to culture Caco-2/HT29-MTX and the LDH assay cannot be used due to Cu interference (section 2.4.2).

4.4.2. Translocation and cellular uptake

Researchers have used Caco-2/HT29-MTX co-cultures to study drug absorption and transportation (Antunes et al. 2013, Boegh et al. 2014, Hilgendorf et al. 2000), as well as NM uptake and translocation (Akbari et al. 2017, Walczak et al. 2015b, Araújo et al. 2014, Calatayud et al. 2012, Jin et al. 2012, Kenzaoui et al. 2012, Yuan et al. 2013). However, none of these studies has investigated the translocation of CuO NMs using a Caco-2/HT29-MTX co-culture. In addition, existing studies with NMs have only assessed the concentration of NMs in the BL compartment. In this study, different concentrations of CuO NMs and $CuSO_4$ were used to investigate the translocation of Cu from the AP to BL compartment over time by assessing the concentration of Cu in cells, AP and BL media. The concentration of Cu in the BL media, and cell increased in a time dependent manner. Increased concentration of Cu in AP compartment (compared to differentiated cells (section 3.3.4)) were observed at 24 and 48 h post exposure whilst increased Cu concentration was observed in the BL media at 48 h suggesting that the mucus covering the cell surface, may have prevented NM penetration and delayed the contact between the enterocytes and Cu. Although, not performed in this study, the trapping of NMs by the

mucus may be studied in future using electron microscopy, which could image the interaction of particle with mucus.

Less than 100 % of the Cu content exposed to cells was recovered in the samples. The unrecovered Cu could have bound to thiol containing peptides and proteins, and cell-culture plastics as previously described (section 3.4.2). In comparison, iron oxide NMs (9–10 nm) coated with either cationic polyvinyl amine (aminoPVA) or anionic oleic acid translocated into the BL compartment (<2 %) 24 h post exposure using Caco-2/HT29-MTX co-culture (Kenzaoui et al. 2012), which was higher than observed for CuO NMs reported in this present study. Walczak et al exposed a Caco-2/HT29-MTX co-culture to neutral, amine and carboxyl-modified polystyrene NMs (50 and 100 nm) for 24 h (Walczak et al. 2015b). They observed a translocation rate of 4.5 and 0.5 % for 50 nm and 100 nm neutral polystyrene NMs respectively, suggesting that NM size can influence NM translocation across the intestinal barrier. In addition, up to 6.8 % of carboxyl-modified polystyrene was translocated across the cells, whereas 1 % of the amine modified counterpart was translocated suggesting that negative modification may enhance translocation. Furthermore, *in vivo* experiments have demonstrated 0.6 % of 48V-radiolabeled (48V) TiO_2 NMs (70 nm) translocated across the gastrointestinal barrier when administered to female wistar-kyoto rats via intra-oesophageal instillation across the gastrointestinal barrier at 1 h post exposure and only 0.05 % were still retained in the body after 7 days (Kreyling et al. 2017). In future, it would be of interest to study the cellular uptake of CuO NMs using TEM, as the method used to quantify Cu (ICP-OES) does not discriminate between particles and ions.

The P_{app} value of Cu translocation across the Caco-2/HT29-MTX co-culture was less than $1x10^{6}$, which implies that CuO NMs and $CuSO_4$ are poorly absorbed by the co-culture model. However, extension of the time of exposure may lead to an increased P_{app} value as a significant increase was observed after 48 h exposure compared 24 h. Exposure of Cruciferin/Calcium (Cru/Ca) and Cruciferin/Chitosan (Cru/Cs) NMs to Caco-2/HT29-MTX co-culture demonstrated higher P_{app} values (Akbari et al. 2017) compared to this present study.

4.4.3. ROS formation

A series of studies have implicated ROS formation as one of the mechanism underlying NM toxicity (section 3.4.3) however only two published papers have studied the impact of NMs on ROS production by Caco-2/HT29-MTX cells (Lai et al. 2013, Georgantzopoulou et al. 2016) and none have used CuO NMs and $CuSO_4$. Therefore, this study fills this gap in knowledge. $CuSO_4$ stimulated a significant increase in ROS formation at 2 h post exposure, whereas CuO NMs did not. This could be attributed to the delayed and incomplete dissolution of CuO NMs at the time point studied as demonstrated in the dissolution studies for this NMs (Ude et al. 2017). Therefore, future studies could assess ROS production over a range of time points. Previous reports have shown that Ag NM (20 and 200 nm) and $AgNO_3$ did not induce ROS production 2 h post exposure to Caco-2/HT29-MTX co-culture (Georgantzopoulou et al. 2016). In addition, a lack of ROS formation was observed after exposure of Caco-2/HT29-MTX cells to carboxylated single-walled carbon nanotubes (SWCNT-COOH), multi-walled carbon nanotubes (MWCNT-COOH) and poly (4-vinylpyrrolidone) (PVP) wrapped multi-walled (MWCNT-PVP) 8 h post exposure (Lai et al. 2013). In future studies, reactive nitrogen species (RNS), antioxidant (e.g. glutathione) depletion and/or lipid peroxidation should be assessed to determine the contribution of oxidative stress to the toxicity of CuO NMs in the Caco-2/HT29-MTX co-culture model.

4.4.4. IL-8 production

CuO NMs and $CuSO_4$ stimulated a concentration dependent increase in IL-8 production 24 h post exposure to Caco-2/HT29-MTX cells. Similarly exposure of the Caco-2/HT29-MTX co-culture to Ag NMs (20 nm) and $AgNO_3$ on Caco-2/HT29-MTX co-culture demonstrated a concentration dependent increase in IL-8 secretion but Ag NM (200 nm) had no significant impact indicating a size dependent effect (Georgantzopoulou et al. 2016). However, SWCNT-COOH, MWCNT-COOH and PVP wrapped MWCNT-PVP demonstrated non-significant effect in all the pro-inflammatory cytokines (TNF-α, IL-1β, IL-6 and IL-8) assessed at 8 h post exposure to Caco-2/HT29-MTX co-culture (Lai et al. 2013). Assessment of cytokine release after treatment of Caco-2/HT29-MTX co-culture with NMs is not frequently performed as only two published papers have been identified, which have used cytokine production to assess NM toxicity in Caco-2/HT29-MTX co-

culture (Lai et al. 2013, Georgantzopoulou et al. 2016). Other researchers who have assessed cytokine release with co-culture cells have used co-culture of different cells other than Caco-2 and HT29-MTX such as BEAS-2B cells and neutrophils(Pang et al. 2012), Caco-2 and human macrophages (THP-1) cells (Susewind et al. 2016), Caco-2, THP-1 and human dendritic cells (MUTZ-3) (Kämpfer et al. 2017) and they observed increased IL-8 secretion. Therefore, the study has shown that IL-8 production could be incorporated in future studies when testing NM toxicity using the Caco-2/HT29-MTX co-culture. Other cytokines such as IL-6, IL-10, TNF-α and IL-1β should be assessed in future studies to investigate the impact of CuO NMs on cytokine production.

4.4.5. Gene expression

As mentioned above (section 4.4.2) most research conducted with Caco-2/HT29-MTX co-cultures are on translocation, uptake and absorption. However, this study has used the Caco-2/HT29-MTX model to investigate the impact of CuO NMs and $CuSO_4$ on oxidative stress genes (*HMOX1*), metal binding genes (*MT1A* and *2A*), a mucus secreting gene (*MUC2*) and a pro-inflammatory response gene (*IL8*) to investigate their mechanism of action and identify biomarkers of toxicity. A time dependent upregulation of the *HMOX1* which was maximal at 12 h post exposure, suggests that CuO NMs and $CuSO_4$ may be stimulating an oxidative response in cells, and that 12 h might be the optimum time point for study of *HMOX1* expression in future. Similar upregulation was also observed in undifferentiated Caco-2 cells after exposure to Au (5nm) (Bajak et al. 2015). Oxidative stress or substance that can generate ROS directly or indirectly stimulates upregulation of the *HMOX1*. *HMOX1* expression alteration may be induced by transcription factors such as NF-E2-regulated factor-2, hypoxia-inducible factor-1 or activator protein including, metal binding compounds and antioxidants (Ryter and Choi 2005, Ryu et al. 2014). Upregulation of *HMOX1* has been reported after exposure of Ag NMs (20 1126 nm) to Caco-2/Raji B co-culture (Bouwmeester et al. 2011) and Hela cells and A549 cells (Miura and Shinohara 2009, Sthijns et al. 2017).

Increased *IL8* expression was observed at all time points after exposure of the Caco-2/HT29-MTX co-culture to CuO NMs and $CuSO_4$, which is consistent with the IL-8 protein secretion assay (ELISA) (section 4.4.4). The maximum stimulation of *IL8* was observed at 12 h. Although, *IL8* mRNA expression by Caco-2/HT29-MTX cells

following exposure to CuO NMs has not been studied previously, reports have shown an increase in IL-8 protein production after exposure of Caco-2/HT29-MTX co-culture to Ag NMs (20 nm) (Georgantzopoulou et al. 2016).

There is no published paper on *MT* expression following exposure of the Caco-2/HT29-MTX co-culture to CuO NMs and $CuSO_4$, hence the need for this study. Upregulation of *MT* expression is dependent on ion release; hence, the toxicity of CuO NMs is likely to rely on the dissolution of the NMs (in the intracellular or extracellular environment). Exposure of A549 and BEAS-2B cells to CuO NMs has been demonstrated to upregulate *MT* (Strauch et al. 2017). This study has shown an induction of *MT1A* and *MT2A* expression after exposure of CuO NMs and $CuSO_4$ to Caco-2/HT29-MTX co-culture at all time points and concentrations tested suggesting that *MT* may be a good marker for metallic NM toxicity study, and in particular Cu NMs. The level of expression of *MT2A* was higher than *MT1A* and maximum at 12 h post exposure as was also observed in differentiated and undifferentiated Caco-2 cells (sections 2.3.5 and 3.3.7). This high level of expression for *MT2A* than *MT1A* was also observed in a previous study with Caco-2/Raji B cells (Bouwmeester et al. 2011) and A549 and BEAS-2B (Strauch et al. 2017). Therefore, *MT2A* may be suggested as a better marker for metallic NM investigation than *MT1A* in intestine.

The principal site of *MUC2* expression is in the intestine (Lesuffleur et al. 1993, Johansson et al. 2008, Johansson et al. 2011). In the Caco-2/HT29-MTX co-culture, *MUC2* expression occurred in time and concentration dependent manner with a maximal response after 24 h exposure, as also shown by differentiated Caco-2 cells (section 3.3.7). In control cells, *MUC2* expression in Caco-2/HT29-MTX co-culture is higher compared to differentiated and undifferentiated Caco-2 cells, which provides additional confirmation that the development of a mucus secreting intestinal *in vitro* model was successful. Taken together, the findings demonstrate that when assessing the toxicity of NMs via investigation of expression in Caco-2/HT29 –MTX cells, *HMOX1*, *IL8*, *MT2A* and *MUC2* may serve as the most sensitive molecular markers, however, *HMOX1* and *MT2A* are suggested for 4 h, *IL8* at 12 h and *MUC2* at 24 h post exposure assessment. In the future, other metallothionein isoforms (such as *MT1B*, *MT1M*, *MT1L*, *MT1E*, *MT1F*, *MT1X*, *MT1G* and *MT1H*), antioxidant genes (catalase, glutathione peroxidase, superoxide dismutase), apoptosis genes (caspases 3 and 7 or cleaved poly (ADP ribose)

polymerase (PARP)) could be studied to perform a more in-depth assessment of molecular markers of the NM toxicity to the intestine *in vitro*. Protein production/activity were not measured in this study and this could be assessed in the future studies.

4.5. Conclusions

The Caco-2/HT29-MTX co-culture *in vitro* model has closer physiological characteristics to intestinal cells *in vivo* than Caco-2 cell monocultures. Interestingly, CuO NMs and $CuSO_4$ compromised barrier integrity like differentiated Caco-2 cells. However, the impact on the integrity of cell monolayer for the co-culture was less than that observed for differentiated Caco-2 cells. This may also explain why there was less Cu translocation in the Caco-2/HT29-MTX co-culture model. The effect is likely to result from the presence of mucus in Caco-2/HT29-MTX co-culture, which limits the interaction of the NMs with the intestinal epithelial cells. Exposure of CuO NMs and $CuSO_4$ mediated increased IL-8 secretion, and expression of *HMOX1*, *IL8*, *MT1A*, *MT2A* and *MUC2* in the Caco-2/HT29-MTX co-culture. As observed previously, CuO NMs and $CuSO_4$ induced a similar impact in Caco-2/HT29-MTX co-culture at all the tested endpoints except ROS production. TEER measurement, IL-8 secretion, *HMOX1*, *IL8*, *MT2A* and *MUC2* expression could be employed as markers when testing the toxicity of CuO NMs in the co-culture model. Further research is required to further probe the mechanism of toxicity of CuO NMs.

CHAPTER 5: Impact of copper oxide NMs and copper sulphate on an intestinal microfold (M) cell *in vitro* model: a Caco-2/Raji B co-culture

5.1 Introduction

One of the largest lymphoid organs is the GALT (which is made up of approximately 70 % of the bodies immunocytes) and comprises of aggregated and isolated lymphoid follicles (Jung et al. 2010, Neutra et al. 2001, Corr et al. 2008). The Peyer's patches are formed from aggregated lymphoid follicles in follicle-associated epithelium (FAE) which includes M cells (Jung et al. 2010, Corr et al. 2008). Microfold cells represent ~10 % of the follicle-associated epithelium and are responsible for luminal antigen sampling (Lefebvre et al. 2015, Gamboa and Leong 2013, Jepson and Ann Clark 1998, Jepson and Clark 2001). M cells lack microvilli in the apical side and are responsible for transporting particles and pathogens across the intestinal epithelium to the underlying immune cells (des Rieux et al. 2007, Brayden et al. 2005, Corr et al. 2008, Shakweh et al. 2004, Jepson and Clark 2001). M cells function as antigen sampling cells and are a site for microbial and particulate matter trafficking (Powell et al. 2007). Translocation of food grade TiO_2 (100-200 nm), mixed environmental silicate (100-700 nm) and aluminium silicate (<100-400 nm) particles have be studied *ex vivo* (using surgically resected intestinal tissues) and the particles were observed in the macrophages within the GALT of human volunteers (Powell et al. 1996).

There are currently three different *in vitro* models of M cells and all are based on Caco-2 co-cultures. The first is the co-culture of murine lymphocytes from the Peyer's patch and Caco-2 cells using transwell plates (Kernéis et al. 1997), but this model has the limitations that it lacks uniformity, is not completely made of human cells, and relies on the use of animals to obtain the lymphocytes, which has ethical and financial implications. The co-culture of murine isolated lymphocytes and Caco-2 cells has been used to study the adhesion, internalization and translocation of *Vibrio cholerae* (Kernéis et al. 1997). This model has also been used to investigate NM transport across the intestinal epithelium. More specifically, 5 fold increase in transportation of chitosan-DNA NMs (390 kDa and 60–100 kDa) were reported in M cell monolayer compared to intestinal monolayer formed from only differentiated Caco-2 cells (Kadiyala et al. 2010). The second model is a co-culture of human Burkitt's Raji B cells with Caco-2 cells in a transwell plate. In this model, Raji B cells are seeded in the BL compartment of the transwell plate after 14 days and are grown for a further 4-6 days (Figure 5.1 A) (des Rieux et al. 2005). This model has been used to study the transport of pharmaceuticals, and carboxylated and aminated

latex NMs from the AP to BL compartments (des Rieux et al. 2005). In addition, other researchers also demonstrated a substantial development of M cells *in vitro* using a Caco-2/Raji B co-culture without inverting the insert (Schimpel et al. 2014). Translocation of *E. coli*, *S. enterica* using un-inverted Caco-2/Raji B co-cultures has been investigated previously (Martinez-Argudo and Jepson 2008, Tahoun et al. 2011).

The third model also involves a co-culture of Caco-2 cells with Raji B cells, but the insert is inverted during the culture (Figure 5.1B), thereby allowing close contact of the Raji B cells with Caco-2 cells, which is thought to promote M cell development (des Rieux et al. 2007). Caco-2 cells are seeded into the apical side of the transwell membrane for 3-5 days, and then the transwell insert is inverted. After 14 days, Raji B cells are seeded to the BL side and the M cells form after 4-6 days of seeding the Raji B cells. Following the formation of the M cells, the inserts are placed back at its original orientation before use for studies (des Rieux et al. 2007). M cell development using inverted and un-inverted transmembrane plates have been used to study insulin translocation from AP to BL compartment (Antunes et al. 2013). Translocation and whole genome gene expresion have also been investigated using this model in response to Ag NMs (Bouwmeester et al. 2011). Antunes et al reported that there was no difference between inverted and un-inverted Caco-2/Raji B co-culture based on WGA staining and insulin translocation studies (Antunes et al. 2013) hence un-inverted model was used for this study. Several methods are used for assessment of M cell development including WGA staining to stain sialic acid and N-acetylglucosamine residues present in M cells, alkaline phosphatase secretion and electron microscopy to identify a lack of microvilli on the M cell (Schimpel et al. 2014, Martinez-Argudo and Jepson 2008, Brun et al. 2014) . It is therefore necessary to confirm the development of M cells prior to using the inverted or un-inverted Caco-2/Raji B co-culture model.

As described for the Caco-2/HT29-MTX co-culture, most researchers who have used *in vitro* M cell models (e.g. Caco-2/Raji B co-culture) to investigate the response of the intestine to NMs *in vitro* have concentrated on investigation of translocation and permeability of NMs with little or no attention to assessment of the toxicity of NMs (des Rieux et al. 2005, des Rieux et al. 2007, Cabellos et al. 2017). Therefore, to elucidate the appropriate marker for studying the toxicity of NMs in the intestine using an M cell *in vitro* model. An extensive range of markers such as tight junction integrity using TEER

measurement, SEM, immunostaining of the tight junction, light microscopy, nuclei count, cytokine production, ROS formation, NMs translocation and gene expression were tested to investigate the toxicity of NMs on Caco-2/Raji B co-cultures.

A

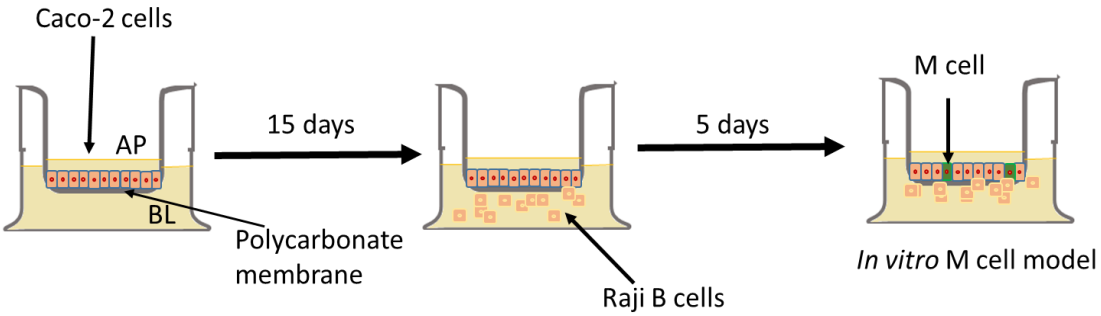

B

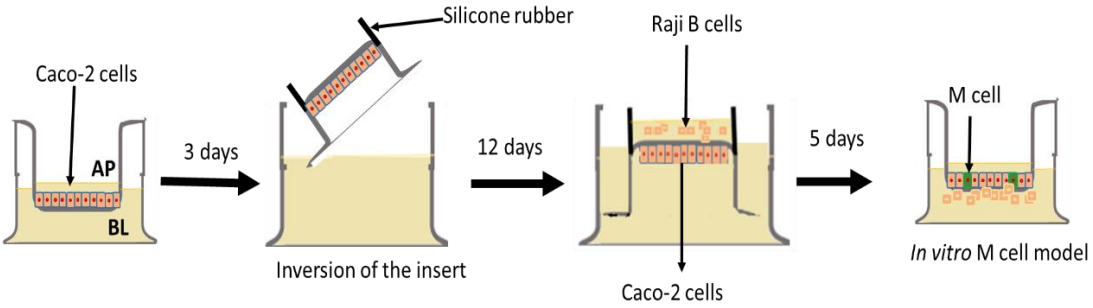

Figure 5.1: Schematic representation of M cell co-culture in vitro model.

Caco-2 cells are seeded into the apical compartment at day 1 followed by Raji B cells into the BL compartment on the 14th to 16th for development of the un-inverted in vitro M cell model (A). Alternatively, Caco-2 cells are seeded into the apical compartment at day 1, and the insert is then inverted at day 3 to 5 and then the Raji B cells are seeded on the 14th to 16th day on the top of the inverted (B). The cells are allowed to grow together until the 20th or 21st day to form the M cell.

5.1.1. Aim and objectives

The aim of this chapter is to investigate the potential use of the Caco-2/Raji B co-culture as an *in vitro* M cell model for the study of NM toxicity, and to identify the most appropriate biochemical and molecular biomarker to employ in the assessment of NM toxicity in intestine using this *in vitro* model. The toxicity of CuO NMs and $CuSO_4$ will be compared to help elucidate the involvement of particle and ions in the toxicity of NMs.

Specific objectives are as follows

i. To elucidate the impact of CuO NMs and $CuSO_4$ on the Caco-2/Raji B co-culture via investigation of cytotoxicity (light and electron microscopy and nuclei counts), barrier integrity (using tight junction staining, TEER measurement) and cell morphology, IL-8 production, ROS formation and expression of genes related to inflammation, oxidative stress, mucus secretion and metal binding (metallothionein).
ii. To investigate the translocation of CuO NMs and $CuSO_4$ across the intestinal epithelium using a Caco-2/Raji B co-culture.

5.1.2. Hypotheses

i. CuO NMs and $CuSO_4$ will induce a loss of cell viability in the Caco-2/Raji B co-culture.
ii. CuO NMs and $CuSO_4$ will induce ROS production in the Caco-2/Raji B co-culture.
iii. CuO NMs and $CuSO_4$ will stimulate IL-8 production in the Caco-2/Raji B co-culture.
iv. CuO NMs and $CuSO_4$ will impair barrier integrity via reduction in TEER, disruption of tight junction staining thereby enhancing Cu ion translocation across the Caco-2/Raji B co-culture.
v. CuO NMs and $CuSO_4$ will mediate increased expression of genes related to inflammation, oxidative stress, mucus secretion and metal binding (metallothionein) in the Caco-2/Raji B co-culture.
vi. The impact of CuO NMs and $CuSO_4$ on the Caco-2/Raji B co-culture will be similar.

5.2. Materials and Methods

5.2.1. Cell culture

Human Burkitti's lymphoma; B lymphocyte (Raji B) cells were obtained from ATCC (USA). The source and maintenance of the Caco-2 cell line is previously described (section 2.2.3). Raji B cells were maintained in Roswell Park Memorial Institute (RPMI)

1640 Medium (Gibco Life Technologies) supplemented with 10 % heat inactivated FBS (Gibco Life Technologies), 100 U/ml Penicillin/Streptomycin (Gibco Life Technologies) and at 37 ºC, 5 % CO_2 and 95 % humidity. The cells were sub-cultured three times a week.

5.2.2. Culturing of the microfold (M) cell model of the intestinal epithelium

The M cell model of the gastrointestinal epithelium was cultivated by modifying the protocol as described (Gullberg et al. 2000, des Rieux et al. 2005, Schimpel et al. 2014). Briefly, 3.13 x 10^5 cells/cm^2 of Caco-2 cells were suspended in 0.5 ml of DMEM and seeded into the AP compartment of 3.0 µm pore polycarbonate transwell inserts in a 12-well plate, with growth area of 1.12 cm^2 (Corning) and grown for 15 days at 37 ºC, 5 % CO_2 and 95 % humidity. The medium on both the AP (0.5 ml) and BL (1.5 ml) compartments was changed every other day. On the 15th day, 5 x 10^5 cells/ml of Raji B cells were suspended in DMEM (1.5 ml) and seeded into the BL compartment. The co-culture was grown for 5 days under standard incubation conditions and the medium was changed only in the AP compartment every day. The TEER was measured every other day following the method described in section 3.2.3.

5.2.3. Transmission electron microscopy (TEM)

Transmission electron microscopy (TEM) is a powerful microscope that transmits electron beams through an ultrathin (< 100 nm) section of a specimen or an aqueous suspension on a grid. The interaction of the specimen with the beam as the beam passes through the specimen leads to image formation. The image formed is magnified by electromagnetic lenses and then the images focused and collected on a screen. In this study, TEM was used to identify a lack of microvilli in Caco-2 /Raji B co-culture as an evidence of M cell formation. Differentiated Caco-2 cells, Caco-2/HT29-MTX and Caco-2/Raji B co-cultures (for methodology please refer to sections 3.2.2, 4.2.2 and 5.2.2) were washed twice with PBS and fixed with 2.5 % glutaraldehyde (in 0.1 M sodium cacodylate) for 2 h at the RT. The cells were washed with wash buffer (0.1 M sodium cacodylate pH 7.3) for 10 min three times, and further processed by Stephen Mitchel (Edinburgh University). Briefly, the cells were rinsed with H_2O for 10 min twice, and post fixed with 1 % osmium teteraoxide (OsO_4 in H_2O) for 45 min then washed again for

10 min twice. Afterwards, the cells were dehydrated with graded concentrations of ethanol (50, 70 and 95 %), for 10 min each, and 100 % ethanol for 10 min three times. This was followed by 50:50 ethanol: resin for 1 h, 100 % resin for 1 h twice. The insert was then carefully excised and embedded in fresh epoxy resin and polymerised at 60 ^{o}C for 24 h. The samples were embedded and cured before being fastened to a trimming block. A trapezoid shape of around 1 µm thickness was obtained with an ultramicrotome (Leica Microsystems Milton) and stained with toluidine blue then viewed under light microscope (Olympus B X 40, Germany) to select an appropriate section to examine. Approximately 60 nm sections were cut and transferred onto TEM grids followed by coating of the grid with 5 nm of evaporated carbon to minimise charging. The cells were examined, and images taken with a Philips/FEI CM120 Bio Twin Transmission Electron Microscope (Germany). The images were processed with image J.

5.2.4 Wheat germ agglutinin (WGA) conjugates staining

In order to confirm the formation of M cells by the Caco-2/Raji B co-culture fluorescein isothiocyanate (FITC) labelled WGA was used to stain Caco-2/Raji B co-cultures due to the high affinity of WGA to sialic acid and N-acetylglucosamine residues present in M cells (Schimpel et al. 2014). Differentiated Caco-2 cells, Caco-2/HT29-MTX and Caco-2/Raji B co-cultures were washed twice with PBS and fixed with 4 % formaldehyde for 25 min at RT. The cells were washed three times with PBS and then 500 µl of 5.0 µg/ml WGA FITC conjugate (in PBS) (Sigma Poole, UK) was used to label the cells for 15 min at RT. The cells were then washed two times with PBS. The polycarbonate inserts were carefully excised and mounted with ProLong® Gold antifade reagent with DAPI (Molecular probes, Life Technology, UK) onto a microscope slide and covered with a glass coverslip then, sealed with nail polish and allowed to dry at 4 ^{o}C for 24 h before visualizing with a Carl Zeiss Axio Scope A 1 Upright Research Microscope (Germany) fixed with a camera (ZEISS Axiocam ERc 5s). More than 4 fields of view were taken.

5.2.5. Investigation of the impact of CuO NMs and $CuSO_4$ on Caco-2/Raji B co-culture barrier integrity

The Caco-2/Raji B co-culture was exposed to cell culture medium (control), 6.34 or 12.68 Cu µg/cm^2 CuO NMs and $CuSO_4$ (500 µl) and the TEER value was measured as described previously (section 3.2.4).

5.2.6. Immunostaining of Caco-2/Raji B co-culture tight junctions

The Caco-2/Raji B co-culture was exposed to cell culture medium (control), 6.34 Cu µg/cm^2 CuO NMs and $CuSO_4$ (500 µl) processed visualised and imaged as detailed in section 3.2.5.

5.2.7. Nuclei counting: Cytotoxicity

The Caco-2/Raji B co-culture was exposed to cell culture medium (control), 6.34 or 12.68 Cu µg/cm^2 CuO NMs and $CuSO_4$ (500 µl). The cells were processed, imaged and the nuclei number counted as outlined in section 3.2.6.

5.2.8. Scanning electron microscopy (SEM)

The Caco-2/Raji B co-culture was exposed to cell culture medium (control) or 6.34 Cu µg/cm^2 CuO NMs (500 µl). The cells were processed and imaged as previously described in section 3.2.7.

5.2.9. Romanowsky staining: Cell morphology

The Caco-2/Raji B co-culture was exposed to cell culture medium (control), 6.34 or 12.68 Cu µg/cm^2 CuO NMs and $CuSO_4$ (500 µl) and processed as outlined in section 3.2.8. The cells were imaged using a light microscope, Carl Zeiss Axio Scope A 1 Upright Research Microscope (Germany) fitted with a camera (EOS 60D Canon, Japan).

5.2.10. Assessment of Cu transport across the intestinal monolayer

The Caco-2/Raji B co-culture was exposed to cell culture medium (control), 3.17, 6.34 or 12.68 Cu µg/cm^2 CuO NMs and $CuSO_4$ (500 µl). Processing of the supernatant and cells,

and measurement of the Cu concentration were performed following the method outlined in section 3.2.9.

5.2.11. Evaluation of intracellular ROS production

The Caco-2/Raji B co-culture was treated with cell culture medium (control), 6.34 or 12.68 Cu µg/cm^2 CuO NMs and $CuSO_4$ (500 µl) and the level of ROS formation was determined as described previously (section 3.2.10).

5.2.12. IL-8 production

The Caco-2/Raji B co-culture treated with cell culture medium (control), 200 ng of TNF-α (positive control), 3.17, 6.34 or 12.68 Cu µg/cm^2 CuO NMs and $CuSO_4$(500 µl). IL-8 secretion was then assessed using ELISA following the method described in section 3.2.11.2.

5.2.13. Gene expression

The Caco-2/Raji B co-culture was exposed to cell culture medium (control), 3.17, 6.34 or 12.68 Cu µg/cm^2 CuO NMs and $CuSO_4$ (500 µl). The RNA was isolated as detailed in section 3.2.12.1 and the cDNA synthesised following the method outlined in section 2.2.11.2. qPCR was performed, and data analysed as described in section 2.2.11.3.

5.2.14. Data analysis

All data were analysed as described in section 3.2.13.

5.3. Results

5.3.1. Verification of M cell and intact monolayer formation

Differentiation of the Caco-2/Raji B co-culture was studied by TEER measurement. TEER was measured from the 5th day after seeding the Caco-2 cells until the 20th day and a continuous increase in TEER was observed from the 5th day (~ 100 Ω.cm^2) to the 15th day (715 Ω.cm^2), which was the day the Raji B cells were seeded to BL compartment. The TEER continued to increase until two days (~755 Ω.cm^2) after the seeding of the Raji B cells and at day 20, a decrease in TEER value to approximately 690 Ω.cm^2 was

observed (Figure 5.2). Only cultures with a TEER value of greater than 500 $\Omega.cm^2$ were used for all experiments in this study. TEM study was also performed to confirm the development of M cells by the Caco-2/Raji B co-culture, as M cells are known to lack microvilli. The TEM image demonstrated a lack of microvilli at the point where an M cell is located as indicated with red arrow in Caco-2/Raji B co-culture (Figure 5.3). Microvilli were present in all the surfaces of the differentiated Caco-2 cell and Caco-2/HT29-MTX co-culture (Figure 5.3).

FITC labelled WGA was used to localise M cells in the Caco-2/Raji B co-culture because of the high affinity of WGA to sialic acid and N-acetylglucosamine residues, which are found in high concentration in M cells compared to other cells of the enterocytes. In this study a high intensity of WGA staining was visualised in the Caco-2/Raji B co-culture compared to differentiated Caco-2 cells and Caco-2/HT29-MTX co-culture indicating the formation of M cells (Figure 5.4).

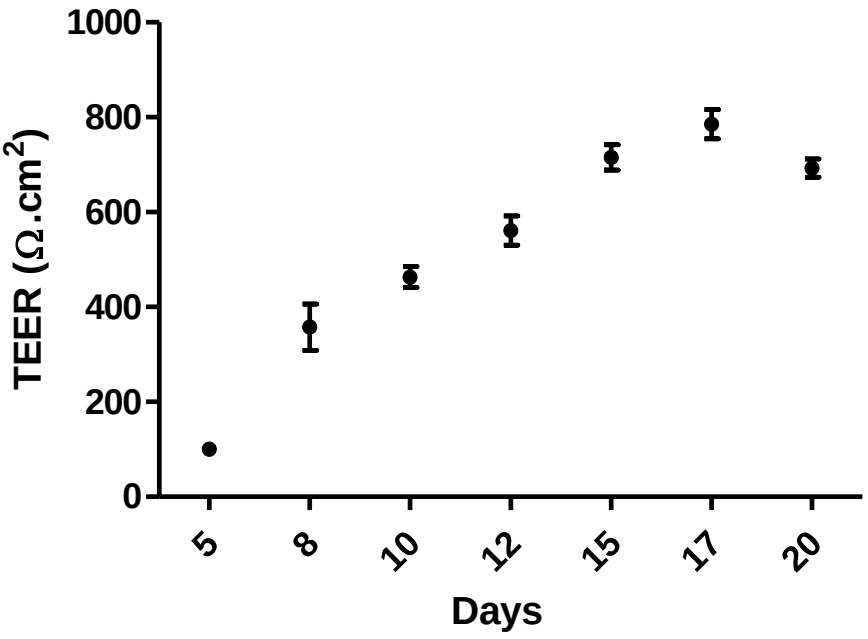

Figure 5.2: TEER value of the Caco-2/Raji B co-culture over 20 days.

A Caco-2/Raji B co-culture was grown in transwell plates, and TEER measurements made at regular intervals to monitor cell differentiation. Data are expressed as mean TEER value ± SEM (n = 3).

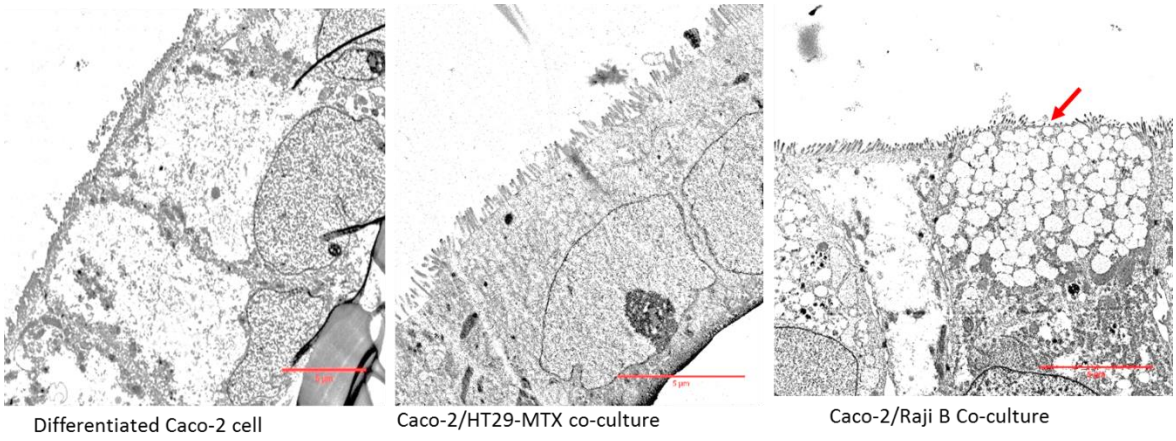

Figure 5.3: TEM image of differentiated Caco-2 cells, Caco-2/HT29-MTX and Caco-2/Raji B co-cultures.

Differentiated Caco-2 cells, Caco-2/HT29-MTX and Caco-2/Raji B co-culture were washed, processed for TEM analysis and examined by TEM. Red arrow indicates the M cell lacking microvilli. Representative images are shown and scale bar=5 µm (n=3).

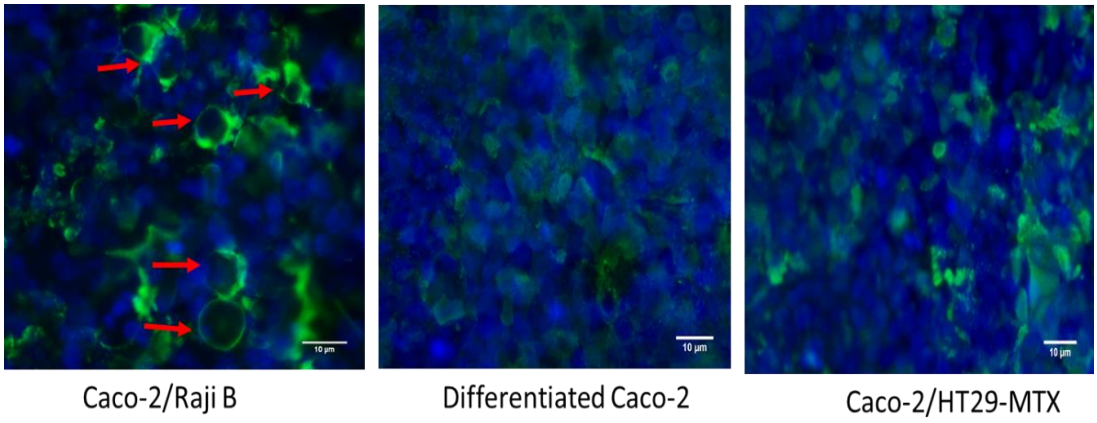

Figure 5. 4: Confirmation of the presence of M cells in Caco-2/Raji B co-cultures using WGA FITC labelling.

Differentiated Caco-2 cells, Caco-2/HT29-MTX and Caco-2/Raji B co-culture were fixed, labelled with WGA FITC (green) and mounted with ProLong with DAPI (nucleus: blue) and the images obtained with a fluorescent Microscope. Red arrows indicate the M cells. Representative images are presented and scale bar = 10 µm (n = 4).

5.3.2. Impact of CuO NMs and $CuSO_4$ on the barrier integrity of Caco-2/Raji B co-cultures: TEER value and tight junction protein staining

Caco-2/Raji B co-cultures demonstrated a significant time dependent decrease in TEER value 12 h post exposure to CuO NMs and $CuSO_4$ at all concentrations tested, compared to control (Figure 5.5). A significant decrease in TEER value was observed from 15 h post treatment with 6.34 Cu µg/cm^2 of CuO NMs and $CuSO_4$. The TEER value of the control remained approximately constant and ranged from 720-820 Ω.cm^2 over the duration of the experiment (Figure 5.5). ZO-1 was visualised in the Caco-2/Raji B co-culture exposed to cell culture medium (control) (Figure 5.6). After exposure to 6.34 Cu µg/cm^2 of CuO NMs and $CuSO_4$ for 24 h, a decreased intensity of ZO-1 staining was observed in the co-culture exposed to CuO NMs and $CuSO_4$ compared to control, implicating a loss of barrier integrity (Figure 5.6).

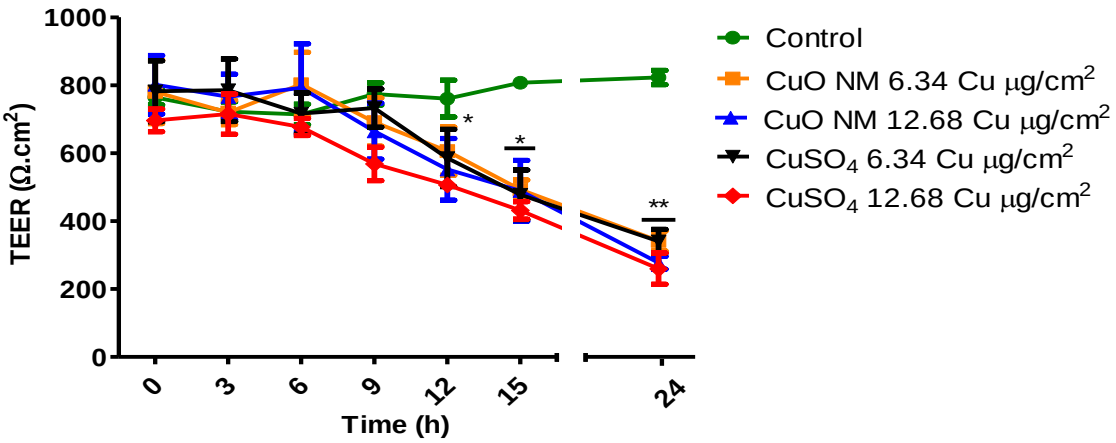

Figure 5.5: Impact of CuO NMs and $CuSO_4$ on Caco-2/Raji B co-culture TEER values.

*The Caco-2/Raji B co-culture was exposed to cell culture medium (control, 0), CuO NMs or $CuSO_4$ at concentrations of 6.34 or 12.68 Cu µg/cm^2 for 24 h. TEER values were measured using epithelial volt-ohmmeter EVOM every 3 h. Data are expressed as mean TEER ± SEM (n = 3). Significance at P<0.05 is indicated by * and P<0.01 is indicated by ** compared with control.*

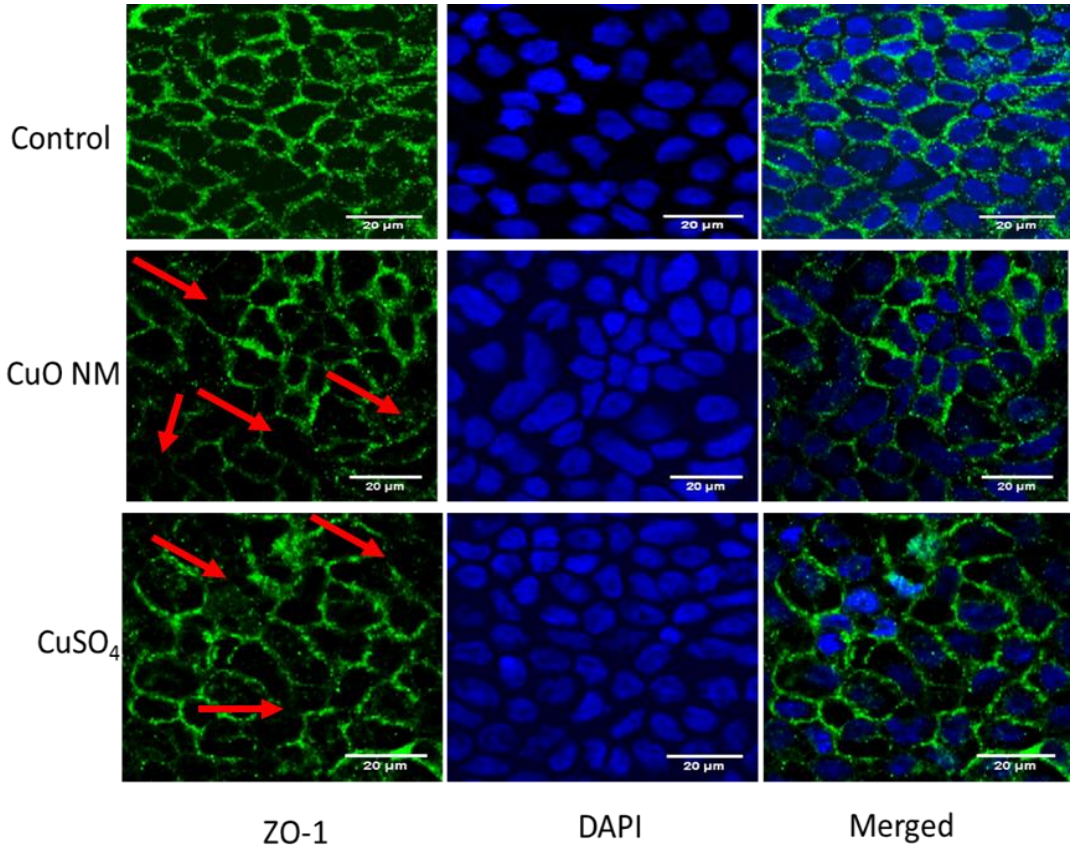

Figure 5.6: The impact of CuO NMs and $CuSO_4$ on Caco-2/Raji B co-culture tight junction proteins.

The Caco-2/Raji B co-culture was exposed to cell culture medium (control) or 6.34 Cu µg/cm^2 of CuO NMs and $CuSO_4$ for 24 h, then fixed, and stained for the tight junction protein ZO-1 (green) and nucleus (blue). The images extended focus were obtained using confocal microscope. Red arrows indicate areas where there is a reduction in ZO-1 staining intensity. Scale bar = 20 µm. Representative images are shown (n=3).

5.3.3. The impact of CuO NMs and $CuSO_4$ on Caco-2/Raji B co-culture cell viability and morphology

The presence of microvilli in the Caco-2/Raji B co-culture and impact of CuO NMs on cell morphology was investigated with SEM. Microvilli were visualised on the surface of the Caco-2/Raji B co-culture, however some cells lacked microvilli (Figure 5.7) suggesting that the M cells were present. Shortening of the microvilli on some of the cells was observed at 24 h post exposure to 12.68 Cu µg/cm^2 CuO NMs to Caco-2/Raji B co-culture (Figure 5.7). The viability and morphology of the Caco-2/Raji B co-culture was studied with light microscopy after exposure to cell culture medium (control), 6.34 or

12.68 Cu µg/cm^2 CuO NMs or $CuSO_4$ and stained with Romanowisky stain. The treated Caco-2/Raji B co-culture showed no visible impact on the cell viability and morphology at all treatment concentrations compared to the control (Figure 5.8). The viability of the Caco-2/Raji B co-culture was further studied by staining the co-culture with DAPI followed by nuclei counts after exposure to cell culture medium (control), 6.34 or 12.68 Cu µg/cm^2 CuO NM or $CuSO_4$ for 24 h. The co-culture treated with CuO NMs or $CuSO_4$ showed no significant difference in nuclei number at all concentrations compared to the control (Figure 5.9A) with representative images shown in Figure 5.9B. This suggests there was no loss of cell viability.

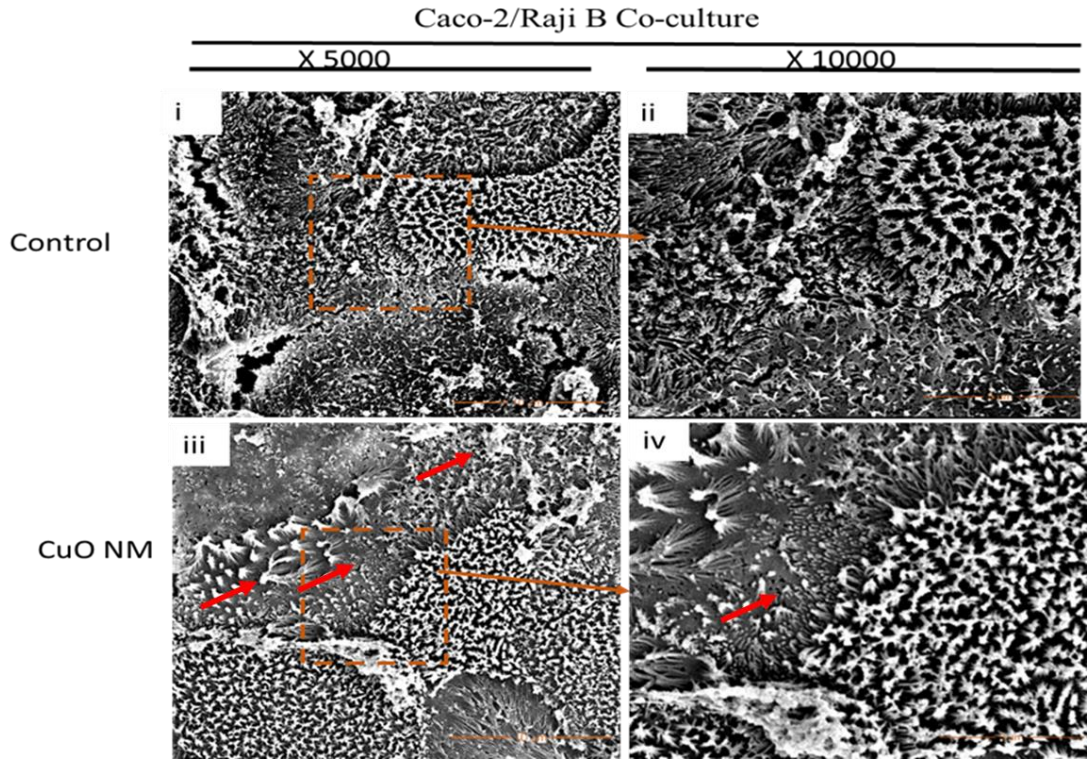

Figure 5.7: SEM images of Caco-2/Raji B co-culture exposed to CuO NMs.

The Caco-2/Raji B co-culture was exposed to cell culture medium (control) or 12.68 Cu µg/cm^2 of CuO NMs for 24 h. The cells were washed, fixed, dehydrated, dried and examined by SEM. i) and ii) are control Caco-2/Raji B co-culture cells imaged at a magnification of X 5000 and X 10000 respectively. iii) and iv) are Caco-2/Raji B co-cultures exposed to 12.68 Cu µg/cm^2 of CuO NMs imaged at a magnification of X 5000 and X 10000 respectively. Representative images are shown (n=3). Red arrows indicate area of shortened microvili.

.

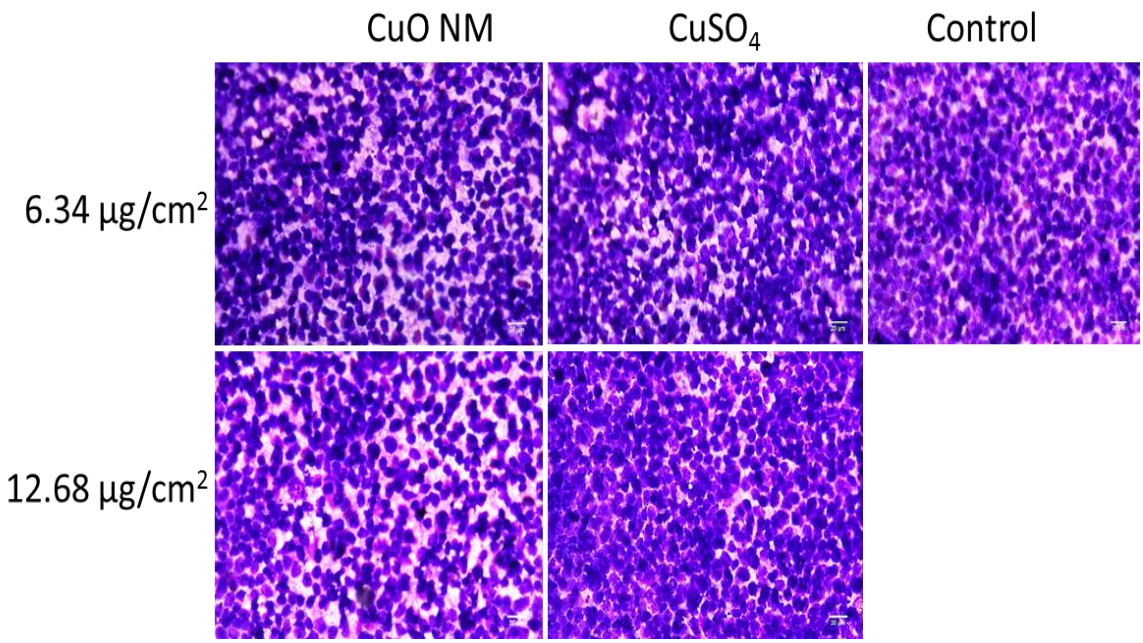

Figure 5.8: Impact of CuO NMs and $CuSO_4$ on Caco-2/Raji B co-culture cell morphology.

The Caco-2/Raji B co-culture was exposed to cell culture medium (control) and 6.34 or 12.68 Cu µg/cm^2 CuO NMs or $CuSO_4$ for 24 h. The cells were then fixed, stained and visualised using a light microscopy (magnification 40 X, scale bar=20 µm). Representative images are shown (n=3).

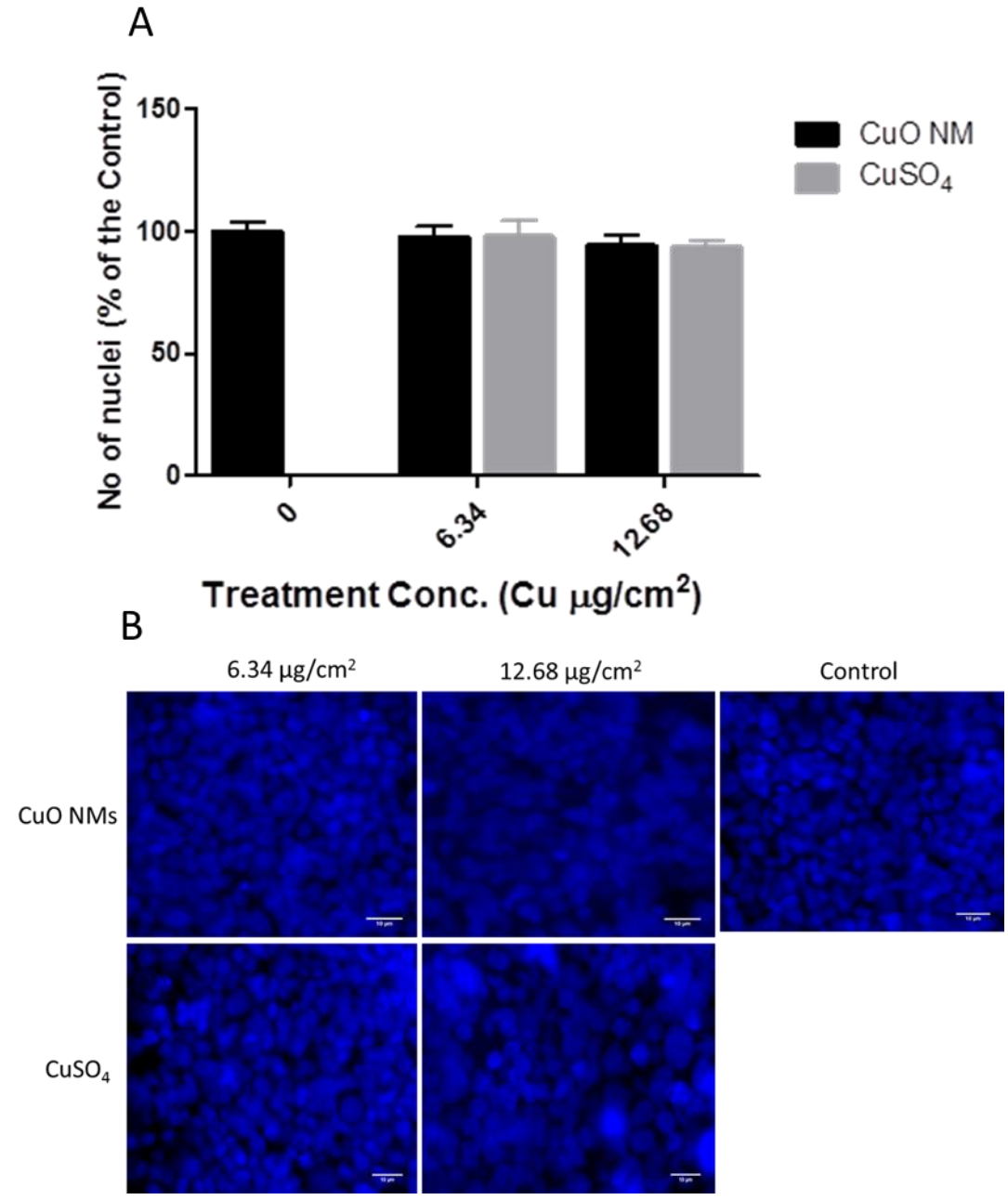

Figure 5.9: Assessment of the viability of the Caco-2/Raji B co-culture using nuclei staining with DAPI.

*The Caco-2/Raji B Co-culture was treated with 6.34 and 12.68 Cu µg/cm² of CuO NMs and $CuSO_4$, fixed and the nucleus (blue) stained and imaged with fluorescent microscope, (magnification 40X) and the nuclei counted using Image J software (A). Data are presented as number of nuclei (expressed in % of the unexposed control) ± SEM. Significance at $P<0.05$ is indicated by * compared to unexposed control. Representative images (B) are presented and scale bar = 10 µm. (n = 3).*

5.3.4. Cellular uptake and translocation of Cu across the intestinal monolayer

Exposure of CuO NMs and $CuSO_4$ to the Caco-2/Raji B co-culture demonstrated a concentration and time dependent decrease in the concentration of Cu ions retained at the AP compartment (Figure 5.10A). Typically, lower levels of Cu were detected at longer time points, and at higher treatment concentrations. A significant decrease in Cu concentration in the AP medium was observed at 48 h post exposure in cells exposed to 12.68 Cu µg/cm^2 of $CuSO_4$ for 24 h (Figure 5.10A). The concentration of Cu after 24 h ranged from 72 to 92 % (expressed as percentage of the initial treatment concentration), with the highest concentration in the AP compartment observed at a concentration of 3.17 Cu µg/cm^2 of CuO NMs and the lowest detectable Cu concentration observed when cells were treated with 12.68 Cu µg/cm^2 of CuO NMs. The detectable range of Cu ion in the AP compartment after a 48 h exposure to CuO NMs and $CuSO_4$ was between ~54 and 79 %. The highest detectable concentration at 48 h was observed when cells were exposed to 3.17 Cu µg/cm^2 $CuSO_4$ (79 %), and the lowest detectable concentration measured when cells were exposed to 12.68 Cu µg/cm^2 of CuO NMs (~54 %) (Figure 5.10A).

A time dependent increase in translocation of Cu across the Caco-2/Raji B co-culture exposed CuO NMs and $CuSO_4$ was observed (Figure 5.10B). Translocation was greatest at 48 h, with a significant increase in translocation of Cu from AP to BL compartment, at all concentrations for both treatments (~4.6-14.2 %). This suggests that the translocation of Cu across the intestinal monolayer increased with time. The concentration of Cu was lowest in the BL compartment after exposure of cells to 3.17 Cu µg/cm^2 CuO NMs and $CuSO_4$ for 24 h (~2.5 %). Whereas treatment of cells with 12.68 Cu µg/cm^2 of CuO NMs for 48 h had the highest concentration of Cu in the BL media, which was ~14 % (Figure 5.10B). There was no significant difference between the translocation of Cu from AP to BL compartment between Caco-2/Raji B co-culture exposed to CuO NMs and $CuSO_4$.

There was no significant time or concentration dependent cellular retention of Cu after exposure of cells to CuO NMs or $CuSO_4$. The concentration of detectable Cu in cells was < 2 % of the initial exposure concentration at 24 and 48 h at all the tested concentrations. The Caco-2/Raji B co-culture exposed to 3.17 Cu µg/cm^2 CuO NMs had the lowest concentration of Cu (0.4 %) at 24 h. At 48 h, exposure of cells to 3.17 Cu µg/cm^2 CuO NMs and $CuSO_4$ demonstrated the highest Cu ion retention (~1.3 %) (Figure 5.10C). No

significant difference was observed in and uptake of CuO NMs and $CuSO_4$ at 24 and 48 h post exposure (Figure 5.10C) and Cu was not detected in the control group.

P_{app} demonstrated a concentration and time dependent increase for treatments. This indicates that translocation from the AP to BL compartment in the Caco-2/Raji B co-culture occurred at the highest rate for cells exposed to 12.68 Cu μg/cm^2 of CuO NMs and $CuSO_4$ (highest P_{app} value) (Figure 5.11).

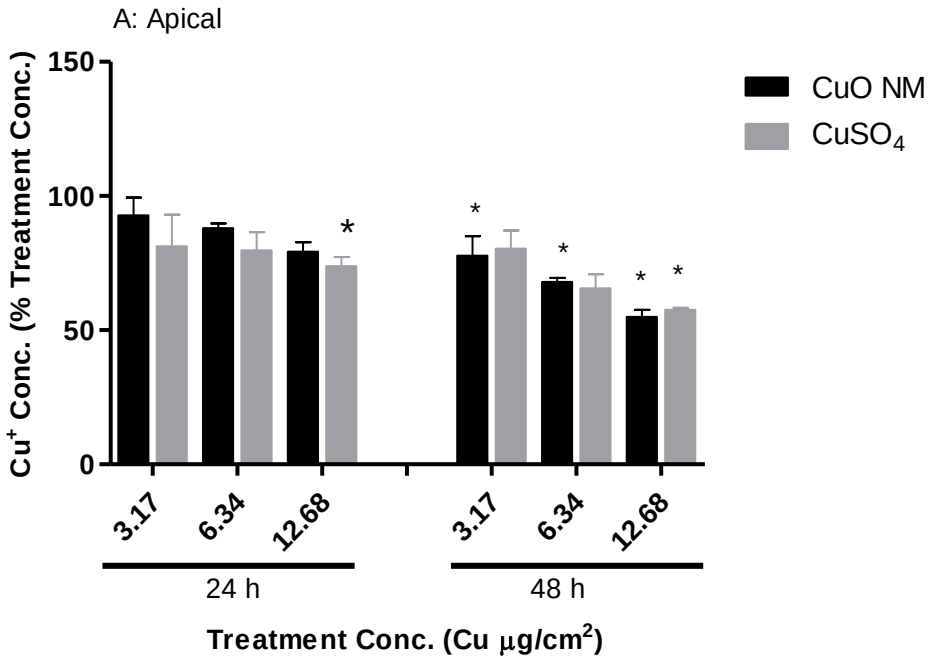

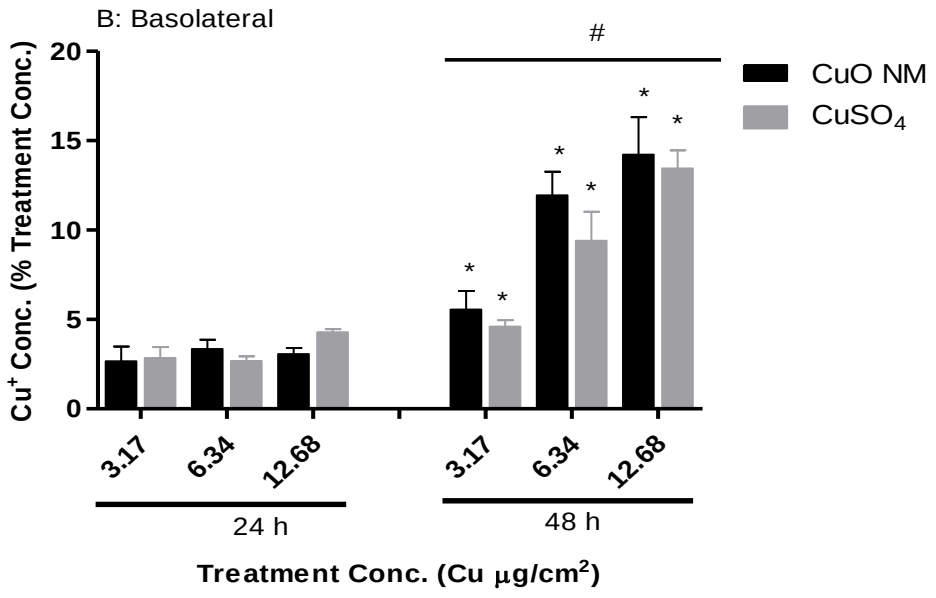

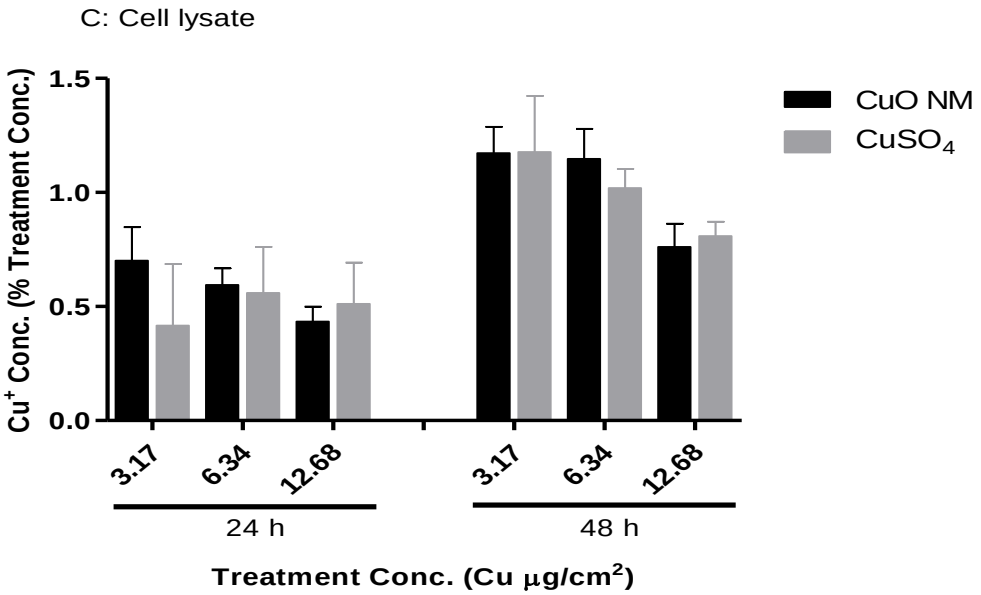

Figure 5.10: CuO NMs or $CuSO_4$ cellular uptake and translocation across the Caco-2/Raji B co-culture.

*The Caco-2/Raji B co-culture was exposed to cell culture medium (control, 0), CuO NMs or $CuSO_4$ at concentrations of 3.17, 6.34 or 12.68 Cu µg/cm^2 for 24 and 48 h. The level of Cu in the AP (A) and BL (B) compartments and the cells (C) was evaluated by ICP-OES. Sample preparation and data analysis was performed by Victor Chibueze Ude and Dr. Lorna Eades performed the ICP-OES analysis. Data are expressed as mean copper concentration (as a percentage of the treatment concentration) ± SEM (n = 3). Significance at P<0.05 are indicted by * for comparison of 24 h post exposure of 3.17 Cu µg/cm^2 of CuO NMs to other treatment concentration within each time point or # for comparison of equivalent concentrations between 24 and 48 h time points.*

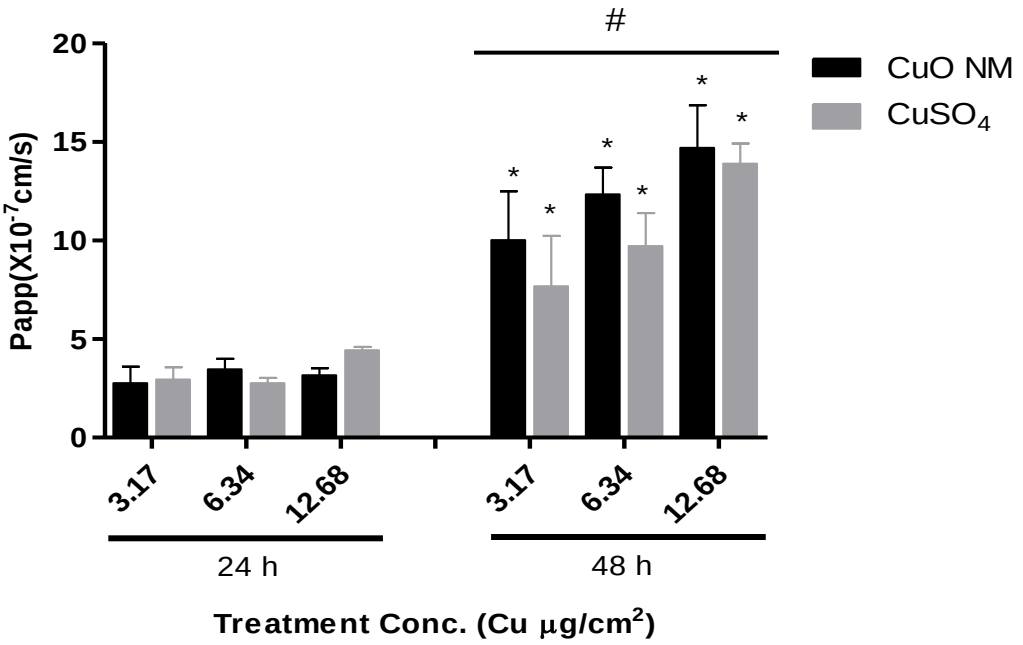

Figure 5.11: Apparent permeability coefficient (P_{app}) of CuO NM and $CuSO_4$.

*The Caco-2/Raji B co-culture was exposed to cell culture medium (control, 0), CuO NMs or $CuSO_4$ at concentrations of 3.17, 6.34 or 12.68 Cu µg/cm^2 for 24 and 48 h. The concentration of Cu in the AP and BL compartments was determined by ICP-OES and P_{app} was calculated. Data are expressed in mean P_{app} ± SEM x10^{-7} cm/s (n = 3). Significance at P<0.05 are indicted by * for comparison of 24 h post exposure of 3.17 Cu µg/cm^2 of CuO NMs to other treatment concentration within each time point or # for comparison of equivalent concentrations between 24 and 48 h time points.*

5.3.5. ROS formation

A significant increase in ROS production (> 4 fold greater than the control) was observed in the Caco-2/Raji B co-culture exposed to all concentration of $CuSO_4$. No increase in ROS production was observed in cells exposed to CuO NMs or positive control (Figure 5.12).

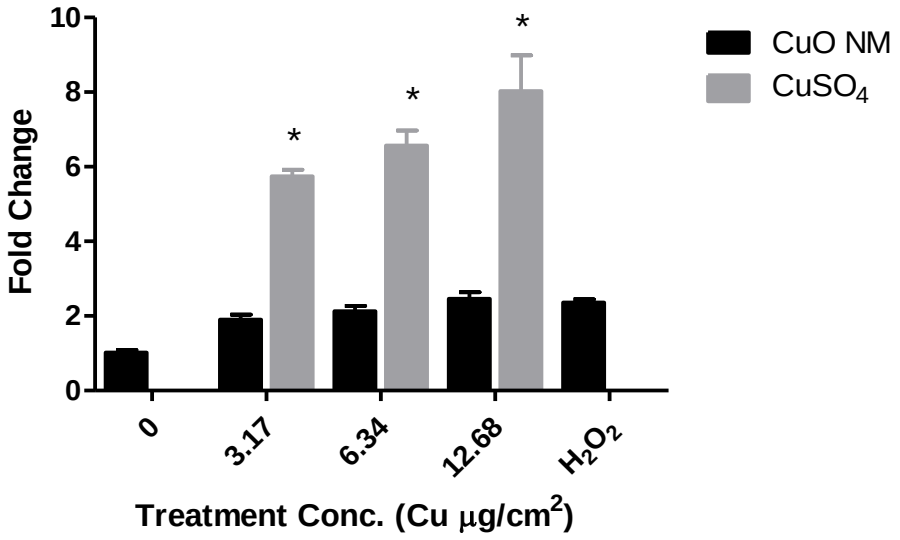

Figure 5.12: ROS formation by the Caco-2/Raji B co-culture following exposure to CuO NMs and $CuSO_4$ for 2 h.

*Intracellular ROS levels were determined using the DCFH-DA assay 2 h post exposure of Caco-2/Raji B co-culture to cell culture medium (control, 0), H_2O_2 (1 mM), CuO NMs and $CuSO_4$ at concentrations of 3.17, 6.34 and 12.68 Cu μg/cm^2. Data are expressed as fold change ± SEM (n = 3). Significance at $P<0.05$ is indicated by * compared to control.*

5.3.6. IL-8 production

Exposure of the Caco-2/Raji B co-culture to CuO NMs and $CuSO_4$ for 24 h stimulated a concentration dependent increase in IL-8 concentration. Both CuO NMs and $CuSO_4$ induced a similar level of IL-8 production, with the highest level of production observed at a concentration of 6.34 Cu μg/cm^2 CuO NMs and $CuSO_4$ (~320 and 349 pg/ml respectively) (Figure 5.13). IL-8 was below detectable level at the control cells (AP and BL media) and in the BL media for all treatments. The positive control (Caco-2/Raji B co-culture exposed to 200 ng/ml TNF-α for 24 h) stimulated IL-8 production of 76.92 ± 13.95 pg/ml.

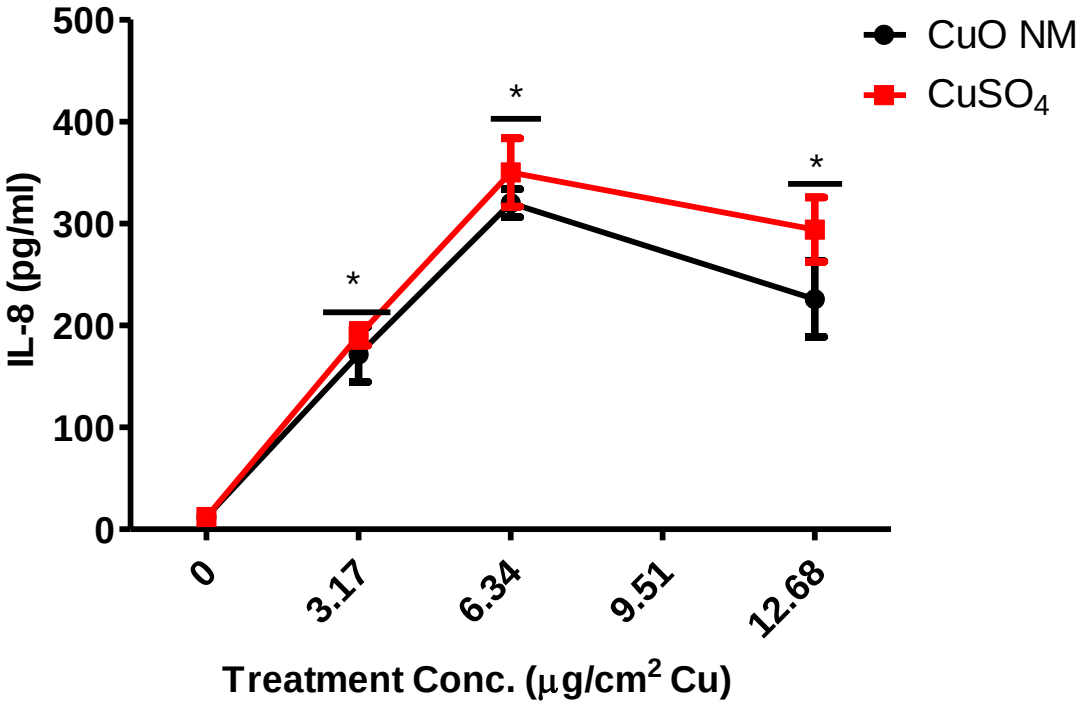

Figure 5.13: IL-8 production by the Caco-2/Raji B co-culture following exposure to CuO NMs and $CuSO_4$.

*The Caco-2/Raji B co-culture was exposed to cell culture medium (control, 0), CuO NMs or $CuSO_4$ at concentrations of 3.17, 6.34 or 12.68 Cu µg/cm^2 for 24 h. The level of IL-8 in the cell supernatant was determined using an ELISA kit. Data are expressed as mean IL-8 concentration (pg/ml) ± SEM (n = 3). Significance at P<0.05 is indicated by * compared to control.*

5.3.7. Gene expression

A significant increase in *HMOX1* expression was observed in the Caco-2/Raji B co-culture at all time points, post exposure to 6.34 and 12.68 Cu µg/cm^2 of CuO NMs and $CuSO_4$ when compared to the control. The level of *HMOX1* expression following exposure to 12.68 Cu µg/cm^2 of CuO NMs and $CuSO_4$ was greater at 4 and 12 h than that observed at 24 h. The highest level of *HMOX1* expression was observed after exposure of cells to a concentration of 12.68 Cu µg/cm^2 of CuO NMs at 4 and 12 h with ~ 13 fold increase. The lowest expression was observed at a concentration of 3.17 µg/cm^2 Cu CuO NMs and $CuSO_4$ (1.5 to 1.8 fold) at 12 and 24 h (Figure 5.14A).

IL8 expression significantly increased at 12 h post exposure of the Caco-2/Raji B co-culture to CuO NMs and $CuSO_4$ (3.4 to 13.6 fold increase) compared to control, except

at a concentration of 3.17 Cu μg/cm^2 $CuSO_4$ (2.2 fold increase) (Figure 5.14B). A significant increase in *IL8* expression was also observed after exposure of cells to 12.68 Cu μg/cm^2 CuO NMs for 24 h (3.6 fold increase). The maximum level of *IL8* expression was observed at a concentration of 12.68 Cu μg/cm^2 of CuO NMs at 12 h, whereas the lowest *IL8* expression was observed at a concentration of 3.17 Cu μg/cm^2 of CuO NMs 4 h post exposure (0.7 fold) (Figure 5.14B).

A significant upregulation in *MT1A* expression in the Caco-2/Raji B co-culture was observed at 12 and 24 h post exposure to 12.68 Cu μg/cm^2 of CuO NMs and $CuSO_4$ compared to control with the fold increase ranging from 3.2 to 4.5 (Figure 5.14C). *MT1A* demonstrated the strongest expression after exposure of cells to 12.68 Cu μg/cm^2 of CuO NMs and $CuSO_4$ at 12 h (~4.5 fold) while the lowest expression was observed at 3.17 Cu μg/cm^2 of CuO NMs for 4 h (0.8 fold) (Figure 5.14C).

Exposure of the Caco-2/Raji B co-culture to 12.68 Cu μg/cm^2 of CuO NMs and $CuSO_4$ for 12 and 24 h elicited a significant increase in *MUC2* expression (3.2 to 4.5 fold increase) compared to control (Figure 5.14D). The strongest response was observed at 12 h post exposure to12.68 Cu μg/cm^2 of CuO NMs and $CuSO_4$ (~4 fold increase) and the lowest expression induced by CuO NMs and $CuSO_4$ (1.2 and 1.8 fold respectively) after 4 h exposure (Figure 5.14D). Comparison of *MUC2* expression by CuO NM and $CuSO_4$ demonstrated a non-significant difference.

The Caco-2/Raji B co-culture exposed to CuO NMs and $CuSO_4$ demonstrated a concentration and time dependent increase in *MT2A* expression (Figure 5.14E). Caco-2/Raji B co-culture exposed to CuO NMs and $CuSO_4$ showed the highest response at 12 h post exposure, with the maximal response observed at concentrations of 6.34 and 12.68 Cu μg/cm^2 of CuO NMs and $CuSO_4$ (fold increase ranged between 24 and 44). However, the lowest level of expression was observed at 4 h post exposure of 3.17 Cu μg/cm^2 CuO NMs and $CuSO_4$ (fold increase 2.4 and 2.9 respectively). There was no significant difference between CuO NM and $CuSO_4$ induced *MT2A* expression exposure (Figure 5.14E). Heatmap representation of the gene expression study is shown in Figure 3.15. In general, the greatest response was observed at 12 h post exposure for all genes with *MT2A* observed to be the most sensitive compared to the other genes.

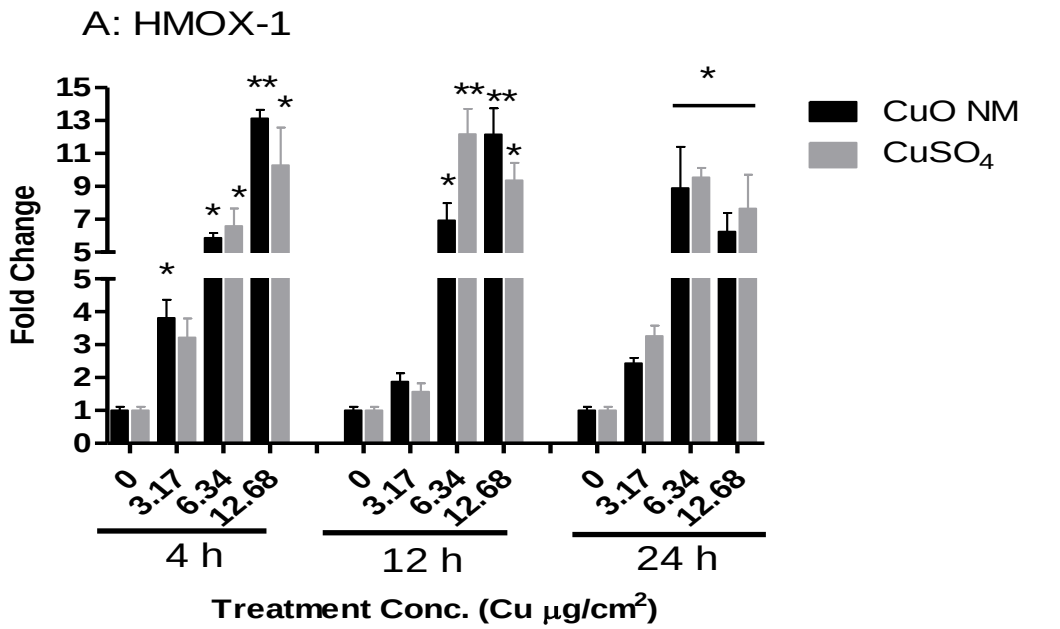
A: HMOX-1
Fold Change
CuO NM
CuSO4
0
3.17
6.34
12.68
4 h
12 h
24 h
Treatment Conc. (Cu μg/cm2)

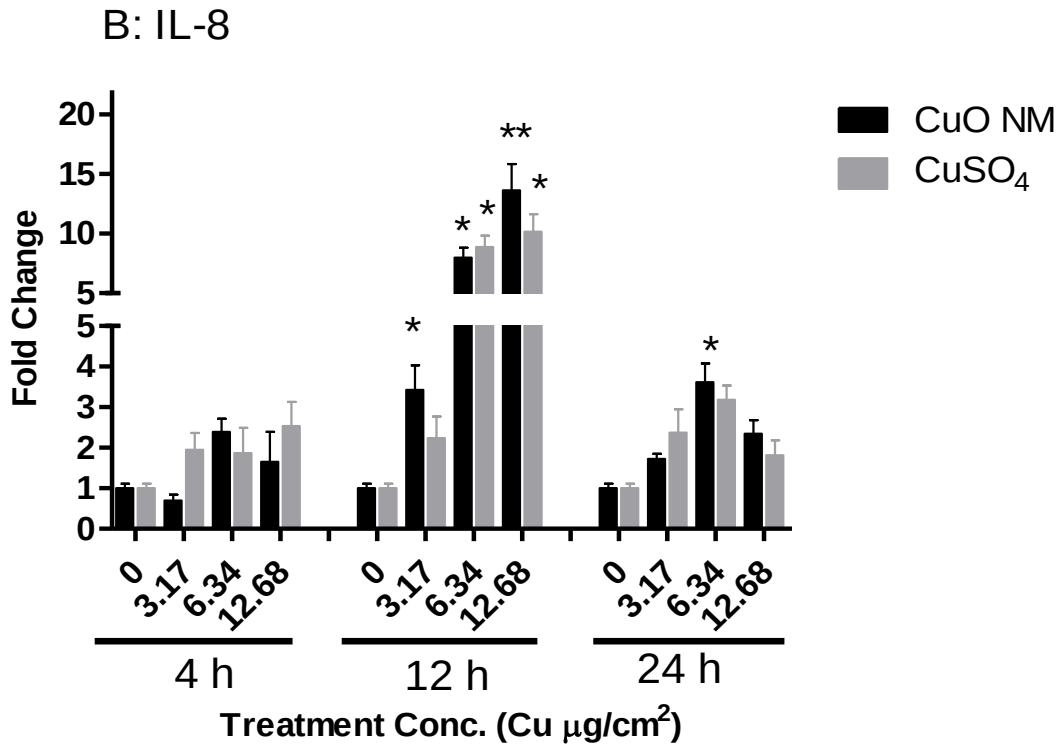
B: IL-8
Fold Change
CuO NM
CuSO4
0
3.17
6.34
12.68
4 h
12 h
24 h
Treatment Conc. (Cu μg/cm2)

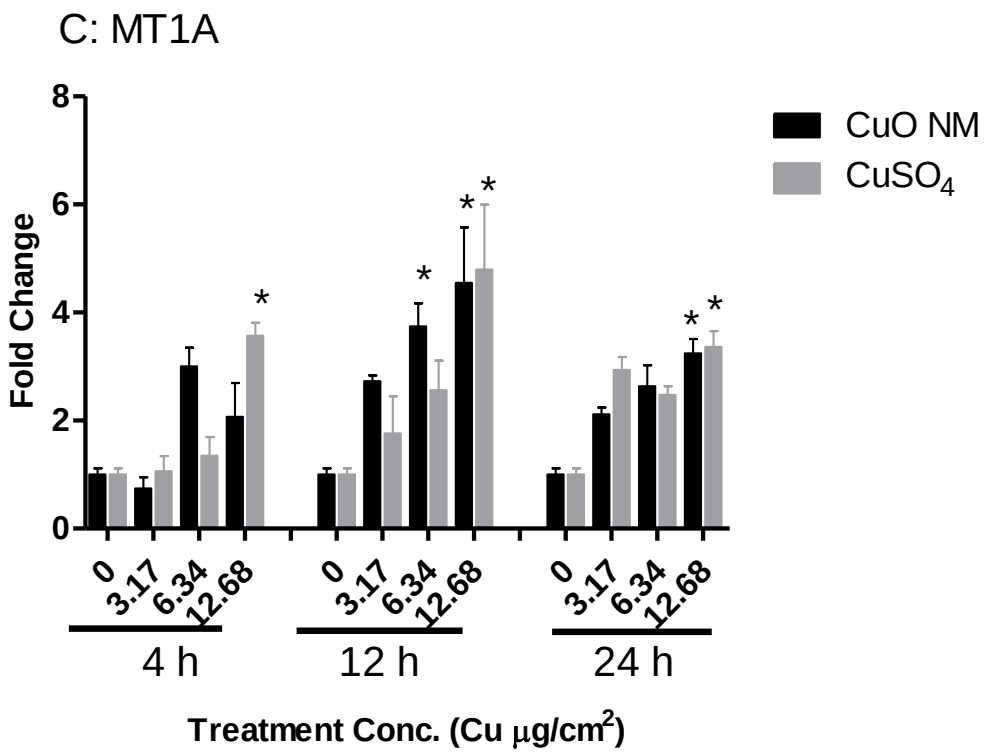
C: MT1A
CuO NM
CuSO4
Fold Change
0
2
4
6
8
0
3.17
6.34
12.68
4 h
12 h
24 h
Treatment Conc. (Cu μg/cm2)

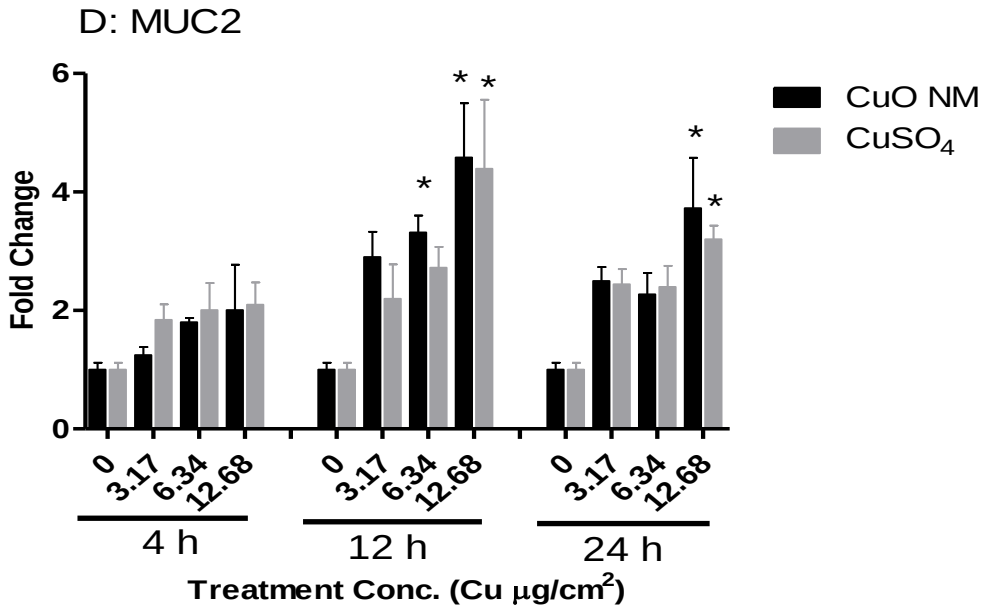
D: MUC2
CuO NM
CuSO4
Fold Change
0
2
4
6
0
3.17
6.34
12.68
4 h
12 h
24 h
Treatment Conc. (Cu μg/cm2)

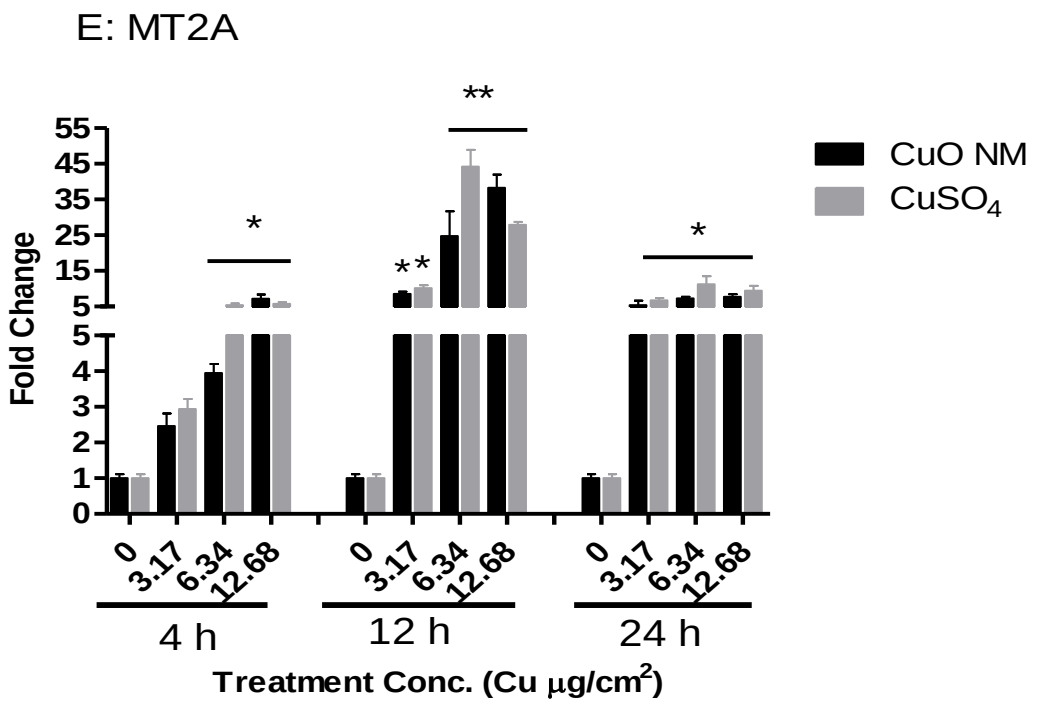

Figure 5.14: Effect of CuO NMs and $CuSO_4$ on gene expression in the Caco-2/Raji B co-culture.

*Caco-2/Raji B cells were exposed to cell culture medium (control, 0), CuO NMs or $CuSO_4$ at concentrations of 3.17, 6.34 or 12.68 Cu μg/cm^2 for 4, 12 and 24 h and changes in HMOX1(A), IL8 (B), MT1A (C), MUC2 (D), MT2A (E) expression assessed using qPCR. Data were expressed as mean fold change ± SEM (n = 3). Significance indicated by * = P<0.05 and ** = P<0.01 compared to control.*

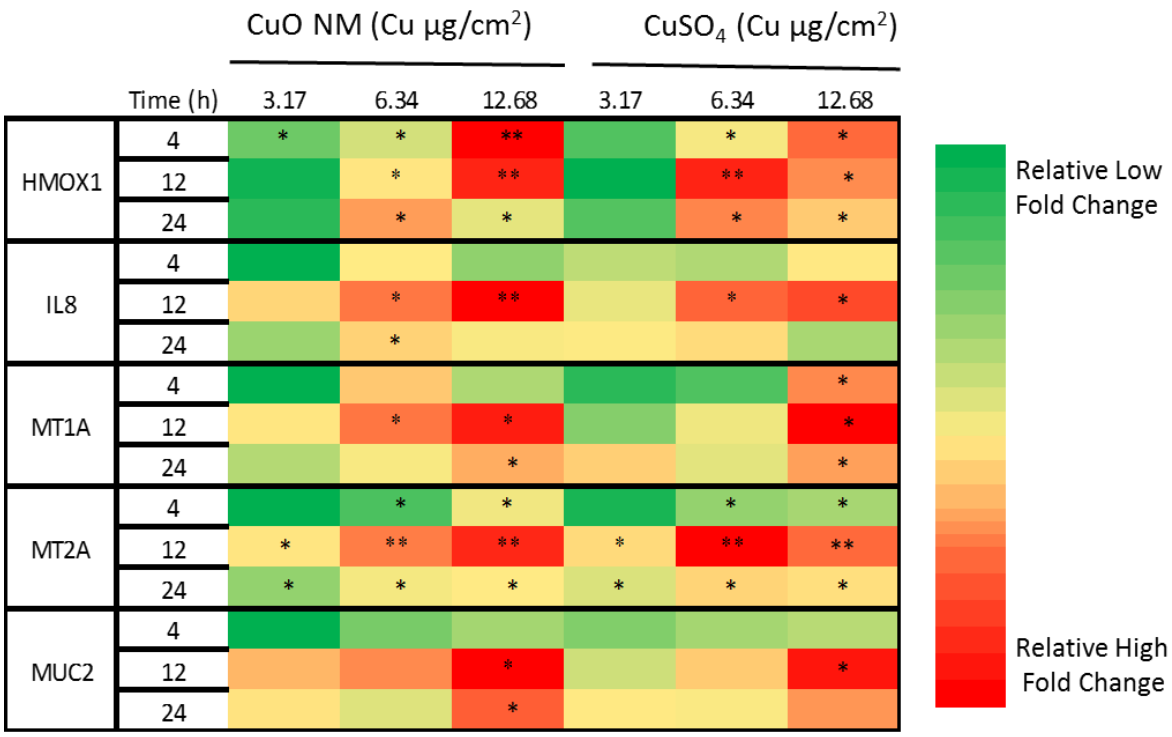

Figure 5.15: Heatmap representation of gene expression by the Caco-2/Raji B co-culture after exposure to CuO NMs and $CuSO_4$.

*Caco-2/Raji B cells were exposed to cell culture medium (control, 0), CuO NMs or $CuSO_4$ at concentrations of 3.17, 6.34 or 12.68 Cu µg/cm² for 4, 12 and 24 h and expression of HMOX1, IL8, MT1A, MUC2, MT2A assessed using qPCR. Genes were compared separately within each time point. Significance indicated by * = P<0.05 and ** = P<0.01 compared to control.*

5.4. Discussion

In this chapter, the findings of the impact of CuO NMs and $CuSO_4$ on the Caco-2/Raji B co-culture were investigated via assessment of cell viability (nuclei count and light microscopy), cell morphology (light microscopy and SEM), IL-8 production, ROS formation and barrier integrity (SEM, TEER and ZO-1 staining). M cell formation by Caco-2/Raji B co-culture was assessed via TEM and WGA staining. Cu translocation (ICP-OES) and expression of *HMOX1* (oxidative stress gene), *IL8* (inflammatory response gene), *MUC2* (mucus secreting gene), *MT1A* and *MT2A* (metal binding genes) (RT qPCR) were also investigated. M cell formation by the co-culture was confirmed by the high intensity of WGA staining and lack of microvilli (TEM). CuO NMs and $CuSO_4$ mediated no significant cell death on the Caco-2/Raji B co-culture as demonstrated by a lack of impact on nuclei number and morphology. CuO NMs and $CuSO_4$ impaired barrier

integrity as shown by a decrease in TEER, tight junction (ZO-1) staining and shortening of the microvilli. The compromise in the barrier integrity is likely to have resulted in a concentration and time dependent translocation of Cu ions across the Caco-2/Raji B co-culture barrier. CuO NMs and $CuSO_4$ also mediated an increase in IL-8 production and upregulated the expression of *HMOX1, IL8, MUC2, MT1A* and *MT2A*. In general, there was no difference between the impact of CuO NMs and $CuSO_4$ on the Caco-2/Raji B co-culture for all the endpoints employed for this study, except ROS formation.

5.4.1. Caco-2/Raji B morphology and viability study

In the small intestine, it is only the M cells that are known to lack some of the characteristics of absorptive cells such as the absence of microvilli, reduced or no hydrolytic enzymes and alkaline phosphatase (Brayden et al. 2005, Schimpel et al. 2014). Other methods such as TEM, alkaline phosphatase expression, and FITC labelled WGA staining have been employed in the identification of the presence of M cells *in vitro* (Schimpel et al. 2014, Ma et al. 2014, des Rieux et al. 2007, Antunes et al. 2013). In this study, FITC labelled WGA staining was used. The WGA staining demonstrated a high intensity in Caco-2/Raji B co-culture compared to that observed for differentiated Caco-2 cells and the Caco-2/HT29-MTX co-culture suggesting a successful formation of M cells by Caco-2/Raji B co-culture. Previous researchers have reported similar findings (Gullberg et al. 2000, Schimpel et al. 2014, Antunes et al. 2013). The staining observed in differentiated Caco-2 cells and the Caco-2/HT29-MTX co-culture may be because of the presence of some WGA receptors or sialic acid and N-acetyl glucosamine, which are usually minimal in epithelial cells (Schimpel et al. 2014, Antunes et al. 2013). The lack of microvilli observed with TEM and SEM in the Caco-2/Raji B co-culture compared to differentiated Caco-2 cells and the Caco-2/HT29-MTX co-culture was similar to the findings of des Rieux et al and Ma et al, and confirmed the development of M cells by the co-culture (des Rieux et al. 2007, Ma et al. 2014).

Assessment of the barrier integrity of the Caco-2/Raji B co-culture is essential when using this *in vitro* model as seeding of Raji B cells to the BL compartment of the Caco-2 cell may lead to disruption in the integrity of the monolayer. Barrier integrity of Caco-2/Raji B co-culture was investigated by measurement of TEER and tight junction staining. TEER measurement is routinely used to study the integrity of the Caco-2/Raji B co-

culture monolayer and it has been shown previously that formation of M cell leads to reduced TEER values (Kernéis et al. 1997, Ma et al. 2014, des Rieux et al. 2007). The TEER value of this study reduced on the 5th day after seeding Raji B cells into the BL compartment, indicating the formation of M cell by the co-culture, compared to differentiated Caco-2 cells. However, the TEER was still over 500 $\Omega.cm^2$, which indicates that the barrier was still functional. Assessment of TEER was also measured after exposure of CuO NMs and $CuSO_4$ to the Caco-2/Raji B co-culture and unexposed control cells in order to investigate impacts on barrier integrity. No change in TEER value after 24 h was observed in control cells. However, when exposed to CuO NMs and $CuSO_4$ the TEER value significantly reduced from 12 to 24 h post exposure, which suggests a disruption in barrier integrity. Previously, decreased TEER values have been reported only at one-time point when assessing the impact of Ag NMs on the integrity of the intestinal barrier using M cell *in vitro* model (Bouwmeester et al. 2011, Antunes et al. 2013, Lozoya-Agullo et al. 2017). In this study, the study design enabled determination of the time when the TEER value started decreasing. The unchanged control TEER value suggests that the monolayer of the co-culture was still intact since there was no further reduction after the formation of M cells.

In addition to the TEER measurement, the Caco-2/Raji B co-culture tight junction protein (ZO-1) was stained after exposure of cells to cell culture medium (control), CuO NMs and $CuSO_4$. Monitoring of tight junction development is frequently investigated by staining ZO-1 protein in different models of intestine *in vitro* including differentiated Caco-2 cells (Price et al. 2014, Qin et al. 2009, Ude et al. 2017) and Caco-2/HT29-MTX co-culture (Brun et al. 2014). However, to my knowledge, there is no published paper on ZO-1 staining of CuO NMs exposed Caco-2/Raji B co-culture. Unexposed Caco-2/Raji B co-culture demonstrated an intense staining indicating the formation of intact tight junctions. When exposed to CuO NMs or $CuSO_4$, reduced tight junction staining was observed in the Caco-2/Raji B co-culture compared to unexposed co-culture. This suggests that CuO NMs and $CuSO_4$ may have caused a disruption in the integrity of the monolayer, which agrees with the findings from the TEER measurement. However, the loss of tight junction staining observed was less (i.e. there was less damage) when compared to that observed for differentiated Caco-2 cells, which suggests that co-culture is less sensitive to NM toxicity.

The Caco-2/Raji B co-culture was imaged with SEM after exposure to cell culture media (control) and CuO NMs. SEM imaging has been used for the identification of M cells in published papers (Schimpel et al. 2014, des Rieux et al. 2007). Indeed, the absence of microvilli in some cells confirmed the formation of M cells in the co-culture. The exposure of CuO NMs to the co-culture caused shortening of microvilli on some cells compared to the control. Although shortening or loss of microvilli have not been reported for the Caco-2/Raji B co culture, exposure of CuO NMs (Ude et al. 2017) and food grade TiO_2 (Faust et al. 2014a, Koeneman et al. 2010) have disrupted the microvilli in differentiated Caco-2 cells. No impact on the morphology of cells or cell number using light microscopy and nuclei number count was observed in this study, suggesting there was no cell loss due to treatment of the cells with CuO NMs or $CuSO_4$. Cell loss due to exposure of undifferentiated Caco-2 cells to CuO NMs or $CuSO_4$ studied via light microscopy and nuclei count have been reported (Ude et al. 2017) (section 2.3.2). This suggests that M cell model is not as sensitive to CuO NMs and $CuSO_4$ toxicity as undifferentiated Caco-2 cells.

5.4.2. Translocation and cellular uptake

The M cell *in vitro* model of intestinal epithelium are used not only for drug absorption and permeability (Antunes et al. 2013, Lozoya-Agullo et al. 2017, Beatriz et al. 2014) but also for investigating NM permeability and translocation. For example, the Caco-2/Raji B co-culture has been used to assess the translocation of Ag NMs (Bouwmeester et al. 2011), TiO_2 (Brun et al. 2014, Cabellos et al. 2017), aminated and carboxylated polystyrene nanoparticles (des Rieux et al. 2005, des Rieux et al. 2007), chitosan-DNA NMs (Kadiyala et al. 2010), and polystyrene NMs (Schimpel et al. 2015). However, none of these studies have used CuO NMs and $CuSO_4$ or assessed the level of NMs in the AP and BL compartments, and cell lysate. A concentration and time dependent translocation of Cu from the AP to BL compartment was observed after exposure of Caco-2/Raji B cells to CuO NMs and $CuSO_4$. The time and concentration dependent translocation could be because the intestinal monolayer is compromised, as demonstrated by the reduction in TEER, shortening of microvilli and reduction in ZO-1 staining intensity described above (section 5.4.1). Indeed, a decrease in TEER value has been shown to induce an increase in the translocation of insulin encapsulated chitosan NMs in M cell (Antunes et al. 2013). Surprisingly, the translocation of CuO NMs and $CuSO_4$ were similar, though the

dissolution study demonstrated < 80 % dissolution of CuO NMs (at 24 h). Since the translocation was investigated via ICP OES analysis, the information about the form in, which CuO NMs was translocated (particle or ion) are not available. In the future, uptake studies via imaging will be included to elucidate whether the CuO NMs are translocated in its particle or ionic form.

As described in previous chapter (section 3.4.2), the summation of the detected Cu concentration in the AP, BL and cell lysate did not add up to 100 %, suggesting a loss of Cu ion during the experiment and the reason for inability to detect 100 % of the treated concentration have been discussed in (section 3.4.2). This study demonstrated a translocation of 5 to 12 % of Cu across the intestinal barrier at 48 h post exposure to 3.17 and 6.34 µg/cm^2 CuO NMs and $CuSO_4$, which was higher than that observed for differentiated Caco-2 cells and Caco-2/HT29-MTX co-culture suggesting that presence of M cell may have caused an increased translocation. *In vivo* translocation studies demonstrated 0.6 % translocation of 48V-radiolabeled (48V) TiO_2 NMs (70 nm) after 1 h intra-oesophageal instillation to rats (Kreyling et al. 2017). In addition, < 1.7 % translocation was observed after administration of polystyrene NMs (50 nm) via oral gavage (Walczak et al. 2015a). Nevertheless, this cannot be compared directly as they did not use the same time point or NMs that was used in this study. However, translocation of NMs *in vitro* has been demonstrated to be greater than observation *in vivo*. The Caco-2/Raji B co-culture exposed to Ag NMs (20 and 30 nm) for 4 h (Bouwmeester et al. 2011) and TiO_2 for 48 h (Cabellos et al. 2017) showed a reduced translocation (<1.5 %) compared to the present study. This could be associated with difference in the physicochemical properties of NMs investigated in these studies (e.g. solubility).

The permeability of Cu across Caco-2/Raji B co-culture measured by P_{app} calculation demonstrated a time dependent translocation after exposure to CuO NMs and $CuSO_4$. The P_{app} value was less than 1x 10^{-6} after 24 h exposure and above 1x 10^{-6} at 48 h post exposure suggesting that at 24 h post exposed Cu was poorly translocated whereas at 48 h post exposure translocation was moderately better. Permeability of Cu in M cell *in vitro* model was greater than that of differentiated Caco-2 cells and Caco-2/HT29-MTX co-culture and this was expected due to the role of M cells and compromise in the barrier integrity. A decrease in TEER value has been shown to corroborate with an increase in permeability in M cell *in vitro* models (Antunes et al. 2013, Akbari et al. 2017). In

comparison, Caco-2/Raji B co-culture demonstrated an increased P_{app} compared to differentiated Caco-2 cell at lower exposure concentration (3.17 and 6.34 Cu µg/cm^2) and similar P_{app} at increased exposure concentration (12.68 Cu µg/cm^2) in this study suggesting that the translocation may have been mediated by M cell. The reason for similar P_{app} between differentiated Caco-2 cells and Caco-2/Raji B co-culture at higher concentration of 12.68 Cu µg/cm^2 of CuO NMs and $CuSO_4$ may be due to saturation of the monolayer by Cu thereby reducing the rate of translocation. (Akbari et al. 2017). The P_{app} of this was similar to the P_{app} of insulin-loaded dextran sulphate/chitosan nanoparticles (Antunes et al. 2013) but lower than the P_{app} of *ex-vivo* study with rat ileum (Woitiski et al. 2011, Yin et al. 2009, Yin et al. 2008).

5.4.3. ROS formation

Literature has demonstrated the involvement of ROS in NM toxicity (section 3.4.3) and in this study, a significant concentration dependent increase in ROS was observed in the Caco-2/Raji B co-culture exposed to $CuSO_4$ but not CuO NMs at 2 h post exposure. The explanation of this behaviour of CuO NMs may be that the exposure time was too short therefore; the CuO NMs had not dissolved completely as it is hypothesised that ion mediate ROS production. Dissolution study in cell culture media has shown that only about 45 % of CuO NMs dissolve after 1h (Ude et al. 2017). Only one-time point was investigated due to the high cost of using co-culture models. In addition, the mechanism of CuO NM toxicity my not be through ROS production. Previously, study with Caco-2/HT29-MTX demonstrated a lack of ROS production after exposure of Ag NM (20 and 200 nm) and $AgNO_3$ for 2 h (Georgantzopoulou et al. 2016) and SWCNT-COOH, MWCNT-COOH and MWCNT-PVP for 8 h (Lai et al. 2013). However more comprehensive investigation of the involvement of oxidative stress could be performed in the future, for example, by performing, Electron Paramagnetic Resonance (EPR) methods of ROS measurement and glutathione depletion.

5.4.4. IL-8 production

Exposure of the Caco-2/Raji B co-culture to CuO NMs and $CuSO_4$ mediated a concentration dependent increase in IL-8 production, reaching maximum at a concentration of 6.34 Cu µg/cm^2. IL-8 production has not been previously assessed while

studying the toxicity of NMs using a Caco-2/Raji B co-culture. However, IL-8 production has been assessed in other intestinal models. For example, IL-8 was produced by Caco-2/THP1 co-culture following exposure to TiO_2 and Au NMs (Susewind et al. 2016). CuO NMs and $CuSO_4$ produced similar level of IL-8 at all concentration, hence suggesting particle and ion mediated toxicity.

5.4.5. Gene expression

Previously, expression of the characteristic *in vivo* M cell genes in the Caco-2/Raji B co-culture have been assessed and Caco-2/Raji B cell demonstrated a substantial correlation with *in vivo* M cell (Lo et al. 2004). However, gene expression is not frequently used as a tool for assessing the toxicity of NMs in the Caco-2/Raji B co-culture. One study was identified, which assessed changes in gene expression after exposure of Caco-2/Raji B co-culture to Ag NMs and demonstrated upregulation of several genes including *HMOX1*, *MT1*, *MT2A* (Bouwmeester et al. 2011). In this study, expression of oxidative stress genes (*HMOX1*), metal binding gene (*MT1A* and *2A*), mucus secreting gene (*MUC2*) and pro-inflammatory response gene (*IL8*) were used to assess the toxicity of CuO NMs and $CuSO_4$. Surprisingly, *HMOX1* expression was induced after exposure of Caco-2/Raji B cells to 6.34 and 12.68 Cu µg/cm^2 of CuO NMs and $CuSO_4$ with no difference between the expression mediated by CuO NMs and $CuSO_4$. This was against the expectation that there will be a decreased *HMOX1* expression in CuO NM as $CuSO_4$ produced significantly elevated ROS than CuO NMs. ROS production is known to induce *HMOX1* expression thereby regulating the injury due to oxidative stress, apoptosis and inflammation (Kundu et al. 2016, Loboda et al. 2016).

IL8 expression was also greatly induced at 12 h post exposure of Caco-2/Raji B co-culture to CuO NMs and $CuSO_4$. Other cell types such HeLa cells and A549 cells (Sthijns et al. 2017, Miura and Shinohara 2009) undifferentiated Caco-2 cells after exposure to Au (5nm) (Bajak et al. 2015) have demonstrated *HMOX1* upregulation on exposure to NMs. In addition, CuO NMs and $CuSO_4$ induced a similar level of expression of *HMOX1* and *IL8* in the Caco-2/Raji B co-culture, which implies that toxicity of CuO NMs may be mediated by both particles and ions since CuO NM dissolution was not 100 % (Ude et al. 2017). Increased *HMOX1* expression was also reported after exposure of Ag NMs to Caco-2/Raji B co-culture (Bouwmeester et al. 2011) and there is no published research

on expression of *IL8* in Caco-2/Raji B co-culture. The increased in *IL8* expression correlated with the observed increase in IL-8 protein secretion (ELISA) in this study however, other models used in this study induced a greater level of *IL8* gene and protein expression. The maximum level of *IL8* at 12 h post exposure indicates that 12 h post exposure may be the optimum time for studying *IL8* expression. Gerloff et al reported upregulation of *IL8* mRNA at post exposure of SiO_2 and ZnO NMs to differentiated Caco-2 cell (Gerloff et al. 2013).

MTs are essential in homeostatic regulation of transition metals such as Zn and Cu (Okita et al. 2017) and function as ROS scavenger (Shiraga et al. 1993) and *HMOX1* modulator (Ryter and Choi 2005). However, inappropriate binding (i.e. when the Cu binds to a wrong binding site) of Cu to MT may result to ROS production (Okita et al. 2017) therefore *MT* expression may be essential for NM toxicity. An increase in expression of *MT1A* and *MT2A* was observed at all time points, with the highest response observed for *MT2A* after exposure of the Caco-2/Raji co-culture to CuO NMs and $CuSO_4$. Both *MT1A* and *MT2A* had the highest expression at 12 h post exposure suggesting that the optimum time point for *MT1A* and *MT2A* is 12 h. *MT2A* response was also clearly high at 4 h post exposure, hence for quick assessment of toxicity of CuO NMs, *MT2A* may be useful. An increase in the expression of *MT1A* and *MT2A* including other isoforms of *MT1* (*MT1B*, *MT1M*, *MT1L*, *MT1E*, *MT1*F, *MT1X*, *MT1G* and *MT1H*) after exposure of Caco-2/Raji B cells was observed for Ag NMs (Bouwmeester et al. 2011). Exposure of A549 and BEAS-2B (pulmonary) cells to CuO NMs (Strauch et al. 2017) and differentiated Caco-2 cells to Au NMs (Bajak et al. 2015) mediated an increase in *MT1A* and *MT2A* expression. Therefore, an increase in *MT* expression may be a useful indicator of (metal and metal oxide) NM toxicity across different cell types. Although, different cell types may vary with respect to what subtype is expressed. CuO NMs and $CuSO_4$ mediated similar level of *MT1A* and *MT2A* as observed by the above-mentioned researchers after exposure to Caco-2/Raji co-culture.

MUC2 is principally expressed in the intestine and are essential for mucus secretion (section 4.4.5). Exposure of the Caco-2/Raji co-culture to CuO NMs and $CuSO_4$ induced a significant increase in *MUC2* expression only at the highest concentration of CuO NMs and $CuSO_4$ (12.68 Cu $\mu g/cm^2$). The increase in *MUC2* expression may occur due to stimulation of a pro-inflammatory response (section 3.4.5). However, there is no mucus

secreting cells in Caco-2/Raji B co-culture therefore low level of *MUC2* expression is expected. Again, *MUC2* expression were similar for both CuO NMs and $CuSO_4$ in Caco-2/Raji B co-culture. *MUC2* expression in Caco-2/Raji B co-culture was lower compared to Caco-2/HT29-MTX co-culture. This is expected as the M cell model lacked mucus secreting cells. As there is no mucus secreting cells in Caco-2/Raji B co-culture therefore low level of *MUC2* expression is expected, and therefore it is not an appropriate biomarker of CuO NM toxicity for this model.

5.5. Conclusions

This study has successfully demonstrated the incorporation of M cells into an *in vitro* co-culture of Caco-2 and Raji B cells. Exposure of the Caco-2/Raji B co-culture CuO NMs and $CuSO_4$ mediated reduced TEER measurement, ZO-1 green emission, and shortened microvilli and time and concentration dependent Cu translocation but did not stimulate cell loss. CuO NMs and $CuSO_4$ stimulated IL-8 protein secretion, *HMOX1*, *IL8*, *MT1A*, *MT2A* and *MUC2* expression in Caco-2/Raji B co-culture. The impact of CuO NMs and $CuSO_4$ on the Caco-2/Raji B co-culture was similar except for ROS production, which was higher for $CuSO_4$. This suggests that the toxicity of CuO NMs may have not been only because of ROS production in this model. TEER measurement, IL-8 secretion, *HMOX1*, *IL8*, and *MT2A* expression may be suggested as useful endpoints for future testing of CuO NMs toxicity in the M cell *in vitro* model. The M cell model was less sensitive to the toxicity of CuO NMs than the undifferentiated and differentiated Caco-2 cell monocultures.

CHAPTER 6: Impact of amorphous silicon dioxide NMs and Montmorillonite on intestinal cells *in vitro*

6.1. Introduction

6.1.1 Silicon dioxide

Silicon dioxide (SiO_2), commonly known as silica, is a group IV metal oxide, which occurs in crystalline and amorphous forms (Napierska et al. 2010, Fruijtier-Pölloth 2012). Crystalline silica is made from tetrahedral units and exists as quartz and porosil in ordered arrangement (Napierska et al. 2010) (Figure 6.1A). Amorphous silica is made of a non-repeating network of tetrahedral units, with neighbouring tetrahedral units attached to the oxygen corners (Figure 6.1B). Amorphous silica exists as pyrogenic silica, precipitated silica, silica gel and colloidal silica depending on the mode of synthesis (van Kesteren et al. 2015, Fruijtier-Pölloth 2012, Napierska et al. 2010). Silica is one of the most abundant metals in nature and humans come in contact with SiO_2 in occupational, environmental and consumer settings. Prior to the emergence of NM hazard studies, the toxicity of crystalline and amorphous silica particles has been assessed (Bouffant et al. 1982, Martin et al. 1984, Marks 1957). For example, synthetic amorphous SiO_2 has already been accepted as food additive since 1950 as an anticaking agent (Fruijtier-Pölloth 2016, Fruijtier-Pölloth 2012). The acceptable daily intake for amorphous SiO_2 particles is designated as "not specified" (very low toxicity) by the Joint FAO/WHO Expert Committee on Food Additives (JCFA) and EU scientific Committee on Food (SCF) (Fruijtier-Pölloth 2016).

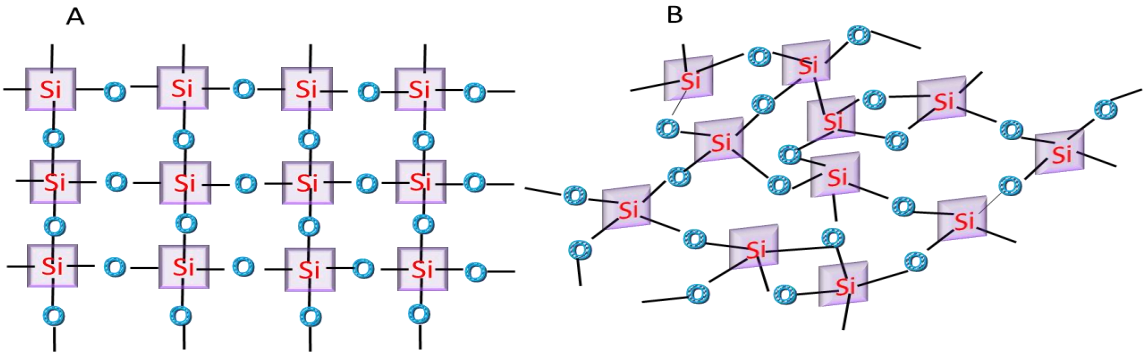

Figure 6.1: Structural representation of crystalline (A) and amorphous form of silicon oxide (B).

The arrangement of atoms in the crystalline form is very ordered whereas the amorphous form are more disarranged. Si in a purple square = silicon and the blue O = oxygen.

The most wildly synthesised NM globally is SiO_2, because of its extensive use by industry and medicine (Decan et al. 2016). For example, SiO_2 NMs are used for drug delivery, bio imaging and cancer therapy (Pasqua et al. 2009, Kim et al. 2015, Sakai-Kato et al. 2014, Schübbe et al. 2012). SiO_2 NMs are also used in biotechnology for DNA transfection and for consumer products such as cosmetics, drugs, paints, and food in the form of additives (anticaking agent) (McCracken et al. 2013, Decan et al. 2016), and in agriculture for gene delivery in plants (Decan et al. 2016). SiO_2 is also used to maintain the flow of powder (vending machine powders, milk and cream powder substitutes, cheese and sugar) (Smolkova et al. 2015). The use of silica NMs in a diverse range of products leads to human exposure via ingestion, inhalation, dermal, adsorption and injection. A series of toxicology studies have been conducted with different type of silica. *In vitro* (using cell lines) have investigated toxicity of SiO_2 NMs to the lungs, intestine and skin and the available results seem to be contradictory. For example, cytotoxicity, increase in ROS levels and modified expression (CAT, GSTA4, TNF-α, CYP1A, POR, SOD1, GSTM3, GPX1, and GSR1) were shown by silica (E 551, 10-50 nm) after exposure to WI-38 cells (human lung normal fibroblasts) for 24 or 48 h (Athinarayanan et al. 2014). Decan et al also observed loss of viability after exposure of lung epithelial cells (FE1 cells) to SiO_2 NMs (5 -20 nm) (Decan et al. 2016). Assessment of cytotoxicity, genotoxicity and nuclear localization of SiO_2 NMs (12-200 nm) exposed to undifferentiated and differentiated Caco-2 cells demonstrated a non-toxic effect after 5, 24, 48 and 72 h exposure (Sakai-Kato et al. 2014, Schübbe et al. 2012, McCracken et al. 2013, McCracken et al. 2016, Gerloff et al. 2013). IL-8 secretion was observed after undifferentiated Caco-2 cells were exposed to SiO_2 NMs (15 nm) at highest concentration (32 µg/ml) whereas 55 nm sized SiO_2 NMs did not induce IL-8 production (Tarantini et al. 2015b). *In vivo* studies have demonstrated that SiO_2 NMs (10-22 nm) are non-toxic after oral, intratracheal instillation and intravenous administration to rat models (Tarantini et al. 2015a, Guichard et al. 2015, Hofmann et al. 2015). Therefore, there is the need to assess the impacts of SiO_2 NMs following ingestion as many consumer products are being impregnated with SiO_2 NMs that may lead to its ingestion, and there is a deficiency of studies, which have assessed their toxicity in the intestine.

6.1.2. Montmorillonite

Nanoclay is a form of layered minerals silicates, which could be natural or synthetic and are used in a diverse array of products (Hayles et al. 2017). For example various health care products such as suspensions, emulsions stabilizers and other rheological modifiers use nanoclays to enhance their stability (Viseras et al. 2007). Nanoclays are also components of materials and substances used for protection against environmental agents, absorption of greases adhesion to the skin and control of heat release (Viseras et al. 2007). Nanoclays are also used in personal care products such as cosmetics and toothpaste (Uddin 2008, Das et al. 2016, Patel et al. 2006), and plastic packaging to decrease gas permeability (Shekarabi et al. 2014, Thomas et al. 2012). Different types of natural nanoclays exist (montmorillonite, bentonite, zeolite, kaolinite, chlorite, halloysite palygorskite and sepiolite) (Lawson and Wendell 1995, Chu and Garwood 1992, Papoulis 2011), but MMT nanoclay is the mostly used nanoclay in health and industrial formulations (Baek et al. 2012, Sharma et al. 2010) hence the reason for selection of MMT for the study.

MMT is a layered material that has a large specific surface area, high cation exchange capacity, high adsorption properties and adhesive ability (Aguzzi et al. 2007, Papoulis 2011, Baek et al. 2012, Maisanaba et al. 2015, Mallakpour and Dinari 2011). These properties of MMT are usually harnessed for pharmaceutical uses such as drug delivery and protection of bioactive substances against harsh degradation in a biological environment (Papoulis 2011, Aguzzi et al. 2007). MMT have the potential of being used for food packaging materials due to its antimicrobial characteristics and impact on gas permeability (Maisanaba et al. 2015, Thomas et al. 2012). The general chemical formula of MMT is expressed as $(Na, Ca)0.33(Al, Mg)_2 (Si_4O_{10})(OH)_2 \cdot nH_2O$ (Baek et al. 2012), which could be modified to obtain more sustainable and suitable form of clay.

MMT has been shown to induce cytotoxic effects only at very high concentration (125 µg/ml) after 72 h exposure to human INT-407 intestinal cells (derived from HeLa cell line) whereas no toxicity was observed after oral administration of up to 1,000 mg/kg to mice (Baek et al. 2012). An increase in TNF-α, IL-6 and LDH secretion and absence of frequency of micronucleus number (FMN) was demonstrated in A549 lung epithelial cells after exposure to MMT (200 µg/ml) (Huo et al. 2015). Other researchers have also demonstrated a non-toxic effect after exposure of MMT to undifferentiated Caco-2 cells

with only organically modified MMT capable of inducing a cytotoxic effect via ROS production, glutathione increase and DNA damage (comet assay) (Maisanaba et al. 2014, Sharma et al. 2010). This implies that the toxicity of MMT is as a result of the organic modification. Cu/Zn loaded MMT induced an increase in TEER *ex vivo*, anti-inflammatory cytokines (TGF-β1) mRNA expression, and protein levels, and downregulation of *TNFα, IL6, IL8* and *IL1β* mRNA expression in the intestine of weaned piglets after 21 days feeding of a mixture of basal diet and 2 g/kg Cu/Zn loaded MMT (Lefei et al. 2017). Due to a lack of published paper on impact of MMT on the intestine and increase in ingestion of MMT as they are incorporated in many consumer products, there is the need to investigate its toxicity to the intestine.

6.1.3. Aims and objectives

In this study, the toxicity of SiO_2 and MMT were assessed in 4 *in vitro* intestinal models (undifferentiated Caco-2 cells, differentiated Caco-2 cells, Caco-2/HT29-MTX and Caco-2/Raji B co-culture, using selected endpoints, which were prioritised based on the toxicity of CuO NMs described in previous chapters. TEER measurement, cytotoxicity, cell morphology (light microscopy) and IL-8 production were selected for this study for rapid and inexpensive comparison between SiO_2 NMs, MMT, CuO NMs and $CuSO_4$ because they were the the most sensitive marker for intestinal *in vitro* toxicity study for CuO NMs.

The aim of this chapter is to investigate the toxicity of SiO_2 NMs and MMT nanoclay on intestinal *in vitro* models (undifferentiated caco-2 cells, differentiated Caco-2 cells, Caco-2/HT29-MTX and Caco-2/Raji B co-cultures) using selected endpoints such as an assessment of cytotoxicity, ROS formation, TEER measurement, light microscopy and IL-8 production.

Specific objectives

i. To assess the impact of SiO_2 NMs and MMT on undifferentiated Caco-2 cell, via investigation of cytotoxicity ROS formation and IL-8 production.
ii. To investigate the impact of SiO_2 NMs and MMT on differentiated Caco-2 cells, via investigation of cytotoxicity, barrier integrity and cell morphology ROS formation and IL-8 production.
iii. To determine the impact of SiO_2 NMs and MMT on the Caco-2 /HT29-MTX co-culture, via investigation of cytotoxicity, barrier integrity and cell morphology

(using TEER measurement and light microscopy), ROS formation and IL-8 production.

iv. To assess the impact of SiO_2 NMs and MMT on the Caco-2/Raji B co-culture, via investigation of cytotoxicity, barrier integrity and cell morphology (using TEER measurement and light microscopy), ROS formation and IL-8 production.

v. To compare the toxicity of SiO_2 NMs and MMT to the toxicity of CuO NMs and $CuSO_4$.

6.1.4. Hypotheses

i. SiO_2 NMs and MMT will induce loss of viability in undifferentiated Caco-2 cells.

ii. SiO_2 NMs and MMT will induce a loss of viability in differentiated Caco-2 cells, and the Caco-2/HT29-MTX and Caco-2/Raji B co-cultures.

iii. SiO_2 NMs and MMT will stimulate IL-8 production in undifferentiated Caco-2 cells, differentiated Caco-2 cells, Caco-2/HT29-MTX and Caco-2/Raji B co-cultures.

iv. The impact of SiO_2 NMs and MMT on the undifferentiated Caco-2 cells, differentiated Caco-2 cells, Caco-2/HT29-MTX and Caco-2/Raji B co-cultures will be similar to CuO NMs and $CuSO_4$.

6.2. Materials and methods

6.2.1. Nanomaterials

Synthetic amorphous silicon dioxide (SiO_2) NMs, also known as NM-202, was provided by the Fraunhofer Institute of Molecular Biology and Applied Ecology (IME, Germany) as a powder. These SiO_2 NMs have been characterised by the European Commission's Joint Research Centre (JRC) Repository in Ispra, Italy. (http://ihcp.jrc.ec.europa.eu/our_activities/nanotechnology/nanomaterials-repository).
The SiO_2 NMs primary particle size, as measured with TEM ranged between 5 and 30 nm, with evidence that the NMs can agglomerate to a size ranging between 10 and 600 nm and the NM had a specific surface area of 184.0 m^2/g (Cotogno et al. 2013, Rasmussen et al. 2013). MMT was provided by BYK additive and instrument Manchester, UK. The manufacturer provided no information on physicochemical properties of MMT.

6.2.1.1. Nanomaterial preparation

MMT and SiO_2 NMs were dispersed by modifying the procedure developed by (Jacobsen et al. 2010). Briefly, the MMT nanoclay was diluted in Mili Q H_2O to obtain 1 mg/ml suspension, vortexed for 30 sec and mixed for 1 h with Dynal sample mixer (MXIC1, 18 RPM) and FBS then added to make up a concentration of 2 % FBS. SiO_2 were dispersed in 2 % FBS in Milli Q de-ionised water. The dispersed MMT nanoclay and SiO_2 suspensions were sonicated for 16 min in a bath sonicator without pause. Following the sonication step, all samples were used immediately. After sonication the required concentration for each experiment were obtained by serial dilution in the appropriate medium. To determine the acute toxicity of MMT and SiO_2 NMs, 10 concentrations of the NMs were prepared and ranged between 0.37 to 78.13 µg/cm^2 (equivalent to 1.17 to 250 µg/ml).

6.2.2. Dynamic light scattering analysis

The hydrodynamic diameter, zeta potential and polydispersity index (PdI) of SiO_2 NMs and MMT nanoclay in biological media (MEM and DMEM complete cell culture medium) were determined using DLS (Malvern Zetasizer Nano series) at 0 h and at 24 h (following incubation at 37 °C). SiO_2 NMs and MMT were prepared as described above (section 6.2.1) and the concentration was adjusted to 100 µg/ml in phenol red free cell culture medium supplemented with 10 % FBS, 100 U/ml penicillin/streptomycin, 100 IU/ml NEAA, and 2 mM L-glutamine). The hydrodynamic diameter, PdI and Zeta potential of the samples were measured in triplicate following 120 sec equilibrations.

6.2.3. Cell culture

The source and maintenance of Caco-2 (section 2.2.3) HT29-MTX (section 4.2.1) and Raji B cell lines (section 5.2.1) are described previously. Caco-2 cell differentiation was performed as described in section 3.2.2. Co-culture of Caco-2/HT29-MTX and Caco-2/Raji B were maintained as described in section 4.2.2 and 5.2.2 respectively.

6.2.4. Alamar blue cell viability assay

The viability of SiO_2 and MMT in undifferentiated Caco-2 cells was assessed via the Alamar blue assay. After culturing the cells using the protocol described in section 2.2.5,

cells were washed twice with PBS (Gibco Life Technologies) and exposed to 100 µl of cell culture medium (negative control), 0.1 % triton-X 100 (positive control), and different concentrations of SiO_2 or MMT (0.37 to 78.13 µg/cm^2) for 24 h. Then the alarmar blue assay was performed as outlined in section 2.2.5.

6.2.5. Evaluation of acellular and intracellular ROS production

The acellular level of ROS production was determined following the method outlined in section 2.2.9.1 using cell culture medium (untreated control), 7.81or 15.63 µg/cm^2 of SiO_2 or MMT and 1mM/cm^2 of H_2O_2 (positive control). For cellular ROS production undifferentiated Caco-2 cells were cultured and treated with 150 µM DCFH-DA as described in section 2.2.9.2 and the cells exposed to cell culture medium (untreated control), 7.81, 15.63 or 31.25 µg/cm^2 of SiO_2 or MMT and 1mM H_2O_2 (positive control). The level of ROS produced at 2 h post exposure was determined as detailed previously in section 2.2.9.2.

5.2.6. Investigation of the impact of SiO_2 NMs and MMT on intestinal cell barrier integrity using TEER measurement

TEER was measured after exposure of differentiated Caco-2 cells, and the Caco-2/HT29-MTX and Caco-2/Raji B co-cultures to cell culture medium (untreated control), 7.81 or 15.63 µg/cm^2 of SiO_2 NMs or MMT for 24 h as previously described in section 3.2.3.

6.2.7. Romanowsky staining: Cell morphology

Undifferentiated Caco-2 cells were exposed to cell culture medium (control), 7.81 or 15.63 µg/cm^2 SiO_2 NMs or MMT for 24 h and processed as described previously (section 2.2.8). The differentiated Caco-2 cell, Caco-2/HT29-MTX and Caco-2/Raji B co-culture were treated with cell culture medium (control) and 15.63 µg/cm^2 of SiO_2 NMs or MMT for 24 h and then processed as described in section 3.2.8. After drying, the cells were imaged using light microscopy.

6.2.8. IL-8 ELISA analysis

The supernatant from undifferentiated Caco-2 cells exposed to cell culture medium (control), 7.81, 15.63 and 31.25 µg/cm^2 of SiO_2 NMs or MMT nanoclay and differentiated

Caco-2 cells, Caco-2/HT29-MTX and Caco-2/Raji B co-cultures exposed to cell culture medium (control), 7.81 and 15.63 µg/cm^2 for 24 h were assessed for IL-8 production following the method outline in section 2.2.10.2.

6.2.8. Data analysis

All data were analysed as described previously in section 3.2.12.

6.3 Results

6.3.1. Characterisation of the SiO_2 and MMT

SiO_2 NMs and MMT were characterised by measuring hydrodynamic diameter, zeta potential and PdI using DLS (Table 6.1 and 6.2) after dispersion in MEM and DMEM complete cell culture medium at 0 and 24 h. The average hydrodynamic diameter of SiO_2 NMs in MEM and DMEM were 133.07 and 125.57 nm at 0 h respectively and 162.58 and 139.34 nm post 24 h incubation respectively. SiO_2 NMs were agglomerated in both MEM and DMEM complete media as the primary size was between 5-30 nm (Rasmussen et al. 2013), at both time points investigated. The zeta potential was negative ranging from -8.61 to -10.01 mV and the PdI ranged between 0.59 and 8.3. The hydrodynamic diameter of MMT were 276.24 and 294.23 at 0 and 24 h respectively. MMT also seemed to have agglomerated and the hydrodynamic diameter increased after 24 h incubation. The zeta potential was negative ranging from -9.2 to -10.1 mV. Incubation of MMT for 24 h did not affect the zeta potential or the PdI (0.56-0.69).

Table 6.1: Hydrodynamic diameter, zeta potential and polydispersity index (PdI) values of SiO_2 NMs in MEM and DMEM complete cell culture medium.

Data are expressed as mean ± SEM (n=3).

	Time (h)	*0*	*24*
Complete MEM	Hydrodynamic diameter (nm)	133.07±7.80	162.58 ±5.81
	Zeta Potential (mV)	-10.01±0.30	-8.61±0.38
	PdI	0.71±0.07	0.69±0.02
Complete DMEM	Hydrodynamic diameter (nm)	125.57±10.09	139.34±12.88
	Zeta Potential (mV)	-9.28±0.50	-8.95±0.69
	PdI	0.83±0.09	0.59±0.05

Table 6.2: Hydrodynamic diameter, zeta potential and polydispersity index (PdI) values of MMT in MEM and DMEM complete cell culture medium.

Data are expressed as mean ± SEM (n=3).

	Time (h)	*0*	*24*
Complete MEM	Hydrodynamic diameter (nm)	276.24±15.44	294.23±13.30
	Zeta Potential (mV)	-9.22±0.20	-10.10±0.089
	PdI	0.57±0.02	0.59±0.03
Complete DMEM	Hydrodynamic diameter (nm)	275.57±13.36	335.04±9.12
	Zeta Potential (mV)	-9.36±0.65	-10.02±0.20
	PdI	0.56±0.02	0.69±0.01

6.3.2. Alamar blue cell viability assay

Assessment of the viability of undifferentiated Caco-2 cells using the Alamar blue assay after treatment with SiO_2 NMs and MMT for 24 h demonstrated a non-significant increase in cell death up to a concentration of 78.13 µg/cm^2 (Figure 6.2). Since there was no impact on the viability of undifferentiated Caco-2 cells, the BMD 20 could not be calculated. Therefore, the equivalent concentrations employed for CuO NMs and $CuSO_4$ investigation were used for further studies with SiO_2 NMs and MMT.

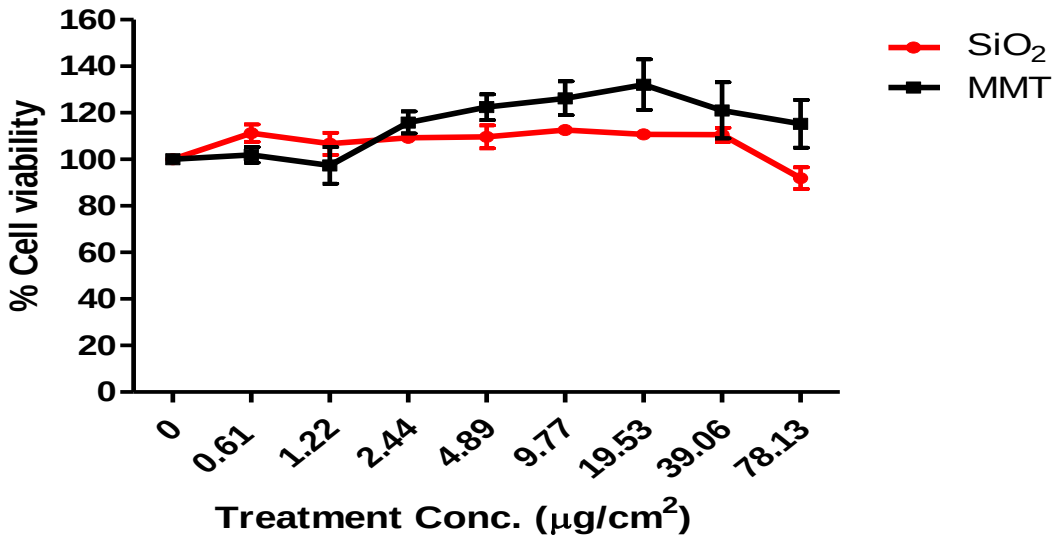

Figure 6.2: Cytotoxicity of SiO_2 NMs and MMT to undifferentiated Caco-2 cells.

Viability of undifferentiated Caco-2 cells was assessed using the Alamar blue assay following exposure of cells to MEM complete cell culture medium (control), SiO_2 or MMT at concentrations ranging from 0.61 and 78.13 µg/cm^2 for 24 h. Viability of Caco-2 cells was assessed using the Alamar blue assay, and data were expressed as a % of the control (i.e. % viability). Data are expressed as mean % viability ± SEM (n = 3).

6.3.3. ROS formation

Acellular ROS production by SiO_2 NMs and MMT was assessed via the DCFH-DA assay (Figure 6.3). There was no significant production of ROS by SiO_2 NMs and MMT for up to 2 h whereas H_2O_2 produced an increase in ROS (~5 fold). ROS production was also assessed in undifferentiated Caco-2 cells at 2 h post exposure (Figure 6.4). SiO_2 NMs and MMT (at all treatment concentrations) did not stimulate ROS production 2 h post exposure. An increase in ROS production was observed in H_2O_2 exposed cells (Figure

6.4). The acellular and cellular ROS production by SiO_2 NMs and MMT were lower than CuO NMs and $CuSO_4$ (Figure 2.8 and 2.10) in undifferentiated Caco-2 cells. Since SiO_2 and MMT did not produce ROS (in acellular conditions and in undifferentiated Caco-2 cells), ROS production was not investigated in the other intestinal co-culture models.

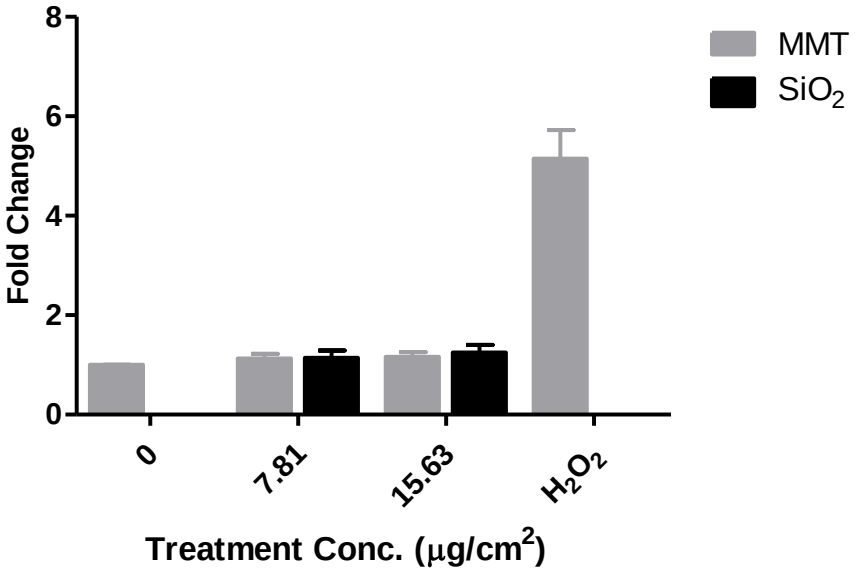

Figure 6.3: Acellular ROS formation by SiO_2 NMs and MMT at 2 h.

Acellular ROS levels were determined in cell culture medium (0), and for SiO_2 NMs and MMT at concentrations of 7.81 and 15.63 µg/cm^2 using the DCFH-DA assay at 2 h. Data are expressed as mean fold change (compared to the control) ± SEM (n = 3).

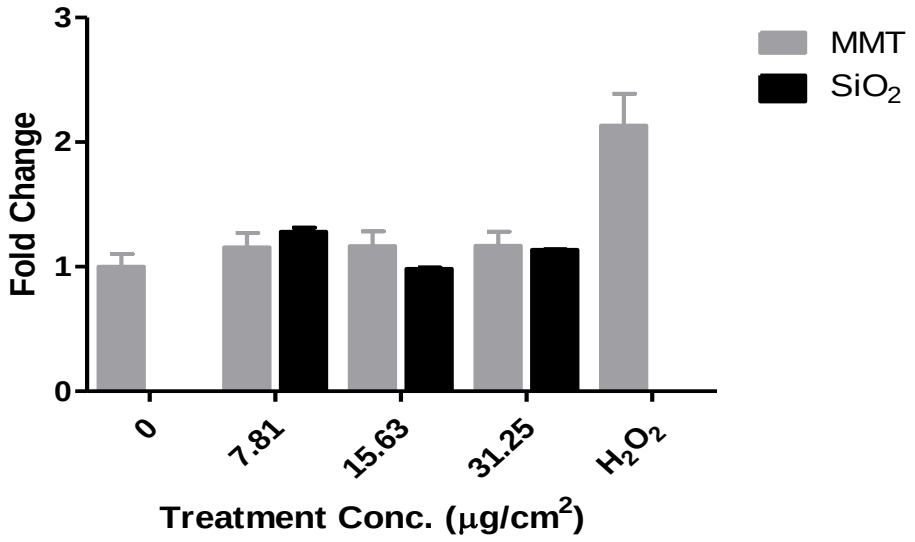

Figure 6.4: ROS formation by undifferentiated Caco-2 cells 2 h post exposure to SiO_2 NMs and MMT.

Intracellular ROS levels were determined using the DCFH-DA assay 2 h post exposure of undifferentiated Caco-2 cells to cell culture medium (control, 0), H_2O_2, SiO_2 NMs or MMT at concentrations of 7.81, 15.63, 31.25 µg/cm^2. Data are expressed as mean fold change ± SEM (n = 3).

6.3.4. Impact of SiO_2 NMs and MMT on cell morphology

The impact of SiO_2 NMs and MMT on intestinal barrier integrity and cell morphology was investigated in differentiated Caco-2 cells, Caco-2/HT29-MTX and Caco-2/Raji B co-culture models via assessment of TEER measurement, and light microscopy (Romanowisky staining). The TEER values were similar to the control following exposure of all cell models to SiO_2 NMs and MMT at all concentrations and time points (Figure 6.5). The TEER value of differentiated Caco-2 cells ranged between 750 and 900 Ω.cm^2 (Figure 6.5A), Caco-2/HT29-MTX co-culture were also from 750 to 900 Ω.cm^2 (Figure 6.5B) and the Caco-2/Raji B co-culture ranged from 650 to 850 Ω.cm^2 (Figure 6.5C) after treatment with SiO_2 NMs or MMT at all concentrations. There was no difference in cell number and structural morphology of undifferentiated Caco-2 cells, differentiated Caco-2 cells, Caco-2/HT29-MTX and Caco-2/Raji B co-culture compared to control after 24 h treatment with SiO_2 NMs and MMT, suggesting that there was no loss in cell viability (Figures 6.6 and 6.7).

A: Differentiated Caco-2 cell

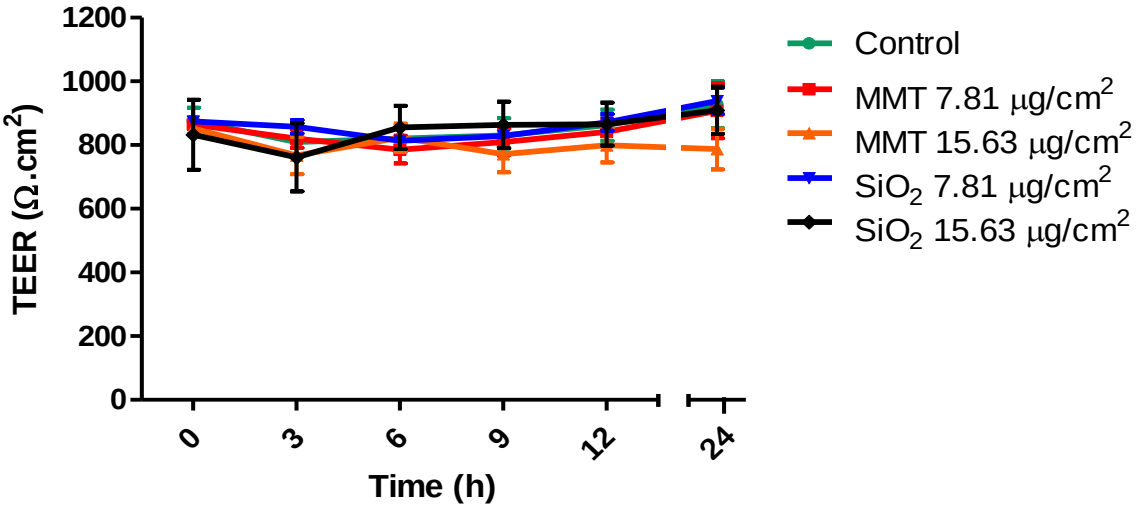

B: Caco-2/HT29-MTX

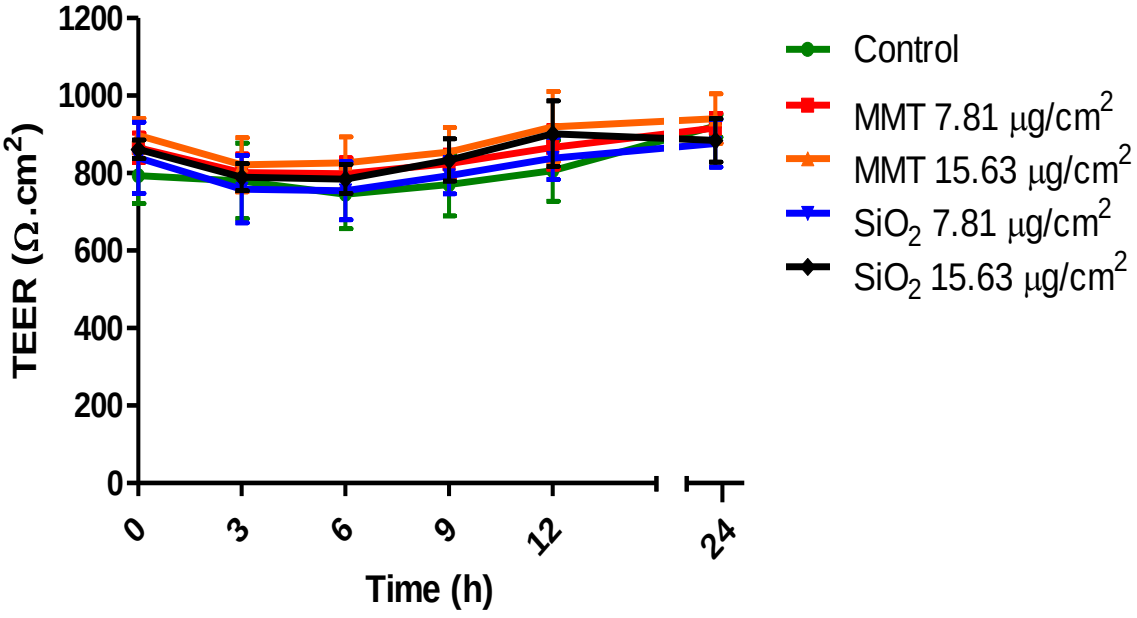

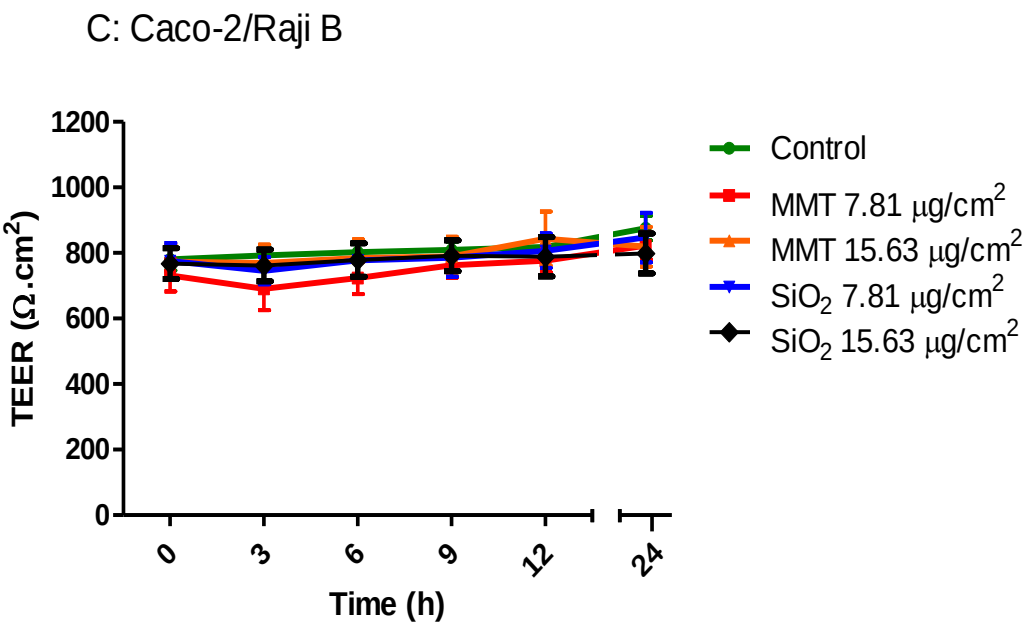

Figure 6.5: Impact of SiO_2 NMs and MMT on in vitro intestinal model TEER values.

Differentiated Caco-2 cells (A), the Caco-2/HT29-MTX co-culture (B), and the Caco-2/Raji B co-culture (C) were exposed to cell culture medium (control, 0), SiO_2 NMs and MMT at concentrations of 7.81 or 15.63 µg/cm² for 24 h. The TEER values were measured using epithelial voltohmmeter EVOM every 3 h Data are expressed as mean TEER value ± SEM (n = 3).

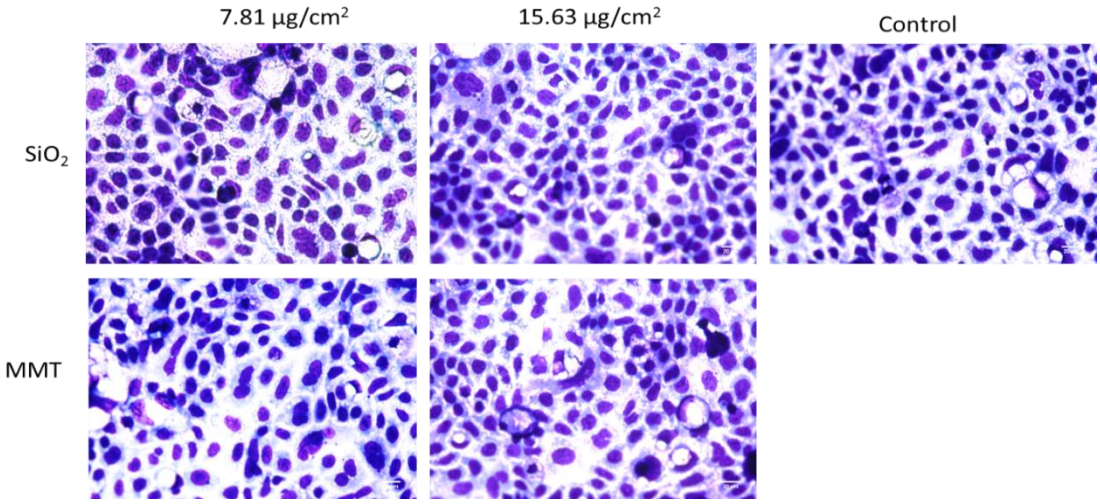

Figure 6.6: Impact of SiO_2 NMs and MMT on undifferentiated Caco-2 cell morphology.

Undifferentiated Caco-2 cells were exposed to cell culture medium (control) and 7.81 or 15.63 µg/cm² of SiO_2 NMs or MMT for 24 h. The cells were then fixed, stained and visualised using the light microscopy (magnification 40 X, scale bar=20 µm. Representative images are shown (n=3).

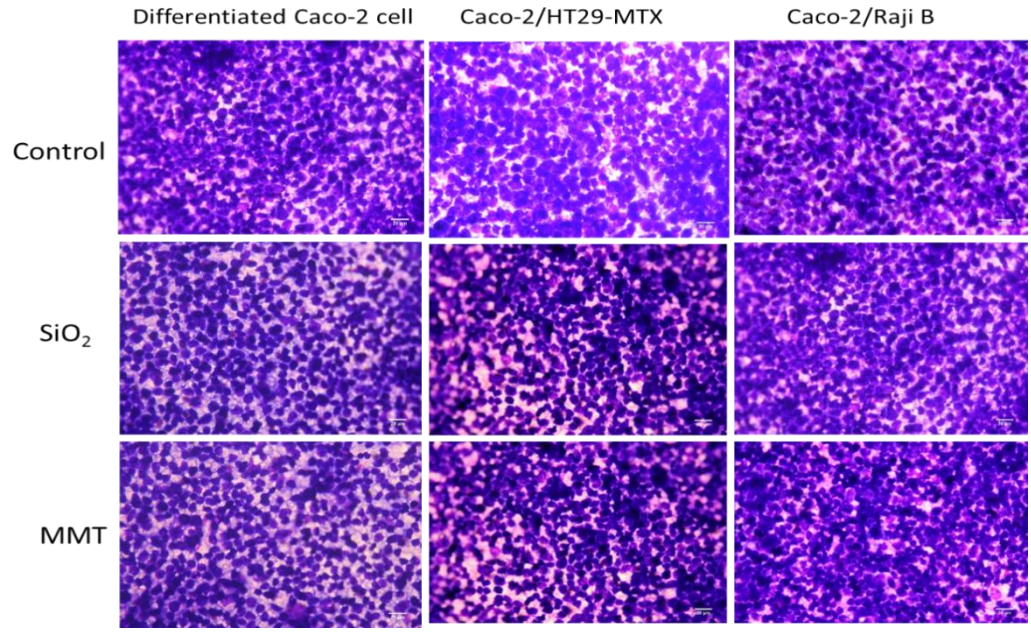

Figure 6.7: Impact of SiO_2 NMs and MMT on differentiated Caco-2 cells, Caco-2/HT29-MTX and Caco-2/Raji B co-culture morphology.

Differentiated Caco-2 cells, Caco-2/HT29-MTX and Caco-2/Raji B co-cultures were exposed to cell culture medium (control), 15.63 µg/cm^2 of SiO_2 NMs or MMT for 24 h. The cells were then fixed, stained and visualised using the light microscopy (magnification 40 X, scale bar=20 µm. Representative images are shown (n=3).

6.3.6. IL-8 production

A significant increase in IL-8 production was observed after exposure of undifferentiated Caco-2 cells to SiO_2 NMs for 24 h at all concentrations compared to control. In contrast IL-8 production was comparable to the control following exposure of undifferentiated Caco-2 cells to 15.63 and 31.25 µg/cm^2 of MMT (Figure 6.8A). Differentiated Caco-2 cells exposed to 7.81 and 15.63 µg/cm^2 SiO_2 NMs demonstrated a significant increase in IL-8 secretion (32.91 and 31.09 pg/ml respectively), compared to control (Figure 6.8B). No IL-8 production was detected following exposure of differentiated Caco-2 cells to MMT. Generally, IL-8 secretion induced by MMT and the untreated control in differentiated Caco-2 cells were below detectable level of the ELISA assay.

SiO_2 NMs (7.81 and 15.63 µg/cm^2) stimulated a significant increase in IL-8 production from the Caco-2/HT29-MTX co-culture at 24 h post exposure compared to control (Figure 6.8C). Caco-2/HT29-MTX cells exposed to 7.81 µg/cm^2 of SiO_2 NMs induced

IL-8 release of 48.55 pg/ml, while exposure to 15.63 µg/cm^2 SiO_2 NMs mediated IL-8 secretion of 69.92 pg/ml. No IL-8 production from the Caco-2/HT29-MTX co-culture exposed to MMT or cell culture medium (control) was detected. (Figure 6.8C). The Caco-2/Raji B co-culture secreted a concentration of 57.91 and 48.13 pg/ml of IL-8 after exposure to SiO_2 NMs (7.81 and 15.63 µg/cm^2 respectively). There was no detectable secretion of IL-8 by MMT and the untreated control by the Caco-2/Raji B co-culture (Figure 6.8D). IL-8 production by undifferentiated Caco-2 cells, differentiated Caco-2 cells, Caco-2/HT29-MTX and Caco-2/Raji B co-culture were less post exposure to MMT compared to SiO_2 NMs.

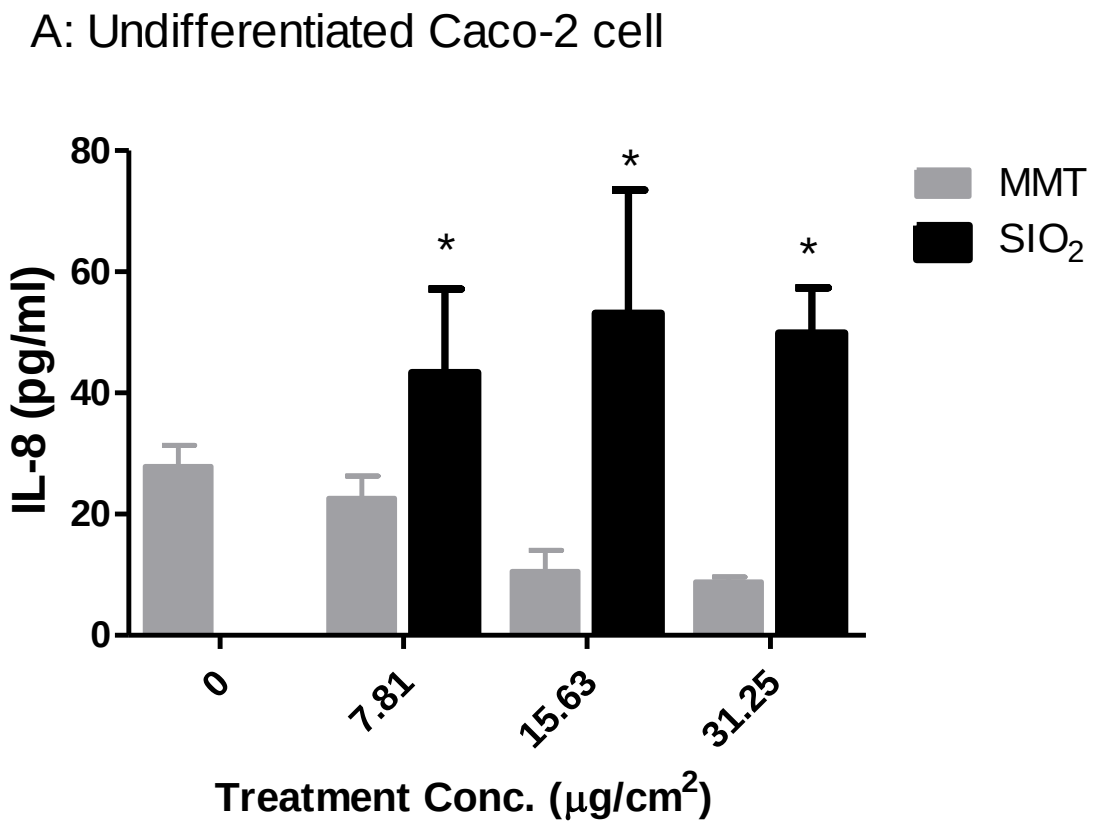

B: Differentiated Caco-2 cell

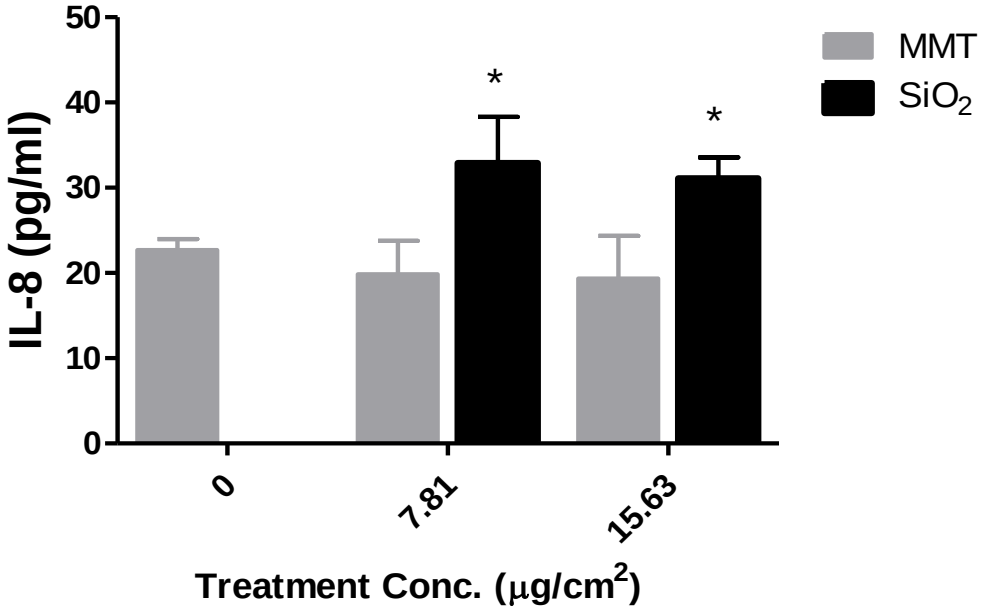

C: Caco-2/HT29-MTX

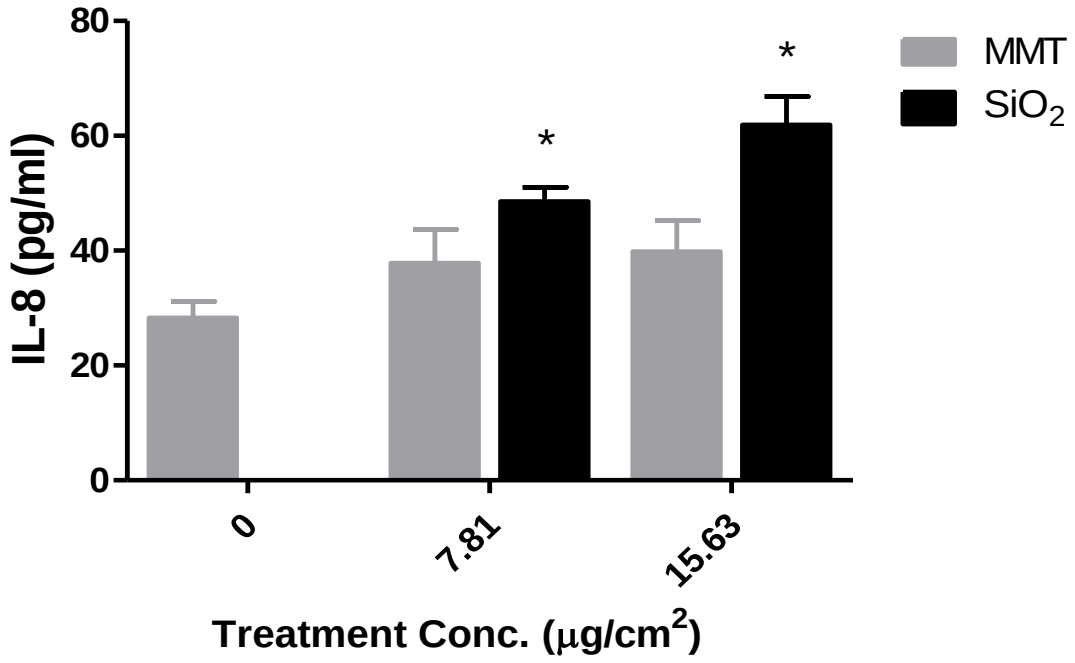

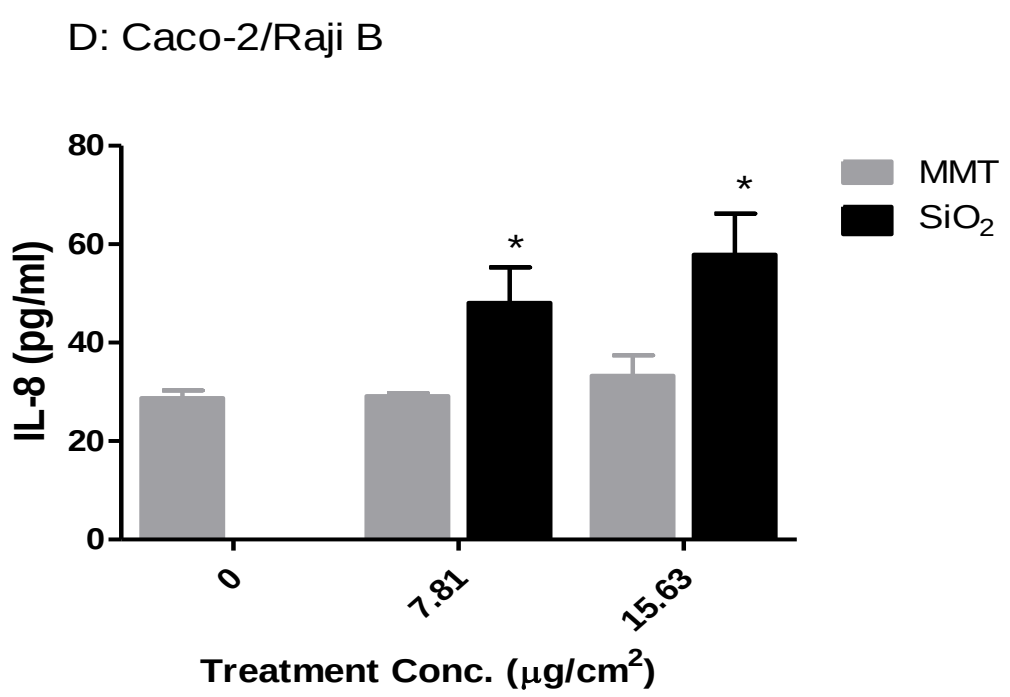

Figure 6.8: IL-8 production by undifferentiated Caco-2 cells, differentiated Caco-2 cells, and the Caco-2/HT29-MTX and Caco-2/Raji B co-cultures following SiO_2 NMs and MMT exposure.

*Undifferentiated Caco-2 cell (A), differentiated Caco-2 cells (B), the Caco-2/HT29-MTX co-culture (C) and the Caco-2/Raji B co-culture (D) were exposed to cell culture medium (control, 0), SiO_2 NMs or MMT at concentrations of 7.81, 15.63, 31.25 µg/cm^2 for 24 h. The level of IL-8 in the cell supernatant was determined using an ELISA. Data are expressed as mean IL-8 concentration (pg/ml) ± SEM (n = 3). Significance at P<0.05 is indicated by * compared to control.*

6.4. Discussion

In this part of the study, a rapid and low-cost screen of the toxicity of SiO_2 NMs and MMT nanoclays to the intestine was performed *in vitro*, with the endpoints selected based on the response of *in vitro* models (of various complexities) to CuO NMs and $CuSO_4$. Furthermore, due to financial and time constraints a more in-depth screen of these NMs could not be performed. Assessment of TEER and IL-8 secretion were selected as they were previously demonstrated to be sensitive markers of CuO NMs and $CuSO_4$ toxicity across *in vitro* intestinal models of various complexities. Light microscopy (as a measure of cytotoxicity) was only sensitive to undifferentiated Caco-2 cells exposed to CuO NMs and $CuSO_4$ and ROS production was only sensitive to $CuSO_4$ but were included to see if

SiO_2 NMs and MMT can induce its response. Non-soluble NMs that are known to be less toxic than CuO NMs were selected to identify if the models and endpoints selected were appropriate to assess the toxicity of NMs of more varied physicochemical properties. The physicochemical characteristics of SiO_2 NMs and MMT in cell culture media were investigated, and their toxicity to the intestinal cell models (undifferentiated Caco-2 cells differentiated Caco-2 cells, Caco-2/HT29-MTX and Caco-2/Raji B co-cultures) was assessed via investigation of cytotoxicity (Alamar blue assay and light microscopy), ROS production (DCFH-DA assay), IL-8 production (ELISA), and cell morphology (via light microscopy). TEER measurement was used to assess the barrier integrity of differentiated Caco-2 cells, Caco-2/HT29-MTX and Caco-2/Raji B co-cultures. SiO_2 NMs and MMT were shown to have no toxic effect when cell viability and cell morphology were used as indicators of toxicity in all models. SiO_2 NMs and MMT did not mediate production of ROS in acellular and cellular conditions. Whilst SiO_2 NMs stimulated IL-8 production, MMT did not in all the intestinal *in vitro* models used for the study. Therefore, the result suggests that SiO_2 NMs and MMT are relatively non-toxic at the tested concentrations and time points.

6.4.1. Physicochemical properties of SiO_2 and MMT

Both SiO_2 and MMT are likely to be agglomerated in the cell culture medium. The primary size of SiO_2 NMs have been shown to range between 5 and 30 nm (Rasmussen et al. 2013) indicating that SiO_2 NMs agglomerated in cell culture media. The primary size of MMT is not known as they are in layered form with a thickness of 1nm and so cannot be imaged. However, incubation of MMT at 37 ^oC for 24 h after dispersion and dilution in complete MEM and DMEM led to increase in hydrodynamic diameter (294.23±13.30 and 335.04±9.12 nm respectively) suggesting that MMT has agglomerated at 24 h post incubation. Agglomeration of synthetic amorphous SiO_2 NMs has been reported (Rasmussen et al. 2013). The hydrodynamic diameter of CuO NMs was smaller than that observed for SiO_2 and MMT (section 2.3.1). Furthermore, the hydrodynamic diameter of CuO NMs reduced in size 24 h post incubation. These differences in the physicochemical properties of NMs may influence their biological response. The result of the SiO_2 characterisation in this study are similar to the observation of JRC. Extensive characterisation of MMT was not assessed in this study as

one of the PhD students in our laboratory is presently carrying out the characterisation. Preliminary results suggest that their toxicity may be cell type dependent.

6.4.2 Cytotoxicity and impact of SiO_2 NMs and MMT on cell morphology

The Alamar blue assay was used to assess the viability of undifferentiated Caco-2 cells after exposure to SiO_2 NMs and MMT 24 h post exposure. Both SiO_2 NMs and MMT did not cause cytotoxicity. A similar lack of cytotoxicity has been reported for up 72 h post exposure of SiO_2 NMs of various properties on undifferentiated Caco-2 cells (Gerloff et al. 2013, McCracken et al. 2013, Sakai-Kato et al. 2014, Schübbe et al. 2012, McCracken et al. 2016). On the other hand, FE1 (human lung epithelial) and WI-38 (human fibroblast) cells demonstrated slight cytotoxicity at 24 and 48 h post exposure of Si and SiO_2 NMs (Decan et al. 2016, Athinarayanan et al. 2014). Although, the study by Athinarayanan et al used the same type of SiO_2 used in this study, cytotoxicity assessment was performed with the MTT assay whereas this study used Alamar blue, which may explain why different results were obtained. Decan et al used amorphous Si NMs (2-20 nm), a pure and smaller sized silicon NMs. Therefore, different cell type and assay method may vary in their sensitivity to SiO_2 NMs. MMT has also showed non-toxic effect at 24 h post exposure to undifferentiated Caco-2 cells (Sharma et al. 2010, Maisanaba et al. 2014) whereas long term exposure of INT-407 cells (HeLa derived cell line) to MMT induced cytotoxicity only at high concentration (125 µg/ml) (Baek et al. 2012). Therefore, overall, the findings are in agreement with those of the wider scientific community.

The toxicity of SiO_2 NMs and MMT on undifferentiated Caco-2 cells was also investigated with light microscopy after exposure to SiO_2 NMs and MMT. The Alamar blue assay cannot be applied to differentiated Caco-2 models, and previous studies using CuO NMs demonstrated that light microscopy provided a useful and rapid insight into the cytotoxicity of NMs (which was comparable to the more time consuming, and complex quantitative approaches used to assess cell death (nuclei counts) or cell morphology (e.g. electron microscopy)). Therefore, light microscopy studies enabled a direct comparison of NM toxicity to be performed across models. SiO_2 NMs and MMT did not impact on the confluence or morphology of the exposed cells (in all models used), compared to the control, suggesting that these NMs are not toxic. CuO NMs exposed to undifferentiated Caco-2 cells induced cell death leading to a loss of cells, which was

identified using the Alamar blue assay and light microscopy (Ude et al. 2017) (Figure 2.6). However, no impact was observed post exposure of differentiated Caco-2 cells, Caco-2/HT29-MTX and Caco-2/Raji B co-culture to CuO NMs (Figures 3.5, 4.6 and 5.7). Light microscopy has not been used to study the toxicity of SiO_2 NMs and MMT in intestinal models (e.g. differentiated Caco-2 cells, Caco-2/HT29-MTX and Caco-2/Raji B co-culture) prior to now. However, use of light microscopy to assess toxicity of NMs has been used previously for other cell types. For example, the toxicity of Ag NMs, ufCB and TiO_2 to differentiated HL-60 has been studied using light microscopy and change in a cell morphology was observed after exposure to Ag NMs and ufCB (Johnston et al. 2015). Therefore, whilst light microscopy does not provide a quantitative assessment of NM cytotoxicity, and has not been commonly used to assess the response of Caco-2 cells to NMs it is a rapid and cost-effective method that can be used to explore the impact of NMs on cell viability and morphology, and it is therefore recommended that it is used more commonly to assess NM toxicity.

TEER measurement was also used to assess the integrity of the intestinal barrier in differentiated Caco-2 cells, Caco-2/HT29-MTX and Caco-2/Raji B co-cultures after exposure to SiO_2 NMs and MMT. No impact was observed after exposure to SiO_2 NMs and MMT compared to control suggesting that SiO_2 NMs and MMT were not toxic at the exposed concentrations. Exposure of CuO NMs and $CuSO_4$ to differentiated Caco-2 cells, Caco-2/HT29-MTX and Caco-2/Raji B co-cultures caused a reduction in the TEER value compared to control (sections 3.31, 4.31 and 5.32). In addition, Cu/Zn loaded MMT exposed to the intestine of weaned piglets has been shown to increase TEER value *ex vivo* (Lefei et al. 2017). A decrease in TEER have been reported after exposure of CuO NMs to differentiated Caco-2 cells (Piret et al. 2012b), Caco-2/HT29-MTX (Walczak et al. 2015b, Brun et al. 2014) and the Caco-2/Raji B co-culture (Bouwmeester et al. 2011, Lozoya-Agullo et al. 2017), although the TEER was only measured at one time point making their study different from this present study. There is no published paper that has studied the toxicity of SiO_2 NMs and MMT to the intestine *in vitro* by measuring the TEER values. Measurement of TEER values maximises the amount of information obtained for other measurements of toxicity, therefore it is recommended that future studies continue to assess TEER over time as an indicator of NM toxicity.

6.4.3. ROS production

Since stimulation of oxidative stress is known as key mechanism underlying NM toxicity (section 3.4.3), acellular and cellular ROS production by SiO_2 NMs and MMT was assessed via the DCFH-DA assay. SiO_2 NMs did not produce ROS in acellular conditions and undifferentiated Caco-2 cells. H_2O_2 was used as positive control, which demonstrated significant increase in ROS formation, hence suggesting that the assay worked. Therefore, this result suggests that SiO_2 NMs was not toxic at the exposed concentration. Similar results were reported after exposure of human gastric epithelial cells (GES-1) and undifferentiated Caco-2 cell to SiO_2 NMs (10-50 nm) (Yang et al. 2014, Kaiser et al. 2013, Tarantini et al. 2015b). However, the same size of SiO_2 NMs used in this study induced ROS production in human lung fibroblast cells (Athinarayanan et al. 2014), indicating a cell dependent toxicity. SiO_2 NMs (14 nm) induced acellular ROS production when assessed in artificial digested and undigested form using EPR (Gerloff et al. 2013). ROS formation was also mediated in A549 and HepG2 epithelial cells and NIH/3T3 fibroblasts at post 24 h exposure to different sizes of SiO_2 NMs (20, 60, 100 and 200 nm) and 100 and 200 nm SiO_2 NMs generated greater ROS compared to 20 and 60 nm (Kim et al. 2015). This suggests a size dependent toxicity of silica.

MMT demonstrated no increase in acellular and cellular ROS with the DCFH-DA assay. Absence of acellular ROS and cellular ROS after exposure of up to 170 µg/ml of MMT to undifferentiated Caco-2 cells for 24 h has been reported (Sharma et al. 2010). Another researcher reported an increase in ROS production after exposure of 40 µg/ml of MMT to undifferentiated Caco-2 cells, but not at lower concentrations at 24 and 48 h post exposure (Maisanaba et al. 2014) however the MMT concentration were higher than the concentration used in this present study. In comparison, equivalent concentration of CuO NMs and $CuSO_4$ induced ROS production in acellular conditions (section 2.3.4). This suggests that SiO_2 NMs and MMT do not stimulate ROS production. Taken together, the results from existing studies suggest that experimental design influences whether NMs stimulate ROS production e.g. physicochemical properties of silica, assay type used to assess ROS production, exposure time, concentrations tested and concentration of DCFH-DA (the reagents). Only undifferentiated cells were used for ROS production studies since acellular condition did not and undifferentiated Caco-2 cells, which are known to be more sensitive did not produce ROS after exposure to SiO_2 NMs and MMT. As

measurement of oxidative stress requires assessment of a range of parameters, future studies could perform a more comprehensive assessment of the involvement of oxidative stress by investigating the impact of NMs on lipid peroxidation and assessment of antioxidants (e.g. glutathione depletion, superoxide dismutase, catalase).

6.4.4. IL-8 production

IL-8 production was one of the prominent markers observed across all the models after exposure to CuO NMs and $CuSO_4$. Assessment of IL-8 production by SiO_2 NMs and MMT allows a comparison of the toxicity of CuO NMs, $CuSO_4$, SiO_2 NMs and MMT to be performed across all the intestinal models used for this study. SiO_2 NMs exposed to undifferentiated Caco-2 cells, differentiated Caco-2 cells, Caco-2/HT29-MTX and Caco-2/Raji B co-cultures for 24 h induced IL-8 production at all concentration tested. Although SiO_2 NMs stimulated IL-8 secretion was statistically significant, it is unlikely to be biologically significant as a relatively small increase was observed.

Furthermore, whilst SiO_2 stimulated IL-8 production by differentiated Caco-2 cells, Caco-2/HT29-MTX and Caco-2/Raji B co-cultures, this was 7 fold lower than that observed from cells exposed to CuO NMs and $CuSO_4$ (sections 3.3.6, 4.3.6, 5.3.6). There are conflicting findings in the literature about whether SiO_2 stimulates IL-8 production from cells *in vitro*. For example, Tarantini et al. (2015b) reported a similar level of IL-8 production after exposure of 32 µg/ml of SiO_2 NMs (15 nm) to undifferentiated Caco-2 cells, with a lack of induction of IL-8 by lower concentrations and at all concentrations of larger SiO_2 NMs (55 nm), indicating a size dependent and concentration dependent IL-8 release. Another researcher reported a lack of *IL-8* expression by undifferentiated and differentiated Caco-2 cells after exposure to SiO_2 NMs (14 nm) (Gerloff et al. 2013). In contrast, an increase in IL-8 secretion has been reported after exposure of A549 monoculture and A549/THP-1 co-cultures to SiO_2 NMs (10 to 60 nm) (Wottrich et al. 2004, Choi et al. 2009). Normal mesothelial cells (MET-5A) exposed to both nano and micro silica particles also demonstrated an increase in IL-8 secretion (Brown et al. 2007). This suggests that IL-8 release after exposure to SiO_2 NMs may be cell dependent, as Caco-2 cells seem to have lower response compared to the other cell types.

In this study, MMT did not mediate IL-8 release after 24 h exposure to undifferentiated Caco-2 cells, differentiated Caco-2 cells, Caco-2/HT29-MTX and Caco-2/Raji B co-

culture. Lefei et al. (2017) reported a decrease in mRNA expression of pro-inflammatory cytokines such as *TNFα, IL6, IL8 and IL1β* after oral exposure of copper/zinc-loaded montmorillonite to weaned piglets *in vivo*. MMT induced significant increase in IL-6 after exposure of 200 μg/ml to A549 lung epithelial cells for 24 h and TNF-α for 3 h (Huo et al. 2015). The level of cytokine produced are unlikely to be physiologically relevant as small levels of IL-8 were produced in all the intestinal models.

6.5. Conclusions

Amorphous silica NMs and MMT agglomerated in cell culture medium. In comparison, the size of CuO NMs agglomerates was smaller and this may explain the higher toxicity of CuO NMs compared to SiO_2 NMs and MMT. In addition, CuO NMs are soluble, which may likely influence their toxicity. SiO_2 NMs and MMT were nontoxic to undifferentiated Caco-2 cells when toxicity was assessed via the Alamar blue assay, light microscopy, and ROS formation. In addition, SiO_2 NMs and MMT did not elicit toxicity to differentiated Caco-2 cells, Caco-2/HT29-MTX and Caco-2/Raji B co-cultures when light microscopy, and TEER was used to assess toxicity. Whilst SiO_2 NMs stimulated IL-8 release in all the intestinal *in vitro* models, no IL-8 secretion was induced by MMT. This suggests that MMT is likely to be pro-inflammatory at the tested concentrations. In addition, since SiO_2 NMs induced very low levels of IL-8 production, it may be inferred that SiO_2 NMs was only slightly pro-inflammatory. However, the overall findings imply that CuO NMs and $CuSO_4$ were more toxic or bioreactive than SiO_2 NMs and MMT as CuO NMs and $CuSO_4$ induced cytotoxicity (Alamar blue assay), reduced TEER value and induced increased IL-8 production. It may be inferred that IL-8 is the most sensitive marker among the endpoints used for NM toxicity or bioreactivity investigation in this study across all models. It is suggested that gene expression of the oxidative stress (*GPX, HMOX1*), inflammation (*IL1β*, *IL8*, *IL10*) and mucus secreting (*MUC2*) will be investigated to determine the toxicity of SiO_2 NMs and MMT in the intestinal *in vitro* models. MMT did not induce toxicity via assessment of cytotoxicity and cell morphology (Alamar blue assay, TEER measurement and light microscopy), ROS formation and IL-8 production, therefore it may be suggested that MMT was not toxic to all the intestinal *in vitro* models at the exposed concentrations.

Chapter 7: General discussion, recommendation and conclusions

7.1. General discussion

In this study a range of tests were employed to assess the toxicity of NMs with the aim of identifying the most appropriate markers for assessment of the toxicity of NMs to the intestine *in vitro*. These endpoints included cytotoxicity (using Alamar blue assay, nuclei count, and light microscopy), cell morphology and barrier integrity (using TEER measurement, tight junction staining and SEM), uptake and translocation (ICP-OES), ROS production, cytokine production and gene expression (*HMOX1*, *IL8*, *MUC2 MT1A* and *MT2A*). Four different *in vitro* intestinal models namely; undifferentiated Caco-2 cells, differentiated Caco-2 cells, Caco-2/HT29-MTX and a Caco-2/Raji B co-culture were used to investigate the toxicity of CuO NMs, $CuSO_4$, SiO_2 NMs and nanoclays in the intestine to identify if *in vitro* models of various complexities varied in their sensitivity to NM toxicity.

7.1.1. Physicochemical properties of the NMs

A thorough characterisation of the physicochemical properties of NMs is recommended in parallel to hazard studies in order to help identify the attributes of NMs, which confer toxicity. The physicochemical properties of NMs (CuO and SiO_2 NMs) used for this study were investigated previously (Gosens et al. 2016, Ude et al. 2017, Rasmussen et al. 2013), and so only limited characterisation was necessary in this study. There is only limited information available on the physicochemical characteristics of the nanoclays, as their size could not be determined via SEM and TEM. The hydrodynamic diameter (as a measure of size), PdI and zeta potential were investigated for all NMs after dispersion in MEM and DMEM complete media at 0 and 24 h incubation. CuO NMs demonstrated a significant reduction in hydrodynamic diameter to less than primary size (10 nm) whereas an increase in hydrodynamic diameter was observed in SiO_2 NMs and MMT after 24 h. This suggests that CuO NMs became less agglomerated in biological media, and may dissociate or dissolve over time (sections 2.4.1). The smaller size, and solubility of CuO NMs may explain why these NMs were more toxic than SiO_2 NMs and MMT nanoclay. $CuSO_4$ was included to help decipher the contribution of ions and particles in CuO NM toxicity. Furthermore, the Cu concentration in CuO NMs and $CuSO_4$ was standardized to facilitate making comparisons between the treatments.

7.1.2. Verification of the models

Confluency of undifferentiated Caco-2 cells was determined using light microscopy and SEM. Three methods confirmed that undifferentiated Caco-2 cells were 100 % confluent prior to their use for toxicity studies. The differentiation status, development of M cells and presence of goblet cells were investigated using TEER measurement, tight junction protein (ZO-1) staining, Alcian blue staining, WGA staining, SEM, TEM and light microscopy. TEER measurement, which was used to confirm the progression of development of barrier integrity confirmed that differentiated Caco-2 cells, and the Caco-2/HT29-MTX and Caco-2/Raji B co-cultures developed an intact monolayer, with all the TEER values greater than 500 $\Omega.cm^2$. In addition, staining of the ZO-1 tight junction protein confirmed the findings observed with TEER measurement. Differentiated Caco-2 cells and Caco-2/HT29-MTX co-cultures also demonstrated elongated microvilli covering the entire cell surface, which is an indication of development of *in vivo* line intestinal monolayer. Caco-2/Raji B cells showed an absence of microvilli in some areas, but not in others, which is an indicative of M cell development. A high intensity of WGA staining in some areas of the surface of Caco-2/Raji B cells confirmed the development of M cells. The presence of mucus on the surface of the Caco-2/HT29-MTX co-culture was confirmed with Alcian blue, and implying that goblet cells developed. The viability of the differentiated Caco-2 cells, Caco-2/HT29-MTX and Caco-2/Raji B cells was confirmed with light microscopy and nuclei count after staining with DAPI, and confirmed that the viability of the cells was not affected by prolonged culturing in a transwell plate. Therefore, our models were all able to mimic features of the intestinal epithelium.

7.1.3. Barrier integrity and cytotoxicity

Cell viability and impact on barrier integrity of cells was determined via the TEER measurement, light microscopy, nuclei count, ZO-1 staining and SEM in differentiated Caco-2 cell models. The impact of NMs on cell viability in undifferentiated Caco-2 cells was assessed using the Alamar blue assay. CuO NMs and $CuSO_4$ demonstrated a significant decrease in viability 24 h post exposure to undifferentiated Caco-2 cells at concentrations $\geq$ 4.89 $\mu g/cm^2$ (equivalent to 15.63 µg/ml) (section 2.3.2). Conversely, MMT nanoclay and SiO_2 NMs did not show any significant decrease in viability, even at the highest concentration tested (500 µg/ml) (section 6.3.2). This suggests that CuO NMs

and $CuSO_4$ were more toxic than MMT nanoclay and SiO_2 NMs. The Alamar blue assay result was used to determine the BMD 20 of CuO NMs (4.4 µg/cm^2) and to select sub-lethal concentrations of CuO NMs and $CuSO_4$ for further mechanistic studies in undifferentiated and differentiated cell models. MMT nanoclay and SiO_2 NM concentrations were also selected based on the BMD 20 of CuO NMs as a BMD 20 could not be determined. The selection of the same concentration, across NMs enabled a direct comparison of NM. Toxicity to be made. Only limited concentration of NMs could be tested in the more complex models due to the higher cost of performing this work, but ideally a range of concentrations would be tested in hazard studies.

Nuclei counts and light microscopy were also used to assess the cytotoxicity of the NMs on undifferentiated Caco-2 cells using selected concentrations. A loss of cells (light microscopy) and decrease in nuclei number was only observed after exposure to CuO NMs, confirming the results from the Alamar blue assay (section 2.4.2). The results therefore suggest that all measures of cytotoxicity provide comparable results. Assessment of the suitability of using other approaches to assess cytotoxicity was required as the Alamar blue assay is not compatible with the transwell plates required for differentiation of the cells, and the LDH assay cannot be performed with CuO Nms, due to interference. Interestingly, when the viability of differentiated Caco-2 cells, Caco-2/HT29-MTX and Caco-2/Raji B cells were assessed post exposure to CuO NMs and $CuSO_4$ via light microscopy and nuclei counts, the viability of the cells was not affected. This suggests that use of undifferentiated cells may overestimate the toxicity of NMs. Exposure of undifferentiated Caco-2 cells, differentiated Caco-2 cells and the Caco-2/HT29-MTX and Caco-2/Raji B co-culture to MMT nanoclays and SiO_2 NMs did not result in a loss of cell viability. It is proposed that nuclei count and light microscopy could be useful measures of intestinal cell viability across different intestinal models when other more commonly used biochemical assays to assess viability (e.g. Alamar blue, WST-1, MTT and LDH) cannot be performed.

As discussed in sections 3.4.1, the reduction in TEER values due to CuO NMs and $CuSO_4$ exposure, indicated a compromise in barrier integrity. Post exposure to 6.34 µg/cm^2 CuO NMs and $CuSO_4$, a reduction in TEER value was identified, but the timing of the effect differed between the models. TEER decreased at 9 h for differentiated Caco-2 cells, at 12 h for the Caco-2/Raji B and at 15 h for the Caco-2/HT29-MTX co-cultures, suggesting

that differentiated Caco-2 cells were most sensitive followed by Caco-2/Raji B and Caco-2/HT29-MTX co-cultures. The reduced sensitivity by Caco-2/HT29-MTX co-culture may be attributed to trapping of the CuO NMs by the mucus thereby hindering their direct contact with intestinal epithelial cells (Cone 2009, Fröhlich 2012). No time dependent change in TEER measurement was observed post exposure of MMT nanoclays and SiO_2 NMs (equivalent concentration of CuO NMs) to differentiated Caco-2 cells, Caco-2/Raji B and Caco-2/HT29-MTX co-cultures. This again suggests that these NMs are less toxic than CuO NMs.

Tight junction (ZO-1) staining confirmed that impact of CuO NMs and $CuSO_4$ compromised barrier integrity in differentiated Caco-2 cells and Caco-2/Raji B co-culture indicating a barrier integrity perturbation. However, the tight junction staining of Caco-2/HT29-MTX co-culture exposed CuO NMs and $CuSO_4$ seem similar to the control, which could be because mucus was covering the cell surface thereby prevent impact on the tight junction or visualisation of the tight junction protein staining. The impact on the tight junction protein staining seem greatest in differentiated Caco-2 cells followed by the Caco-2/Raji B and Caco-2/HT29-MTX co-cultures. Again, this suggests a protection by the mucus present on Caco-2/HT29-MTX co-culture. Although a reduction in ZO-1 staining was observed, it will be important to quantify the intensity of the staining to confirm the degree of damage stimulated by CuO NMs and $CuSO_4$ on tight junction proteins. Shortening of the microvilli was also observed in a small proportion of cells in differentiated Caco-2 cells, Caco-2/Raji B and Caco-2/HT29-MTX co-cultures after exposure to CuO NMs but was not assessed for other NMs or $CuSO_4$ due to cost.

Overall, the results imply that CuO NMs and $CuSO_4$ induced toxicity and tight junction dysfunction in all the cell models, and it may be suggested that light microscopy, nuclei count, time dependent TEER measurement, ZO-1 staining and SEM imaging be included in routine laboratory toxicity studies which investigate the toxicity of ingested NMs *in vitro*. As light microscopy and TEER measurement are the quickest and most cost effective, they could be prioritised.

7.1.4. Translocation and cellular uptake

Translocation and uptake studies using differentiated Caco-2 cells, and the Caco-2/Raji B and Caco-2/HT29-MTX co-cultures indicated a time and concentration dependent

retention of Cu on the AP compartment. Translocation from the AP to BL compartment occurred in a time dependent manner as discussed in sections 3.4.2, 4.4.2 and 5.4.2. The level of Cu in BL compartment was lowest in Caco-2/HT29-MTX co-culture followed by the differentiated Caco-2 cells and then Caco-2/Raji B co-culture suggesting that transport was lowest Caco-2/HT29-MTX co-culture. The Caco-2/Raji B co-culture demonstrated the highest accumulation of Cu in the BL compartment compared to both differentiated Caco-2 cells and Caco-2/HT29-MTX co-culture at concentrations of 3.17 and 6.34 µg/cm^2 CuO NMs and $CuSO_4$, 48 h post exposure. In addition, Caco-2/Raji B co-culture also had less accumulation of Cu in the AP compartment at all concentrations compared to differentiated Caco-2 cells despite lower level of impact on monolayer integrity. This reflects the physiological role of the M cell in sampling the GI tract lumen contents and presenting them to immune cells via aiding translocation. This finding may be studied further by investigating the translocation of CuO NMs at a shorter time point (1 h post exposure). The increased level of Cu in the AP compartment in Caco-2/HT29-MTX co-culture compared to differentiated Caco-2 cells and Caco-2/Raji B co-culture agrees with the reduced effect of CuO NMs and $CuSO_4$ on TEER values and ZO-1 staining compared to differentiated Caco-2 cells and Caco-2/Raji B co-culture (sections 3.4.1, 4.4.1 and 5.4.1). This may imply that there was a reduced impact of CuO NMs and $CuSO_4$ on cell monolayer integrity because of the presence of mucus as mentioned above (section 7.1.3), and that the NMs were trapped in the mucus of the AP. The decreased effect on cell monolayer integrity was also made evident by the reduced detectable Cu observed in the BL compartment and decreased P_{app} value compared to differentiated Caco-2 cells and Caco-2/Raji B co-culture (Figures 3.8, 4.10 and 5.11). Overall, the accumulation of Cu in cells was low (<3 %), for all modes. The high translocation in differentiated Caco-2 cells may be attributed to excessive compromise in monolayer integrity, as the same trend of translocation was not observed at lower treatment concentration (3.17 and 6.34 µg/cm^2). The level of detectable copper in the cell lysate was highest in Caco-2/HT29-MTX cells and approximately the same in both differentiated Caco-2 cells and Caco-2/Raji B cells. Mucus may have attracted some of the Cu hindering its translocation, and was released during acidic digestion of cells thereby increasing the amount of Cu detected in the cell extract. It is known that the mucus layer formed after Caco-2/HT29-MTX cannot not be washed off easily (Mahler et al. 2009), therefore cell monolayer washing prior to digestion may have not washed off the

Cu ions that were attached to the monolayer. In comparison with *in vivo* studies (Walczak et al. 2015a, Schleh et al. 2012, Kreyling et al. 2017), differentiated Caco-2 cells, Caco-2/HT29-MTX and Caco-2/Raji B co-culture may overestimate the translocation of NMs, as a higher translocation was observed using all the *in vitro* models. Perhaps, lack of food components increases potential for exposure to NMs as trapping of NMs in the GI tract mix might lead to less bioavailability.

7.1.5. ROS formation

ROS production was increased by CuO NMs and $CuSO_4$ in an acellular condition, with $CuSO_4$ demonstrating greater than double the fold increase of ROS produced by CuO NMs at 2 h post exposure. In cellular conditions, only $CuSO_4$ induced a significant increase in ROS production after a 2 h exposure to undifferentiated Caco-2 cells, differentiated Caco-2 cells, Caco-2/HT29-MTX and Caco-2/Raji B cells. The level of ROS produced by undifferentiated Caco-2 cells was the highest followed by the Caco-2/Raji B co-culture then differentiated Caco-2 cells and the Caco-2/HT29-MTX co-culture. There was no significant increase in intracellular ROS for all the models at 2 h post exposure to CuO NMs. Since the toxicity of CuO NMs and $CuSO_4$ were similar using other endpoints, it may be suggested that at 2 h post exposure CuO NMs had not dissolved or that CuO NMs stimulate its toxicity via a Trojan horse mechanism (section 2.4.3), which may take longer time for uptake and dissociation intracellularly before mediating ROS production. Reports have shown that CuO NMs may induce ROS through Fenton and or Haber-Weiss process (Chumakov et al. 2016). The Fenton and or Haber-Weiss process involves the use of transition metal ion to induce ROS production (Chumakov et al. 2016, Gaggelli et al. 2006). As expected, SiO_2 NMs and MMT nanoclays did not induce ROS production both in acellular and cellular conditions, as all other endpoints used to assess their toxicity demonstrated that they are less toxic. The involvement of oxidative stress may be assessed in future following the methods outline in section 5.4.4.

7.1.6. Cytokine production

Only IL-8 and ICAM-1 were identified using proteome profiler after exposure of CuO NMs to undifferentiated and differentiated Caco-2 cells. IL-8 has a direct relationship with inflammatory response whereas ICAM-1 is an adhesive molecule, which is present in all adherent cells at high concentrations (Sumagin et al. 2008). Since a similar level of

ICAM-1 production was observed in both treated and untreated cells and due to financial constraints, IL-8 was prioritized in this study. However, assessing ICAM -1 via ELISA and gene expression may give insight on the impact of CuO NMs on the inflammatory response and adherent capability of the cells. Exposure to CuO NMs and $CuSO_4$ of undifferentiated Caco-2 cells, differentiated Caco-2 cells, the Caco-2/HT29-MTX and the Caco-2/Raji B cells stimulated an increase IL-8 production, whereas IL-8 was not detected in control cells and the BL compartments of all the intestinal models post exposure to CuO NMs and $CuSO_4$. Undifferentiated Caco-2 cells mediated the highest level of IL-8, followed by differentiated Caco-2 cells, then the Caco-2/HT29-MTX and Caco-2/Raji B co-cultures suggesting that undifferentiated cells are more sensitive than the other models. As previously discussed using undifferentiated cells may therefore, lead to an overestimation of the toxicity or bioreactivity of NMs (section 2.5). Surprisingly, SiO_2 NMs induced IL-8 production when exposed to undifferentiated Caco-2 cells, differentiated Caco-2 cells, Caco-2/HT29-MTX and Caco-2/Raji B co-cultures, but MMT nanoclay did not. However, the level of IL-8 produced was low for SiO_2 NMs, and whilst statistically significant is unlikely to be biologically significant. Therefore, this study suggests that IL-8 investigation via ELISA is very sensitive in intestinal cell models and may be used for investigation of NM toxicity or bioreactivity in the intestine, across models. Other cytokines such as IL-10, IL-1β, IL-6, TNF-α may also be assessed in future.

7.1.7. Gene expression

Gene expressions of antioxidants (*HMOX1*), inflammatory response (*IL8*), mucus secretion (*MUC2*) and metal binding (*MT1A* and *MT2A*) were assessed to determine the most appropriate molecular markers for the assessment of toxicity in the intestine *in vitro* and to decipher the contribution of ions and particles in the toxicity of CuO NMs. The undifferentiated Caco-2 cells mediated the greatest upregulation of all the genes assessed in this study except *MT1A*, further confirming the possible overestimation of toxicity when using undifferentiated Caco-2 cells to assess the toxicity of NMs. A lack of differentiation may have affected the expression of *MT1A* in undifferentiated Caco-2 cells. All the intestinal models induced a time and concentration dependent *HMOX1* expression. Undifferentiated Caco-2 cells, Caco-2/HT29-MTX and Caco-2/Raji B cells mediated a significant increase in *HMOX1* at 4 h post exposure, which reached the peak

at 12 h, and declined at 24 h post exposure. Although, the highest upregulation of *HMOX1* was observed at 12 h post exposure in most of the intestinal models, *HMOX1* expression may be assessed at 4 h post exposure in order to perform a more rapid assessment of toxicity. Maximum *IL8* expression was observed at 12 h post exposure of CuO NMs and $CuSO_4$ to undifferentiated Caco-2 cells, Caco-2/HT29-MTX and Caco-2/Raji B co-cultures, while differentiated Caco-2 cells induced greatest *IL8* expression at 24 h post exposure. The highest level of *IL8* expression at 12 h observed in the Caco-2/HT29-MTX and Caco-2/Raji B co-cultures may be because of the presence of other cell types (HT29-MTX or Raji B cells), which may have enhanced early induction of the gene compared to differentiated Caco-2 cells. All the cells induced a concentration dependent *IL8* expression at 12 h post exposure hence, 12 h may be suggested as the appropriate time point for assessment of *IL8* expression in the intestine *in vitro*.

MT1A was expressed at the lowest level in undifferentiated Caco-2 cells and highest in differentiated cells indicating that differentiation may have an impact on its expression. However, it was observed in this study that *MT2A* was not expressed in control undifferentiated Caco-2 cells, whereas unexposed differentiated cells were able to express *MT2A*, suggesting that expression of *MT2A* may also be affected by differentiation. There was no correlation between level of *MT1A* expression and time point or concentration. *MT2A* was upregulated in a concentration and time dependent manner in all the intestinal cell models except undifferentiated Caco-2 cells. Among all the genes assessed in this study *MT2A* was the most highly expressed gene, and the maximum expression was observed at 12 h post exposure of CuO NMs and $CuSO_4$. A similar level of expression was observed in differentiated Caco-2 cells and Caco-2/HT29-MTX cells, and the lowest level of expression was observed in the Caco-2/Raji B co-culture. Since a substantial level of *MT2A* expression was observed at 4 h post exposure to CuO NMs and $CuSO_4$, *MT2A* expression could be assessed at 4 h as an early indicator of NM toxicity. *MT2A* may be suggested as a good molecular marker for investigation of metal containing NMs in the intestine whereas *MT1A* may not. However, other subunits of *MT1* (e.g. *MT1B*, *MT1M*, *MT1L*, *MT1E*, *MT1F*, *MT1X*, *MT1G*, *MT1H* and *GPX*) may be assessed in future to ascertain the MT1 subunit that may be employed in the toxicity study of NMs. Since expression of metallothionein are induced by ions and not particles (section 2.4.5), our

result implicates ion involvement in the toxicity of CuO NMs dissolved either before or after uptake (Trojan horse mechanism).

MUC2 expression was highest at 12 h post exposure of CuO NMs and $CuSO_4$ to undifferentiated Caco-2 cells and Caco-2/Raji B co-culture, and 24 h for differentiated Caco-2 cells and Caco-2/HT29-MTX co-culture. Expression of *MUC2* was lowest in the Caco-2/Raji B co-culture at all time points and highest in Caco-2/HT29-MTX cells. This was not a surprise as the Caco-2/HT29-MTX co-culture contains mucus-secreting cells (HT29-MTX). Increased expression of *MUC2* may be as a result of toxicity or physiologically relevant protective mechanism as previously discussed (section 2.4.5) therefore, *MUC2* expression is suggested to be included in assessment of NMs toxicity or bioreactivity in intestinal models at 24 h post exposure since *MUC2* expression is specific to the intestine (Pelaseyed et al. 2014, Johansson et al. 2008, Johansson et al. 2011).

7.2. Further direction of research

Although a battery of tests were employed to assess NM toxicity across *in vitro* models of various complexities, there are still some areas that would benefit from further investigation. The hydrodynamic diameter of CuO NMs increased immediately after dispersion and decreased below the primary size after incubation for 24 h suggesting dissolution in cell culture media assessed via DLS. However, future studies may need to use TEM analysis to confirm the change in CuO NM agglomeration status over time.

TEER measurement was associated with some difficulties as the cells are removed from incubator and equilibrated for 15 min prior to taking TEER measurements and this may introduce errors into the results. However, to eliminate this, measurement of the impact on cell morphology and viability may be investigated using automated impedance instrument (e.g. cellZscope® device) (Benson et al. 2013) in future as measurements are taken *in situ* (while the cell is in incubator).

In this study, it was suggested that toxicity of CuO NMs was mediated by ions and particles. It will be of benefit to investigate the contribution of intracellular Cu ion release to CuO NM toxicity via the following methods: detection of the free and labile metal ions, qualitative determination of the presence of dissolved metal ions by chelation, and separation of dissolved metal ions by filtration or centrifugation (Ivask et al. 2012) in the

future. Translocation and uptake of CuO NMs were studied by measuring the Cu ion concentration with ICP-OES, which are not able to separate the ions from particles. However, visualisation of uptake of CuO NMs using TEM attached with energy dispersion spectroscopy (EDS) could be performed to confirm particle uptake by cells. This will also help to determine the contribution of ions and particles in the toxicity of CuO NMs. TEM attached with energy dispersion spectroscopy (EDS) will also facilitated the clarification of possible trapping of CuO NMs by the mucus formed on the surface of Caco-2/HT29-MTX co-culture. Short time point (e.g. 1 h post exposure) translocation studies with CuO NMs could be performed to demonstrate the functionality of M cell models (transport properties) Furthermore, latex microspheres transport studies may also be employed to demonstrate that Caco-2/Raji B cells functionally resemble *in vivo* M cells (i.e. to demonstrate grater particle transport properties in the M cells *in vitro*).

In this study, Trojan horse, indiscriminate binding of Cu to thiol, amine and carboxyl groups of amino acids in their active site were suggested as the mechanism of CuO NMs toxicity. Nevertheless, to understand the actual mechanism underlying the toxicity of CuO NMs, other methods of ROS detection such as EPR, impact of these NMs on lipid peroxidation, and assessment of antioxidants (e.g. glutathione depletion, superoxide dismutase, catalase) may be employed in future to investigate ROS formation and involvement of oxidative stress in CuO NMs toxicity.

The use of more concentrations, other NMs, and *in vitro* models such as triple co-culture models and epithelial cell derived stem cells, organ and body on the chip would ideally be included. This was not possible due financial and time constraints. In addition, introduction of flow/bacteria to cell cultures to improve physiological relevance may be employed in future studies. It would also be essential to directly compare the same NMs with *in vivo* studies, as there is lack of published data, which have compared *in vitro* and *in vivo* models using the same NMs and the available *in vivo* literature demonstrated a lower toxicity compared to *in vitro* models.

7.3. Final conclusions

CuO NMs and $CuSO_4$ demonstrated strikingly similar trends of toxicity to undifferentiated Caco-2 cells, differentiated Caco-2 cells, and and the Caco-2/HT29-MTX and Caco-2/Raji B co-cultures. CuO NMs and $CuSO_4$ caused a reduction in

viability, TEER value, ZO-1 staining intensity, diminished the length of microvilli, and mediated tight junction integrity dysfunction in the entire *in vitro* intestinal models. CuO NMs and $CuSO_4$ also upregulated IL-8 secretion, expression of *HMOX1*, IL8, *MT1A*, MT2A and *MUC2* in a concentration and time dependent manner. CuO NMs and $CuSO_4$ were translocated in a concentration dependent manner with the greatest translocation observed in Caco-2/Raji B co-culture. Although, there was an increase in ROS production in acellular conditions by CuO NMs and $CuSO_4$, no intestinal cell models showed a significant increase in ROS production and $CuSO_4$ produced greater than double of the ROS produced by CuO NMs. This suggests that CuO NMs toxicity may be mediated by ion and particles as CuO NMs $CuSO_4$ stimulated similar level of toxicity using other endpoints and CuO NMs dissolution was not up to 100 % after 24 h incubation in cell culture medium. Assessing the impact of SiO_2 NMs and MMT nanoclay on the four intestinal models using ROS production, light microscopy, TEER measurement, viability assay (Alamar blue) and IL-8 production demonstrated a lack of toxicity. The results suggest that among the tested endpoints, IL-8 was the most sensitive marker for NM toxicity study.

Undifferentiated Caco-2 cells seem most sensitive followed by differentiated Caco-2 cells then, the Caco-2/Raji B and Caco-2/HT29-MTX co-cultures suggesting that lack of differentiation to *in vivo*-like intestinal cells may have been the reason for their higher sensitivity. It is therefore, possible that the use of undifferentiated Caco-2 cells will overestimate the toxicity of NMs in the intestine. However, the use of undifferentiated Caco-2 may not be completely discarded as the use of transwell plates is more expensive and time consuming. Therefore, it is suggested that undifferentiated Caco-2 cells be used for screening of wide range of NMs for selection of sub lethal concentration prior to the use differentiated Caco-2 cells, and the Caco-2/Raji B and Caco-2/HT29-MTX co-cultures. Differentiated Caco-2 cells, Caco-2/Raji B and Caco-2/HT29-MTX co-cultures are very robust for NM toxicity studies in the intestine; however, Caco-2/Raji B and Caco-2/HT29-MTX co-culture may be prioritized when carrying out translocation studies as they mimic the *in vivo* situation more than undifferentiated and differentiated Caco-2 cells. In addition, molecular markers (*HMOX1*, *IL8*, *MT2A* and *MUC2*) and biochemical (IL-8 secretion) time dependent TEER measurement, impact on cell morphology (using ZO-1 staining, light and electron microscopy) are suggested for routine assessment of

toxicity in the intestine *in vitro*. Finally, the relevancy of these markers to NMs of more varied physicochemical properties requires further investigation as NMs are diverse in nature and toxicity mechanism.

References

Abbasi, N. A., Zahoor, M., Khan, H. A. and Qureshi, A. A. (2012) 'Effect of encapsulated calcium carbide application at different growth stages on potato (Solanum tuberosum L.) growth, yield and tuber quality', *Pakistan Journal of Botany*, 44(5), 1543-1550.

Abbott Chalew, T. E. and Schwab, K. J. (2013) 'Toxicity of commercially available engineered nanoparticles to Caco-2 and SW480 human intestinal epithelial cells', *Cell Biol Toxicol*, 29(2), 101-16.

Abdal Dayem, A., Hossain, M. K., Lee, S. B., Kim, K., Saha, S. K., Yang, G.-M., Choi, H. Y. and Cho, S.-G. (2017) 'The Role of Reactive Oxygen Species (ROS) in the Biological Activities of Metallic Nanoparticles', *Int J Mol Sci*, 18(1), 120.

Aguzzi, C., Cerezo, P., Viseras, C. and Caramella, C. (2007) 'Use of clays as drug delivery systems: Possibilities and limitations', *Applied Clay Science*, 36(1), 22-36.

Ahamed, M., Alhadlaq, H. A., Khan, M. A. M., Karuppiah, P. and Al-Dhabi, N. A. (2014) 'Synthesis, Characterization, and Antimicrobial Activity of Copper Oxide Nanoparticles', *Journal of Nanomaterials*, 2014, 1-4.

Aitken, R. J., Chaudhry, M. Q., Boxall, A. B. and Hull, M. (2006) 'Manufacture and use of nanomaterials: current status in the UK and global trends', *Occup Med (Lond)*, 56(5), 300-6.

Akbari, A., Lavasanifar, A. and Wu, J. (2017) 'Interaction of cruciferin-based nanoparticles with Caco-2 cells and Caco-2/HT29-MTX co-cultures', *Acta Biomaterialia*, 64, 249-258.

Al-Jubory, A. R. and Handy, R. D. (2013) 'Uptake of titanium from TiO2 nanoparticle exposure in the isolated perfused intestine of rainbow trout: nystatin, vanadate and novel CO2-sensitive components', *Nanotoxicology*, 7(8), 1282-1301.

Al-Nasiry, S., Geusens, N., Hanssens, M., Luyten, C. and Pijnenborg, R. (2007) 'The use of Alamar Blue assay for quantitative analysis of viability, migration and invasion of choriocarcinoma cells', *Human Reproduction*, 22(5), 1304-1309.

Alam, N., Amin, R., Khan, A., Ara, I., Shim, M. J., Lee, M. W. and Lee, T. S. (2008) 'Nutritional Analysis of Cultivated Mushrooms in Bangladesh - Pleurotus ostreatus, Pleurotus sajor-caju, Pleurotus florida and Calocybe indica', *Mycobiology*, 36(4), 228-232.

Amiri, M., Etemadifar, Z., Daneshkazemi, A. and Nateghi, M. (2017) 'Antimicrobial Effect of Copper Oxide Nanoparticles on Some Oral Bacteria and Candida Species', *Journal of Dental Biomaterials*, 4(1), 347-352.

Angelé-Martínez, C., Nguyen, K. V. T., Ameer, F. S., Anker, J. N. and Brumaghim, J. L. (2017) 'Reactive oxygen species generation by copper(II) oxide nanoparticles determined by DNA damage assays and EPR spectroscopy', *Nanotoxicology*, 11(2), 278-288.

Antunes, F., Andrade, F., Araújo, F., Ferreira, D. and Sarmento, B. (2013) 'Establishment of a triple co-culture *in vitro* cell models to study intestinal absorption of peptide drugs', *European Journal of Pharmaceutics and Biopharmaceutics*, 83(3), 427-435.

Araújo, F., Shrestha, N., Shahbazi, M.-A., Fonte, P., Mäkilä, E. M., Salonen, J. J., Hirvonen, J. T., Granja, P. L., Santos, H. A. and Sarmento, B. (2014) 'The impact of nanoparticles on the mucosal translocation and transport of GLP-1 across the intestinal epithelium', *Biomaterials,* 35(33), 9199-9207.

Araya, M., Olivares, M., Pizarro, F., González, M., Speisky, H. and Uauy, R. (2003) 'Gastrointestinal symptoms and blood indicators of copper load in apparently healthy adults undergoing controlled copper exposure', *Am J Clin Nutr,* 77, 646-650.

Argueta-Figueroa, L., Morales-Luckie, R. A., Scougall-Vilchis, R. J. and Olea-Mejía, O. F. (2014) 'Synthesis, characterization and antibacterial activity of copper, nickel and bimetallic Cu–Ni nanoparticles for potential use in dental materials', *Progress in Natural Science: Materials International,* 24(4), 321-328.

Aruoja, V., Dubourguier, H.-C., Kasemets, K. and Kahru, A. (2009) 'Toxicity of nanoparticles of CuO, ZnO and TiO2 to microalgae Pseudokirchneriella subcapitata', *Science of The Total Environment,* 407(4), 1461-1468.

Aruoja, V., Pokhrel, S., Sihtmae, M., Mortimer, M., Madler, L. and Kahru, A. (2015) 'Toxicity of 12 metal-based nanoparticles to algae, bacteria and protozoa', *Environmental Science: Nano,* 2(6), 630-644.

Athinarayanan, J., Periasamy, V. S., Alsaif, M. A., Al-Warthan, A. A. and Alshatwi, A. A. (2014) 'Presence of nanosilica (E551) in commercial food products: TNF-mediated oxidative stress and altered cell cycle progression in human lung fibroblast cells', *Cell Biol Toxicol,* 30(2), 89-100.

Atuma, C., Strugala, V., Allen, A. and Holm, L. (2001) 'The adherent gastrointestinal mucus gel layer: thickness and physical state *in vivo*', *American Journal of Physiology - Gastrointestinal and Liver Physiology,* 280(5), G922-G929.

Au - Mateer, S. W., Au - Cardona, J., Au - Marks, E., Au - Goggin, B. J., Au - Hua, S. and Au - Keely, S. (2016) 'Ex Vivo Intestinal Sacs to Assess Mucosal Permeability in Models of Gastrointestinal Disease', *JoVE,* (108), e53250.

Aueviriyavit, S., Phummiratch, D. and Maniratanachote, R. (2014) 'Mechanistic study on the biological effects of silver and gold nanoparticles in Caco-2 cells--induction of the Nrf2/HO-1 pathway by high concentrations of silver nanoparticles', *Toxicol Lett,* 224(1), 73-83.

Awwad, A. M., Albiss, B. A. and Salem, N. M. (2015) 'Antibacterial Activity of synthesized Copper Oxide Nanoparticles using Malva sylvestris Leaf Extract', *SMU Medical Journal,* 2(1), 91-101.

Azzam, M. M. M., Zou, X. T., Dong, X. Y. and Xie, P. (2011) 'Effect of supplemental l-threonine on mucin 2 gene expression and intestine mucosal immune and digestive enzymes activities of laying hens in environments with high temperature and humidity', *Poultry Science,* 90(10), 2251-2256.

Baek, M., Lee, J.-A. and Choi, S.-J. (2012) 'Toxicological effects of a cationic clay, montmorillonite *in vitro* and *in vivo*', *Molecular & Cellular Toxicology,* 8(1), 95-101.

Bajak, E., Fabbri, M., Ponti, J., Gioria, S., Ojea-Jimenez, I., Collotta, A., Mariani, V., Gilliland, D., Rossi, F. and Gribaldo, L. (2015) 'Changes in Caco-2 cells

transcriptome profiles upon exposure to gold nanoparticles', *Toxicol Lett*, 233(2), 187-99.

Banerjee, A., Qi, J., Gogoi, R., Wong, J. and Mitragotri, S. (2016) 'Role of nanoparticle size, shape and surface chemistry in oral drug delivery', *Journal of Controlled Release,* 238, 176-185.

Banga, A., Witzmann, F. A., Petrache, H. I. and Blazer-Yost, B. L. (2012) 'Functional Effects of Nanoparticle Exposure on Calu-3 Airway Epithelial Cells', *Cellular Physiology and Biochemistry,* 29(1-2), 197-212.

Bannunah, A. M., Vllasaliu, D., Lord, J. and Stolnik, S. (2014) 'Mechanisms of nanoparticle internalization and transport across an intestinal epithelial cell model: effect of size and surface charge', *Mol Pharm,* 11(12), 4363-73.

Bansal, S., Biswas, G. and Avadhani, N. G. (2014) 'Mitochondria-targeted heme oxygenase-1 induces oxidative stress and mitochondrial dysfunction in macrophages, kidney fibroblasts and in chronic alcohol hepatotoxicity()', *Redox Biol,* 2, 273-283.

Baricevic, M. (2012) *The Digestive System: Introduction and Primary Organs,* Pearson Education Inc.

Beasley, D. E., Koltz, A. M., Lambert, J. E., Fierer, N. and Dunn, R. R. (2015) 'The Evolution of Stomach Acidity and Its Relevance to the Human Microbiome', *PLoS One,* 10(7), e0134116.

Beatriz, L.-S., Melissa, G., Victor, S. and Maria, J. B.-P. (2014) *'In Vitro* Intestinal Co-Culture Cell Model to Evaluate Intestinal Absorption of Edelfosine Lipid Nanoparticles', *Current Topics in Medicinal Chemistry*, 14(9), 1124-1132.

Bellmann, S., Carlander, D., Fasano, A., Momcilovic, D., Scimeca, J. A., Waldman, W. J., Gombau, L., Tsytsikova, L., Canady, R., Pereira, D. I. and Lefebvre, D. E. (2015) 'Mammalian gastrointestinal tract parameters modulating the integrity, surface properties, and absorption of food-relevant nanomaterials', *Wiley Interdiscip Rev Nanomed Nanobiotechnol,* 7(5), 609-22.

Benn, T., Cavanagh, B., Hristovski, K., Posner, J. D. and Westerhoff, P. (2010) 'The Release of Nanosilver from Consumer Products Used in the Home', *Journal of Environmental Quality,* 39(6), 1875-1882.

Benn, T. M. and Westerhoff, P. (2008) 'Nanoparticle Silver Released into Water from Commercially Available Sock Fabrics', *Environ. Sci. Technol.,* 42, 4133–4139.

Benson, K., Cramer, S. and Galla, H.-J. (2013) 'Impedance-based cell monitoring: barrier properties and beyond', *Fluids and Barriers of the CNS,* 10(1), 5.

Bergin, I. L. and Witzmann, F. A. (2013) 'Nanoparticle toxicity by the gastrointestinal route: evidence and knowledge gaps', *Int J Biomed Nanosci Nanotechnol,* 3(1-2).

Besinis, A., De Peralta, T. and Handy, R. D. (2014) 'The antibacterial effects of silver, titanium dioxide and silica dioxide nanoparticles compared to the dental disinfectant chlorhexidine on Streptococcus mutans using a suite of bioassays', *Nanotoxicology,* 8(1), 1-16.

Beyth, N., Houri-Haddad, Y., Domb, A., Khan, W. and Hazan, R. (2015) 'Alternative Antimicrobial Approach: Nano-Antimicrobial Materials', *Evidence-based Complementary and Alternative Medicine : eCAM,* 2015, 246012.

Bhattacharyya, A., Chattopadhyay, R., Mitra, S. and Crowe, S. E. (2014) 'Oxidative stress: an essential factor in the pathogenesis of gastrointestinal mucosal diseases', *Physiol Rev,* 94(2), 329-54.

Birben, E., Sahiner, U. M., Sackesen, C., Erzurum, S. and Kalayci, O. (2012) 'Oxidative Stress and Antioxidant Defense', *The World Allergy Organization journal,* 5(1), 9-19.

Boegh, M., Baldursdóttir, S. G., Müllertz, A. and Nielsen, H. M. (2014) 'Property profiling of biosimilar mucus in a novel mucus-containing *in vitro* model for assessment of intestinal drug absorption', *European Journal of Pharmaceutics and Biopharmaceutics,* 87(2), 227-235.

Bolea, E., Jimenez-Lamana, J., Laborda, F., Abad-Alvaro, I., Blade, C., Arola, L. and Castillo, J. R. (2014) 'Detection and characterization of silver nanoparticles and dissolved species of silver in culture medium and cells by AsFlFFF-UV-Vis-ICPMS: application to nanotoxicity tests', *Analyst,* 139(5), 914-922.

Bondarenko, O., Ivask, A., Käkinen, A., Kurvet, I. and Kahru, A. (2013) 'Particle-Cell Contact Enhances Antibacterial Activity of Silver Nanoparticles', *PLoS One,* 8(5), e64060.

Bony, S., Carcelen, M., Olivier, L. and Devaux, A. (2006) 'Genotoxicity assessment of deoxynivalenol in the Caco-2 cell line model using the Comet assay', *Toxicol Lett,* 166(1), 67-76.

Bossi, E., Zanella, D., Gornati, R. and Bernardini, G. (2016) 'Cobalt oxide nanoparticles can enter inside the cells by crossing plasma membranes', *Scientific Reports,* 6, 22254.

Bouffant, L. L., Daniel, H., Martin, J. and Bruyere, S. (1982) 'Effect of impurities and associated minerals on quartz toxicity' in *Inhaled Particles V,* Elsevier, 625-634.

Bouwmeester, H., Dekkers, S., Noordam, M. Y., Hagens, W. I., Bulder, A. S., de Heer, C., ten Voorde, S. E. C. G., Wijnhoven, S. W. P., Marvin, H. J. P. and Sips, A. J. A. M. (2009) 'Review of health safety aspects of nanotechnologies in food production', *Regulatory Toxicology and Pharmacology,* 53(1), 52-62.

Bouwmeester, H., Poortman, J., Peters, R. J., Wijma, E., Kramer, E., Makama, S., Puspitaninganindita, K., Marvin, H. J. P., Peijnenburg, A. A. C. M. and Hendriksen, P. J. M. (2011) 'Characterization of Translocation of Silver Nanoparticles and Effects on Whole-Genome Gene Expression Using an *In Vitro* Intestinal Epithelium Coculture Model', *ACS Nano,* 5(5), 4091-4103.

Bouwmeester, H., van der Zande, M. and Jepson, M. A. (2018) 'Effects of food-borne nanomaterials on gastrointestinal tissues and microbiota', *Wiley Interdisciplinary Reviews: Nanomedicine and Nanobiotechnology,* 10(1).

Boyles, M. S. P., Ranninger, C., Reischl, R., Rurik, M., Tessadri, R., Kohlbacher, O., Duschl, A. and Huber, C. G. (2016) 'Copper oxide nanoparticle toxicity profiling using untargeted metabolomics', *Part Fibre Toxicol,* 13(1), 49.

Braakhuis, H. M., Park, M. V., Gosens, I., De Jong, W. H. and Cassee, F. R. (2014) 'Physicochemical characteristics of nanomaterials that affect pulmonary inflammation', *Part Fibre Toxicol,* 11(1), 1-25.

Brandon, E. F. A., Oomen, A. G., Rompelberg, C. J. M., Versantvoort, C. H. M., van Engelen, J. G. M. and Sips, A. J. A. M. (2006) 'Consumer product *in vitro* digestion model: Bioaccessibility of contaminants and its application in risk assessment', *Regulatory Toxicology and Pharmacology,* 44(2), 161-171.

Brayden, D. J., Jepson, M. A. and Baird, A. W. (2005) 'Keynote review: Intestinal Peyer's patch M cells and oral vaccine targeting', *Drug Discovery Today,* 10(17), 1145-1157.

Bremner, I. (1987) 'Involvement of Metallothionein in the Hepatic Metabolism of Copper', *The Journal of Nutrition,* 117, 19-29.

Brown, D. M., Dickson, C., Duncan, P., Al-Attili, F. and Stone, V. (2010) 'Interaction between nanoparticles and cytokine proteins: impact on protein and particle functionality', *Nanotechnology,* 21(21), 215104.

Brown, D. M., Donaldson, K., Borm, P. J., Schins, R. P., Dehnhardt, M., Gilmour, P., Jimenez, L. A. and Stone, V. (2004) 'Calcium and ROS-mediated activation of transcription factors and TNF-α cytokine gene expression in macrophages exposed to ultrafine particles', *American Journal of Physiology - Lung Cellular and Molecular Physiology,* 286(2 30-2), L344-L353.

Brown, D. M., Johnston, H., Gubbins, E. and Stone, V. (2014) 'Cytotoxicity and Cytokine Release in Rat Hepatocytes, C3A Cells and Macrophages Exposed to Gold Nanoparticles—Effect of Biological Dispersion Media or Corona', *Journal of Biomedical Nanotechnology,* 10(11), 3416-3429.

Brown, D. M., Johnston, H. J., Gaiser, B., Pinna, N., Caputo, G., Culha, M., Kelestemur, S., Altunbek, M., Stone, V., Roy, J. C., Kinross, J. H. and Fernandes, T. F. (2018) 'A cross-species and model comparison of the acute toxicity of nanoparticles used in the pigment and ink industries', *NanoImpact,* 11, 20-32.

Brown, D. M., Wilson, M. R., MacNee, W., Stone, V. and Donaldson, K. (2001) 'Size-Dependent Proinflammatory Effects of Ultrafine Polystyrene Particles: A Role for Surface Area and Oxidative Stress in the Enhanced Activity of Ultrafines', *Toxicology and Applied Pharmacology,* 175(3), 191-199.

Brown, S. C., Kamal, M., Nasreen, N., Baumuratov, A., Sharma, P., Antony, V. B. and Moudgil, B. M. (2007) 'Influence of shape, adhension and simulated lung mechanics on amorphous silica nanoparticle toxicity', *Advanced Powder Technology,* 18(1), 69-79.

Brun, E., Barreau, F., Veronesi, G., Fayard, B., Sorieul, S., Chanéac, C., Carapito, C., Rabilloud, T., Mabondzo, A., Herlin-Boime, N. and Carrière, M. (2014) 'Titanium dioxide nanoparticle impact and translocation through ex vivo, *in vivo* and *in vitro* gut epithelia', *Part Fibre Toxicol,* 11(1), 13.

Burden, N., Aschberger, K., Chaudhry, Q., Clift, M. J. D., Doak, S. H., Fowler, P., Johnston, H., Landsiedel, R., Rowland, J. and Stone, V. (2017) 'The 3Rs as a framework to support a 21st century approach for nanosafety assessment', *Nano Today,* 12, 10-13.

Burkhead, J. L., Reynolds, K. A. G., Abdel-Ghany, S. E., Cohu, C. M. and Pilon, M. (2009) 'Copper homeostasis', *New Phytologist,* 182(4), 799-816.

Cabellos, J., Delpivo, C., Fernández-Rosas, E., Vázquez-Campos, S. and Janer, G. (2017) 'Contribution of M-cells and other experimental variables in the translocation of TiO2 nanoparticles across *in vitro* intestinal models', *NanoImpact*, 5, 51-60.

Calatayud, M., Vázquez, M., Devesa, V. and Vélez, D. (2012) '*In Vitro* Study of Intestinal Transport of Inorganic and Methylated Arsenic Species by Caco-2/HT29-MTX Cocultures', *Chemical Research in Toxicology*, 25(12), 2654-2662.

Calvo, J., Jung, H. and Meloni, G. (2017) 'Copper metallothioneins', *IUBMB Life*, 69(4), 236-245.

Canli, E. G. and Canli, M. (2017) 'Effects of aluminum, copper, and titanium nanoparticles on some blood parameters in Wistar rats', *Turkish Journal of Zoology*, 41(2), 259-266.

Carpene, E., Andreani, G. and Isani, G. (2007) 'Metallothionein functions and structural characteristics', *J Trace Elem Med Biol*, 21 Suppl 1, 35-9.

Catto-Smith, A. G., Emselle, S. and Bishop, R. F. (2008) 'Changes in macromolecular transport appear early in Caco-2 cells infected with a human rotavirus', *Scandinavian Journal of Gastroenterology*, 43(3), 314-322.

Chakraborty, M., Jain, S. and Rani, V. (2011) 'Nanotechnology: Emerging Tool for Diagnostics and Therapeutics', *Applied Biochemistry and Biotechnology*, 165(5), 1178-1187.

Chakraborty, U. and Pradhan, D. (2011) 'High temperature-induced oxidative stress in Lens culinaris, role of antioxidants and amelioration of stress by chemical pre-treatments', *Journal of Plant Interactions*, 6(1), 43-52.

Chang, A. Y., Chan, J. Y., Cheng, H.-L., Tsai, C.-Y. and Chan, S. H. (2009) 'Hypoxia-inducible factor 1/heme oxygenase 1 cascade as upstream signals in the prolife role of heat shock protein 70 at rostral ventrolateral medulla during experimental brain stem death', *Shock*, 32(6), 651-658.

Chang, H.-J., Choi, S.-W., Ko, S.-H. and Chun, H.-S. (2011) 'Effect of Particle Size of Zinc Oxides on Cytotoxicity and Cell Permeability in Caco-2 Cells', *Journal of Food Science and Nutrition*, 16(2), 174-178.

Chang, H., Jwo, C. S., Lo, C. H., Tsung, T. T., Kao, M. J. and Lin, H. M. (2005) 'Rheology of CuO nanoparticle suspension prepared by ASNSS', *Rev. Adv.Mater. sci.*, 10, 128-132.

Chang, Y.-N., Zhang, M., Xia, L., Zhang, J. and Xing, G. (2012) 'The toxic effects and mechanisms of CuO and ZnO nanoparticles', *Materials*, 5(12), 2850-2871.

Chen, C.-C. and Chen, J. J. (2014) 'Benchmark Dose Calculation for Ordered Categorical Responses', *Risk Analysis*, 34(8), 1435-1447.

Chen, E. Y. T., Garnica, M., Wang, Y.-C., Chen, C.-S. and Chin, W.-C. (2011) 'Mucin Secretion Induced by Titanium Dioxide Nanoparticles', *PLoS One*, 6(1), e16198.

Chen, G., Lianqin, Z., Fenghua, Z., Fang, Z., Mingming, S. and Kai, H. (2015) 'Comparative evaluation of nano-CuO crossing Caco-2 cell monolayers and cellular uptake', *Journal of Nanoparticle Research*, 17(4), 1-10.

Chen, L., Lu, X., Liang, X., Hong, D., Guan, Z., Guan, Y. and Zhu, W. (2016) 'Mechanistic studies of the transport of peimine in the Caco-2 cell model', *Acta Pharmaceutica Sinica B,* 6(2), 125-131.

Chen, N., Song, Z.-M., Tang, H., Xi, W.-S., Cao, A., Liu, Y. and Wang, H. (2016) 'Toxicological effects of Caco-2 cells following short-term and long-term exposure to Ag nanoparticles', *Int J Mol Sci,* 17(6), 974.

Chen, X.-M., Elisia, I. and Kitts, D. D. (2010) 'Defining conditions for the co-culture of Caco-2 and HT29-MTX cells using Taguchi design', *Journal of Pharmacological and Toxicological Methods,* 61(3), 334-342.

Chen, Z., Meng, H., Xing, G., Chen, C., Zhao, Y., Jia, G., Wang, T., Yuan, H., Ye, C., Zhao, F., Chai, Z., Zhu, C., Fang, X., Ma, B. and Wan, L. (2006) 'Acute toxicological effects of copper nanoparticles *in vivo'*, *Toxicol Lett,* 163(2), 109-120.

Cheng, K. C., Li, C. and Uss, A. S. (2008) 'Prediction of oral drug absorption in humans – from cultured cell lines and experimental animals', *Expert Opinion on Drug Metabolism & Toxicology,* 4(5), 581-590.

Cherian, M. G., Jayasurya, A. and Bay, B.-H. (2003) 'Metallothioneins in human tumors and potential roles in carcinogenesis', *Mutation Research/Fundamental and Molecular Mechanisms of Mutagenesis,* 533(1–2), 201-209.

Cho, W.-S., Duffin, R., Howie, S. E. M., Scotton, C. J., Wallace, W. A. H., MacNee, W., Bradley, M., Megson, I. L. and Donaldson, K. (2011) 'Progressive severe lung injury by zinc oxide nanoparticles; the role of Zn(2+)dissolution inside lysosomes', *Part Fibre Toxicol,* 8, 27-27.

Choi, S.-J., Oh, J.-M. and Choy, J.-H. (2009) 'Toxicological effects of inorganic nanoparticles on human lung cancer A549 cells', *Journal of Inorganic Biochemistry,* 103(3), 463-471.

Christensen, F. M., Johnston, H. J., Stone, V., Aitken, R. J., Hankin, S., Peters, S. and Aschberger, K. (2010) 'Nano-silver – feasibility and challenges for human health risk assessment based on open literature', *Nanotoxicology,* 4(3), 284-295.

Chu, P. and Garwood, W. E. (1992) 'Zeolite-clay composition and uses thereof',

Chumakov, A., Batalova, V. and Slizhov, Y. (2016) *Electro-Fenton-like reactions of transition metal ions with electrogenerated hydrogen peroxide,* translated by AIP Publishing, 040004.

Clark, M. A., Jepson, M. A., Simmons, N. L., Booth, T. A. and Hirst, B. H. (1993) 'Differential expression of lectin-binding sites defines mouse intestinal M-cells', *Journal of Histochemistry & Cytochemistry,* 41(11), 1679-1687.

Clift, M. J. D., Brandenberger, C., Rothen-Rutishauser, B., Brown, D. M. and Stone, V. (2011a) 'The uptake and intracellular fate of a series of different surface coated quantum dots *in vitro*', *Toxicology,* 286(1), 58-68.

Clift, M. J. D., Gehr, P. and Rothen-Rutishauser, B. (2011b) 'Nanotoxicology: a perspective and discussion of whether or not *in vitro* testing is a valid alternative', *Arch Toxicol,* 85(7), 723-731.

Cobo, E. R., Kissoon-Singh, V., Moreau, F. and Chadee, K. (2015) 'Colonic MUC2 mucin regulates the expression and antimicrobial activity of β-defensin 2', *Mucosal Immunol,* 8(6), 1360-1372.

Cone, R. A. (2009) 'Barrier properties of mucus', *Advanced Drug Delivery Reviews,* 61(2), 75-85.

Cooper, K. L., Liu, K. J. and Hudson, L. G. (2009) 'Enhanced ROS production and redox signaling with combined arsenite and UVA exposure: Contribution of NADPH oxidase', *Free Radical Biology and Medicine,* 47(4), 381-388.

Cornick, S., Tawiah, A. and Chadee, K. (2015) 'Roles and regulation of the mucus barrier in the gut', *Tissue Barriers,* 3(1-2), e982426.

Corr, S. C., Gahan, C. C. and Hill, C. (2008) 'M-cells: origin, morphology and role in mucosal immunity and microbial pathogenesis', *FEMS Immunol Med Microbiol,* 52(1), 2-12.

Cotogno, G., Gibson, P., Per Axel Clausen, P.-J. d., Temmerman, S. H. N. and Ceccone, G. (2013) 'Synthetic Amorphous Silicon Dioxide (NM-200, NM-201, NM-202, NM-203, NM-204): Characterisation and Physico-Chemical Properties In: NM-Series of Representative Manufactured Nanomaterials', *Ispra, Italy: Joint Research Centre of the European Commission*.

Crater, J. S. and Carrier, R. L. (2010) 'Barrier Properties of Gastrointestinal Mucus to Nanoparticle Transport', *Macromolecular Bioscience,* 10(12), 1473-1483.

Crawley, S. W., Mooseker, M. S. and Tyska, M. J. (2014) 'Shaping the intestinal brush border', *J Cell Biol,* 207(4), 441-51.

Dameron, C. T. and Harrison, M. D. (1998) 'Mechanisms for protection against copper toxicity', *The American Journal of Clinical Nutrition,* 67, 1091S- 1097S.

Das, K., Rawat, K. and Bohidar, H. (2016) 'Surface patch binding induced interaction of anisotropic nanoclays with globular plasma proteins', *RSC Advances,* 6(106), 104117-104125.

Decan, N., Wu, D., Williams, A., Bernatchez, S., Johnston, M., Hill, M. and Halappanavar, S. (2016) 'Characterization of *in vitro* genotoxic, cytotoxic and transcriptomic responses following exposures to amorphous silica of different sizes', *Mutation Research/Genetic Toxicology and Environmental Mutagenesis,* 796, 8-22.

Derk, R., Davidson, D. C., Manke, A., Stueckle, T. A., Rojanasakul, Y. and Wang, L. (2015) 'Potential *in vitro* model for testing the effect of exposure to nanoparticles on the lung alveolar epithelial barrier', *Sensing and Bio-Sensing Research,* 3, 38-45.

des Rieux, A., Fievez, V., Garinot, M., Schneider, Y. J. and Preat, V. (2006) 'Nanoparticles as potential oral delivery systems of proteins and vaccines: a mechanistic approach', *J Control Release,* 116(1), 1-27.

des Rieux, A., Fievez, V., Theate, I., Mast, J., Preat, V. and Schneider, Y. J. (2007) 'An improved *in vitro* model of human intestinal follicle-associated epithelium to study nanoparticle transport by M cells', *Eur J Pharm Sci,* 30(5), 380-91.

des Rieux, A., Ragnarsson, E. G., Gullberg, E., Preat, V., Schneider, Y. J. and Artursson, P. (2005) 'Transport of nanoparticles across an *in vitro* model of the human intestinal follicle associated epithelium', *Eur J Pharm Sci,* 25(4-5), 455-65.

Desai, V. and Kaler, S. G. (2008) 'Role of copper in human neurological disorders1–3', *Am J Clin Nutr,* 88, 855S–858S.

Duffin, R., Tran, L., Brown, D., Stone, V. and Donaldson, K. (2007) 'Proinflammogenic Effects of Low-Toxicity and Metal Nanoparticles *In Vivo* and *In Vitro:* Highlighting the Role of Particle Surface Area and Surface Reactivity', *Inhalation Toxicology,* 19(10), 849-856.

Duncan, T. V. (2011) 'Applications of nanotechnology in food packaging and food safety: Barrier materials, antimicrobials and sensors', *J Colloid Interface Sci,* 363(1), 1-24.

Dusinska, M., Rundén-Pran, E., Schnekenburger, J. and Kanno, J. (2017) 'Chapter 3 - Toxicity Tests: *In Vitro* and *In Vivo* A2 - Fadeel, Bengt' in Pietroiusti, A. and Shvedova, A. A., eds., *Adverse Effects of Engineered Nanomaterials (Second Edition)*, Academic Press, 51-82.

Ebabe Elle, R., Rahmani, S., Lauret, C., Morena, M., Bidel, L. P. R., Boulahtouf, A., Balaguer, P., Cristol, J.-P., Durand, J.-O., Charnay, C. and Badia, E. (2016) 'Functionalized Mesoporous Silica Nanoparticle with Antioxidants as a New Carrier That Generates Lower Oxidative Stress Impact on Cells', *Mol Pharm,* 13(8), 2647-2660.

EFSA (2009) 'Guidance of the Scientific Committee on the request from EFSA on the use of the benchmark dose approach in risk assessment', *EFSA Journal,* 1150, 1-72.

Elamin, E., Masclee, A., Troost, F., Dekker, J. and Jonkers, D. (2014) 'Cytotoxicity and metabolic stress induced by acetaldehyde in human intestinal LS174T goblet-like cells', *American Journal of Physiology-Gastrointestinal and Liver Physiology,* 307(3), G286-G294.

Ellingsen, D. G., Horn, N. and Aaseth, J. A. N. (2007) 'CHAPTER 26 - Copper' in *Handbook on the Toxicology of Metals (Third Edition)*, Burlington: Academic Press, 529-546.

Elsaesser, A., Barnes, C. A., McKerr, G., Salvati, A., Lynch, I., Dawson, K. A. and Howard, C. V. (2011) 'Quantification of nanoparticle uptake by cells using an unbiased sampling method and electron microscopy', *Nanomedicine,* 6(7), 1189-1198.

Erickson, K. L., Medina, E. A. and Hubbard, N. E. (2000) 'Micronutrients and Innate Immunity', *The Journal of Infectious Diseases 2000;182(Suppl 1):S5–10,* 182((Suppl 1)), s5-10.

Estrela-Lopis, I., Romero, G., Rojas, E., Moya, S. and Donath, E. (2011) *Nanoparticle uptake and their co-localization with cell compartments–a confocal Raman microscopy study at single cell level,* translated by IOP Publishing, 012017.

European-Commision (2011) 'Recommendation on the difinition of nanomaterials', [online], available: <http://ec.europa.eu/environment/chemicals/nanotech/pdf/commission_recommendation.pdf>. [accessed 5/ 25/2015].

Evans, D. F., Pye, G., Bramley, R., Clark, A. G., Dyson, T. J. and Hardcastle, J. D. (1988) 'Measurment of gastrointestinal pH profile in normal ambulant human subjects', *Gut,* 29, 1035-1041.

Even-Tzur, N., Kloog, Y., Wolf, M. and Elad, D. (2008) 'Mucus Secretion and Cytoskeletal Modifications in Cultured Nasal Epithelial Cells Exposed to Wall Shear Stresses', *Biophysical Journal,* 95(6), 2998-3008.

Fahmy, B. and Cormier, S. A. (2009) 'Copper oxide nanoparticles induce oxidative stress and cytotoxicity in airway epithelial cells', *Toxicology in Vitro,* 23(7), 1365-1371.

Fallingborg, J. (1999) 'Intraluminal pH of the human gastrointestinal tract', *Danish medical bulletin,* 46(3), 183-196.

Fanning, A. S., Ma, T. Y. and Anderson, J. M. (2002) 'Isolation and functional characterization of the actin binding region in the tight junction protein ZO-1', *The FASEB Journal,* 16(13), 1835-1837.

Farcal, L., Torres Andon, F., Di Cristo, L., Rotoli, B. M., Bussolati, O., Bergamaschi, E., Mech, A., Hartmann, N. B., Rasmussen, K., Riego-Sintes, J., Ponti, J., Kinsner-Ovaskainen, A., Rossi, F., Oomen, A., Bos, P., Chen, R., Bai, R., Chen, C., Rocks, L., Fulton, N., Ross, B., Hutchison, G., Tran, L., Mues, S., Ossig, R., Schnekenburger, J., Campagnolo, L., Vecchione, L., Pietroiusti, A. and Fadeel, B. (2015) 'Comprehensive *In Vitro* Toxicity Testing of a Panel of Representative Oxide Nanomaterials: First Steps towards an Intelligent Testing Strategy', *PLoS One,* 10(5), e0127174.

Faust, J. J., Doudrick, K., Yang, Y., Westerhoff, P. and Capco, D. G. (2014a) 'Food grade titanium dioxide disrupts intestinal brush border microvilli *in vitro* independent of sedimentation', *Cell Biol Toxicol,* 30(3), 169-188.

Faust, J. J., Zhang, W., Chen, Y. and Capco, D. G. (2014b) 'Alpha-Fe2O3 elicits diameter-dependent effects during exposure to an *in vitro* model of the human placenta', *Cell Biol Toxicol,* 30(1), 31-53.

Ferrec, E. L. and Fardel, O. (2012) 'Applications Using Caco-2 and TC7 Cells for Drug Metabolism Studies' in *Encyclopedia of Drug Metabolism and Interactions,* First Edition ed., John Wiley & Sons, Inc, 1-16.

Ferruzza, S., Rossi, C., Scarino, M. L. and Sambuy, Y. (2012a) 'A protocol for differentiation of human intestinal Caco-2 cells in asymmetric serum-containing medium', *Toxicology in Vitro,* 26(8), 1252-1255.

Ferruzza, S., Rossi, C., Scarino, M. L. and Sambuy, Y. (2012b) 'A protocol for in situ enzyme assays to assess the differentiation of human intestinal Caco-2 cells', *Toxicol In Vitro,* 26(8), 1247-51.

Florez, L., Herrmann, C., Cramer, J. M., Hauser, C. P., Koynov, K., Landfester, K., Crespy, D. and Mailänder, V. (2012) 'How Shape Influences Uptake: Interactions of Anisotropic Polymer Nanoparticles and Human Mesenchymal Stem Cells', *Small,* 8(14), 2222-2230.

Fogh, J., Fogh, J. M. and Orfeo, T. (1977) 'One Hundred and Twenty-Seven Cultured Human Tumor Cell Lines Producing Tumors in Nude Mice', *J Natl. Cancer Inst.,* 59(1), 221-226.

Fogh, J. and Trempe, G. (1975) 'New Human Tumor Cell Lines' in Fogh, J., ed. *Human Tumor Cells in Vitro*, Boston, MA: Springer US, 115-159.

Foster, A. W., Osman, D. and Robinson, N. J. (2014) 'Metal Preferences and Metallation', *The Journal of Biological Chemistry,* 289(41), 28095-28103.

Foucaud, L., Wilson, M. R., Brown, D. M. and Stone, V. (2007) 'Measurement of reactive species production by nanoparticles prepared in biologically relevant media', *Toxicol Lett,* 174(1), 1-9.

Fröhlich, E. (2012) 'The role of surface charge in cellular uptake and cytotoxicity of medical nanoparticles', *Int J Nanomedicine,* 7, 5577-5591.

Fruijtier-Pölloth, C. (2012) 'The toxicological mode of action and the safety of synthetic amorphous silica—A nanostructured material', *Toxicology,* 294(2), 61-79.

Fruijtier-Pölloth, C. (2016) 'The safety of nanostructured synthetic amorphous silica (SAS) as a food additive (E 551)', *Arch Toxicol,* 90(12), 2885-2916.

Fu, P. P., Xia, Q., Hwang, H.-M., Ray, P. C. and Yu, H. (2014) 'Mechanisms of nanotoxicity: Generation of reactive oxygen species', *Journal of Food and Drug Analysis,* 22(1), 64-75.

Gabbay, J. (2006) 'Copper Oxide Impregnated Textiles with Potent Biocidal Activities', *Journal of Industrial Textiles,* 35(4), 323-335.

Gaetke, L. M., Chow-Johnson, H. S. and Chow, C. K. (2014) 'Copper: Toxicological relevance and mechanisms', *Arch Toxicol,* 88(11), 1929-1938.

Gaggelli, E., Kozlowski, H., Valensin, D. and Valensin, G. (2006) 'Copper Homeostasis and Neurodegenerative Disorders (Alzheimer's, Prion, and Parkinson's Diseases and Amyotrophic Lateral Sclerosis)', *Chem. Rev.,* 106, 1995-2044.

Gaiser, B. K., Hirn, S., Kermanizadeh, A., Kanase, N., Fytianos, K., Wenk, A., Haberl, N., Brunelli, A., Kreyling, W. G. and Stone, V. (2013) 'Effects of silver nanoparticles on the liver and hepatocytes *in vitro*', *Toxicol Sci,* 131(2), 537-47.

Gamboa, J. M. and Leong, K. W. (2013) '*In vitro* and *in vivo* models for the study of oral delivery of nanoparticles', *Advanced Drug Delivery Reviews,* 65(6), 800-810.

Garrett, W. S., Gordon, J. I. and Glimcher, L. H. (2010) 'Homeostasis and inflammation in the intestine', *Cell,* 140(6), 859-70.

Gassler, N., Newrzella, D., Böhm, C., Lyer, S., Li, L., Sorgenfrei, O., van Laer, L., Sido, B., Mollenhauer, J., Poustka, A., Schirmacher, P. and Gretz, N. (2006) 'Molecular characterisation of non-absorptive and absorptive enterocytes in human small intestine', *Gut,* 55(8), 1084-1089.

Gatoo, M. A., Naseem, S., Arfat, M. Y., Mahmood Dar, A., Qasim, K. and Zubair, S. (2014) 'Physicochemical Properties of Nanomaterials: Implication in Associated Toxic Manifestations', *BioMed Research International,* 2014, 498420.

Gebert, A., Fassbender, S., Werner, K. and Weissferdt, A. (1999) 'The Development of M Cells in Peyer's Patches Is Restricted to Specialized Dome-Associated Crypts', *The American Journal of Pathology,* 154(5), 1573-1582.

Gebert, A., Rothkötter, H.-J. and Pabst, R. (1996) 'M Cells in Peyer's Patches of the Intestine' in Kwang, W. J., ed. *International Review of Cytology,* Academic Press, 91-159.

Geiser, M. and Kreyling, W. G. (2010) 'Deposition and biokinetics of inhaled nanoparticles', *Part Fibre Toxicol,* 7(1), 1-17.

Georgantzopoulou, A., Serchi, T., Cambier, S., Leclercq, C. C., Renaut, J., Shao, J., Kruszewski, M., Lentzen, E., Grysan, P., Eswara, S., Audinot, J.-N., Contal, S., Ziebel, J., Guignard, C., Hoffmann, L., Murk, A. J. and Gutleb, A. C. (2016) 'Effects of silver nanoparticles and ions on a co-culture model for the gastrointestinal epithelium', *Part Fibre Toxicol,* 13(1), 9.

Gerloff, K., Albrecht, C., Boots, A. W., Förster, I. and Schins, R. P. F. (2009) 'Cytotoxicity and oxidative DNA damage by nanoparticles in human intestinal Caco-2 cells', *Nanotoxicology*, 3(4), 355-364.

Gerloff, K., Fenoglio, I., Carella, E., Kolling, J., Albrecht, C., Boots, A. W., Förster, I. and Schins, R. P. F. (2012) 'Distinctive Toxicity of TiO2 Rutile/Anatase Mixed Phase Nanoparticles on Caco-2 Cells', *Chemical Research in Toxicology*, 25(3), 646-655.

Gerloff, K., Pereira, D. I. A., Faria, N., Boots, A. W., Kolling, J., Förster, I., Albrecht, C., Powell, J. J. and Schins, R. P. F. (2013) 'Influence of simulated gastrointestinal conditions on particle-induced cytotoxicity and interleukin-8 regulation in differentiated and undifferentiated Caco-2 cells', *Nanotoxicology,* 7(4), 353-366.

Giannasca, P. J., Giannasca, K. T., Leichtner, A. M. and Neutra, M. R. (1999) 'Human Intestinal M Cells Display the Sialyl Lewis A Antigen', *Infection and Immunity,* 67(2), 946-953.

Goodman, C. M., McCusker, C. D., Yilmaz, T. and Rotello, V. M. (2004) 'Toxicity of Gold Nanoparticles Functionalized with Cationic and Anionic Side Chains', *Bioconjugate Chemistry,* 15(4), 897-900.

Gosens, I., Cassee, F. R., Zanella, M., Manodori, L., Brunelli, A., Costa, A. L., Bokkers, B. G. H., de Jong, W. H., Brown, D., Hristozov, D. and Stone, V. (2016) 'Organ burden and pulmonary toxicity of nano-sized copper (II) oxide particles after short-term inhalation exposure', *Nanotoxicology*, 1-12.

Gotteland, M., Araya, M., Pizarro, F. and Olivares, M. (2001) 'Effect of Acute Copper Exposure on Gastrointestinal Permeability in Healthy Volunteers', *Digestive Diseases and Sciences,* 46(9), 1909-1914.

Granger, B. and Baker, R. F. (1950) 'Electron microscope investigation of the striated border of intestinal epithelium', *The Anatomical Record,* 107(4), 423-441.

Granger, D. N. and Kvietys, P. R. (2015) 'Reperfusion injury and reactive oxygen species: The evolution of a concept()', *Redox Biol,* 6, 524-551.

Gree, A. D. (2015) 'The-History-and-Working-Principle-of-the-Scanning-Electron-Microscope-(SEM).'.

Guichard, Y., Maire, M. A., Sébillaud, S., Fontana, C., Langlais, C., Micillino, J. C., Darne, C., Roszak, J., Stępnik, M. and Fessard, V. (2015) 'Genotoxicity of synthetic amorphous silica nanoparticles in rats following short-term exposure, part 2: Intratracheal instillation and intravenous injection', *Environmental and molecular mutagenesis,* 56(2), 228-244.

Gullberg, E., Leonard, M., Karlsson, J., Hopkins, A. M., Brayden, D., Baird, A. W. and Artursson, P. (2000) 'Expression of Specific Markers and Particle Transport in a

New Human Intestinal M-Cell Model', *Biochemical and Biophysical Research Communications,* 279(3), 808-813.

Gullberg, E. and Soderholm, J. D. (2006) 'Peyer's patches and M cells as potential sites of the inflammatory onset in Crohn's disease', *Ann N Y Acad Sci,* 1072, 218-32.

Halasi, M., Wang, M., Chavan, T. S., Gaponenko, V., Hay, N. and Gartel, A. L. (2013) 'ROS inhibitor N-acetyl-l-cysteine antagonizes the activity of proteasome inhibitors', *Biochem J,* 454(2), 201-208.

Halpern, M. D. and Denning, P. W. (2015) 'The role of intestinal epithelial barrier function in the development of NEC', *Tissue Barriers,* 3(1-2), e1000707.

Han, X., Gelein, R., Corson, N., Wade-Mercer, P., Jiang, J., Biswas, P., Finkelstein, J. N., Elder, A. and Oberdörster, G. (2011) 'Validation of an LDH Assay for Assessing Nanoparticle Toxicity', *Toxicology,* 287(0), 99-104.

Hansson, G. C. (2012) 'Role of mucus layers in gut infection and inflammation', *Current opinion in microbiology,* 15(1), 57-62.

Haq, F., Mahoney, M. and Koropatnick, J. (2003) 'Signaling events for metallothionein induction', *Mutation Research/Fundamental and Molecular Mechanisms of Mutagenesis,* 533(1), 211-226.

Hauri, J. F. and Niece, B. K. (2011) 'Leaching of Silver from Silver-Impregnated Food Storage Containers', *Journal of Chemical Education,* 88(10), 1407-1409.

Hayles, J., Johnson, L., Worthley, C. and Losic, D. (2017) '5 - Nanopesticides: a review of current research and perspectives A2 - Grumezescu, Alexandru Mihai' in *New Pesticides and Soil Sensors,* Academic Press, 193-225.

Helander, H. F. and Fändriks, L. (2014) 'Surface area of the digestive tract – revisited', *Scandinavian Journal of Gastroenterology,* 49(6), 681-689.

Hilgendorf, C., Spahn-Langguth, H., Regårdh, C. G., Lipka, E., Amidon, G. L. and Langguth, P. (2000) 'Caco-2 versus Caco-2/HT29-MTX Co-cultured Cell Lines: Permeabilities Via Diffusion, Inside- and Outside-Directed Carrier-Mediated Transport', *Journal of Pharmaceutical Sciences,* 89(1), 63-75.

Hoet, P. H., Brüske-Hohlfeld, I. and Salata, O. V. (2004) 'Nanoparticles – known and unknown health risks', *J Nanobiotechnology,* 2(1), 1-15.

Hoffmann, E., Dittrich-Breiholz, O., Holtmann, H. and Kracht, M. (2002) 'Multiple control of interleukin-8 gene expression', *Journal of Leukocyte Biology,* 72(5), 847-855.

Hofmann, T., Schneider, S., Wolterbeek, A., van de Sandt, H., Landsiedel, R. and van Ravenzwaay, B. (2015) 'Prenatal toxicity of synthetic amorphous silica nanomaterial in rats', *Reproductive Toxicology,* 56, 141-146.

Horobin, R. W. (2011) 'How Romanowsky stains work and why they remain valuable — including a proposed universal Romanowsky staining mechanism and a rational troubleshooting scheme', *Biotechnic & Histochemistry,* 86(1), 36-51.

Hörter, D. and Dressman, J. B. (2001) 'Influence of physicochemical properties on dissolution of drugs in the gastrointestinal tract1', *Advanced Drug Delivery Reviews,* 46(1–3), 75-87.

House of the Lords (2009) *Nanotechnologies and Food*, 1, The Stationery Office Limited, London.

Hsiao, I. L., Hsieh, Y.-K., Wang, C.-F., Chen, I. C. and Huang, Y.-J. (2015) 'Trojan-Horse Mechanism in the Cellular Uptake of Silver Nanoparticles Verified by Direct Intra- and Extracellular Silver Speciation Analysis', *Environmental Science & Technology,* 49(6), 3813-3821.

Huang, Y.-W., Wu, C.-h. and Aronstam, R. S. (2010) 'Toxicity of Transition Metal Oxide Nanoparticles: Recent Insights from *in vitro* Studies', *Materials,* 3(10), 4842-4859.

Hubatsch, I., Ragnarsson, E. G. E. and Artursson, P. (2007) 'Determination of drug permeability and prediction of drug absorption in Caco-2 monolayers', *Nat. Protocols,* 2(9), 2111-2119.

Huo, T., Dong, F., Wang, M., Sun, S., Deng, J., Zhang, Q. and Yu, S. (2015) 'Cytotoxicity of Quartz and Montmorillonite in Human Lung Epithelial Cells (A549)' in Dong, F., ed. *Proceedings of the 11th International Congress for Applied Mineralogy (ICAM)*, Cham: Springer International Publishing, 159-171.

Hussain, S. M., Hess, K. L., Gearhart, J. M., Geiss, K. T. and Schlager, J. J. (2005) '*In vitro* toxicity of nanoparticles in BRL 3A rat liver cells', *Toxicol In Vitro,* 19(7), 975-83.

Ivask, A., George, S., Bondarenko, O. and Kahru, A. (2012) 'Metal-Containing Nano-Antimicrobials: Differentiating the Impact of Solubilized Metals and Particles' in Cioffi, N. and Rai, M., eds., *Nano-Antimicrobials: Progress and Prospects*, Berlin, Heidelberg: Springer Berlin Heidelberg, 253-290.

Ivask, A., Juganson, K., Bondarenko, O., Mortimer, M., Aruoja, V., Kasemets, K., Blinova, I., Heinlaan, M., Slaveykova, V. and Kahru, A. (2014) 'Mechanisms of toxic action of Ag, ZnO and CuO nanoparticles to selected ecotoxicological test organisms and mammalian cells *in vitro*: A comparative review', *Nanotoxicology,* 8(sup1), 57-71.

Jacobsen, N. R., Pojano, G., Wallin, H. and Jensen, K. A. (2010) 'Nanomaterial dispersion protocol for toxicological studies in ENPRA. Internal ENPRA Project Report.', *The National 885 Research Centre for the Working Environment.*

Jain, S., Suzuki, T., Seth, A., Samak, G. and Rao, R. (2011) 'Protein kinase Cζ phosphorylates occludin and promotes assembly of epithelial tight junctions', *Biochemical Journal,* 437(2), 289-299.

Jandhyala, S. M., Talukdar, R., Subramanyam, C., Vuyyuru, H., Sasikala, M. and Reddy, D. N. (2015) 'Role of the normal gut microbiota', *World Journal of Gastroenterology : WJG,* 21(29), 8787-8803.

Jepson, M. A. (2012) 'Chapter 12 - Gastrointestinal Tract A2 - Fadeel, Bengt' in Pietroiusti, A. and Shvedova, A. A., eds., *Adverse Effects of Engineered Nanomaterials*, Boston: Academic Press, 209-224.

Jepson, M. A. and Ann Clark, M. (1998) 'Studying M cells and their role in infection', *Trends in Microbiology,* 6(9), 359-365.

Jepson, M. A. and Clark, M. A. (2001) 'The role of M cells in Salmonella infection', *Microbes and Infection,* 3(14), 1183-1190.

Jepson, M. A., Mason, C. M., Simmons, N. L. and Hirst, B. H. (1995) 'Enterocytes in the follicle-associated epithelia of rabbit small intestine display distinctive lectin-binding properties', *Histochemistry and Cell Biology,* 103(2), 131-134.

Jiménez, I., Aracena, P., Letelier, M. E., Navarro, P. and Speisky, H. (2002) 'Chronic exposure of HepG2 cells to excess copper results in depletion of glutathione and induction of metallothionein', *Toxicology in Vitro,* 16(2), 167-175.

Jin, Y., Song, Y., Zhu, X., Zhou, D., Chen, C., Zhang, Z. and Huang, Y. (2012) 'Goblet cell-targeting nanoparticles for oral insulin delivery and the influence of mucus on insulin transport', *Biomaterials,* 33(5), 1573-1582.

Joanne, W., Ricker, M. and Muench, J. (2006) 'Copper Deficiency as Cause of Unexplained Hematologic and Neurologic Deficits in Patient with Prior Gastrointestinal Surgery', *J Am Board Fam Med 2006;19:191– 4.),* 19, 191-194.

Johansson, M. E. V., Larsson, J. M. H. and Hansson, G. C. (2011) 'The two mucus layers of colon are organized by the MUC2 mucin, whereas the outer layer is a legislator of host–microbial interactions', *Proceedings of the National Academy of Sciences,* 108(Supplement 1), 4659-4665.

Johansson, M. E. V., Phillipson, M., Petersson, J., Velcich, A., Holm, L. and Hansson, G. C. (2008) 'The inner of the two Muc2 mucin-dependent mucus layers in colon is devoid of bacteria', *Proceedings of the National Academy of Sciences,* 105(39), 15064-15069.

Johnston, H., Brown, D. M., Kanase, N., Euston, M., Gaiser, B. K., Robb, C. T., Dyrynda, E., Rossi, A. G., Brown, E. R. and Stone, V. (2015) 'Mechanism of neutrophil activation and toxicity elicited by engineered nanomaterials', *Toxicol In Vitro,* 29(5), 1172-84.

Johnston, H. J., Hutchison, G., Christensen, F. M., Peters, S., Hankin, S. and Stone, V. (2010) 'A review of the *in vivo* and *in vitro* toxicity of silver and gold particulates: Particle attributes and biological mechanisms responsible for the observed toxicity', *Crit Rev Toxicol,* 40(4), 328-346.

Johnston, H. J., Verdon, R., Gillies, S., Brown, D. M., Fernandes, T. F., Henry, T. B., Rossi, A. G., Tran, L., Tucker, C., Tyler, C. R. and Stone, V. (2018) 'Adoption of *in vitro* systems and zebrafish embryos as alternative models for reducing rodent use in assessments of immunological and oxidative stress responses to nanomaterials', *Crit Rev Toxicol,* 48(3), 252-271.

Jones, K., Morton, J., Smith, I., Jurkschat, K., Harding, A.-H. and Evans, G. (2015) 'Human *in vivo* and *in vitro* studies on gastrointestinal absorption of titanium dioxide nanoparticles', *Toxicol Lett,* 233(2), 95-101.

Jung, C., Hugot, J. P. and Barreau, F. (2010) 'Peyer's Patches: The Immune Sensors of the Intestine', *Int J Inflam,* 2010, 823710.

Kadiyala, I., Loo, Y., Roy, K., Rice, J. and Leong, K. W. (2010) 'Transport of chitosan–DNA nanoparticles in human intestinal M-cell model versus normal intestinal enterocytes', *European Journal of Pharmaceutical Sciences,* 39(1–3), 103-109.

Kaiser, J.-P., Roesslein, M., Diener, L. and Wick, P. (2013) 'Human Health Risk of Ingested Nanoparticles That Are Added as Multifunctional Agents to Paints: an *In Vitro* Study', *PLoS One,* 8(12), e83215.

Kalbassi, M. R., Johari, S. A., Soltani, M. and Yu, I. (2013) 'Particle Size and Agglomeration Affect the Toxicity Levels of Silver Nanoparticle Types in Aquatic Environment', *ECOPERSIA,* 1(3), 273-290.

Kaler, S. G. (1998) 'Metabolic and Molecular Bases of Menkes Disease and Occipital Horn Syndrome', *Pediatric and Developmental Pathology,* 1, 85-98.

Kämpfer, A. A. M., Urbán, P., Gioria, S., Kanase, N., Stone, V. and Kinsner-Ovaskainen, A. (2017) 'Development of an *in vitro* co-culture model to mimic the human intestine in healthy and diseased state', *Toxicology in Vitro,* 45, 31-43.

Kanaya, T., Aso, H., Miyazawa, K., Kido, T., Minashima, T., Watanabe, K., Ohwada, S., Kitazawa, H., Rose, M. T. and Yamaguchi, T. (2007) 'Staining patterns for actin and villin distinguish M cells in bovine follicle-associated epithelium', *Research in Veterinary Science,* 82(2), 141-149.

Kang, T., Guan, R., Chen, X., Song, Y., Jiang, H. and Zhao, J. (2013) '*In vitro* toxicity of different-sized ZnO nanoparticles in Caco-2 cells', *Nanoscale Research Letters,* 8, 496.

Karlsson, H. L., Cronholm, P., Gustafsson, J. and Möller, L. (2008) 'Copper Oxide Nanoparticles Are Highly Toxic: A Comparison between Metal Oxide Nanoparticles and Carbon Nanotubes', *Chemical Research in Toxicology,* 21(9), 1726-1732.

Kasemets, K., Ivask, A., Dubourguier, H.-C. and Kahru, A. (2009) 'Toxicity of nanoparticles of ZnO, CuO and TiO2 to yeast Saccharomyces cerevisiae', *Toxicology in Vitro,* 23(6), 1116-1122.

Kavanaugh, D. W., O'Callaghan, J., Buttó, L. F., Slattery, H., Lane, J., Clyne, M., Kane, M., Joshi, L. and Hickey, R. M. (2013) 'Exposure of Bifidobacterium longum subsp. infantis to Milk Oligosaccharides Increases Adhesion to Epithelial Cells and Induces a Substantial Transcriptional Response', *PLoS One,* 8(6), e67224.

Kenzaoui, B. H., Vilà, M. R., Miquel, J. M., Cengelli, F. and Juillerat-Jeanneret, L. (2012) 'Evaluation of uptake and transport of cationic and anionic ultrasmall iron oxide nanoparticles by human colon cells', *Int J Nanomedicine,* 7, 1275-1286.

Kermanizadeh, A. (2012) 'Engineered Nanomaterial Impact in the Liver following Exposure via an Intravenous Route–The Role of Polymorphonuclear Leukocytes and Gene Expression in the Organ', *Journal of Nanomedicine & Nanotechnology,* 04(01).

Kermanizadeh, A., Pojana, G., Gaiser, B. K., Birkedal, R., Bilanicova, D., Wallin, H., Jensen, K. A., Sellergren, B., Hutchison, G. R., Marcomini, A. and Stone, V. (2013a) '*In vitro* assessment of engineered nanomaterials using a hepatocyte cell line: cytotoxicity, pro-inflammatory cytokines and functional markers', *Nanotoxicology,* 7(3), 301-13.

Kermanizadeh, A., Vranic, S., Boland, S., Moreau, K., Baeza-Squiban, A., Gaiser, B. K., Andrzejczuk, L. A. and Stone, V. (2013b) 'An *in vitro* assessment of panel of engineered nanomaterials using a human renal cell line: cytotoxicity, pro-inflammatory response, oxidative stress and genotoxicity', *BMC Nephrology,* 14, 96.

Kernéis, S., Bogdanova, A., Kraehenbuhl, J.-P. and Pringault, E. (1997) 'Conversion by Peyer's Patch Lymphocytes of Human Enterocytes into M Cells that Transport Bacteria', *Science,* 277(5328), 949-952.

Kim, I.-Y., Joachim, E., Choi, H. and Kim, K. (2015) 'Toxicity of silica nanoparticles depends on size, dose, and cell type', *Nanomedicine: Nanotechnology, Biology and Medicine,* 11(6), 1407-1416.

Kim, M. J., Lee, H. H., Jeong, J. W., Seo, M. J., Kang, B. W., Park, J. U., Kim, K. S., Cho, Y. S., Seo, K. I., Kim, G. Y., Kim, J. I., Choi, Y. H. and Jeong, Y. K. (2014) 'Anti-inflammatory effects of 5-hydroxy-3,6,7,8,3',4'-hexamethoxyflavone via NF-kappaB inactivation in lipopolysaccharide-stimulated RAW 264.7 macrophage', *Mol Med Rep,* 9(4), 1197-203.

Kim, Y. H., Boykin, E., Stevens, T., Lavrich, K. and Gilmour, M. I. (2014) 'Comparative lung toxicity of engineered nanomaterials utilizing *in vitro*, *ex vivo* and *in vivo* approaches', *J Nanobiotechnology,* 12(1), 47.

Kim, Y. J., Kim, E.-H. and Hahm, K. B. (2012) 'Oxidative stress in inflammation-based gastrointestinal tract diseases: Challenges and opportunities', *Journal of Gastroenterology and Hepatology,* 27(6), 1004-1010.

Kim, Y. S. and Ho, S. B. (2010) 'Intestinal Goblet Cells and Mucins in Health and Disease: Recent Insights and Progress', *Current Gastroenterology Reports,* 12(5), 319-330.

Kirch, J., Guenther, M., Doshi, N., Schaefer, U. F., Schneider, M., Mitragotri, S. and Lehr, C.-M. (2012) 'Mucociliary clearance of micro- and nanoparticles is independent of size, shape and charge—an *ex vivo* and *in silico* approach', *Journal of Controlled Release,* 159(1), 128-134.

Kleczkowski, M., Kluciński, W., Sikora, J., Kasztelan, R. and Zdanowicz, M. (2002) 'Role of transition metals ion and reactive oxygen species in biological oxidation in cattle (part 1)', *Polish journal of veterinary sciences,* 5(4), 263-268.

Koeneman, B. A., Zhang, Y., Westerhoff, P., Chen, Y., Crittenden, J. C. and Capco, D. G. (2010) 'Toxicity and cellular responses of intestinal cells exposed to titanium dioxide', *Cell Biol Toxicol,* 26(3), 225-238.

König, J., Wells, J., Cani, P. D., García-Ródenas, C. L., MacDonald, T., Mercenier, A., Whyte, J., Troost, F. and Brummer, R.-J. (2016) 'Human Intestinal Barrier Function in Health and Disease', *Clinical And Translational Gastroenterology,* 7, e196.

Kovvuru, P., Mancilla, P. E., Shirode, A. B., Murray, T. M., Begley, T. J. and Reliene, R. (2015) 'Oral ingestion of silver nanoparticles induces genomic instability and DNA damage in multiple tissues', *Nanotoxicology,* 9(2), 162-171.

Kreyling, W. G., Holzwarth, U., Schleh, C., Kozempel, J., Wenk, A., Haberl, N., Hirn, S., Schäffler, M., Lipka, J., Semmler-Behnke, M. and Gibson, N. (2017) 'Quantitative biokinetics of titanium dioxide nanoparticles after oral application in rats: Part 2', *Nanotoxicology,* 11(4), 443-453.

Kroll, A., Pillukat, M. H., Hahn, D. and Schnekenburger, J. (2012) 'Interference of engineered nanoparticles with *in vitro* toxicity assays', *Arch Toxicol,* 86(7), 1123-1136.

Kucharzik, T., LÜGering, N., Rautenberg, K., LÜGering, A., Schmidt, M. A., Stoll, R. and Domschke, W. (2000) 'Role of M Cells in Intestinal Barrier Function', *Ann N Y Acad Sci,* 915(1), 171-183.

Kuhn, D. A., Vanhecke, D., Michen, B., Blank, F., Gehr, P., Petri-Fink, A. and Rothen-Rutishauser, B. (2014) 'Different endocytotic uptake mechanisms for nanoparticles in epithelial cells and macrophages', *Beilstein Journal of Nanotechnology,* 5, 1625.

Kumar, K. K. V., Karnati, S., Reddy, M. B. and Chandramouli, R. (2010) 'Caco-2 cell lines in drug discovery- An updated perspective', *Journal of Basic and Clinical Pharmacy*, 1(2), 63-69.

Kumari, Y. P., Chandra, J. S., Rao, B. S. and Sunandamma, Y. (2012) 'Synthesis, characterization and antibacterial activity of Alloxanthiosemicarbazone Au (III) complexes', *Journal of Current Pharmaceutical Research,* 10(1), 28-33.

Kundu, J., Chae, I. G. and Chun, K.-S. (2016) 'Fraxetin Induces Heme Oxygenase-1 Expression by Activation of Akt/Nrf2 or AMP-activated Protein Kinase α/Nrf2 Pathway in HaCaT Cells', *Journal of Cancer Prevention,* 21(3), 135-143.

Kung, M.-L., Hsieh, S.-L., Wu, C.-C., Chu, T.-H., Lin, Y.-C., Yeh, B.-W. and Hsieh, S. (2015) 'Enhanced reactive oxygen species overexpression by CuO nanoparticles in poorly differentiated hepatocellular carcinoma cells', *Nanoscale,* 7(5), 1820-1829.

La Fontaine, S. and Mercer, J. F. B. (2007) 'Trafficking of the copper-ATPases, ATP7A and ATP7B: Role in copper homeostasis', *Archives of Biochemistry and Biophysics*, 463(2), 149-167.

Lai, S. K., Wang, Y.-Y. and Hanes, J. (2009) 'Mucus-penetrating nanoparticles for drug and gene delivery to mucosal tissues', *Advanced Drug Delivery Reviews,* 61(2), 158-171.

Lai, X., Blazer-Yost, B. L., Clack, J. W., Fears, S. L., Mitra, S., Ntim, S. A., Ringham, H. N. and Witzmann, F. A. (2013) 'Protein expression profiles of intestinal epithelial co-cultures: effect of functionalised carbon nanotube exposure', *Int J Biomed Nanosci Nanotechnol,* 3(1-2), 10.1504/IJBNN.2013.054508.

Lai, X., Zhao, H., Zhang, Y., Guo, K., Xu, Y., Chen, S. and Zhang, J. (2018) 'Intranasal Delivery of Copper Oxide Nanoparticles Induces Pulmonary Toxicity and Fibrosis in C57BL/6 mice', *Scientific Reports,* 8(1), 4499.

Landy, J., Ronde, E., English, N., Clark, S. K., Hart, A. L., Knight, S. C., Ciclitira, P. J. and Al-Hassi, H. O. (2016) 'Tight junctions in inflammatory bowel diseases and inflammatory bowel disease associated colorectal cancer', *World J Gastroenterol,* 22(11), 3117-3126.

Lara, H. H., Ayala-Núñez, N. V., Ixtepan Turrent, L. d. C. and Rodríguez Padilla, C. (2010) 'Bactericidal effect of silver nanoparticles against multidrug-resistant bacteria', *World Journal of Microbiology and Biotechnology*, 26(4), 615-621.

Lawson, F. W. and Wendell, R. M. (1995) 'Animal litter containing a water-swellable clay, carboxymethylcellulose, and siliceous coated bicarbonate particles',

LeBlanc, J. G., Milani, C., de Giori, G. S., Sesma, F., van Sinderen, D. and Ventura, M. (2013) 'Bacteria as vitamin suppliers to their host: a gut microbiota perspective', *Current Opinion in Biotechnology,* 24(2), 160-168.

Lee, C.-M., Jeong, H.-J., Yun, K.-N., Kim, D. W., Sohn, M.-H., Lee, J. K., Jeong, J. and Lim, S. T. (2012) 'Optical imaging to trace near infrared fluorescent zinc oxide nanoparticles following oral exposure', *Int J Nanomedicine,* 7, 3203-3209.

Lee, I.-C., Ko, J.-W., Park, S.-H., Shin, N.-R., Shin, I.-S., Moon, C., Kim, J.-H., Kim, H.-C. and Kim, J.-C. (2016) 'Comparative toxicity and biodistribution assessments in rats following subchronic oral exposure to copper nanoparticles and microparticles', *Part Fibre Toxicol,* 13, 56.

Lee, S. H. (2015) 'Intestinal permeability regulation by tight junction: implication on inflammatory bowel diseases', *Intest Res,* 13(1), 11-8.

Lefebvre, D. E., Venema, K., Gombau, L., Valerio, L. G., Jr., Raju, J., Bondy, G. S., Bouwmeester, H., Singh, R. P., Clippinger, A. J., Collnot, E. M., Mehta, R. and Stone, V. (2015) 'Utility of models of the gastrointestinal tract for assessment of the digestion and absorption of engineered nanomaterials released from food matrices', *Nanotoxicology,* 9(4), 523-42.

Lefei, J., Chun Chun, W., Huan, W., Rong, G., Fang Hui, L., Jie, F. and Caihong, H. (2017) 'Copper/zinc-loaded montmorillonite influences intestinal integrity, the expression of genes associated with inflammation, TLR4–MyD88 and TGF-β1 signaling pathways in weaned pigs after LPS challenge', *Innate Immunity,* 23(8), 648-655.

Lesuffleur, T., Porchet, N., Aubert, J. P., Swallow, D., Gum, J. R., Kim, Y. S., Real, F. X. and Zweibaum, A. (1993) 'Differential expression of the human mucin genes MUC1 to MUC5 in relation to growth and differentiation of different mucus-secreting HT-29 cell subpopulations', *Journal of Cell Science,* 106(3), 771.

Letelier, M. E., Lepe, A. M., Faúndez, M., Salazar, J., Marín, R., Aracena, P. and Speisky, H. (2005) 'Possible mechanisms underlying copper-induced damage in biological membranes leading to cellular toxicity', *Chemico-Biological Interactions,* 151(2), 71-82.

Li, J., Volpe, D. A., Wang, Y., Zhang, W., Bode, C., Owen, A. and Hidalgo, I. J. (2011) 'Use of transporter knockdown Caco-2 cells to investigate the *in vitro* efflux of statin drugs', *Drug Metabolism and Disposition,* 39(7), 1196-1202.

Li, Y. and Monteiro-Riviere, N. A. (2016) 'Mechanisms of cell uptake, inflammatory potential and protein corona effects with gold nanoparticles', *Nanomedicine,* 11(24), 3185-3203.

Lim, C.-H., Kang, M., Han, J.-H. and Yang, J.-S. (2012) 'Effect of Agglomeration on the Toxicity of Nano-sized Carbon Black in Sprague-Dawley Rats', *Environmental Health and Toxicology,* 27, e2012015.

Lin, Z., Karthik, P. S., Hada, M., Nishikawa, T. and Hayashi, Y. (2017) 'Simple Technique of Exfoliation and Dispersion of Multilayer Graphene from Natural Graphite by Ozone-Assisted Sonication', *Nanomaterials,* 7(6), 125.

Liu, M., Zhang, J., Shan, W. and Huang, Y. (2015) 'Developments of mucus penetrating nanoparticles', *Asian Journal of Pharmaceutical Sciences,* 10(4), 275-282.

Liu, S., Kawai, K., Tyurin, V. A., Tyurina, Y. Y., Borisenko, G. G., Fabisiak, J. P., Quinn, P. J., Pitt, B. R. and Kagan, V. E. (2001) 'Nitric oxide-dependent pro-oxidant and pro-apoptotic effect of metallothioneins in HL-60 cells challenged with cupric nitrilotriacetate', *Biochemical Journal,* 354(Pt 2), 397-406.

Liu, X., Zheng, S., Qin, Y., Ding, W., Tu, Y., Chen, X., Wu, Y., Yanhua, L. and Cai, X. (2017) 'Experimental Evaluation of the Transport Mechanisms of PoIFN-α in Caco-2 Cells', *Frontiers in Pharmacology*, 8, 781, available: [accessed 2017].

Lo, D., Tynan, W., Dickerson, J., Scharf, M., Cooper, J., Byrne, D., Brayden, D., Higgins, L., Evans, C. and O'Mahony, D. J. (2004) 'Cell culture modeling of specialized tissue: identification of genes expressed specifically by follicle-associated epithelium of Peyer's patch by expression profiling of Caco-2/Raji co-cultures', *International Immunology,* 16(1), 91-99.

Loboda, A., Damulewicz, M., Pyza, E., Jozkowicz, A. and Dulak, J. (2016) 'Role of Nrf2/HO-1 system in development, oxidative stress response and diseases: an evolutionarily conserved mechanism', *Cellular and Molecular Life Sciences,* 73, 3221-3247.

Long, T. C., Saleh, N., Tilton, R. D., Lowry, G. V. and Veronesi, B. (2006) 'Titanium Dioxide (P25) Produces Reactive Oxygen Species in Immortalized Brain Microglia (BV2): Implications for Nanoparticle Neurotoxicity', *Environmental Science & Technology,* 40(14), 4346-4352.

Lozoya-Agullo, I., Araújo, F., González-Álvarez, I., Merino-Sanjuán, M., González-Álvarez, M., Bermejo, M. and Sarmento, B. (2017) 'Usefulness of Caco-2/HT29-MTX and Caco-2/HT29-MTX/Raji B Coculture Models To Predict Intestinal and Colonic Permeability Compared to Caco-2 Monoculture', *Mol Pharm,* 14(4), 1264-1270.

Lubelska, K., Misiewicz-Krzemińska, I., Milczarek, M., Krzysztoń-Russjan, J., Anuszewska, E., Modzelewska, K. and Wiktorska, K. (2012) 'Isothiocyanate–drug interactions in the human adenocarcinoma cell line Caco-2', *Molecular and Cellular Biochemistry,* 367(1), 19-29.

Lundquist, P. and Artursson, P. (2016) 'Oral absorption of peptides and nanoparticles across the human intestine: Opportunities, limitations and studies in human tissues', *Advanced Drug Delivery Reviews,* 106, 256-276.

Luther, E. M., Schmidt, M. M., Diendorf, J., Epple, M. and Dringen, R. (2012) 'Upregulation of metallothioneins after exposure of cultured primary astrocytes to silver nanoparticles', *Neurochem Res,* 37(8), 1639-48.

Lutsenko, S. (2010) 'Human copper homeostasis: a network of interconnected pathways', *Current Opinion in Chemical Biology,* 14(2), 211-217.

Lutsenko, S., Barnes, N. L., Bartee, M. Y. and Dmitriev, O. Y. (2007) 'Function and regulation of human copper-transporting ATPases', *Physiol Rev,* 87(3), 1011-46.

Ma, H., Williams, P. L. and Diamond, S. A. (2013) 'Ecotoxicity of manufactured ZnO nanoparticles – A review', *Environmental Pollution,* 172, 76-85.

Ma, T., Wang, L., Yang, T., Ma, G. and Wang, S. (2014) 'M-cell targeted polymeric lipid nanoparticles containing a Toll-like receptor agonist to boost oral immunity', *Int J Pharm,* 473(1-2), 296-303.

Ma, T. Y., Anderson, J. M. and Turner, J. R. (2012) 'Chapter 38 - Tight Junctions and the Intestinal Barrier A2 - Johnson, Leonard R' in Ghishan, F. K., Kaunitz, J. D., Merchant, J. L., Said, H. M. and Wood, J. D., eds., *Physiology of the Gastrointestinal Tract (Fifth Edition)*, Boston: Academic Press, 1043-1088.

Madara, J. L. (2011) 'Functional morphology of epithelium of the small intestine', *Comprehensive Physiology*.

Mahe, M. M., Sundaram, N., Watson, C. L., Shroyer, N. F. and Helmrath, M. A. (2015) 'Establishment of Human Epithelial Enteroids and Colonoids from Whole Tissue and Biopsy', *J Vis Exp*, (97), 52483.

Mahler, G. J., Shuler, M. L. and Glahn, R. P. (2009) 'Characterization of Caco-2 and HT29-MTX cocultures in an *in vitro* digestion/cell culture model used to predict iron bioavailability', *The Journal of Nutritional Biochemistry*, 20(7), 494-502.

Mailänder, V. and Landfester, K. (2009) 'Interaction of Nanoparticles with Cells', *Biomacromolecules*, 10(9), 2379-2400.

Maisanaba, S., Gutiérrez-Praena, D., Pichardo, S., Moreno, F. J., Jordá, M., Cameán, A. M., Aucejo, S. and Jos, Á. (2014) 'Toxic effects of a modified montmorillonite clay on the human intestinal cell line Caco-2', *Journal of Applied Toxicology*, 34(6), 714-725.

Maisanaba, S., Prieto, A. I., Pichardo, S., Jordá-Beneyto, M., Aucejo, S. and Jos, Á. (2015) 'Cytotoxicity and mutagenicity assessment of organomodified clays potentially used in food packaging', *Toxicology in Vitro*, 29(6), 1222-1230.

Majeed, K., Jawaid, M., Hassan, A., Abu Bakar, A., Abdul Khalil, H. P. S., Salema, A. A. and Inuwa, I. (2013) 'Potential materials for food packaging from nanoclay/natural fibres filled hybrid composites', *Materials & Design*, 46, 391-410.

Mallakpour, S. and Dinari, M. (2011) 'Preparation and characterization of new organoclays using natural amino acids and Cloisite Na+', *Applied Clay Science*, 51(3), 353-359.

Malysheva, A., Ivask, A., Hager, C., Brunetti, G., Marzouk, E. R., Lombi, E. and Voelcker, N. H. (2016) 'Sorption of silver nanoparticles to laboratory plastic during (eco)toxicological testing', *Nanotoxicology*, 10(4), 385-390.

Manabe, M., Kanzato, H. and Shimizu, M. (2002) 'An *In Vitro* Approach to the Evaluation of the Cross Talk Between Intestinal Epithelium and Macrophages' in *Animal Cell Technology: Basic & Applied Aspects*, Springer, 479-483.

Manke, A., Wang, L. and Rojanasakul, Y. (2013) 'Mechanisms of Nanoparticle-Induced Oxidative Stress and Toxicity', *BioMed Research International*, 2013, 15.

Marano, F., Hussain, S., Rodrigues-Lima, F., Baeza-Squiban, A. and Boland, S. (2011) 'Nanoparticles: molecular targets and cell signalling', *Arch Toxicol*, 85(7), 733-741.

Margoshes, M. and Vallee, B. L. (1957) 'A Cadmium Protein from Equine Kidney Cortex.', *Journal of the American Chemical Society*, 79(17), 4813-4814.

Marks, J. (1957) 'The neutralization of silica toxicity *in vitro*', *British journal of industrial medicine*, 14(2), 81.

Martin, T. R., Ayars, G., Butler, J. and Altman, L. C. (1984) 'The comparative toxicity of volcanic ash and quartz: effects on cells derived from the human lung', *American Review of Respiratory Disease,* 130(5), 778-782.

Martinez-Argudo, I. and Jepson, M. A. (2008) 'Salmonella translocates across an *in vitro* M cell model independently of SPI-1 and SPI-2', *Microbiology,* 154(12), 3887-3894.

Martínez-Maqueda, D., Miralles, B. and Recio, I. (2015) 'HT29 Cell Line' in Verhoeckx, K., Cotter, P., López-Expósito, I., Kleiveland, C., Lea, T., Mackie, A., Requena, T., Swiatecka, D. and Wichers, H., eds., *The Impact of Food Bioactives on Health: in vitro and ex vivo models*, Cham: Springer International Publishing, 113-124.

Martirosyan, A., Polet, M., Bazes, A., Sergent, T. and Schneider, Y.-J. (2012) 'Food Nanoparticles and Intestinal Inflammation: A Real Risk?'.

Martirosyan, A. and Schneider, Y. J. (2014) 'Engineered nanomaterials in food: implications for food safety and consumer health', *Int J Environ Res Public Health,* 11(6), 5720-50.

McCracken, C., Dutta, P. K. and Waldman, W. J. (2016) 'Critical assessment of toxicological effects of ingested nanoparticles', *Environmental Science: Nano,* 3(2), 256-282.

McCracken, C., Zane, A., Knight, D. A., Dutta, P. K. and Waldman, W. J. (2013) 'Minimal Intestinal Epithelial Cell Toxicity in Response to Short- and Long-Term Food-Relevant Inorganic Nanoparticle Exposure', *Chemical Research in Toxicology,* 26(10), 1514-1525.

McShan, D., Ray, P. C. and Yu, H. (2014) 'Molecular Toxicity Mechanism of Nanosilver', *Journal of Food and Drug Analysis,* 22(1), 116-127.

Merrifield, D. L., Shaw, B. J., Harper, G. M., Saoud, I. P., Davies, S. J., Handy, R. D. and Henry, T. B. (2013) 'Ingestion of metal-nanoparticle contaminated food disrupts endogenous microbiota in zebrafish (Danio rerio)', *Environmental Pollution,* 174, 157-163.

Misra, S. K., Nuseibeh, S., Dybowska, A., Berhanu, D., Tetley, T. D. and Valsami-Jones, E. (2014) 'Comparative study using spheres, rods and spindle-shaped nanoplatelets on dispersion stability, dissolution and toxicity of CuO nanomaterials', *Nanotoxicology,* 8(4), 422-432.

Miura, N. and Shinohara, Y. (2009) 'Cytotoxic effect and apoptosis induction by silver nanoparticles in HeLa cells', *Biochemical and Biophysical Research Communications,* 390(3), 733-737.

Miyayama, T. and Matsuoka, M. (2016) 'Involvement of lysosomal dysfunction in silver nanoparticle-induced cellular damage in A549 human lung alveolar epithelial cells', *Journal of Occupational Medicine and Toxicology (London, England),* 11, 1.

Molloy, S. A. and Kaplan, J. H. (2009) 'Copper-dependent Recycling of hCTR1, the Human High Affinity Copper Transporter', *The Journal of Biological Chemistry,* 284(43), 29704-29713.

Morowitz, M. J., Carlisle, E. and Alverdy, J. C. (2011) 'Contributions of Intestinal Bacteria to Nutrition and Metabolism in the Critically Ill', *The Surgical clinics of North America,* 91(4), 771-785.

Muñoz , C., López, M., Olivares, M., Pizarro, F., Arredondo, M. and Araya, M. (2005) 'Differential response of interleukin-2 production to chronic copper supplementation in healthy humans', *Eur. Cytokine Netw,* 16(4), 261-265.

Mura, S., Hillaireau, H., Nicolas, J., Le Droumaguet, B., Gueutin, C., Zanna, S., Tsapis, N. and Fattal, E. (2011) 'Influence of surface charge on the potential toxicity of PLGA nanoparticles towards Calu-3 cells', *Int J Nanomedicine,* 6, 2591-2605.

Murphy, B. J., Andrews, G. K., Bittel, D., Discher, D. J., McCue, J., Green, C. J., Yanovsky, M., Giaccia, A., Sutherland, R. M., Laderoute, K. R. and Webster, K. A. (1999) 'Activation of Metallothionein Gene Expression by Hypoxia Involves Metal Response Elements and Metal Transcription Factor-1', *Cancer Res,* 59(6), 1315.

Naika, H. R., Lingaraju, K., Manjunath, K., Kumar, D., Nagaraju, G., Suresh, D. and Nagabhushana, H. (2015) 'Green synthesis of CuO nanoparticles using Gloriosa superba L. extract and their antibacterial activity', *Journal of Taibah University for Science,* 9(1), 7-12.

Napierska, D., Thomassen, L. C., Lison, D., Martens, J. A. and Hoet, P. H. (2010) 'The nanosilica hazard: another variable entity', *Part Fibre Toxicol,* 7(1), 39.

Naresh, R., Song, Y. and Hampson, D. J. (2009) 'The intestinal spirochete Brachyspira pilosicoli attaches to cultured Caco-2 cells and induces pathological changes', *PLoS One,* 4(12), e8352.

Natoli, M., Leoni, B. D., D'Agnano, I., D'Onofrio, M., Brandi, R., Arisi, I., Zucco, F. and Felsani, A. (2011) 'Cell growing density affects the structural and functional properties of Caco-2 differentiated monolayer', *J Cell Physiol,* 226(6), 1531-43.

Navabi, N., McGuckin, M. A. and Linden, S. K. (2013) 'Gastrointestinal cell lines form polarized epithelia with an adherent mucus layer when cultured in semi-wet interfaces with mechanical stimulation', *PLoS One,* 8(7), e68761.

Nel, A., Xia, T., Mädler, L. and Li, N. (2006) 'Toxic Potential of Materials at the Nanolevel', *Science,* 311(5761), 622-627.

Neutra, M. R., Mantis, N. J. and Kraehenbuhl, J.-P. (2001) 'Collaboration of epithelial cells with organized mucosal lymphoid tissues', *Nature Immunology,* 2, 1004.

Nichols, G., Byard, S., Bloxham, M. J., Botterill, J., Dawson, N. J., Dennis, A., Diart, V., North, N. C. and Sherwood, J. D. (2002) 'A review of the terms agglomerate and aggregate with a recommendation for nomenclature used in powder and particle characterization', *Journal of Pharmaceutical Sciences,* 91(10), 2103-2109.

Nishitani, Y., Zhang, L., Yoshida, M., Azuma, T., Kanazawa, K., Hashimoto, T. and Mizuno, M. (2013) 'Intestinal anti-inflammatory activity of lentinan: influence on IL-8 and TNFR1 expression in intestinal epithelial cells', *PLoS One,* 8(4), e62441.

Nose, Y., Kim, B.-E. and Thiele, D. J. (2006) 'Ctr1 drives intestinal copper absorption and is essential for growth, iron metabolism, and neonatal cardiac function', *Cell Metabolism,* 4(3), 235-244.

O'Flaherty, S. and Klaenhammer, T. R. (2012) 'Influence of exposure time on gene expression by human intestinal epithelial cells exposed to Lactobacillus acidophilus', *Applied and Environmental Microbiology*, 78(14), 5028-5032.

Oberdörster, G., Maynard, A., Donaldson, K., Castranova, V., Fitzpatrick, J., Ausman, K., Carter, J., Karn, B., Kreyling, W., Lai, D., Olin, S., Monteiro-Riviere, N., Warheit, D. and Yang, H. (2005) 'Principles for characterizing the potential human health effects from exposure to nanomaterials: elements of a screening strategy', *Part Fibre Toxicol*, 2(1), 1-35.

Ock, C. Y., Kim, E. H., Choi, D. J., Lee, H. J., Hahm, K. B. and Chung, M. H. (2012) '8-Hydroxydeoxyguanosine: not mere biomarker for oxidative stress, but remedy for oxidative stress-implicated gastrointestinal diseases', *World J Gastroenterol*, 18(4), 302-8.

Ogra, Y., Tejima, A., Hatakeyama, N., Shiraiwa, M., Wu, S., Ishikawa, T., Yawata, A., Anan, Y. and Suzuki, N. (2016) 'Changes in intracellular copper concentration and copper-regulating gene expression after PC12 differentiation into neurons', *Scientific Reports*, 6, 33007.

Okita, Y., Rcom-H'cheo-Gauthier, A. N., Goulding, M., Chung, R. S., Faller, P. and Pountney, D. L. (2017) 'Metallothionein, Copper and Alpha-Synuclein in Alpha-Synucleinopathies', *Frontiers in Neuroscience*, 11(114).

Ong, K. J., MacCormack, T. J., Clark, R. J., Ede, J. D., Ortega, V. A., Felix, L. C., Dang, M. K. M., Ma, G., Fenniri, H., Veinot, J. G. C. and Goss, G. G. (2014) 'Widespread Nanoparticle-Assay Interference: Implications for Nanotoxicity Testing', *PLoS One*, 9(3), e90650.

Ong, S. L., Gravante, G., Metcalfe, M. S. and Dennison, A. R. (2013) 'History, ethics, advantages and limitations of experimental models for hepatic ablation', *World Journal of Gastroenterology : WJG*, 19(2), 147-154.

Onodera, A., Nishiumi, F., Kakiguchi, K., Tanaka, A., Tanabe, N., Honma, A., Yayama, K., Yoshioka, Y., Nakahira, K., Yonemura, S., Yanagihara, I., Tsutsumi, Y. and Kawai, Y. (2015) 'Short-term changes in intracellular ROS localisation after the silver nanoparticles exposure depending on particle size', *Toxicology Reports*, 2, 574-579.

Oomen, A. G., Hack, A., Minekus, M., Zeijdner, E., Cornelis, C., Schoeters, G., Verstraete, W., Van de Wiele, T., Wragg, J., Rompelberg, C. J. M., Sips, A. J. A. M. and Van Wijnen, J. H. (2002) 'Comparison of Five *In Vitro* Digestion Models To Study the Bioaccessibility of Soil Contaminants', *Environmental Science & Technology*, 36(15), 3326-3334.

Oomen, A. G., Rompelberg, C. J., Bruil, M. A., Dobbe, C. J., Pereboom, D. P. and Sips, A. J. (2003) 'Development of an *in vitro* digestion model for estimating the bioaccessibility of soil contaminants', *Arch Environ Contam Toxicol*, 44(3), 281-7.

Ortega, R., Bresson, C., Darolles, C., Gautier, C., Roudeau, S., Perrin, L., Janin, M., Floriani, M., Aloin, V., Carmona, A. and Malard, V. (2014) 'Low-solubility particles and a Trojan-horse type mechanism of toxicity: the case of cobalt oxide on human lung cells', *Part Fibre Toxicol*, 11(1), 14.

Pan, F., Han, L., Zhang, Y., Yu, Y. and Liu, J. (2015) 'Optimization of Caco-2 and HT29 co-culture *in vitro* cell models for permeability studies', *International Journal of Food Sciences and Nutrition,* 66(6), 680-685.

Pang, W., Lan, X.-m. and Wang, C.-b. (2012) 'Effect of puerarin on the release of interleukin-8 in co-culture of human bronchial epithelial cells and neutrophils', *Chinese Journal of Integrative Medicine,* 18(4), 283-287.

Papoulis, D. (2011) 'Clay-based Nanocomposites Possibilities and Limitations', *AIP Conference Proceedings,* 1389(1), 1450-1453.

Park, E.-J., Yi, J., Kim, Y., Choi, K. and Park, K. (2010) 'Silver nanoparticles induce cytotoxicity by a Trojan-horse type mechanism', *Toxicology in Vitro,* 24(3), 872-878.

Park, J.-W., Lee, I.-C., Shin, N.-R., Jeon, C.-M., Kwon, O.-K., Ko, J.-W., Kim, J.-C., Oh, S.-R., Shin, I.-S. and Ahn, K.-S. (2016) 'Copper oxide nanoparticles aggravate airway inflammation and mucus production in asthmatic mice via MAPK signaling', *Nanotoxicology,* 10(4), 445-452.

Park, K., Park, E. J., Chun, I. K., Choi, K., Lee, S. H., Yoon, J. and Lee, B. C. (2011) 'Bioavailability and toxicokinetics of citrate-coated silver nanoparticles in rats', *Arch Pharm Res,* 34(1), 153-8.

Pasqua, L., Cundari, S., Ceresa, C. and Cavaletti, G. (2009) 'Recent Development, Applications, and Perspectives of Mesoporous Silica Particles in Medicine and Biotechnology', *Current Medicinal Chemistry,* 16(23), 3054-3063.

Patel, H. A., Somani, R. S., Bajaj, H. C. and Jasra, R. V. (2006) 'Nanoclays for polymer nanocomposites, paints, inks, greases and cosmetics formulations, drug delivery vehicle and waste water treatment', *Bulletin of Materials Science,* 29(2), 133-145.

Peckys, D. B. and de Jonge, N. (2011) 'Visualizing Gold Nanoparticle Uptake in Live Cells with Liquid Scanning Transmission Electron Microscopy', *Nano Letters,* 11(4), 1733-1738.

Peixe, T. S., Souza Nascimento, E. d., Schofield, K. L., Arcuri, A. S. A. and Bulcão, R. P. (2015) 'Nanotoxicology and Exposure in the Occupational Setting', *Occupational Diseases and Environmental Medicine,* 03(03), 35-48.

Pelaseyed, T., Bergström, J. H., Gustafsson, J. K., Ermund, A., Birchenough, G. M. H., Schütte, A., van der Post, S., Svensson, F., Rodríguez-Piñeiro, A. M., Nyström, E. E. L., Wising, C., Johansson, M. E. V. and Hansson, G. C. (2014) 'The mucus and mucins of the goblet cells and enterocytes provide the first defense line of the gastrointestinal tract and interact with the immune system', *Immunological reviews,* 260(1), 8-20.

Pele, L. C., Thoree, V., Bruggraber, S. F. A., Koller, D., Thompson, R. P. H., Lomer, M. C. and Powell, J. J. (2015) 'Pharmaceutical/food grade titanium dioxide particles are absorbed into the bloodstream of human volunteers', *Part Fibre Toxicol,* 12, 26.

Piana, C., Wirth, M., Gerbes, S., Viernstein, H., Gabor, F. and Toegel, S. (2008) 'Validation of reference genes for qPCR studies on Caco-2 cell differentiation', *European Journal of Pharmaceutics and Biopharmaceutics,* 69(3), 1187-1192.

Pietroiusti, A., Magrini, A. and Campagnolo, L. (2016) 'New frontiers in nanotoxicology: Gut microbiota/microbiome-mediated effects of engineered nanomaterials', *Toxicology and Applied Pharmacology,* 299, 90-95.

Pietroiusti, A., Massimiani, M., Fenoglio, I., Colonna, M., Valentini, F., Palleschi, G., Camaioni, A., Magrini, A., Siracusa, G., Bergamaschi, A., Sgambato, A. and Campagnolo, L. (2011) 'Low Doses of Pristine and Oxidized Single-Wall Carbon Nanotubes Affect Mammalian Embryonic Development', *ACS Nano,* 5(6), 4624-4633.

Piret, J. P., Jacques, D., Audinot, J. N., Mejia, J., Boilan, E., Noel, F., Fransolet, M., Demazy, C., Lucas, S., Saout, C. and Toussaint, O. (2012a) 'Copper(II) oxide nanoparticles penetrate into HepG2 cells, exert cytotoxicity via oxidative stress and induce pro-inflammatory response', *Nanoscale,* 4(22), 7168-84.

Piret, J. P., Vankoningsloo, S., Mejia, J., Noel, F., Boilan, E., Lambinon, F., Zouboulis, C. C., Masereel, B., Lucas, S., Saout, C. and Toussaint, O. (2012b) 'Differential toxicity of copper (II) oxide nanoparticles of similar hydrodynamic diameter on human differentiated intestinal Caco-2 cell monolayers is correlated in part to copper release and shape', *Nanotoxicology,* 6(7), 789-803.

Powell, J. J., Ainley, C. C., Harvey, R. S., Mason, I. M., Kendall, M. D., Sankey, E. A., Dhillon, A. P. and Thompson, R. P. (1996) 'Characterisation of inorganic microparticles in pigment cells of human gut associated lymphoid tissue', *Gut,* 38.

Powell, J. J., Faria, N., Thomas-McKay, E. and Pele, L. C. (2010) 'Origin and fate of dietary nanoparticles and microparticles in the gastrointestinal tract', *Journal of Autoimmunity,* 34(3), J226-J233.

Powell, J. J., Thoree, V. and Pele, L. C. (2007) 'Dietary microparticles and their impact on tolerance and immune responsiveness of the gastrointestinal tract', *The British journal of nutrition,* 98(Suppl 1), S59-S63.

Price, D. B., Ackland, M. L., Burks, W., Knight, M. I. and Suphioglu, C. (2014) 'Peanut Allergens Alter Intestinal Barrier Permeability and Tight Junction Localisation in Caco-2 Cell Cultures¹', *Cellular Physiology and Biochemistry,* 33(6), 1758-1777.

Prohaska, J. R. (2008) 'Role of copper transporters in copper homeostasis', *The American Journal of Clinical Nutrition,* 88(3), 826S-829S.

Puthothu, B., Krueger, M., Heinze, J., Forster, J. and Heinzmann, A. (2006) 'Impact of IL8 and IL8-Receptor alpha polymorphisms on the genetics of bronchial asthma and severe RSV infections', *Clinical and Molecular Allergy,* 4(1), 1-6.

Qin, H., Zhang, Z., Hang, X. and Jiang, Y. (2009) 'L. plantarum prevents Enteroinvasive Escherichia coli-induced tight junction proteins changes in intestinal epithelial cells', *BMC Microbiol,* 9, 63-63.

Quintanar, L. and Rivillas-Acevedo, L. (2013) 'Studying Metal Ion–Protein Interactions: Electronic Absorption, Circular Dichroism, and Electron Paramagnetic Resonance' in Williams, M. A. and Daviter, T., eds., *Protein-Ligand Interactions: Methods and Applications,* Totowa, NJ: Humana Press, 267-297.

Rasmussen, K., Mech, A., Mast, J., De Temmerman, P., Waegeneers, N., Van Steen, F., Pizzolon, J. C., De Temmerman, L., Van Doren, E. and Jensen, K. A. (2013) 'Synthetic Amorphous Silicon Dioxide (NM-200, NM-201, NM-202, NM-203,

NM-204). Characterisation and Physico-Chemical Properties', *JRC Scientific and Policy Reports*.

Ren, G., Hu, D., Cheng, E. W., Vargas-Reus, M. A., Reip, P. and Allaker, R. P. (2009) 'Characterisation of copper oxide nanoparticles for antimicrobial applications', *Int J Antimicrob Agents,* 33(6), 587-90.

Rinaldi, A. C. (2000) 'Meeting report – Copper research at the top', *BioMetals,* 13, 9-13.

Romero-Isart, N. and Vašák, M. (2002) 'Advances in the structure and chemistry of metallothioneins', *Journal of Inorganic Biochemistry,* 88(3–4), 388-396.

Round, A. N., Rigby, N. M., Garcia de la Torre, A., Macierzanka, A., Mills, E. N. C. and Mackie, A. R. (2012) 'Lamellar Structures of MUC2-Rich Mucin: A Potential Role in Governing the Barrier and Lubricating Functions of Intestinal Mucus', *Biomacromolecules,* 13(10), 3253-3261.

Ruttkay-Nedecky, B., Nejdl, L., Gumulec, J., Zitka, O., Masarik, M., Eckschlager, T., Stiborova, M., Adam, V. and Kizek, R. (2013) 'The role of metallothionein in oxidative stress', *Int J Mol Sci,* 14(3), 6044-66.

Ryter, S. W. and Choi, A. M. K. (2005) 'Heme Oxygenase-1: Redox Regulation of a Stress Protein in Lung and Cell Culture Models', *Antioxidants & Redox Signaling,* 7(1-2), 80-91.

Ryu, W.-I., Park, Y.-H., Bae, H. C., Kim, J. H., Jeong, S. H., Lee, H. and Son, S. W. (2014) 'ZnO nanoparticle induces apoptosis by ROS triggered mitochondrial pathway in human keratinocytes', *Molecular & Cellular Toxicology,* 10(4), 387-391.

Sabella, S., Carney, R. P., Brunetti, V., Malvindi, M. A., Al-Juffali, N., Vecchio, G., Janes, S. M., Bakr, O. M., Cingolani, R. and Stellacci, F. (2014) 'A general mechanism for intracellular toxicity of metal-containing nanoparticles', *Nanoscale,* 6(12), 7052-7061.

Sahu, D., Kannan, G. M., Vijayaraghavan, R., Anand, T. and Khanum, F. (2013) 'Nanosized Zinc Oxide Induces Toxicity in Human Lung Cells', *ISRN Toxicology,* 2013, 8.

Sakai-Kato, K., Hidaka, M., Un, K., Kawanishi, T. and Okuda, H. (2014) 'Physicochemical properties and *in vitro* intestinal permeability properties and intestinal cell toxicity of silica particles, performed in simulated gastrointestinal fluids', *Biochimica et Biophysica Acta (BBA) - General Subjects,* 1840(3), 1171-1180.

Sambuy, Y., De Angelis, I., Ranaldi, G., Scarino, M. L., Stammati, A. and Zucco, F. (2005) 'The Caco-2 cell line as a model of the intestinal barrier: influence of cell and culture-related factors on Caco-2 cell functional characteristics', *Cell Biol Toxicol,* 21, 1-26.

Sambuy, Y., Ferruzza, S., Ranaldi, G. and De Angelis, I. (2001) *Intestinal Cell Culture Models: Applications in Toxicology and Pharmacology, Cell Biology and Toxicology.,* Netherlands: C Kluwer Academic Publishers.

Sancho, E., Batlle, E. and Clevers, H. (2004) 'Signaling pathways in intestinal development and cancer', *Annu Rev Cell Dev Biol,* 20, 695-723.

Sauvain, J.-J., Rossi, M. J. and Riediker, M. (2013) 'Comparison of Three Acellular Tests for Assessing the Oxidation Potential of Nanomaterials', *Aerosol Science and Technology,* 47(2), 218-227.

Schimpel, C., Rinner, B., Absenger-Novak, M., Meindl, C., Fröhlich, E., Falk, A., Zimmer, A. and Roblegg, E. (2015) 'A novel *in vitro* model for studying nanoparticle interactions with the small intestine', *EURO-NanoTox-Letters,* 6(1), 1-14.

Schimpel, C., Teubl, B., Absenger, M., Meindl, C., Fröhlich, E., Leitinger, G., Zimmer, A. and Roblegg, E. (2014) 'Development of an Advanced Intestinal *In Vitro* Triple Culture Permeability Model To Study Transport of Nanoparticles', *Mol Pharm,* 11(3), 808-818.

Schleh, C., Semmler-Behnke, M., Lipka, J., Wenk, A., Hirn, S., Schäffler, M., Schmid, G., Simon, U. and Kreyling, W. G. (2012) 'Size and surface charge of gold nanoparticles determine absorption across intestinal barriers and accumulation in secondary target organs after oral administration', *Nanotoxicology,* 6(1), 36-46.

Schübbe, S., Schumann, C., Cavelius, C., Koch, M., Müller, T. and Kraegeloh, A. (2012) 'Size-dependent localization and quantitative evaluation of the intracellular migration of silica nanoparticles in Caco-2 cells', *Chemistry of Materials,* 24(5), 914-923.

Schulzke, J. D., Ploeger, S., Amasheh, M., Fromm, A., Zeissig, S., Troeger, H., Richter, J., Bojarski, C., Schumann, M. and Fromm, M. (2009) 'Epithelial Tight Junctions in Intestinal Inflammation', *Ann N Y Acad Sci,* 1165(1), 294-300.

Sekine, R., Khurana, K., Vasilev, K., Lombi, E. and Donner, E. (2015) 'Quantifying the adsorption of ionic silver and functionalized nanoparticles during ecotoxicity testing: Test container effects and recommendations', *Nanotoxicology,* 9(8), 1005-1012.

Shakweh, M., Ponchel, G. and Fattal, E. (2004) 'Particle uptake by Peyer's patches: a pathway for drug and vaccine delivery', *Expert Opinion on Drug Delivery,* 1(1), 141-163.

Sharma, A. K., Schmidt, B., Frandsen, H., Jacobsen, N. R., Larsen, E. H. and Binderup, M.-L. (2010) 'Genotoxicity of unmodified and organo-modified montmorillonite', *Mutation Research/Genetic Toxicology and Environmental Mutagenesis,* 700(1), 18-25.

Shaw, C. A., Mortimer, G. M., Deng, Z. J., Carter, E. S., Connell, S. P., Miller, M. R., Duffin, R., Newby, D. E., Hadoke, P. W. F. and Minchin, R. F. (2016) 'Protein corona formation in bronchoalveolar fluid enhances diesel exhaust nanoparticle uptake and pro-inflammatory responses in macrophages', *Nanotoxicology,* 10(7), 981-991.

Shekarabi, A. S., Oromiehie, A. R., Vaziri, A., Ardjmand, M. and Safekordi, A. A. (2014) 'Investigation of the effect of nanoclay on the properties of quince seed mucilage edible films', *Food Science & Nutrition,* 2(6), 821-827.

Shinohara, N., Zhang, G., Oshima, Y., Kobayashi, T., Imatanaka, N., Nakai, M., Sasaki, T., Kawaguchi, K. and Gamo, M. (2017) 'Kinetics and dissolution of intratracheally administered nickel oxide nanomaterials in rats', *Part Fibre Toxicol,* 14, 48.

Shiraga, H., Pfeiffer, R. and Ebadi, M. (1993) 'The effects of 6-hydroxydopamine and oxidative stress on the level of brain metallothionein', *Neurochemistry international,* 23(6), 561-566.

Siddiqui, M. A., Alhadlaq, H. A., Ahmad, J., Al-Khedhairy, A. A., Musarrat, J. and Ahamed, M. (2013) 'Copper oxide nanoparticles induced mitochondria mediated apoptosis in human hepatocarcinoma cells', *PLoS One,* 8(8), e69534.

Sigurdsson, H. H., Kirch, J. and Lehr, C.-M. (2013) 'Mucus as a barrier to lipophilic drugs', *Int J Pharm,* 453(1), 56-64.

Smolkova, B., El Yamani, N., Collins, A. R., Gutleb, A. C. and Dusinska, M. (2015) 'Nanoparticles in food. Epigenetic changes induced by nanomaterials and possible impact on health', *Food and Chemical Toxicology,* 77, 64-73.

Snoeck, V., Goddeeris, B. and Cox, E. (2005) 'The role of enterocytes in the intestinal barrier function and antigen uptake', *Microbes and Infection,* 7(7), 997-1004.

Sthijns, M. M. J. P. E., Thongkam, W., Albrecht, C., Hellack, B., Bast, A., Haenen, G. R. M. M. and Schins, R. P. F. (2017) 'Silver nanoparticles induce hormesis in A549 human epithelial cells', *Toxicology in Vitro,* 40, 223-233.

Stone, V., Johnston, H. J., Balharry, D., Gernand, J. M. and Gulumian, M. (2016) 'Approaches to Develop Alternative Testing Strategies to Inform Human Health Risk Assessment of Nanomaterials', *Risk Analysis,* 36(8), 1538-1550.

Stone, V., Pozzi-Mucelli, S., Tran, L., Aschberger, K., Sabella, S., Vogel, U., Poland, C., Balharry, D., Fernandes, T., Gottardo, S., Hankin, S., Hartl, M. G., Hartmann, N., Hristozov, D., Hund-Rinke, K., Johnston, H., Marcomini, A., Panzer, O., Roncato, D., Saber, A. T., Wallin, H. and Scott-Fordsmand, J. J. (2014) 'ITS-NANO - Prioritising nanosafety research to develop a stakeholder driven intelligent testing strategy', *Part Fibre Toxicol,* 1, 9.

Stone, V., Shaw, J., Brown, D. M., Macnee, W., Faux, S. P. and K., D. (1998) 'The Role of Oxidative Stress in the Prolonged Inhibitory E€ ect of Ultra®ne Carbon Black on Epithelial Cell Function', *Toxicology In Vitro,* 12, 649-659.

Strauch, B. M., Niemand, R. K., Winkelbeiner, N. L. and Hartwig, A. (2017) 'Comparison between micro- and nanosized copper oxide and water soluble copper chloride: interrelationship between intracellular copper concentrations, oxidative stress and DNA damage response in human lung cells', *Part Fibre Toxicol,* 14, 28.

Struyf, S., Gouwy, M., Dillen, C., Proost, P., Opdenakker, G. and Van Damme, J. (2005) 'Chemokines synergize in the recruitment of circulating neutrophils into inflamed tissue', *European journal of immunology,* 35(5), 1583-1591.

Suliman, Y. A., Ali, D., Alarifi, S., Harrath, A. H., Mansour, L. and Alwasel, S. H. (2015) 'Evaluation of cytotoxic, oxidative stress, proinflammatory and genotoxic effect of silver nanoparticles in human lung epithelial cells', *Environ Toxicol,* 30(2), 149-60.

Sumagin, R., Lomakina, E. and Sarelius, I. H. (2008) 'Leukocyte-endothelial cell interactions are linked to vascular permeability via ICAM-1-mediated signaling', *American Journal of Physiology - Heart and Circulatory Physiology,* 295(3), H969-H977.

Sun, T., Yan, Y., Zhao, Y., Guo, F. and Jiang, C. (2012) 'Copper oxide nanoparticles induce autophagic cell death in A549 cells', *PLoS One,* 7(8), e43442.

Susewind, J., de Souza Carvalho-Wodarz, C., Repnik, U., Collnot, E.-M., Schneider-Daum, N., Griffiths, G. W. and Lehr, C.-M. (2016) 'A 3D co-culture of three human cell lines to model the inflamed intestinal mucosa for safety testing of nanomaterials', *Nanotoxicology,* 10(1), 53-62.

Suzuki, K. T., A. Someya, Y.Komada and Ogra, Y. (2002) 'Roles of metallothionein in copper homeostasis: responses to Cu-deficient diets in mice', *Journal of Inorganic Biochemistry,* 88, 173–182.

Syed, H. K., Iqbal, M. A., Haque, R. A. and Peh, K.-K. (2015) 'Synthesis, characterization and antibacterial activity of a curcumin–silver(I) complex', *Journal of Coordination Chemistry,* 68(6), 1088-1100.

Tahoun, A., Siszler, G., Spears, K., McAteer, S., Tree, J., Paxton, E., Gillespie, T. L., Martinez-Argudo, I., Jepson, M. A., Shaw, D. J., Koegl, M., Haas, J., Gally, D. L. and Mahajan, A. (2011) 'Comparative Analysis of EspF Variants in Inhibition of Escherichia coli Phagocytosis by Macrophages and Inhibition of E. coli Translocation through Human- and Bovine-Derived M Cells', *Infection and Immunity,* 79(11), 4716-4729.

Taipalensuu, J., Törnblom, H., Lindberg, G., Einarsson, C., Sjöqvist, F., Melhus, H., Garberg, P., Sjöström, B., Lundgren, B. and Artursson, P. (2001) 'Correlation of gene expression of ten drug efflux proteins of the ATP-binding cassette transporter family in normal human jejunum and in human intestinal epithelial Caco-2 cell monolayers', *Journal of Pharmacology and Experimental Therapeutics,* 299(1), 164-170.

Takahashi, S. (2012) 'Molecular functions of metallothionein and its role in hematological malignancies', *J Hematol Oncol,* 5, 41.

Takenaka, S., Karg, E., Roth, C., Schulz, H., Ziesenis, A., Heinzmann, U., Schramel, P. and Heyder, J. (2001) 'Pulmonary and systemic distribution of inhaled ultrafine silver particles in rats', *Environmental Health Perspectives,* 109(Suppl 4), 547-551.

Tarantini, A., Huet, S., Jarry, G., Lanceleur, R., Poul, M., Tavares, A., Vital, N., Louro, H., João Silva, M. and Fessard, V. (2015a) 'Genotoxicity of synthetic amorphous silica nanoparticles in rats following short-term exposure. Part 1: Oral route', *Environmental and molecular mutagenesis,* 56(2), 218-227.

Tarantini, A., Lanceleur, R., Mourot, A., Lavault, M. T., Casterou, G., Jarry, G., Hogeveen, K. and Fessard, V. (2015b) 'Toxicity, genotoxicity and proinflammatory effects of amorphous nanosilica in the human intestinal Caco-2 cell line', *Toxicology In Vitro,* 29(2), 398-407.

Taylor, A. A., Marcus, I. M., Guysi, R. L. and Walker, S. L. (2015) 'Metal Oxide Nanoparticles Induce Minimal Phenotypic Changes in a Model Colon Gut Microbiota', *Environmental Engineering Science,* 32(7), 602-612.

Teitelbaum, R., Schubert, W., Gunther, L., Kress, Y., Macaluso, F., Pollard, J. W., McMurray, D. N. and Bloom, B. R. (1999) 'The M Cell as a Portal of Entry to the Lung for the Bacterial Pathogen Mycobacterium tuberculosis', *Immunity,* 10(6), 641-650.

The Royal Society (2004) *Nanoscience and nanotechnologies: opportunities and uncertainties*, Clyvedon Press, Cardiff, UK.

Thirumoorthy, N., Shyam Sunder, A., Manisenthil Kumar, K., Senthil Kumar, M., Ganesh, G. and Chatterjee, M. (2011) 'A review of metallothionein isoforms and their role in pathophysiology', *World J Surg Oncol*, 9, 54.

Thomas, S., Meera, A. and Maria, H. J. (2012) 'Enhancing Gas-Barrier Properties of Polymer-Clay Nanocomposites', *Soc. Plast. Eng. Plast. Res. Online*, 10.

Tian, X., Jiang, X., Welch, C., Croley, T. R., Wong, T.-Y., Chen, C., Fan, S., Chong, Y., Li, R., Ge, C., Chen, C. and Yin, J.-J. (2018) 'Bactericidal Effects of Silver Nanoparticles on Lactobacilli and the Underlying Mechanism', *ACS Applied Materials & Interfaces*, 10(10), 8443-8450.

Titma, T., Shimmo, R., Siigur, J. and Kahru, A. (2016) 'Toxicity of antimony, copper, cobalt, manganese, titanium and zinc oxide nanoparticles for the alveolar and intestinal epithelial barrier cells *in vitro*', *Cytotechnology*, 68(6), 2363-2377.

Tokuda, S., Higashi, T. and Furuse, M. (2014) 'ZO-1 Knockout by TALEN-Mediated Gene Targeting in MDCK Cells: Involvement of ZO-1 in the Regulation of Cytoskeleton and Cell Shape', *PLoS One*, 9(8), e104994.

Tsuda, A. and Gehr, P. (2014) *Nanoparticles in the lung: environmental exposure and drug delivery*, CRC Press.

Tsuji, T., Kato, A., Yasuda, H., Miyaji, T., Luo, J., Sakao, Y., Ito, H., Fujigaki, Y. and Hishida, A. (2009) 'The dimethylthiourea-induced attenuation of cisplatin nephrotoxicity is associated with the augmented induction of heat shock proteins', *Toxicology and Applied Pharmacology*, 234(2), 202-208.

Uddin, F. (2008) 'Clays, Nanoclays, and Montmorillonite Minerals', *Metallurgical and Materials Transactions A*, 39(12), 2804-2814.

Ude, V. C., Brown, D. M., Viale, L., Kanase, N., Stone, V. and Johnston, H. J. (2017) 'Impact of copper oxide nanomaterials on differentiated and undifferentiated Caco-2 intestinal epithelial cells; assessment of cytotoxicity, barrier integrity, cytokine production and nanomaterial penetration', *Part Fibre Toxicol*, 14(1), 31.

Ueno, T., Yokoi, N., Abe, S. and Watanabe, Y. (2007) 'Crystal structure based design of functional metal/protein hybrids', *Journal of Inorganic Biochemistry*, 101(11), 1667-1675.

Usman, M. S., El Zowalaty, M. E., Shameli, K., Zainuddin, N., Salama, M. and Ibrahim, N. A. (2013) 'Synthesis, characterization, and antimicrobial properties of copper nanoparticles', *Int J Nanomedicine*, 8, 4467-79.

Valdez, C. E., Smith, Q. A., Nechay, M. R. and Alexandrova, A. N. (2014) 'Mysteries of Metals in Metalloenzymes', *Accounts of Chemical Research*, 47(10), 3110-3117.

van Kesteren, P. C. E., Cubadda, F., Bouwmeester, H., van Eijkeren, J. C. H., Dekkers, S., de Jong, W. H. and Oomen, A. G. (2015) 'Novel insights into the risk assessment of the nanomaterial synthetic amorphous silica, additive E551, in food', *Nanotoxicology*, 9(4), 442-452.

Vandamme, T. F. (2014) 'Use of rodents as models of human diseases', *Journal of Pharmacy & Bioallied Sciences*, 6(1), 2-9.

Velarde, G., Ait-Aissa, S., Gillet, C., Rogerieux, F., LaMbre, C., Vindimian, E. and Porcher, J. M. (1999) 'Use of the CaCo-2 Model in the Screening of Polluting Substance Toxicity', *Toxicology In Vitro,* 13(4), 719-722.

Velikorodnaya, Y. I., Pocheptsov, A. Y., Sokolov, O. I., Bogatyrev, V. A. and Dykman, L. A. (2015) 'Effect of gold nanoparticles on proliferation and apoptosis during spermatogenesis in rats', *Nanotechnologies in Russia,* 10(9-10), 814-819.

Verma, G., Marella, A., Shaquiquzzaman, M. and Alam, M. M. (2013) 'Immunoinflammatory responses in gastrointestinal tract injury and recovery', *Acta Biochemica Polonica,* 60(2), 143–149.

Versantvoort, C. H. M., Oomen, A. G., Van de Kamp, E., Rompelberg, C. J. M. and Sips, A. J. A. M. (2005) 'Applicability of an *in vitro* digestion model in assessing the bioaccessibility of mycotoxins from food', *Food and Chemical Toxicology,* 43(1), 31-40.

Viseras, C., Aguzzi, C., Cerezo, P. and Lopez-Galindo, A. (2007) 'Uses of clay minerals in semisolid health care and therapeutic products', *Applied Clay Science,* 36(1), 37-50.

Vllasaliu, D., Exposito-Harris, R., Heras, A., Casettari, L., Garnett, M., Illum, L. and Stolnik, S. (2010) 'Tight junction modulation by chitosan nanoparticles: comparison with chitosan solution', *Int J Pharm,* 400(1-2), 183-193.

Vllasaliu, D., Fowler, R., Garnett, M., Eaton, M. and Stolnik, S. (2011) 'Barrier characteristics of epithelial cultures modelling the airway and intestinal mucosa: A comparison', *Biochemical and Biophysical Research Communications,* 415(4), 579-585.

Vreeburg, R. A. M., Bastiaan-Net, S. and Mes, J. J. (2011) 'Normalization genes for quantitative RT-PCR in differentiated Caco-2 cells used for food exposure studies', *Food & Function,* 2(2), 124-129.

Walczak, A. P., Hendriksen, P. J. M., Woutersen, R. A., van der Zande, M., Undas, A. K., Helsdingen, R., van den Berg, H. H. J., Rietjens, I. M. C. M. and Bouwmeester, H. (2015a) 'Bioavailability and biodistribution of differently charged polystyrene nanoparticles upon oral exposure in rats', *Journal of Nanoparticle Research,* 17(5), 231.

Walczak, A. P., Kramer, E., Hendriksen, P. J. M., Tromp, P., Helsper, J. P. F. G., van der Zande, M., Rietjens, I. M. C. M. and Bouwmeester, H. (2015b) 'Translocation of differently sized and charged polystyrene nanoparticles in *in vitro* intestinal cell models of increasing complexity', *Nanotoxicology,* 9(4), 453-461.

Walter, E., Janich, S., Roessler, B. J., Hilfinger, J. M. and Amidon, G. L. (1996) 'HT29-MTX/Caco-2 Cocultures as an in Vitro Model for the Intestinal Epithelium: I*n Vitro–in Vivo* Correlation with Permeability Data from Rats and Humans', *Journal of Pharmaceutical Sciences,* 85(10), 1070-1076.

Wang, L., Nagesha, D. K., Selvarasah, S., Dokmeci, M. R. and Carrier, R. L. (2008) 'Toxicity of CdSe Nanoparticles in Caco-2 Cell Cultures', *J Nanobiotechnology,* 6, 11.

Wang, T., Bai, J., Jiang, X. and Nienhaus, G. U. (2012) 'Cellular Uptake of Nanoparticles by Membrane Penetration: A Study Combining Confocal Microscopy with FTIR Spectroelectrochemistry', *ACS Nano,* 6(2), 1251-1259.

Wang, Y., Mortimer, M., Chang, C. H. and Holden, P. A. (2018) 'Alginic Acid-Aided Dispersion of Carbon Nanotubes, Graphene, and Boron Nitride Nanomaterials for Microbial Toxicity Testing', *Nanomaterials,* 8(2), 76.

Wang, Z., Li, N., Zhao, J., White, J. C., Qu, P. and Xing, B. (2012) 'CuO Nanoparticle Interaction with Human Epithelial Cells: Cellular Uptake, Location, Export, and Genotoxicity', *Chemical Research in Toxicology,* 25(7), 1512-1521.

Wick, P., Manser, P., Limbach, L. K., Dettlaff-Weglikowska, U., Krumeich, F., Roth, S., Stark, W. J. and Bruinink, A. (2007) 'The degree and kind of agglomeration affect carbon nanotube cytotoxicity', *Toxicol Lett,* 168(2), 121-131.

Wijnhoven, S. W. P., Peijnenburg, W. J. G. M., Herberts, C. A., Hagens, W. I., Oomen, A. G., Heugens, E. H. W., Roszek, B., Bisschops, J., Gosens, I., Van De Meent, D., Dekkers, S., De Jong, W. H., van Zijverden, M., Sips, A. J. A. M. and Geertsma, R. E. (2009) 'Nano-silver – a review of available data and knowledge gaps in human and environmental risk assessment', *Nanotoxicology,* 3(2), 109-138.

Williams, K., Milner, J., Boudreau, M. D., Gokulan, K., Cerniglia, C. E. and Khare, S. (2015) 'Effects of subchronic exposure of silver nanoparticles on intestinal microbiota and gut-associated immune responses in the ileum of Sprague-Dawley rats', *Nanotoxicology,* 9(3), 279-289.

Woitiski, C. B., Sarmento, B., Carvalho, R. A., Neufeld, R. J. and Veiga, F. (2011) 'Facilitated nanoscale delivery of insulin across intestinal membrane models', *Int J Pharm,* 412(1), 123-131.

Wottrich, R., Diabaté, S. and Krug, H. F. (2004) 'Biological effects of ultrafine model particles in human macrophages and epithelial cells in mono- and co-culture', *International Journal of Hygiene and Environmental Health,* 207(4), 353-361.

Xiao, J., Zhu, Y., Huddleston, S., Li, P., Xiao, B., Farha, O. K. and Ameer, G. A. (2018) 'Copper Metal–Organic Framework Nanoparticles Stabilized with Folic Acid Improve Wound Healing in Diabetes', *ACS Nano*.

Xie, X., Liao, J., Shao, X., Li, Q. and Lin, Y. (2017) 'The Effect of shape on Cellular Uptake of Gold Nanoparticles in the forms of Stars, Rods, and Triangles', *Scientific Reports,* 7(1), 3827.

Xu, C., Liu, Y., Xu, G. and Wang, G. (2002) 'Preparation and characterization of CuO nanorods by thermal decomposition of CuC2O4 precursor', *Materials Research Bulletin,* 37(14), 2365-2372.

Yan, H., Duan, X., Pan, H., Holguin, N., Rai, M. F., Akk, A., Springer, L. E., Wickline, S. A., Sandell, L. J. and Pham, C. T. N. (2016) 'Suppression of NF-κB activity via nanoparticle-based siRNA delivery alters early cartilage responses to injury', *Proceedings of the National Academy of Sciences of the United States of America,* 113(41), E6199-E6208.

Yan, Z., Wang, W., Wu, Y., Wang, W., Li, B., Liang, N. and Wu, W. (2017) 'Zinc oxide nanoparticle-induced atherosclerotic alterations *in vitro* and *in vivo*', *Int J Nanomedicine,* 12, 4433-4442, available: [accessed

Yang, L., Yan, W., Wang, H., Zhuang, H. and Zhang, J. (2017) 'Shell thickness-dependent antibacterial activity and biocompatibility of gold@silver core-shell nanoparticles', *RSC Advances,* 7(19), 11355-11361.

Yang, Y.-X., Song, Z.-M., Cheng, B., Xiang, K., Chen, X.-X., Liu, J.-H., Cao, A., Wang, Y., Liu, Y. and Wang, H. (2014) 'Evaluation of the toxicity of food additive silica nanoparticles on gastrointestinal cells', *Journal of Applied Toxicology,* 34(4), 424-435.

Yao, M., He, L., McClements, D. J. and Xiao, H. (2015) 'Uptake of Gold Nanoparticles by Intestinal Epithelial Cells: Impact of Particle Size on Their Absorption, Accumulation, and Toxicity', *Journal of Agricultural and Food Chemistry,* 63(36), 8044-8049.

Ye, D., Bramini, M., Hristov, D. R., Wan, S., Salvati, A., Åberg, C. and Dawson, K. A. (2017) 'Low uptake of silica nanoparticles in Caco-2 intestinal epithelial barriers', *Beilstein Journal of Nanotechnology,* 8, 1396-1406.

Yee, S. (1997) '*In vitro* permeability across Caco-2 cells (colonic) can predict *in vivo* (small intestinal) absorption in man—fact or myth', *Pharmaceutical research,* 14(6), 763-766.

Yin, L., Ding, J., Fei, L., He, M., Cui, F., Tang, C. and Yin, C. (2008) 'Beneficial properties for insulin absorption using superporous hydrogel containing interpenetrating polymer network as oral delivery vehicles', *Int J Pharm,* 350(1), 220-229.

Yin, L., Ding, J., He, C., Cui, L., Tang, C. and Yin, C. (2009) 'Drug permeability and mucoadhesion properties of thiolated trimethyl chitosan nanoparticles in oral insulin delivery', *Biomaterials,* 30(29), 5691-5700.

Yuan, H., Chen, C.-Y., Chai, G.-h., Du, Y.-Z. and Hu, F.-Q. (2013) 'Improved Transport and Absorption through Gastrointestinal Tract by PEGylated Solid Lipid Nanoparticles', *Mol Pharm,* 10(5), 1865-1873.

Zhang, H., Wang, X., Wang, M., Li, L., Chang, C. H., Ji, Z., Xia, T. and Nel, A. E. (2015) 'Mammalian Cells Exhibit a Range of Sensitivities to Silver Nanoparticles that are Partially Explicable by Variations in Antioxidant Defense and Metallothionein Expression', *Small,* 11(31), 3797-805.

Zhang, W., Kalive, M., Capco, D. G. and Chen, Y. (2010) 'Adsorption of hematite nanoparticles onto Caco-2 cells and the cellular impairments: effect of particle size', *Nanotechnology,* 21(35), 355103.

Zhang, X.-F., Shen, W. and Gurunathan, S. (2016) 'Silver Nanoparticle-Mediated Cellular Responses in Various Cell Lines: An *In Vitro* Model', *Int J Mol Sci,* 17(10), 1603.

Zhang, Y., Shareena Dasari, T. P., Deng, H. and Yu, H. (2015) 'Antimicrobial Activity of Gold Nanoparticles and Ionic Gold', *Journal of Environmental Science and Health, Part C,* 33(3), 286-327.

Zhou, G., Zhang, J., Pan, C., Liu, N., Wang, Z. and Zhang, J. (2017) 'Enhanced Uptake of Fe3O4 Nanoparticles by Intestinal Epithelial Cells in a State of Inflammation', *Molecules,* 22(8), 1240.

Zhou, Y., Kong, Y., Kundu, S., Cirillo, J. D. and Liang, H. (2012) 'Antibacterial activities of gold and silver nanoparticles against Escherichia coli and bacillus Calmette-Guérin', *J Nanobiotechnology,* 10, 19-19.

Zhu, X., Fan, W.-G., Li, D.-P., Kung, H. and Lin, M. C. (2011) 'Heme oxygenase-1 system and gastrointestinal inflammation: a short review', *World Journal of Gastroenterology: WJG*, 17(38), 4283.

Zucconi, G. G., Cipriani, S., Scattoni, R., Balgkouranidou, I., Hawkins, D. P. and Ragnarsdottir, K. V. (2007) 'Copper deficiency elicits glial and neuronal response typical of neurodegenerative disorders', *Neuropathology and Applied Neurobiology*, 33(2), 212-225.

Appendices

Appendix 1

Hydrodynamic diameter, zeta potential and polydispersity index (PdI) values of MEM and DMEM complete cell culture medium. Data are expressed as mean ± SEM (n=3). Asterisk (*) represents significant (P<0.05) size decrease at comparison of incubation at time point 0 and 24 h.

	Time (h)	*0*	*24*
Complete MEM	Hydrodynamic diameter (nm)	26.22±4.28	19.58±0.61
	Zeta Potential (mV)	-7.98±0.43	-8.04±0.38
	PdI	0.34±0.08	0.42±0.06
Complete DMEM	Hydrodynamic diameter (nm)	20.45±0.33	19.74±0.46
	Zeta Potential (mV)	-8.32±0.24	-7.90±0.28
	PdI	0.62±0.03	0.33±0.02

Appendix 2

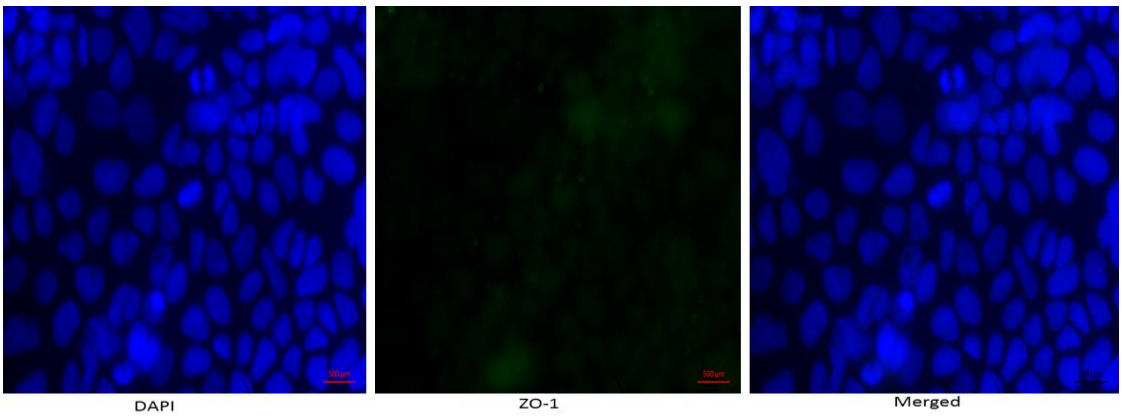

ZO-1 staining of undifferentiated Caco-2 cells. Cells (3.13 x 10^5 cells/cm^2) were grown on a 10 mm glass coverslip in a 24 well plate (Costar Corning, Flintshire, UK). After 24 h of incubation, the cells were fixed and stained for the tight junction protein ZO-1 (green) and nucleus with DAPI (blue). The images were obtained with Zeiss fluorescence microscopy equipped with AxioCam camera. Scale bar = 500 µm.